

NMR Spectroscopic Investigations of Catalyzed Reactions

—

Mechanisms, Kinetics & Unexpected Intermediates

Inaugural-Dissertation

zur

Erlangung des Doktorgrades

der Mathematisch-Naturwissenschaftlichen Fakultät

der Universität zu Köln

vorgelegt von

Markus H. Leutzsch

aus Meerane (Sachsen)

Köln 2015

Berichtersteller: Prof. Dr. B. List
Prof. Dr. A. Berkessel

Tag der mündlichen Prüfung: 25. November 2015

Table of Contents

Table of Contents	1
Kurzzusammenfassung	IV
Abstract	V
List of Abbreviations	VI
Acknowledgements	VIII
1. Introduction	1
2. Background	3
2.1 <i>Asymmetric Organocatalysis</i>	3
2.1.1 Proline Catalyzed Aldol Reactions and the Origin of Enantioselectivity	5
2.1.2 Brønsted Acid Catalysis	11
2.1.3 Organic Lewis Acid Catalysis	13
2.2 <i>ParaHydrogen Induced Hyperpolarization (PHIP) in Homogeneous Catalysis</i>	14
2.2.1 Theory	14
2.2.2 Applications	17
2.2.2.1 Wilkinson's Catalyst	17
2.2.2.2 Trans-Stereoselective Hydrogenation of Alkynes by [RuCp*] ⁺ Catalysts	18
3. Objectives of this Ph.D. Thesis	23
3.1 <i>Direct Experimental Observation of a Hydrogen Bond in a Transition State Model for Proline Catalyzed Aldol Reactions</i>	23
3.2 <i>NMR Spectroscopy as a Versatile Tool for Studying Organocatalytic Reactions and Intermediates</i>	24
3.3 <i>Parahydrogen Induced Polarization (PHIP) as Tool for the Discovery of New, Unknown Intermediates</i>	26
4. Results and Discussion	27
4.1 <i>Aminocatalysis</i>	27
4.1.1 Hydrogen Bonds in Proline Catalyzed Aldol Reactions	27
4.1.1.1 Towards the In Situ Observation of Hydrogen Bonding	27
4.1.1.2 Synthesis of Proline-Derived Enaminones as Stable Transition State Analogues	32

Table of Contents

4.1.1.3	Synthesis of Proline-Derived Aryl Amines as Stable Transition State Analogues	40
4.1.2	Enamine Intermediates in the α -Benzoylation of α -Branched Aldehydes	46
4.2	<i>Disulfonimides as Brønsted- and Lewis-Acid Catalysts</i>	50
4.2.1	Reaction Monitoring of the Asymmetric Torgov Cyclisation	50
4.2.2	Silylation Trends of Disulfonimides	53
4.2.3	Intermediates and Reaction Profiles of the DSI catalyzed Synthesis of β^3 -Amino Esters from <i>N</i> -Boc-Amino Sulfones	56
4.3	<i>Unexpected Carbene Intermediates in the Trans-Hydrogenation of Internal Alkynes</i>	61
4.3.1	<i>Parahydrogen</i> Enrichment	61
4.3.2	Initial Experiment on the <i>Trans</i> -Hydrogenation of Internal Alkynes	62
4.3.3	Observation and Characterization of (Metastable) Carbene-Intermediates.....	69
4.3.4	The Role of the Carbene Intermediates in the Catalytic Cycle	75
4.3.5	Characterization of Other Carbenes	82
4.3.6	Influence of the Catalyst on the Carbene Formation	86
5.	Summary	89
5.1	<i>Transition State Analogues for Proline Catalyzed Aldol reactions</i>	89
5.2	<i>NMR Studies of Organocatalytic Reactions</i>	90
5.3	<i>Carbenes as Intermediates in the Trans-Hydrogenation of Internal Alkynes</i>	91
6.	Outlook	93
6.1	<i>New and Advanced Proline Catalyzed Aldol Enamine Transition State Models</i>	93
6.2	<i>Further NMR Studies of Brønsted Acid Catalyzed Reactions and their Intermediates</i>	94
6.3	<i>Carbene Intermediates</i>	96
7.	Experimental Section	97
7.1	<i>General Remarks</i>	97
7.2	<i>In Situ Observation of Enamines with an Intramolecular H-Bond Acceptor</i>	99
7.2.1	Aldehyde Synthesis	99
7.2.2	In Situ Preparation of Enamines.....	104
7.3	<i>Synthesis of Proline Derived Enaminones with an Intramolecular Hydrogen Bond Acceptor</i> ...	105
7.4	<i>Synthesis of an Proline Derived Aryl Amine with an Intramolecular Hydrogen Bond Acceptor</i>	120
7.5	<i>Kinetic NMR Experiments</i>	131
7.5.1	Torgov Cyclisation.....	131
7.5.2	Mannich Reaction	131

7.6	<i>PHIP Experiments</i>	133
7.6.1	Sample Preparation	133
7.6.2	NMR Measurements	133
7.6.3	<i>Parahydrogen</i> Enrichment	133
7.6.4	Substrates.....	135
7.6.5	Theoretical Methods.....	136
8.	Bibliography	137
9.	Appendix	145
9.1	<i>Pulse Sequences</i>	145
9.2	<i>X-Ray Structures</i>	148
9.3	<i>Eigenständigkeitserklärung</i>	154
9.4	<i>Curriculum Vitae / Lebenslauf</i>	155

Kurzzusammenfassung

Die vorliegende Doktorarbeit beschreibt mechanistische Studien in unterschiedlichen Teilgebieten der homogenen Katalyse mittels NMR-Spektroskopie.

In den letzten Jahren wurde eine Vielzahl an Organokatalysatoren entwickelt, welche unterschiedlichste Transformationen mit hohen Enantioselektivitäten und Ausbeuten ermöglichen. Trotz einer hohen Anzahl an Publikationen auf dem Gebiet, mangelt es vielen Systemen an einem fundierten mechanistischen Verständnis. Die ersten beiden Teile dieser Arbeit befassen sich deshalb mit verschiedenen (NMR-) mechanistischen Studien der Enaminkatalyse sowie der Brønsted- und Lewis Säure Katalyse. Neben der Synthese von Übergangszustands-Analoga der Prolin-katalysierten Aldolreaktion, um die lang debattierte und schwer zu fassende Wasserstoffbrücke zwischen der Carbonsäure des Enamins und dem Elektrophil im enantioselektivitätsbestimmendem Schritt experimentell nachzuweisen, wurden Untersuchungen zum Einfluss von Säure- und Base-Additiven auf die Enaminbildung während der α -Benzylierung von α -verzweigten Aldehyden durchgeführt. Im Weiteren wurden die Reaktionsverläufe der asymmetrischen Torgov-Cyclisierung und der Disulfonimid katalysierten Synthese von β^3 -Amino Estern aus *N*-Boc-Amino Sulfonen mittels kinetischer NMR-Messungen untersucht, mit denen die vorliegenden mechanistischen Modelle bestätigt werden konnten. Außerdem wurde das Silylierungsverhalten von Disulfonimiden mit Hilfe von verschiedenen NMR-Experimenten bestimmt.

Der letzte Teil der vorliegenden Arbeit befasst sich mit mechanistischen Untersuchungen zur katalytischen *trans*-Hydrierung von internen Alkinen mit [RuCp*]-Komplexen mit Hilfe von *para*-Wasserstoff induzierter Polarisierung (PHIP). Während der Untersuchungen konnten verschiedene, unerwartete Carben-Spezies beobachtet und charakterisiert werden. Die Rolle dieser Carbene als Intermediat für verschiedene Nebenreaktionen konnte mittels OPSY-EXSY-Experimenten und ausführlicher DFT Studien bestimmt und etabliert werden.

Abstract

This thesis describes mechanistic studies by NMR spectroscopy in different areas of homogenous catalysis.

Over the last years a wide range of organocatalysts were developed enabling highly diverse transformations with high enantioselectivities and excellent yields. In contrast to the high amount of publications on this field, a mechanistic understanding based on experimental evidences is often underinvestigated. Therefore the first two chapters of this thesis are focused on various (NMR-) mechanistic studies in the fields of enamine catalysis and Brønsted and Lewis acid catalysis. Besides the synthesis towards stable transition state analogues of proline catalyzed aldol reactions in order to detect the elusive and highly debated hydrogen bond interaction between the carboxylic acid moiety of the enamine and the electrophile in the enantiodetermining step, the influence of acid and base additives on the enamine formation in the α -benzylation of α -branched aldehydes was studied. Furthermore the course of the asymmetric Torgov cyclisation and the disulfonimide (DSI) catalyzed synthesis of β^3 -amino esters from *N*-Boc amino sulfones were investigated by kinetic NMR-measurements and the underlying mechanistic models were confirmed by the experimental results. Additionally, the silylation behavior of DSIs was studied by different NMR experiments.

The last part of this dissertation investigates the mechanism of the catalytic *trans*-hydrogenation of internal alkynes with [RuCp*]-complexes by *para*hydrogen induced polarization (PHIP). During the studies different unexpected carbene species were observed and characterized. The role of the carbene as intermediate for several, mostly unwanted, side reactions was determined by OPSY-EXSY-experiments and extensive DFT calculations.

List of Abbreviations

°C	degree Celsius
Ac	acetyl
ALTADENA	Adiabatic Longitudinal Transport After Dissociation Engenders Nuclear Alignment
Ar	aryl
BINOL	1,1'-bi-naphthol
Bn	benzyl
BOC	<i>tert</i> -butyloxycarbonyl
cat.	catalyst or catalytic
COD	1,5-cyclooctadiene
COSY	correlation spectroscopy
Cp*	pentamethylcyclopentadienyl
dba	dibenzylideneacetone
DEPT	Distorsionless Enhancement by Polarization Transfer
DIBAL-H	diisobutylaluminiumhydrid (<i>i</i> -Bu) ₂ AlH
DMSO	dimethylsulfoxide
dr	diastomeric ratio
DSI	disulfonimide
equiv	equivalent(s)
er	enantiomeric ratio
ESI	electrospray ionization
Et	ethyl
et al.	et alii/et aliae – and others
EXSY	EXchange SpectroscopY
FC	flash chromatography
GC	gas chromatography
h	hour(s)
HMBC	heteronuclear multiple bond correlation
HPLC	high performance liquid chromatography
HRMS	high resolution mass spectrometry
HSQC	Heteronuclear Single Quantum Correlation
Hz	Hertz
<i>i</i> -Bu	<i>iso</i> -butyl
INEPT	Insensitive Nuclei Enhanced by Polarization Transfer
K	Kelvin

<i>m/z</i>	mass-to-charge ratio
<i>m</i> CPBA	<i>meta</i> -chloroperoxybenzoic acid
Me	methyl
n.d.	not detected
NBS	<i>N</i> -bromosuccinimide
NMR	nuclear magnetic resonance
NOE(SY)	Nuclear Overhauser Effect (SpectroscopY)
<i>o</i> H ₂	<i>ortho</i> hydrogen
OPSY	Only <i>Para</i> hydrogen Spectroscopy
PASADENA	PArahydrogen and Synthesis Allow Dramatically Enhanced Nuclear Alignment
Ph	phenyl
<i>p</i> H ₂	<i>para</i> hydrogen
PHIP	<i>Para</i> Hydrogen Induced Polarization
ppm	part(s) per million
quant.	quantitative
<i>rac</i>	racemic
rt	room temperature
sat.	saturated
SPINOL	1,1'-spirobiindane-7,7'-diol
TADDOL	$\alpha,\alpha',\alpha',\alpha'$ -tetraaryl-1,3-dioxolan-4,5-dimethanol
TBS	<i>tert</i> -butyl dimethyl silyl (<i>t</i> BuMe ₂ Si)
Tf	trifluoromethanesulfonyl
THF	tetrahydrofuran
TLC	thin layer chromatography
TMS	trimethyl silyl ((CH ₃) ₃ Si)
TRIP	3,3'-bis(2,4,6-triisopropylphenyl)-1,1'-binaphthyl-2,2'-diyl hydrogenphosphat

Acknowledgements

The work presented in this dissertation was conducted between November 2011 and September 2015 at the Max-Planck-Institut für Kohlenforschung in Mülheim an der Ruhr under the guidance of Prof. Dr. Benjamin List and Dr. Christophe Farès.

I would like to thank Prof. Dr. Benjamin List for giving me the opportunity to be part of his outstanding group and to conduct research at this unique institute. His helpful suggestions and discussions and the freedom in performing different NMR investigations with various collaborators are gratefully acknowledged. Furthermore I would also like to thank him for initializing events outside the lab, as for instance the annual boat trip and the Christmas market visits.

My gratitude extends to my second supervisor Dr. Christophe Farès, who was always open for NMR spectroscopic discussions and solving problems. Furthermore, I thank him for the support and the experimental freedom during the PHIP investigations and the opportunity to visit several NMR conferences.

I am grateful to Prof. Dr. A. Berkessel for accepting to review this thesis, and to Prof. Dr. Prof. Dr. U. Ruschewitz and PD Dr. M. Prechtl for acting as my defense committee.

I thank Dr. C. Farés, G. Shevchenko, L. Kötzner and L. Schreyer for careful proofreading of this thesis.

Many of the results presented in this work would not have been possible without great collaboration partners. For initial studies on the enaminone systems I thank Dr. A. D. Bock. For the studies on the α -benzylation I thank Dr. A. Lee, P. S. J. Kaib and Dr. M. van Gemmeren. The studies on several DSI catalyzed reactions were conducted together with Dr. Q. Wang, Dr. Z. Zhang, Dr. S. Prévost and Dr. N. Dupré and I am thankful for the possibility to work together with them. I thank M. Monaco and L. Liu for the collaborative work on their projects. Furthermore I am very thankful to Prof. Dr. A. Fürstner, Dr. M. Fuchs, Dr. L. M. Wolf, Dr. P. Gupta, Prof. Dr. W. Thiel, Dr. D.-A. Roşca and S. Rummelt for the great collaboration in our investigations of *trans*-hydrogenation. I am grateful to Dr. Kerstin Münnemann and her coworkers for the initial introduction into their PHIP techniques. For the work on other interesting projects not presented in this work I am grateful to Dr. V. Wakchaure, Dr. Denis Chusov and G. Shevchenko.

I thank all the recent and former administration and technician team of the List group: A. Hermes, A. Kaltsidis, A. Döhning, H. van Thienen, N. R. Wippich, S. Dehn, S. Marcus, M. Hannappel and Dr. M. M. Lindner for their support in the lab and with administrative work. I would also like to thank my colleagues from the NMR-department: P. Philips, C.

Wirtz, W. Endler, M. Kochius, J. B. Lingnau, W. Wisniewski, B. Gabor and D. Bartels for the good working atmosphere, the maintenance of spectrometers and structure discussions.

Additionally I thank all the recent and former members of the List, Maulide and Klußmann groups, who have not been mentioned so far for the nice working atmosphere during the time I spent at the institute.

I thank W. Kersten and K. Gräfenstein for the design and production of the U-shaped tube for the PHIP studies. For the support in the Drucktechnikum and the maintenance of the glovebox L. Winkel and N. Fuhrmann are gratefully acknowledged.

I would also like to thank the members of the HPLC department: A. Deege, H. Heinrichs and G. Breitenbruch for their support. The members of the mass department are acknowledged for the measurement of several low- and high resolution mass spectra. Additionally, I thank J. Rust, Prof. Dr. Lehmann and all the other members of the X-ray department for measuring and solving the X-ray structures.

I am grateful to project Sustainable Chemical Synthesis (SusChemSys) for funding exiting work on CO₂ as a C1 building block. Although the results obtained are not presented in this work, I highly appreciate the experiences I gained during the project.

For the initial instruction into the field of NMR and his support prior to this thesis I would kindly thank my former supervisor Prof. Dr. S. Berger. Without him I would have never discovered my big interest for NMR.

Zu guter Letzt danke ich meinen Eltern und Großeltern für die Unterstützung während der Promotion und des Studiums. Ohne euch wäre diese Arbeit nicht möglich gewesen.

1. Introduction

“The scientist does not study nature because it is useful to do so. He studies it because he takes pleasure in it, and he takes pleasure in it because it is beautiful. If nature were not beautiful it would not be worth knowing, and life would not be worth living.”

Henri Poincaré, *Science and Method*, 1914

For decades scientists have been driven by fundamental questions to understand nature and to solve problems of mankind. Therefore they study phenomena like signaling pathways and receptors of various organisms in order to develop new drugs, find new pesticides to prevent crop failures or simply discover new good smelling compounds for the perfume industry. In all of these areas small organic molecules are important targets. To facilitate an efficient synthesis of such compounds, chemical research has focused on the development of highly selective catalytic systems. Some big discoveries have been made by accident. In order to realize, understand and explain them, the development of analytical tools played an important role. In addition, these methods help to improve known processes by understanding the mechanism behind them. Nuclear magnetic resonance (NMR) spectroscopy has become one of the most prominent tools in analytical chemistry. The first discovery of nuclear magnetic resonance by *Rabi* in 1938^[1] and the development of liquid and solid NMR methods by *Bloch* and *Purcell* in the late 1940s^[2,3] resulted in the first applications in chemistry in the late 50s.^[4] With the commercial availability of NMR magnets and the development of the first 2D NMR methods by *Ernst* in the 70s, NMR has become one of the most powerful methods in determining structures of molecules and to follow the course of chemical reactions. Despite these advantages, NMR measurements are of relatively low sensitivity at ambient temperatures due to the thermal Boltzmann distribution of the nuclear spins in the magnetic field. In the last decades, discoveries were made to improve the sensitivity with new hardware or hyperpolarization methods.



Figure 1.1: First published ^1H -NMR spectrum of EtOH. For clarity the colors of this picture were inverted.^[4]

Introduction

This thesis will show the symbiosis between the development of catalytic reactions and the importance of analytical tools, especially NMR, for a better understanding of underlying mechanisms and principles. The following chapter will introduce briefly the field of asymmetric organocatalysis including some long standing mechanistic discussions. Afterwards modern methods for improving the NMR sensitivity by the utilization of the *para*-spin isomer of hydrogen for the study of hydrogenation reactions will be introduced. After the outline of the aims of this PhD work, selected attempts in improving the mechanistic understanding of a variety of organocatalyzed, but also metal-catalyzed reactions, over the last years will be shown.

2. Background

2.1 Asymmetric Organocatalysis

Following the year 2000, asymmetric organocatalysis has been established as a third pillar, besides the classical fields of metal- and biocatalysis.^[5] Organocatalytic reactions are accelerated by catalytic to substoichiometric amounts of relatively small, organic molecules. Organocatalysts are more and more applicable in enantioselective transformations.^[6–8]

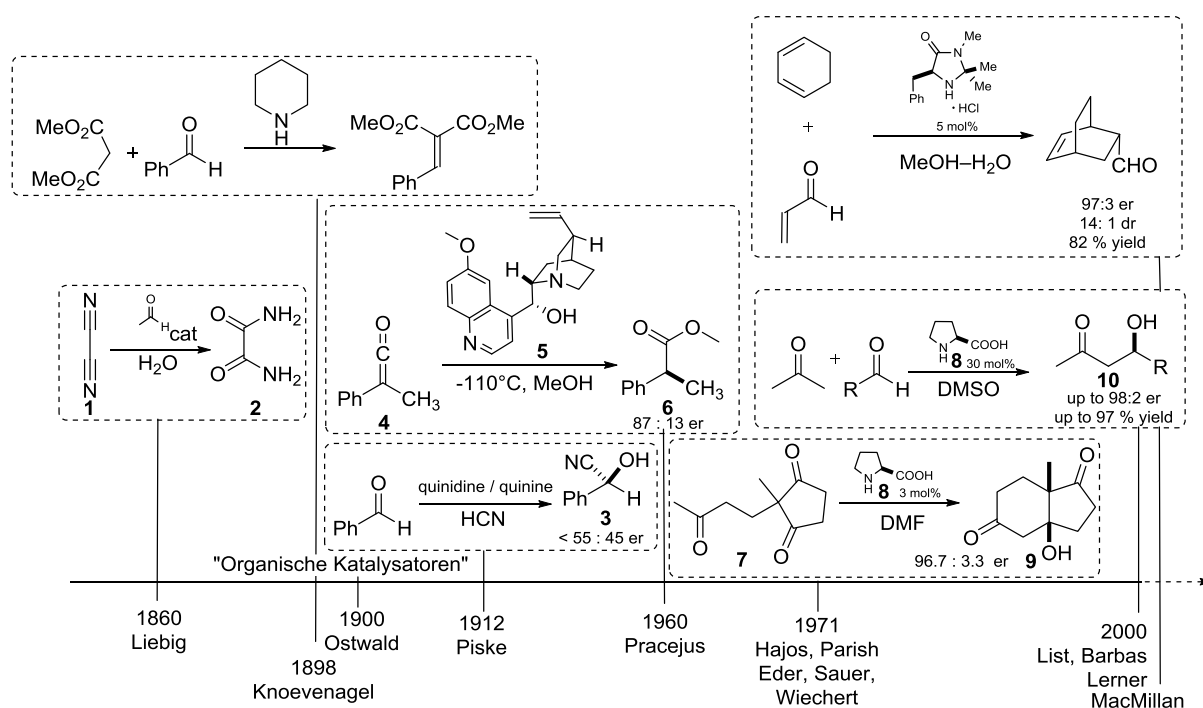


Figure 2.1: Timeline of important organocatalytic reactions until 2000.

Despite its recent rise in popularity, the first examples of organocatalytic reactions date back to the 19th century. In 1860, *Liebig* described the reaction of cyanogen **1** and water in the presence of acetaldehyde to form oxamide **2**.^[9] He came to the conclusion in his report, that the aldehyde plays a crucial role in this transformation and is still present after full conversion of the starting material. An important report, especially for the later development of aminocatalysis^[10], was published by *Knoevenagel* in 1898.^[11] The author reported the condensation reaction of malonic acid and benzaldehyde in the presence of an amine. This was the first example of an amine-catalyzed reaction, inspiring many scientists through the next decades. In the beginning of the 20th century, *Ostwald* mentioned the term "Organische Katalysatoren" (*ger.*: organic catalysts) in one of his publications for the first time.^[12,13] In 1912, *Bredig* and *Fiske* reported the first organocatalytic asymmetric reaction. Although the authors achieved an enantiomeric ratio (er) of lower than 45:55 in the synthesis of cyanohydrins **3** from benzaldehyde and hydrogen cyanide, using quinine and quinidine as catalysts, it is the first example

Background

showing that small organic molecules can induce chirality.^[14] Almost half a century after these observations, *Pracejus* in 1960 reported the synthesis of α -phenyl-propionic esters **6** with 87:13 er after the addition of methanol to phenyl methyl ketene **4** with 1 mol% of *O*-acetyl quinine **5** as the catalyst. The next big step in the history of organocatalysis was reported independently by *Hajos and Parrish*^[15,16] and *Wiechert, Sauer and Eder*^[17] in 1971. Both groups described the synthesis of the bicyclic ketol **9** starting from the achiral triketone **7** using the amino acid L-proline **8** as the catalyst. This was the first example of an organocatalytic asymmetric aldol reaction and also the first example giving the desired products **10** in excellent enantioselectivities (96:4 er). Considering these excellent results, the potential of this discovery was not realized until 2000, when *List, Barbas and Lerner* reported the L-proline **8** catalyzed direct asymmetric aldol reaction introducing the concept of enamine catalysis.^[5] Shortly afterwards *MacMillan* and coworkers reported a highly enantioselective Diels-Alder reaction utilizing the concept of iminium catalysis.^[18] From these days on, organocatalysis has become an intensively investigated research area leading to the discovery of several new organocatalysts and new applications. Besides aminocatalysis, several other concepts of activation have been utilized resulting in highly enantioselective transformations. A brief overview of the various fields of organocatalysis can be found in Figure 2.2. In the next subchapters some selected areas, which are an essential part of this thesis will be introduced.^[7,8]

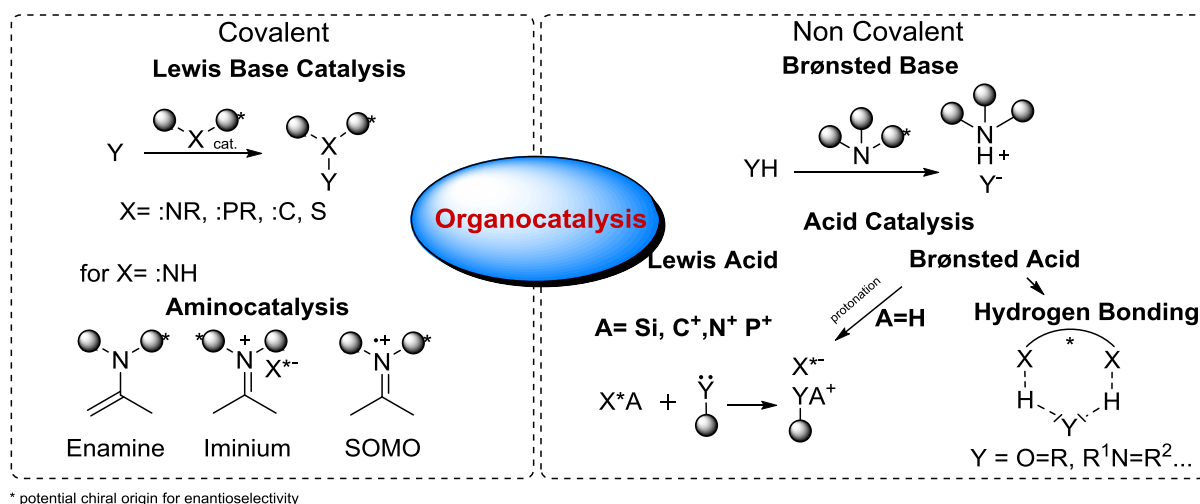
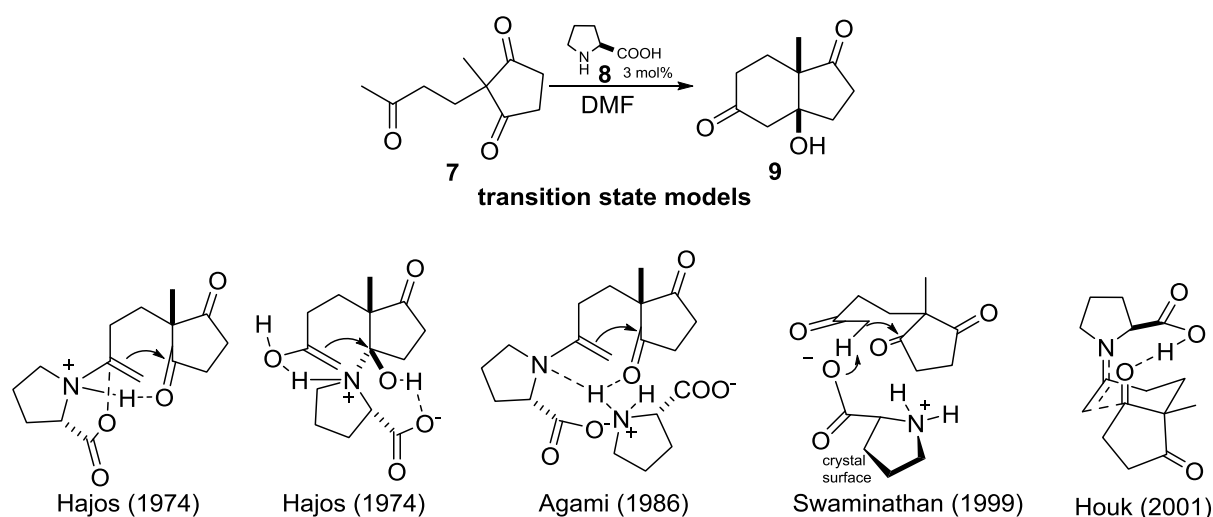


Figure 2.2: Classification of modern organocatalysis sorted by the activation of the electrophile or nucleophile.

2.1.1 Proline Catalyzed Aldol Reactions and the Origin of Enantioselectivity

Since the discovery of the first asymmetric proline-catalyzed intramolecular aldol condensation, a big debate about the origin of enantioselectivity evolved. Many models have been proposed for this so-called Hajos–Parrish–Eder–Sauer–Wiechert reaction (Scheme 2.1).



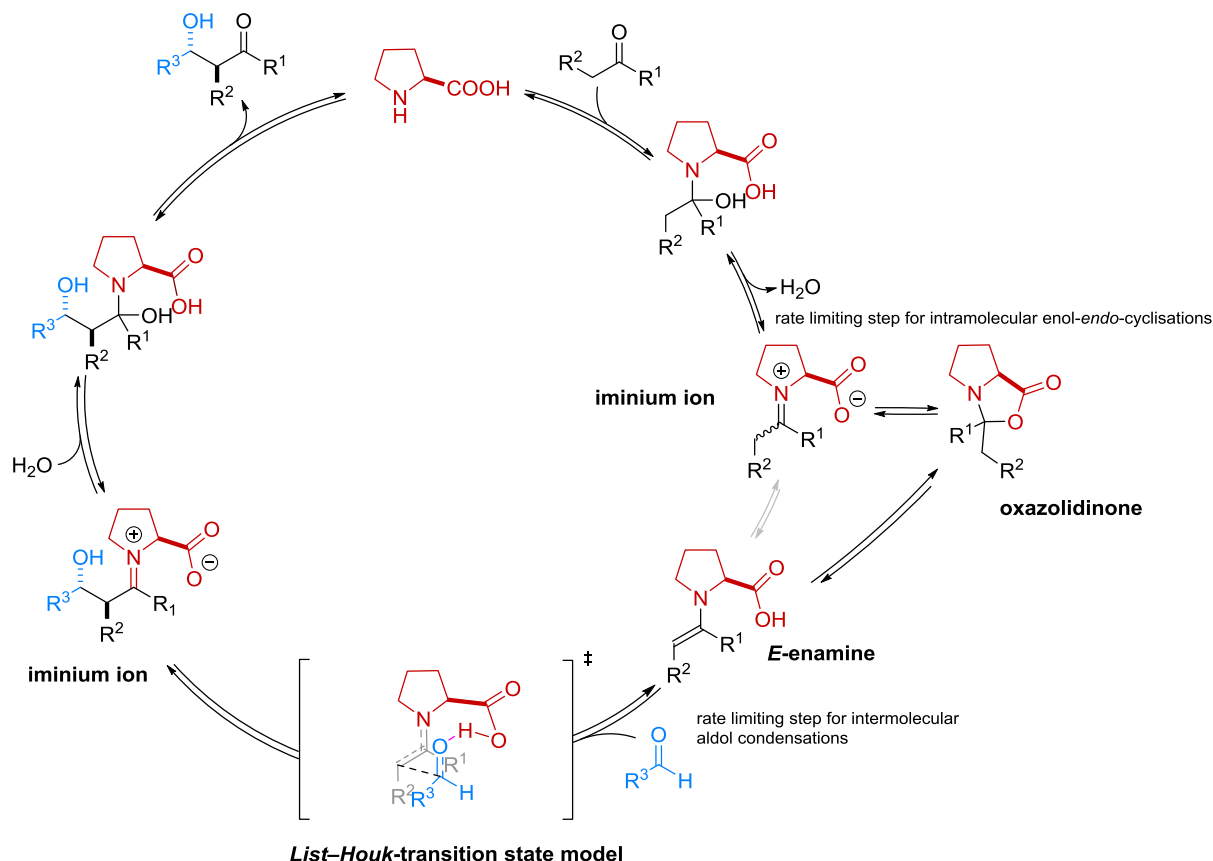
Scheme 2.1: Proposed mechanisms of the Hajos–Parrish–Eder–Sauer–Wiechert reaction.

In his first manuscript *Hajos* discussed two possible transition states that could explain the obtained results.^[16] The first model involved enamine formation between proline **8** and the acyclic ketone **7** and the selectivity was explained by an H-bond interaction of the protonated nitrogen and the side-chain carbonyl group. This model was in good agreement with the proposed aldolase mechanism proposed by *Rutter* in 1964.^[19] In order to confirm this mechanism, he performed the reaction in the presence of H_2^{18}O . If an enamine is formed during the reaction, the product should be ^{18}O enriched. Unfortunately, the result was negative and a second possible model to explain the observations was proposed, in which a hemiaminal is formed between proline and the cyclic carbonyl. This intermediate is then attacked by the enol of the exocyclic ketone in an S_{N} reaction. *Jung* questioned this observation soon after its initial proposal^[20] and also other groups preferred the enamine mechanism.^[21,22] Some years later *Agami et al.* reinvestigated the mechanism and performed nonlinear effect studies^[23]. Interestingly, they could show that two proline molecules have to be involved in the enantiodetermining step, leading to the proposal of a new side-chain enamine mechanism. One proline molecule is responsible for the enamine formation, the other one is a proton transfer mediator. This model was widely accepted by the scientific community for the next decades. In 1999, *Swaminathan et al.* came up with the

Background

hypothesis that the reaction has to occur on the crystal surface, because they could not observe any dissolved proline during an NMR investigation.^[24] Due to known similar reactions that are proceeding in completely homogenous solutions, this mechanism can be rejected. One year after the reports of the proline-catalyzed intermolecular aldol reaction by *List et al.*^[5], *Houk* and his coworkers came up with a new model that included several previously made observations, such as the important role of the enamine, the essential role of the carboxylic acid group and the pyrrolidine ring for asymmetric induction. In this model, the formation of the C–C-bond occurs via a chair like transition state and the hydrogen bond between the acidic proton and the carbonyl oxygen is further stabilizing the transition, leading to the observed (S,S)-enantiomer. After this work, *List* and his coworkers repeated the ¹⁸O-incorporation^[25] studies. Surprisingly, they could observe the efficient ¹⁸O-enrichment in the product and disproved *Hajos* initial result. In addition to these studies, *List et al.* also repeated the nonlinear effect studies of *Agami*.^[26] Interestingly, they found an absence of the nonlinear effect, which finally proved, that only one proline molecule is part of the enantiodetermining step. The authors explained this difference by the high error of the polarimetric enantioselectivity determination compared to the modern determination of the enantiomeric ratio with HPLC on a chiral stationary phase. In addition to this discussion about the origin of enantio- and stereoselectivity of this reaction, other steps of this reaction were also discussed. In 2009, a ¹³C-kinetic isotope effect study at natural abundance in combination with theoretical calculations showed that the C–C-bond formation is not the rate determining step in this intramolecular enol-*endo*-cyclisation, but rather the hemiaminal or the imine/enamine formation.^[27]

Besides the Hajos–Parrish–Eder–Sauer–Wiechert reaction, other aldol reactions were of high interest and the topic of many literature reports. A wide range of studies has tried to clarify the mechanism and will be discussed on the next paragraphs (Scheme 2.2).



Scheme 2.2: Generalized mechanism for proline catalyzed aldol reactions.

Since the first report of intermolecular aldol reactions by *List et al.*, proline derived enamines were proposed as key intermediates in the catalytic cycles^[28–31] based on the established class I aldolase-mechanism. Several theoretical investigations could show that these intermediates explain the observed enantioselectivities. In the first report^[5], the enantioselectivity was explained by a metal-free version of the classical *Zimmermann–Traxler* model (Figure 2.3, **A** and **B**). This model was further advanced after the results of *Houk's* calculation results, showing that the N \cdots H hydrogen bond is not lowering the energy of the transition state (Figure 2.3, **C**). An alternative mechanism for this transformation was reported by *Seebach* and *Eschenmoser* in 2007 (Figure 2.3, **D**).^[32] The authors proposed that oxazolidinones, whose formation have been observed in situ by NMR,^[25] are the catalytically active species and not a parasitic side species. After its formation, the oxazolidinone forms an iminium carboxylate, which is isomerizing to the *cis*-enamine carboxylate. Alternatively the enamine carboxylate is directly formed via a base catalyzed E2 elimination. In the transition state this enamine undergoes a *trans* addition to the electrophile and a new oxazolidinone is formed. In contrast to the *List–Houk*-model, this mechanism suggests that the C–C-bond formation does not involve an activation of the electrophile by the carboxylic acid. Instead, the carboxylic acid acts in its deprotonated form. Recently *Sunoj et. al.* investigated the stereochemical

Background

outcome of both models in the proline-catalyzed self-aldol reaction of propanal by DFT calculations.^[33] The authors found, that the *List-Houk*-model **C** explains the stereochemical outcome in good agreement with experimental enantio- and diastereoselectivities. In contrast to this, the *Seebach-Eschenmoser* model **D** was inadequate in the calculations to predict the experimental results. Interestingly the less favored *syn*, product was found to be main product of this pathway.

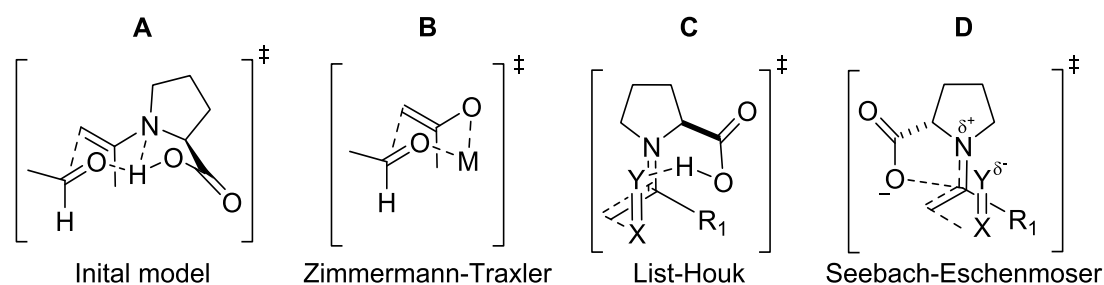


Figure 2.3: Transition state models for intermolecular proline catalyzed reactions.

In 2010, *List et al.*^[34] and *Gschwind et al.*^[35] reported X-ray structures of proline derived enamines and the first in situ detection of proline-derived enamines from aldehydes (Figure 2.4).

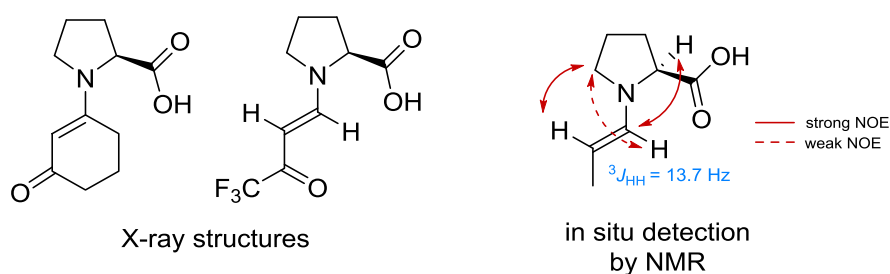


Figure 2.4: Characterized enamines by X-ray and NMR studies by *List et al.*^[34] and *Gschwind et al.*^[35]

The X-ray structures were obtained from stabilized vinylogous amides and were of high interest based on the proposed similarity to the transition state models **C** and **D** due to their electronic structure (Figure 2.5).

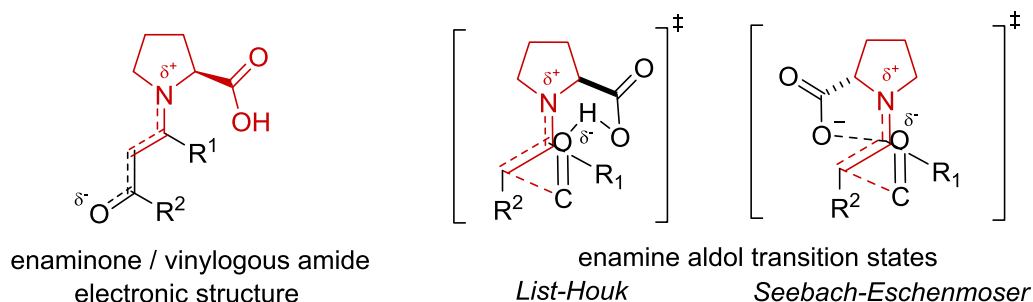


Figure 2.5: Potential relationship between enaminones and the enamine aldol transition state models.

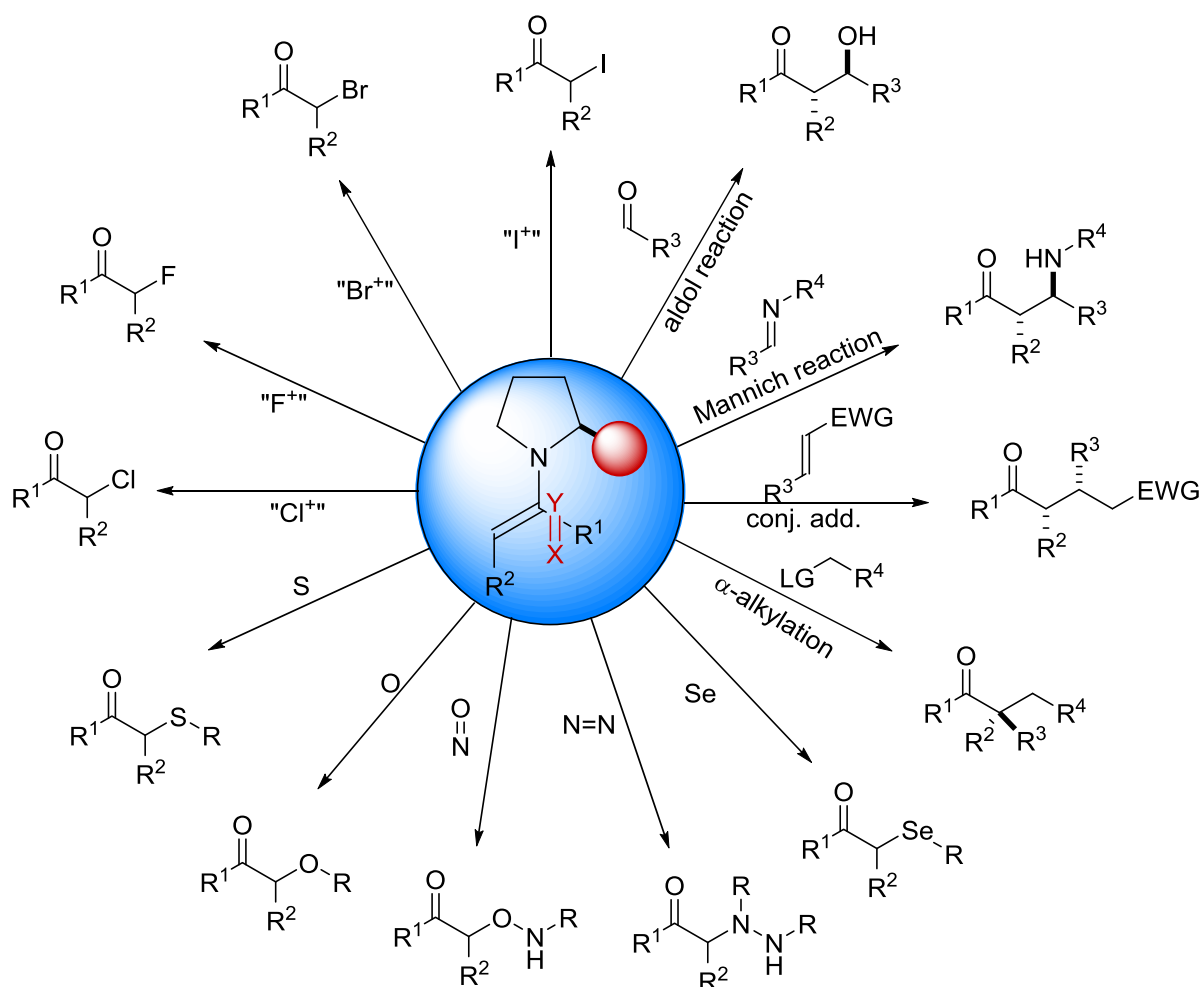
These enaminones were previously described as solid compounds. In solution state NMR studies they have been characterized as (*E*)-configured on the double bond and with a *trans/cis* ratio of 85:15 of the C–N-bond.^[36] After reinvestigation of these compounds, *List* and coworkers were able to obtain crystals that were suitable for a single X-ray analysis.^[37] Their crystalized aldehyde derived enaminones were all (*E*)-enamines, as expected, with a *trans* conformation of the C–N-bond. The key for the enhanced stability of this enaminones and the unobserved formation of oxazolidinones is easily explained by a stabilization of the enamine by an additional carbonyl group. The vinylogous amide resonance decreases the electrophilicity of the α -carbon connected to the nitrogen of the proline and the nucleophilicity of the enamine. The bond lengths obtained from the X-ray structures were in good agreement to the calculated enamine transition states of the intermolecular aldol reaction by *Houk* verifying the initial proposal of the relationship between enaminones and the transition state. Interestingly, some crystals were packed via an intermolecular C–OH \cdots O=C hydrogen bond, suggesting that this could also be possible in solution state during a reaction.

The characterization of the corresponding enamines by *Gschwind* was carried out directly in solution during an intermolecular self-aldol condensation. In agreement with the results of the X-ray structures, the authors also observed *trans*-(*E*)-conformation of the enamine as the preferred conformer, although some small amount of the *cis*-(*E*)-enamine (due to the weak observed NOE) might also be present. As an extension to *List*'s work, they could further investigate the role of the enamine intermediate by exchange NMR spectroscopy (EXSY). Interestingly, the experimental data suggested that the enamine is formed from the corresponding oxazolidinones and not via a central iminium intermediate directly from the aldehyde as it was previously presumed. Solvents had a big influence of the enamine formation: polar aprotic solvents such as DMSO, resulted in a high amount of enamines and oxazolidinones, whereas more apolar solvents, such as CH₃CN, and polar protic solvents, as for instance MeOH, have much lower enamine concentrations (or they are not observable at all). Water as additive had no influence on the equilibrium of the intermediates, but on the overall amount of detected intermediates in solution. This is in agreement with *Blackmond*'s^[38] work, which describes a decreased reaction rate in reactions where enamine formation is the rate limiting step. *Blackmond* and her coworkers intensively studied the kinetics of enamine-catalyzed reactions, as for instance the intermolecular aldol condensation^[39,40] or α -aminations.^[41–43] They observed that, depending on the electrophile, the rate determining step of the reaction changes. In the proline-catalyzed α -amination of aldehydes, the enamine formation is rate determining, whereas in the intermolecular aldol reaction it is the C–C-bond formation.

Background

Despite all the mechanistic investigations which have been published so far, there are still open questions to be answered. Until today, the mechanism of enamine formation starting from oxazolidinone intermediates is still unclear. Additionally, a direct experimental evidence of the hydrogen bond activation of the electrophiles by the carboxylic acid moiety of proline via a stable transition state analogue has not been reported so far.

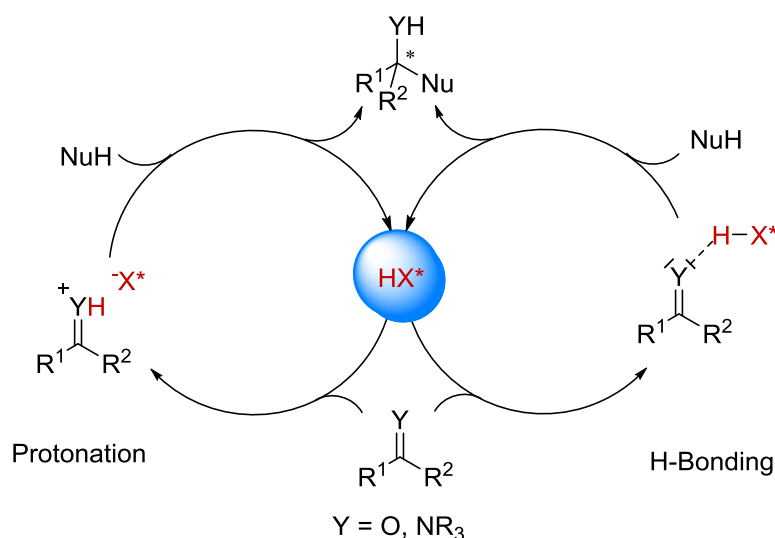
Nevertheless, proline **8** and its derivatives have shown to catalyze various reactions thus making enamine catalysis an attractive field of research. An overview of developed reactions is shown in Scheme 2.3 and several review articles will give a deeper insight for interested readers.^[44–47]



Scheme 2.3: Overview of asymmetric enamine catalysis (adapted with changes from *Pikho et al.*^[46]).

2.1.2 Brønsted Acid Catalysis

Asymmetric Brønsted acid catalysis has emerged as one of the most investigated organocatalytic classes over the last years.^[48–50] A generalized classification results from the possible different activation modes of the electrophile (Scheme 2.4). Nevertheless, the electrophile is acting as a Brønsted base; therefore, it is accepting a proton from the corresponding acid. Once the substrate is activated either by direct protonation or hydrogen bonding, the LUMO of the C=Y is lowered, making it easier for the HOMO of the nucleophile to attack.



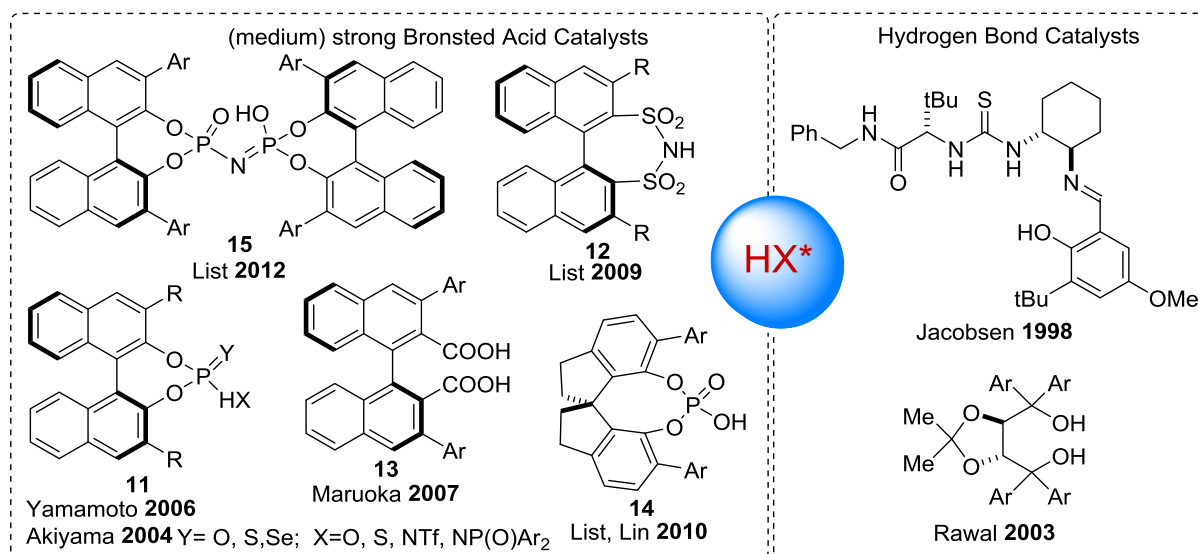
Scheme 2.4: Generalized activation modes and mechanism of Brønsted acid catalyzed reactions.

One of the early examples of highly enantioselective Brønsted acid catalysis was reported by *Jacobsen et al.*, employing hydrogen-bond donating thiourea derivatives to promote an asymmetric Strecker reaction between hydrogen cyanide and allyl imines.^[51] In 2003 *Rawal* and his coworkers showed, that TADDOL derived hydrogen-bond donors are accelerating hetero-Diels–Alder reactions of dienes and aldehydes.^[52]

One year later, *Akiyama* and his coworkers introduced BINOL-derived chiral phosphoric acids **11** as catalysts for the Mannich reaction of aryl imines and silyl ketene acetals.^[50] In the following years several reactions catalyzed by chiral phosphoric acids and their derivatives, as for instance Pictet–Spengler reactions,^[53] Friedel–Crafts alkylations^[54] or transfer hydrogenations,^[55] were discovered. To improve the activation of simple carbonyl compounds, which are hardly activated by phosphoric acids, Yamamoto developed a more acidic *N*-triflyl phosphoramidate facilitating a catalytic Diels–Alder reaction of ethyl vinyl ketone with various silyloxydienes.^[56] Disulfonimides **12**, another strong BINOL-based type of chiral acids, was introduced in 2009 by the group of *List*.^[57,58] Although the authors did not use this scaffold as Brønsted acid in this report

Background

(see next chapter), the motif has shown to be highly reactive and enantioselective in the Friedel–Crafts alkylation of indoles with imines by *Lee* [59] or more recently by *List* and his coworkers in the Torgov cyclisation.[60]



Scheme 2.5: Common catalyst motifs for Brønsted acid catalysis.

Whereas less reactive substrates require stronger acids, activated substrates may decompose under strongly acidic conditions, thus requiring weaker Brønsted acid catalysts as for instance carboxylic acids. An asymmetric alkylation of diazo compounds with *N*-Boc imines was reported to be catalyzed with a chiral BINOL derived dicarboxylic acid **13** by *Maruoka*. [61]

Although BINOL-derived Brønsted acids are widely used in asymmetric organocatalysis, other chiral backbones, derived from TADDOL, [62] VAPOL [63] or SPINOL **14** [64] were developed to improve selectivities by varying the size of the active pocket.

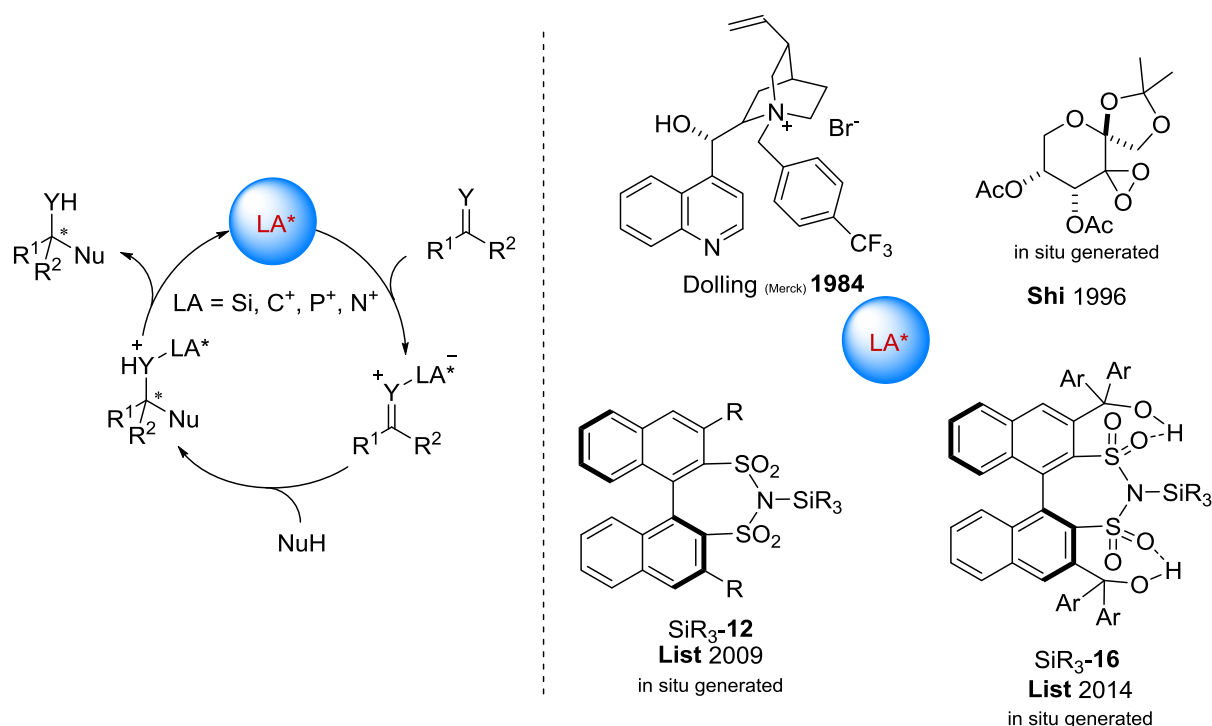
Recently, the group of *List* reported a new class of Brønsted acids **15** having a very confined, active pocket with an imidodiphosphate scaffold allowing the functionalization of small molecules in various transformations, as for instance acetalizations, [65–67] oxidations of sulfones [68] or Prins cyclisations. [69]

2.1.3 Organic Lewis Acid Catalysis

In 1923, complementary to Brønsted, Lewis gave a generalized definition of acids and bases.^[70] A Lewis acid is a chemical compound with an unoccupied orbital and an electron demand, which accepts an electron pair from a Lewis base. From definition, the smallest possible Lewis acid is the free proton H^+ , having only a free 1s orbital.

For many years the field of asymmetric Lewis acid catalysis was associated with Lewis acidic metals coordinated by chiral ligands. The rise of organocatalysis has also led to various examples where organic Lewis acids, as dioxiranes,^[71] ammonium-salts^[72] and silylcations,^[57] promote reactions with high enantioselectivities.

The general mechanism (Scheme 2.6) of these reactions is comparable to Brønsted acid catalyzed reactions. After accepting an electron pair from the Lewis base, the vicinal bond is polarized enabling the attack of a nucleophile. After the reaction with the nucleophile, the Lewis acid diffuses away from the product due to a lower Lewis basicity and is able to activate a new molecule.



Scheme 2.6: Generalized mechanism of asymmetric Lewis acid catalysis (left) and some selective catalysts (right).

In 2009, *List* and his coworkers reported the in situ generation of a chiral silylated disulfonimide **TMS-12** catalyzing the Mukaiyama aldol reaction of aromatic aldehydes and silyl ketene acetals with high yields and enantioselectivities.^[57] More recently, the

same group was able to further increase the acidity and reactivity of these motifs by an intramolecular Brønsted acid activation enabling the reaction of 2-naphthaldehyde with 1,2-bis(trimethylsilyloxy)-cycloalkanes, substrates of usually lower nucleophilicity.^[73]

2.2 *Para*Hydrogen Induced Hyperpolarization (PHIP) in Homogeneous Catalysis

Nuclear Magnetic Resonance Spectroscopy (NMR) is a commonly used method to study and characterize the structure of organic molecules. Like no other method, it delivers information about their covalent connections of NMR active nuclei as well as their three dimensional structure in solution. However, due to its relatively low sensitivity compared to other spectroscopic/metric methods, the detection and characterization of low concentrated reaction intermediates is challenging. Recent studies by the groups of *Gschwind*^[35] and *Berkessel*^[74] have shown the power of NMR in the detection and characterization of reaction intermediates. When the concentration of the reactive intermediates decreases, the detection becomes impossible due to weak Boltzmann polarization of the nuclei in the magnetic field. One possible solution to overcome this drawback is the utilization of hyperpolarization methods,^[75] like chemically induced dynamic nuclear polarization (CIDNP),^[76,77] dynamic nuclear polarization (DNP) or *parahydrogen* induced polarization (PHIP).^[78,79] Although these methods are usually limited to reactions involving radicals or hydrogenation reactions, they have shown their power in several applications.^[75] The next chapter will focus on PHIP as one of these techniques. After a short introduction into the theory behind PHIP, some selected applications on hydrogenation reactions and the characterization of reaction intermediates will be discussed.

2.2.1 Theory

Parahydrogen induced polarization (PHIP) is a NMR technique, which leads to a strongly enhanced NMR signal after hydrogenation of unsaturated bonds via an pairwise transfer of hydrogen. The first reports of two independent experimental NMR applications by *Bowers and Weitekamp*^[80] and *Eisenschmid*^[81] and his coworkers appeared in 1987 after it was predicted earlier.^[82] These experiments gave strong antiphase NMR signals with a signal enhancement above a factor 100. Experiments, which are acquired after hydrogenation in a magnetic field, are called PASADENA, “*Parahydrogen and synthesis allow dramatically enhanced nuclear alignment*”, in honor of the title of the work by *Weitekamp and Bowers*, who worked at Caltech in Pasadena. One year later, *Weitekamp and Pravica*^[82] reported the hydrogenation of styrene to ethylbenzene with

parahydrogen. This time they transferred the sample from a low into a high magnetic field. The observed signal was different compared to the PASADENA signal and showed two individual transitions with opposite phase. They named this effect ALTADENA (Adiabatic Longitudinal Transport After Dissociation Engenders Nuclear Alignment).

In order to understand the origin of the observed hyperpolarization effect, a short look in the physics behind the hydrogen molecule is given in the next paragraphs.^[83]

The hydrogen molecule contains two different atoms with two different nuclear spins (Figure 2.6). A combination of the two will lead two spin isomers: *para*- (total spin $S = 0$) and *ortho*hydrogen ($S = 1$); only the oH_2 is magnetic and will give rise to an NMR signal.

The total wave function of a hydrogen molecule can be described by the following product of different wave functions:

$$\Psi = \Psi_e^{orb} \Psi_e^s \Psi_n^{vib} \Psi_n^{rot} \Psi_n^s \quad (1)$$

The first two functions ($\Psi_e^{orb} \Psi_e^s$) describe the orbital motion and the spin state of the electrons. The others the vibrational, rotational and spin state of the nuclei. The overall symmetry of the wave function is depending on the product $\Psi_n^{rot} \Psi_n^s$. The combination of two different spins will lead to four possible functions. To simplify the formula it can be written as the linear combination of the product of the two different spin states α and β . α represents the lower energy spin state, whereas β stands for the higher energy spin state in a magnetic field.

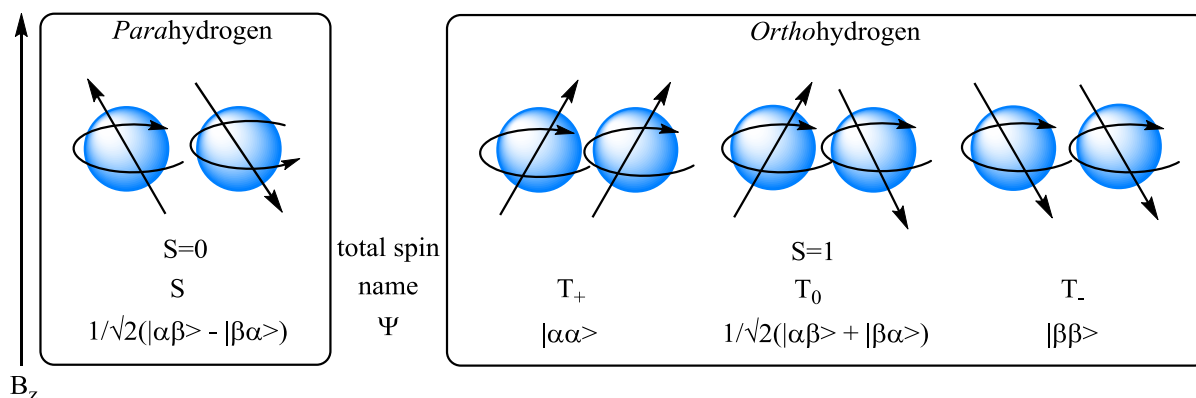


Figure 2.6: Spin states of a hydrogen molecule.

Both isomers are in equilibrium and can slowly convert into each other. Although forbidden by the Pauli exclusion principle, this conversion can be catalyzed by a paramagnetic species, as for instance oxygen, the surface of activated charcoal or iron(III) salts. At room temperature hydrogen gas contains $\sim 75\%$ *ortho*- and 25% *parahydrogen*. At lower temperatures the ratio changes in favor of the *para* isomer, due to its lower rotational energy. At 77 K, the boiling point of liquid nitrogen, the *ortho* to *para* ratio is approximately 1:1, at 0 K only the *para*-form would theoretical be present.

Background

The mechanism that leads to the signal enhancement can be understood by taking a closer look on the energy levels of the spins in a field during a hydrogenation reaction. (Figure 2.7)

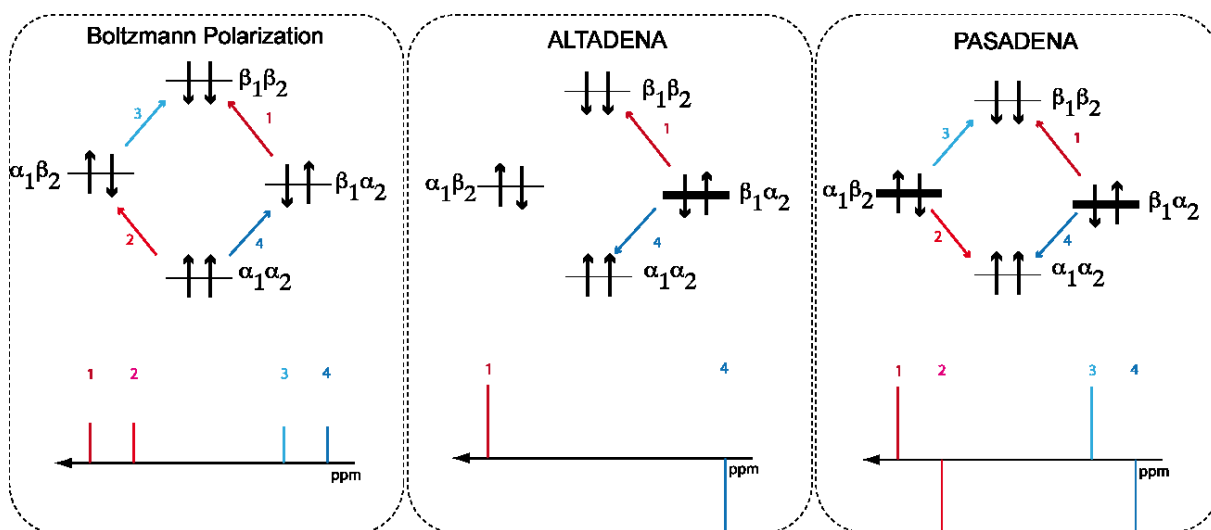


Figure 2.7: Energy diagrams of AB spin systems with different polarization and the resulting NMR spectra (left: Boltzmann polarization, middle: ALTADENA, right: PASADENA). Bars indicate the population in the states. (grey: not populated, thin black: normally populated, thick black: highly populated)

When performing the hydrogenation reaction with thermal hydrogen (25% $p\text{H}_2$), all spin states in the generated AX spin system are almost equally populated (Figure 2.7, left). The small difference in the population of the spin states is explained by the Boltzmann factor ($\Delta P \sim \gamma \hbar B_0 / k_B T$). At room temperature and common high field spectrometers ($B_0 = 5 - 15\text{T}$) this factor is in the range of $10^{-5} * P$ ($P = \text{total population of the spins}$). The spectrum will show transitions with equal intensities that are linear to the Boltzmann distribution.

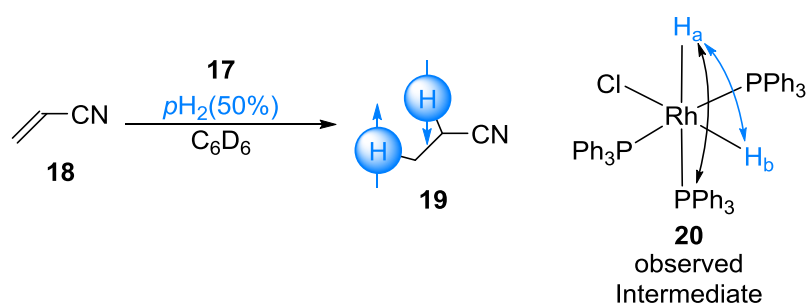
If the reaction is conducted under PASADENA conditions with 100% *para*-hydrogen, (Figure 2.7, right), the population of the single spin states in the resulting AX spin system changes. The energy levels with the *para* spins $|\alpha\beta\rangle$ and $|\beta\alpha\rangle$ are completely populated, whereas the $|\alpha\alpha\rangle$ and $|\beta\beta\rangle$ states are empty. The resulting transitions that lead to the spectrum now give four signals. Two transitions ($|\alpha\beta\rangle \rightarrow |\beta\beta\rangle$ and $|\beta\alpha\rangle \rightarrow |\beta\beta\rangle$) lead to positive NMR signals, whereas the other two ($|\alpha\beta\rangle \rightarrow |\alpha\alpha\rangle$ and $|\beta\alpha\rangle \rightarrow |\alpha\alpha\rangle$) give negative NMR signals. The intensity of these signals mainly depends on the population difference of the excess of population in the *para*-state ΔP . The magnitude of the signal enhancement can be up to factor 10^5 higher compared to normally acquired signals with in the Boltzmann equilibrium.

When the hydrogenation is performed in a low magnetic field and is afterwards transferred into a high field (ALTADENA conditions), the population distribution of the different energy levels will again be different (Figure 2.7, middle). At the low magnetic field all the spin states are equal in energy. During the transfer into the higher field, the population of the *para* spins ends up in the lower energy $|\beta\alpha\rangle$ state. Since all spins populate this energy level, only two transitions are possible. One ($|\beta\alpha\rangle \rightarrow |\alpha\alpha\rangle$) leads to a negative signal, while the other one ($|\beta\alpha\rangle \rightarrow |\beta\beta\rangle$) to a positive. In comparison to PASADENA, the maximum achievable signal enhancement is a factor of two higher, because all the spins end up in one state instead of two.

2.2.2 Applications

2.2.2.1 Wilkinson's Catalyst

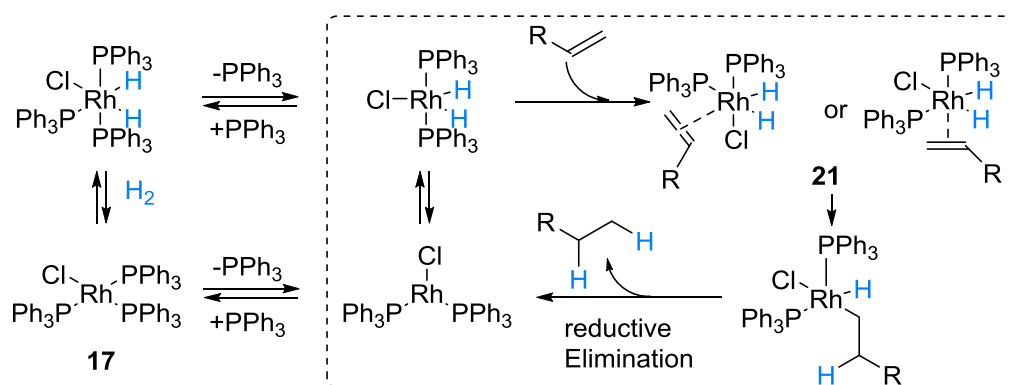
In the first report of the PASADENA effect by *Bowers and Weitekamp*,^[80] the authors used Wilkinson's catalyst **17** ($\text{Rh}(\text{PPh}_3)_3\text{Cl}$)^[84] in C_6D_6 in order to hydrogenate acrylonitrile **18** in the presence of $p\text{H}_2$ (50%) (Scheme 2.7).



Scheme 2.7: Hydrogenation of acrylonitrile by Wilkinson's catalyst.

The authors observed hyperpolarized signals of two different species. One set belongs to the aliphatic protons of the product, propionitrile **19**. This observation proves that the transfer of hydrogen occurs in a pairwise manner. The other observed signals were assigned to hydride protons of the catalyst hydride complex **20** $\text{RhH}_2\text{Cl}(\text{PPh}_3)_3$, which was known to be an intermediate in the reaction as initially reported by *Wilkinson* in 1965.^[84]

Some years later, *Eisenberg* and his student *Duckett*^[85] reinvestigated the corresponding hydrogenation mechanism by PHIP NMR, after several groups investigated the mechanism (Scheme 2.8) including extensive (kinetic) NMR studies of catalytic and stoichiometric reactions.^[86,87]

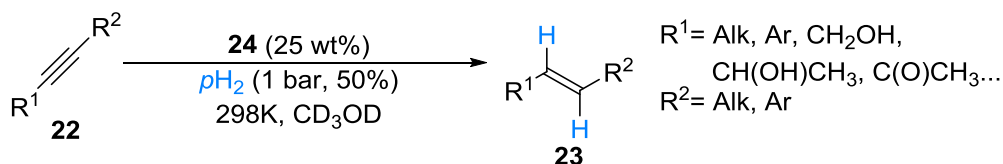


Scheme 2.8: General mechanism for the hydrogenation of olefins by Wilkinson's catalyst.

Up to that point, complexes containing hydrides and an olefin had never been reported. After reproducing the initial results, *Eisenberg et al.* studied extensively the formation of different hydride complexes under various conditions at high and low temperatures taking advantage of the signal enhancement gained from pH_2 . In addition to several dimeric complexes, they were able to observe and characterize a dihydride-olefin-complex $RhH_2Cl(PPh_3)_2(\text{olefin})$ **21** for the first time.^[85,88] This complex contains a hydride that is positioned *trans* to a phosphine assigned by a characteristic 1H - ^{31}P coupling constant of ~ 160 Hz. The other hydride, which is shifted to higher field, did not show this coupling. In addition to that, the fourth ligand in the plane is not certain and is either a chloride or the olefin. The enhanced sensitivity of PHIP enabled the detection of this species and showed the power of this methodology; however, it has to be mentioned, that the kinetic relevance of this olefin complex **21** could not be determined.

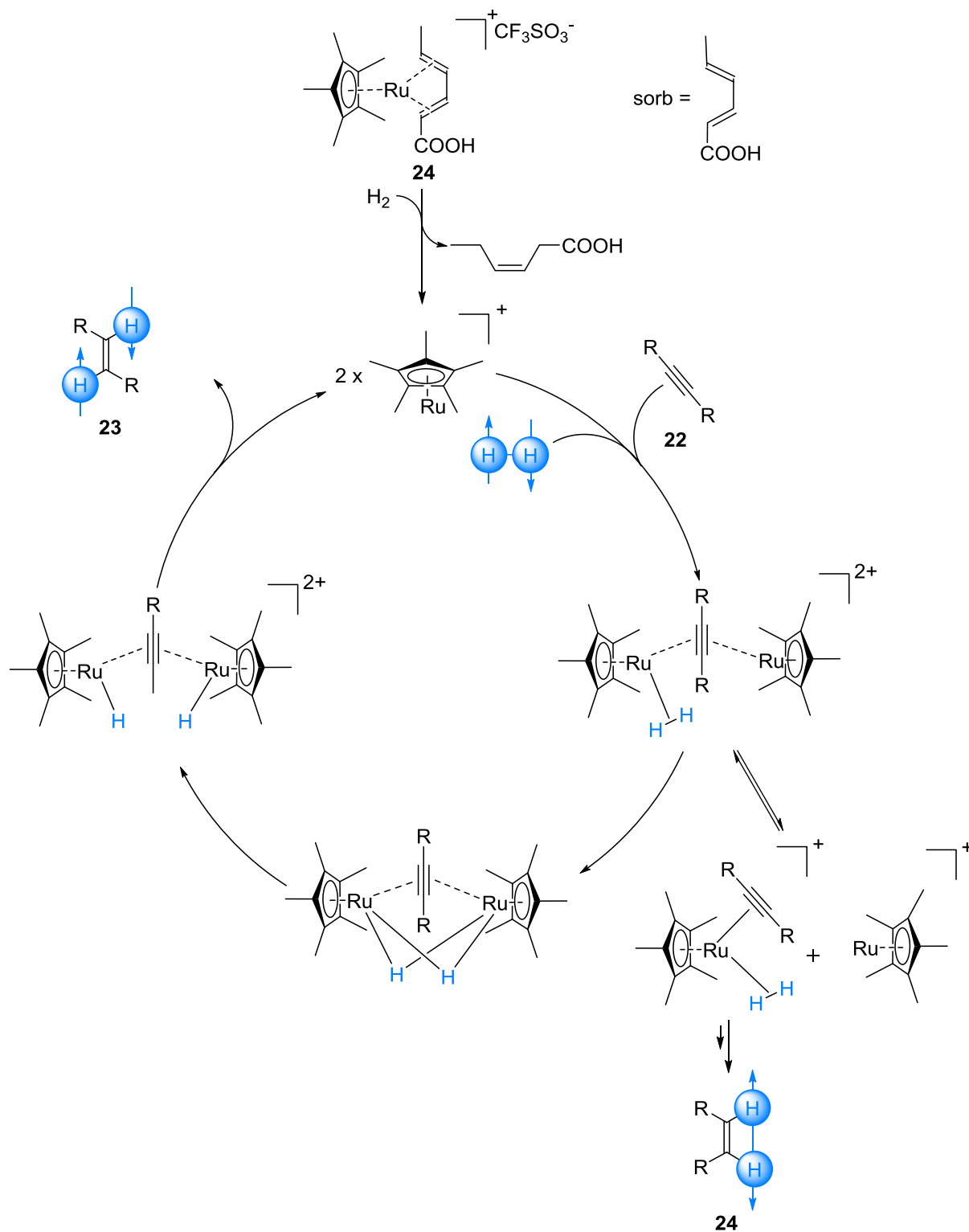
2.2.2.2 *Trans*-Stereoselective Hydrogenation of Alkynes by $[RuCp^*]^+$ Catalysts

Upon hydrogenation of alkynes, two possible products can be formed: a *cis*- or a *trans*-olefin. In literature many example of homo- and heterogeneous hydrogenation catalysts are known, that enable a *cis*-hydrogenation.^[89] The most commonly used catalysts for these transformations are poisoned heterogeneous catalysts, as for instance the Lindlar catalyst,^[90] that stops at the alkene stage and does not overreduce the product to the unwanted alkane. Catalytic reductions to *trans*-alkenes are more challenging and just a few examples were reported in literature, using rhodium^[91,92] or iridium^[93] based metal catalysts.^[91–93] These systems do not have good turnover numbers, are restricted to diarylalkynes or are not functional group tolerant. In 2001, the group of *Bargon* reported a stereoselective hydrogenation of internal alkynes **22** to (*E*)-alkenes **23**^[94] using $[Cp^*Ru(\text{sorb})]OTf$ **24**^[95] as catalyst (Scheme 2.9).



Scheme 2.9: A stereoselective *trans*-hydrogenation of alkynes.

The reaction was studied by PHIP-NMR in order to get a deeper understanding of the mechanism and answer the question whether the transferred hydrogen comes from a single or from multiple hydrogen molecules. Indeed, they observed hyperpolarized signals on several products from different substrates. This shows that the transfer must take place rapidly with the same H_2 so that no loss of the pair correlation of the hydrogen atoms can occur. Additionally, the temperature dependence of the reaction was investigated. When the reaction was conducted in the magnet between 10 °C and 30 °C, exclusively or mainly the (*E*)-product was observed. A further increase of the temperature up to 50 °C generated mostly the (*Z*)-product. This behavior was explained by a change of a binuclear to a mononuclear ruthenium complex catalyzing the reaction. The authors conjectured that at lower temperatures the *trans*-product might be formed by a binuclear complex (Scheme 2.10), in accordance with observations with previous results in literature.^[91,92] The authors did not observe other additional intermediates. This can be explained in their proposed catalytic cycles, which shows that all the proposed intermediates are highly symmetrical so that no hyperpolarization could be observed (Scheme 2.10). One has to mention that a chiral secondary alcohol substrate is also reported by the authors. In this case the hydrogen substrate complex is asymmetric and potential hyperpolarized signals might be observed. The reaction of terminal alkynes does not yield any product due to the formation of a stable vinylidene complex. However, the influence of hydrogen pressure on this reaction was not investigated and also no yields were reported for this reaction. Overall this was so far the only study of a *trans*-selective hydrogenation by PHIP and the reaction mechanism is still under debate.

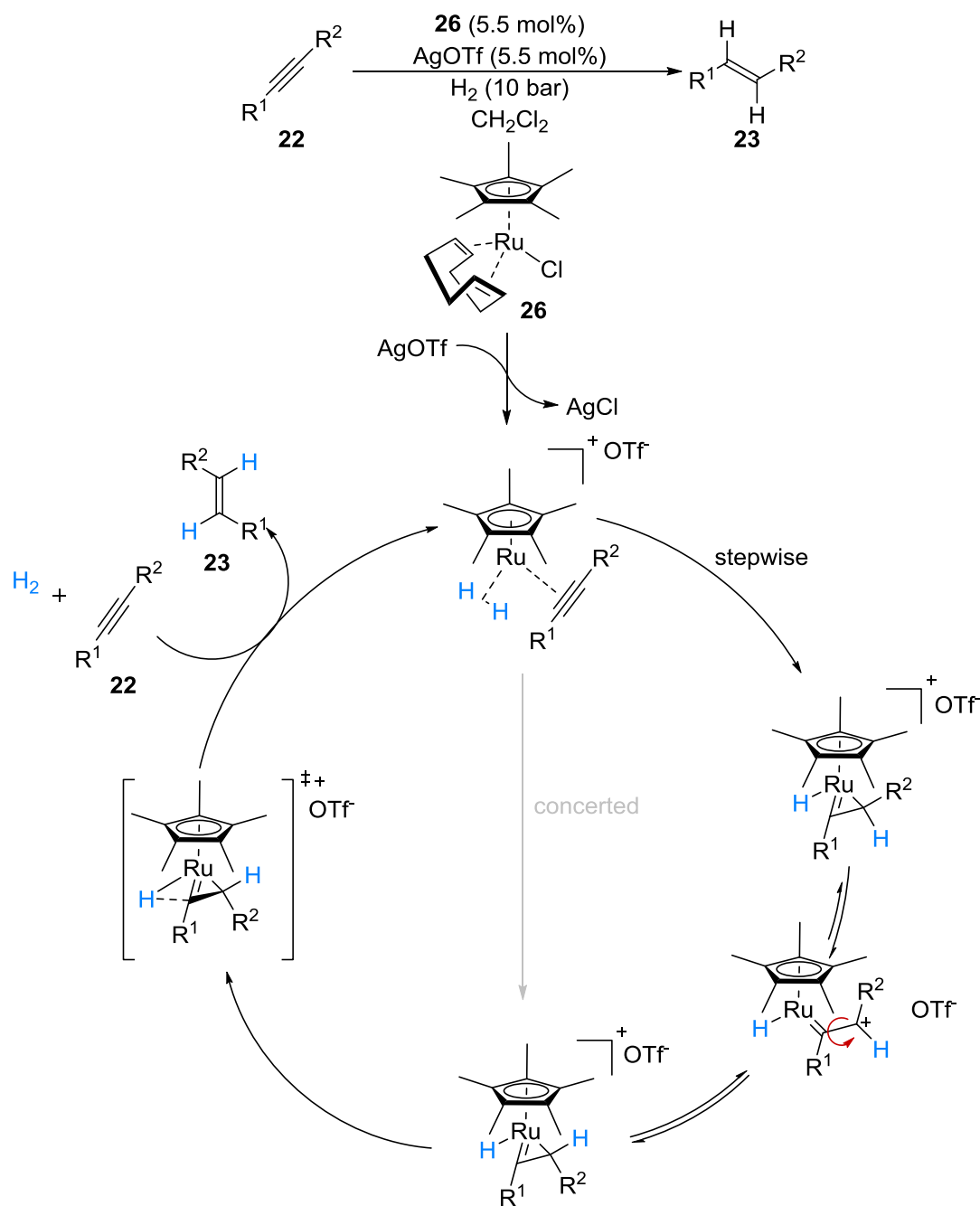


Scheme 2.10: Proposed mechanism for the *trans*-selective hydrogenation of internal alkynes catalyzed by $\text{Cp}^*\text{Ru}(\text{sorb})\text{OTf}$.

In 2004, *Duckett* and his coworkers reported another PHIP NMR study on the hydrogenation reaction of diphenylacetylenes yielding *trans*- and *cis*-stilbenes using a cationic palladium (II) diphosphine complex as the catalyst. Interestingly, hyperpolarized signals were observed for the *cis* olefin, but not for the *trans*.^[96] Additionally, they

observed a covalent palladium intermediate containing three hydrogens. This complex is the precursor of the *trans*-species as proven by EXSY spectroscopy. In the following years, this group was intensively studying the mechanism of this reaction.^[97–99] A palladium hydride turned out to be the active species. The complex with the *cis* product yields the characterized intermediate. After β -hydride elimination, where two different hydrogens are mixed, the *trans*-stilbene is formed, resulting in weak enhancement of the olefinic product signals.

Recently, *Fürstner et al.* reported a hydrogenation protocol for a functional group tolerant and stereoselective *trans*-hydrogenation of alkynes yielding (*E*)-alkenes **23** with good *E/Z* ratios and yields.^[100] The authors started their catalyst screening with the conditions reported initially by *Bargon*^[94] and optimized these by changing the solvent to CH₂Cl₂, using the in situ prepared cationic complex [Cp*Ru(cod)]OTf from [Cp*Ru(cod)]Cl **26** and AgOTf as the catalyst and 10 bar of hydrogen pressure. Initial mechanistic studies showed the formation of several hydride species in the NMR spectrum ($\delta_{\text{H}} = -4.96, -8.02$ and -13.42 ppm) when the sample was kept under hydrogen pressure for one hour. In further experiments it could be shown that [Cp*Ru(H₂)(cod)] **27** yields the corresponding alkenes with the same high *E/Z* ratio as under catalytic hydrogenation conditions, indicating that both species might form similar active intermediates. More recently, *Fürstner* and his coworkers extended the scope of this catalytic systems with slight modulations on the catalyst to *trans*-selective hydroborations,^[101] hydrostannations,^[102] hydrosilylations and hydrogermylations^[103] and a generalized mechanism for product formation was proposed (Scheme 2.11, applied to hydrogenations). In contrast to the previously proposed mechanism by *Bargon* the product formation occurs via a stepwise or concerted formation of a ruthenium metallacycle, which might open and isomerize during the course of the reaction. After hydrogen transfer the catalyst is regenerated through reductive elimination. The concept for this postulated mechanism is inspired by previously conducted computational studies by *Trost* and *Wu* on *trans*-hydrosilylation reactions^[104] and on control experiments with the σ -H₂ ruthenium hydride complex **27**.



Scheme 2.11: Proposed mechanism for the *trans*-selective hydrogenation of internal alkynes by Fürstner.

The newly proposed mechanism contains several intermediates that could potentially be observable through PHIP investigations, depending on their lifetime. Several observations could not be explained by this mechanism, as for instance overreductions and isomerizations. Therefore a reinvestigation of this mechanism would be of high interest.¹

¹ Personal communication with Prof. Fürstner and his coworkers.

3. Objectives of this Ph.D. Thesis

3.1 Direct Experimental Observation of a Hydrogen Bond in a Transition State Model for Proline Catalyzed Aldol Reactions

Proline and its derivatives have emerged as powerful organocatalysts since their first application by *Hajos, Parrish, Eder, Sauer* and *Wiechert* in the intramolecular aldol reaction^[16,17] and the report of *List* et al. on intermolecular aldol reaction.^[5] In all of these reactions a proline-derived enamine and a hydrogen bond activation of the electrophile are proposed as the key for reactivity and enantioselectivity. Recently these enamines have been described in situ by *Gschwind* et al. and in the solid state by *List* and coworkers.^[34,35] The obtained results are in a good agreement to all of the proposed reactions models. Until today no hydrogen bond has been observed directly during these reactions. In the first part of this Ph.D. thesis a (meta-)stable transition state analogue should be synthesized, enabling the NMR-spectroscopic or X-ray observation and characterization of an intramolecular hydrogen bond. On the one hand, in situ generated meta stable enamine intermediates inspired by previous reports by *Gschwind*^[35] and on the other hand stable enamines, that have previously been crystallized by our group,^[34] are envisioned to achieve these goals (Figure 3.1).

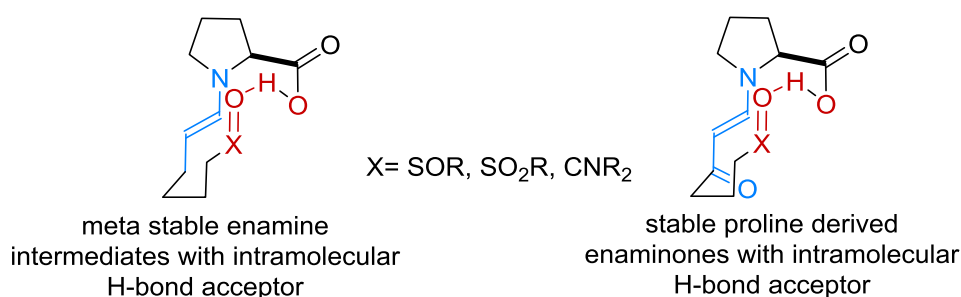


Figure 3.1: Envisioned transition state analogues for proline catalyzed intramolecular aldol reactions

3.2 NMR Spectroscopy as a Versatile Tool for Studying Organocatalytic Reactions and Intermediates

In the last decade, organocatalysis has been established as the third pillar of catalysis. Although various new reactions and catalysts have been discovered, the underlying mechanisms are often underinvestigated or not well understood. The second part of this Ph.D. work is aiming in understanding reactions that are recently developed in the *List* group in the fields of amino-, Brønsted- and organo-Lewis acid catalysis.

Recently, a protocol for the first α -benzylation of α -branched aldehydes has been developed by our group. The aim of the NMR-investigations is to understand the role of acid and base additives in this transformation and to observe enamine intermediates that are the proposed reactive intermediates leading to the desired α -benzylated aldehydes (Figure 3.2).

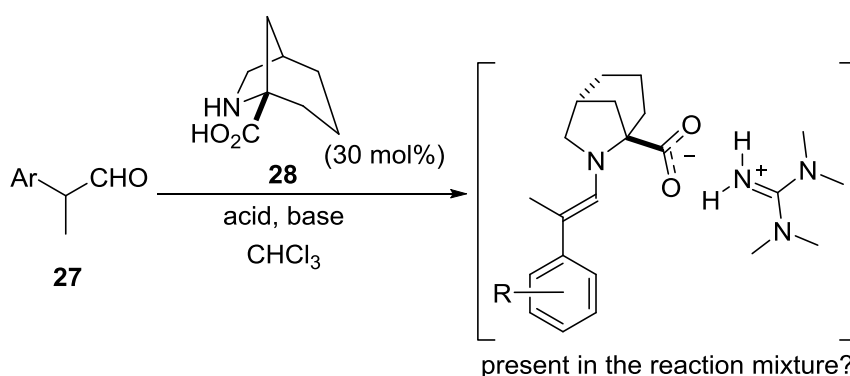
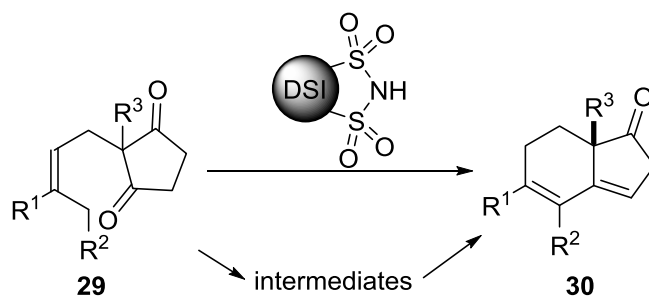


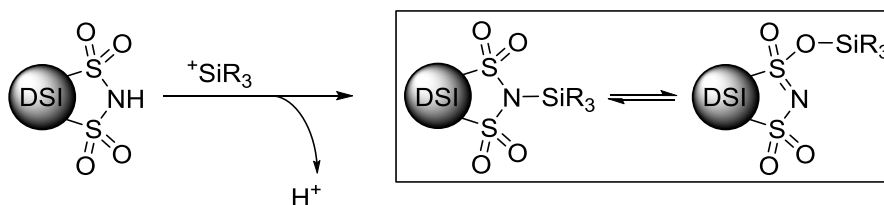
Figure 3.2: Detection of enamine intermediates in the α -benzylation of α -branched aldehydes.

In 2009, our group reported chiral disulfonimides as new powerful motifs for Brønsted acid and precursors for Lewis acid catalyzed reactions. Recently, a protocol for an asymmetric Torgov cyclisation (Scheme 3.1) was developed. The reaction is proposed to proceed via several steps. A kinetic NMR analysis should show the course of the reaction and intermediates that might be formed.



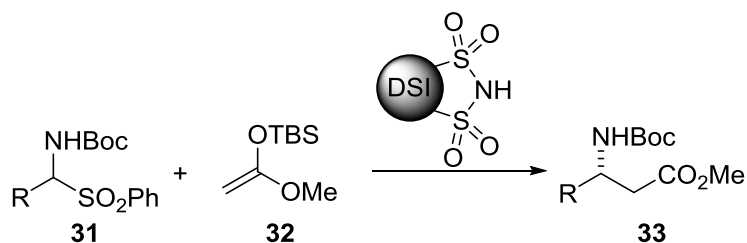
Scheme 3.1: The DSI catalyzed Torgov cyclisation.

Since the first report, DSIs are known as Lewis acid catalysts upon in situ silylation. Initial investigations in our group have shown that two species, *N*- and an *O*-silylated forms of the DSIs, are present in solution. This work should extend these studies and show the dependence of the substitution on the silicon and give experimental evidences for the exchange between these species (Scheme 3.2).



Scheme 3.2: The silatropy of DSIs upon in situ silylation.

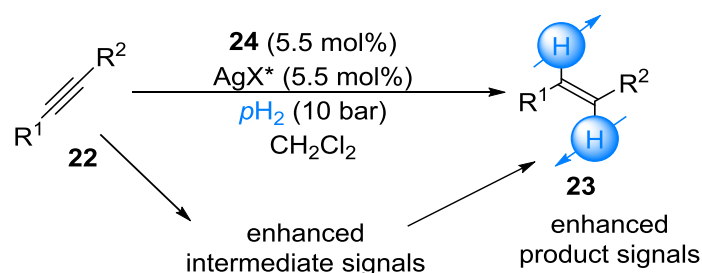
In addition to these studies, the recently developed synthesis of β^3 -amino esters from *N*-Boc-amino sulfones^[105] is investigated by NMR in order to understand the course of the reaction.



Scheme 3.3: DSI catalyzed synthesis of β^3 -amino esters from *N*-Boc-amino sulfones.

3.3 Parahydrogen Induced Polarization (PHIP) as Tool for the Discovery of New, Unknown Intermediates

Recently, *Fürstner* and coworkers have reported a new protocol for a functional group tolerant and selective *trans*-hydrogenation of internal alkynes.^[100] Despite all the advantages of this protocol, several substrates are leading to overreduced or isomerized side products. With the help of PHIP (*parahydrogen* induced polarization), an NMR hyperpolarization technique for hydrogenations, this reaction will be reinvestigated. *Bargon* et al. have already studied this transformation under different reaction conditions.^[94] The PHIP studies should answer the question, whether the new protocol proceeds via a similar mechanism (with the hydrogen being transferred pairwise to the substrate). In addition we hope to observe new, yet unknown intermediates by slightly modifying the catalyst or the substrate in order to further understand the underlying mechanism and the occurrence of side products (Scheme 3.4).



Scheme 3.4: PHIP studies of the selective *trans*-hydrogenation of internal alkynes.

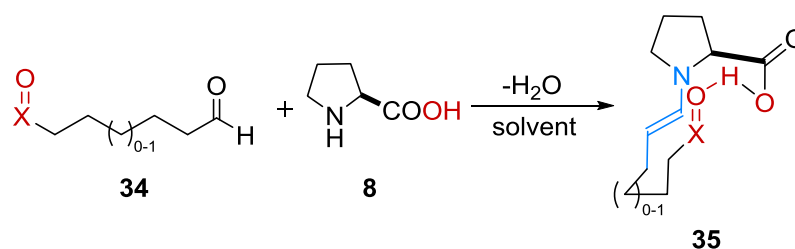
4. Results and Discussion

4.1 Aminocatalysis

4.1.1 Hydrogen Bonds in Proline Catalyzed Aldol Reactions

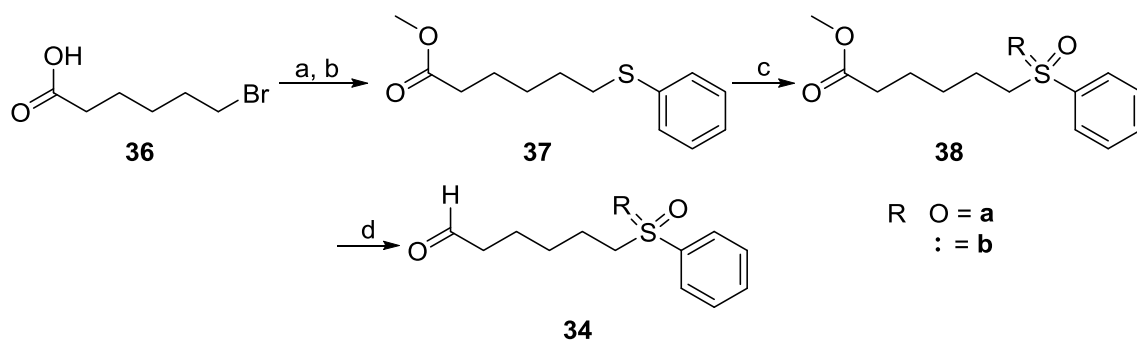
4.1.1.1 Towards the In Situ Observation of Hydrogen Bonding

Inspired by the recent work of *Gschwind* et al.,^[35] we envisioned to observe the generation of a hydrogen bond in an in situ formed enamine. To achieve this goal, the intermediate should bear a strong intramolecular hydrogen bond acceptor in analogy to the proposed transition state and it should not further react via an intramolecular aldol reaction to enable an unambiguous characterization by NMR (Scheme 4.1). This hydrogen bond acceptor can be an amide, a sulfoxide or a sulfone.^[106,107] In addition, these structures are closer to the List–Houk transition state^[30] due to their amide-resonance^[108] or geometry.^[109]



Scheme 4.1: In situ formation of a metastable enamine intermediate.

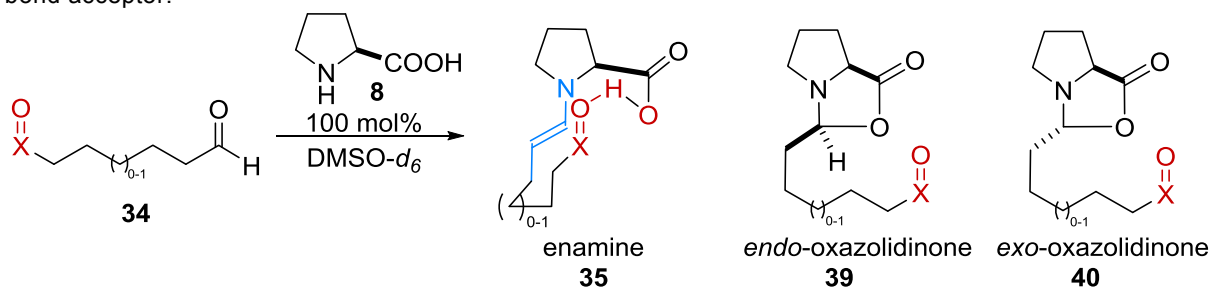
Aldehydes bearing sulfones or sulfoxides as hydrogen bond acceptors could easily be obtained in 4 steps starting from commercially available 5-bromohexanoic acid **36** (Scheme 4.2). After nucleophilic substitution of the bromine with sodium thiophenolate and Fischer esterification in methanol, the corresponding 5-phenylthio-hexanoic acid methyl ester **37** could be obtained with good yields (85%) over 2 steps. In the next step the thioether was oxidized with aqueous hydrogen peroxide solution and diphenylphosphate as the catalyst. This reaction yielded the corresponding sulfoxide **38a** by employing one equivalent of oxidant or the sulfone **38b**, when the double amount was used. At this stage of the synthesis enantioenriched sulfoxides could be obtained by using chiral confined imidodiphosphates as the catalyst.^[68] To prove whether we obtain a chiral discrimination of the starting material with enantiomerically pure proline, we decided to perform the non-asymmetric reaction first. The desired products **34a/b** were obtained by a reduction of the methyl esters **38** using (*i*-Bu)₂AlH (DIBAL-H) as reductant.



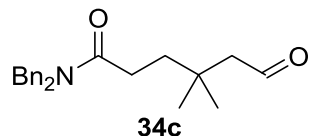
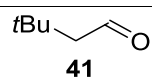
Scheme 4.2: Synthetic route for the synthesis of aldehydes with a sulfone/sulfoxide as H-bond acceptor. Conditions: a) PhSNa, EtOH, rt, 16 h, 85%; b) MeOH, H₂SO₄, quant.; c) aq. H₂O₂ (15%), (PhO)₂POOH; d) DIBAL-H, THF.

The synthesized aldehydes were directly used for the in situ preparation of the enamine species derived from L-proline (Table 4.1, entry 2 and 3). To our disenchantment, the observed enamine : oxazolidinones ratio was very similar to the previously reported results by *Gschwind* (Table 4.1, entry 1). If an interaction of the proton acceptor and the carboxylic acid function had been present, a change of this ratio would have been expected. Additionally, we were not able to observe any enantiodifferentiation at the enamine protons. This suggests that the chiral center is not spatial to the enamine and so probably the aliphatic chain is not in a cyclic structure due to hydrogen bonding but in the energetically more favored zigzag conformation.

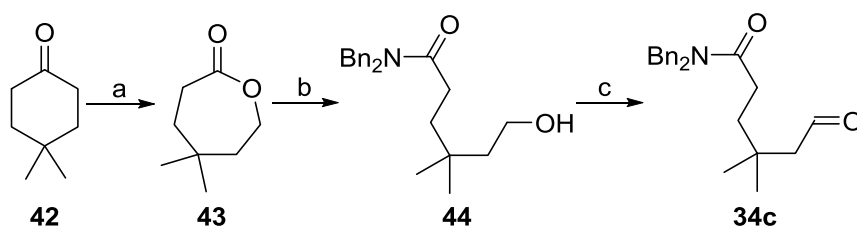
Table 4.1: Observed enamine: oxazolidinone ratio of different aldehydes with an intramolecular hydrogen bond acceptor.



Entry	Aldehyde	Ratio enamine : endo ox : exo ox.
1 ^[35]		13 : 23 : 64
2		20 : 18 : 62
3		18 : 19 : 64

4	 <p style="text-align: center;">34c</p>	56 : 17 : 27
5	 <p style="text-align: center;">41</p>	36 : 28 : 36

We wondered, whether the cyclic conformation of the intermediate could be more favored by simply introducing the Thorpe–Ingold effect on the chain. We decided to start our synthesis from 4,4-dimethylcyclohexanone **42**. For synthetical reasons, we decided to use an amide as the hydrogen bond acceptor. The introduction of a sulfone or sulfoxide would require several more steps to introduce the required functional group. The H-bond acceptor strengths of both variants are similar.^[106,107] After Baeyer–Villiger oxidation of **42** and ring opening of the corresponding lactone **43** with dibenzylamine, the amido-alcohol **44** was obtained. The oxidation of the primary alcohol with Dess–Martin-periodinane (DMP) gave the desired aldehyde **34c** in good yields.

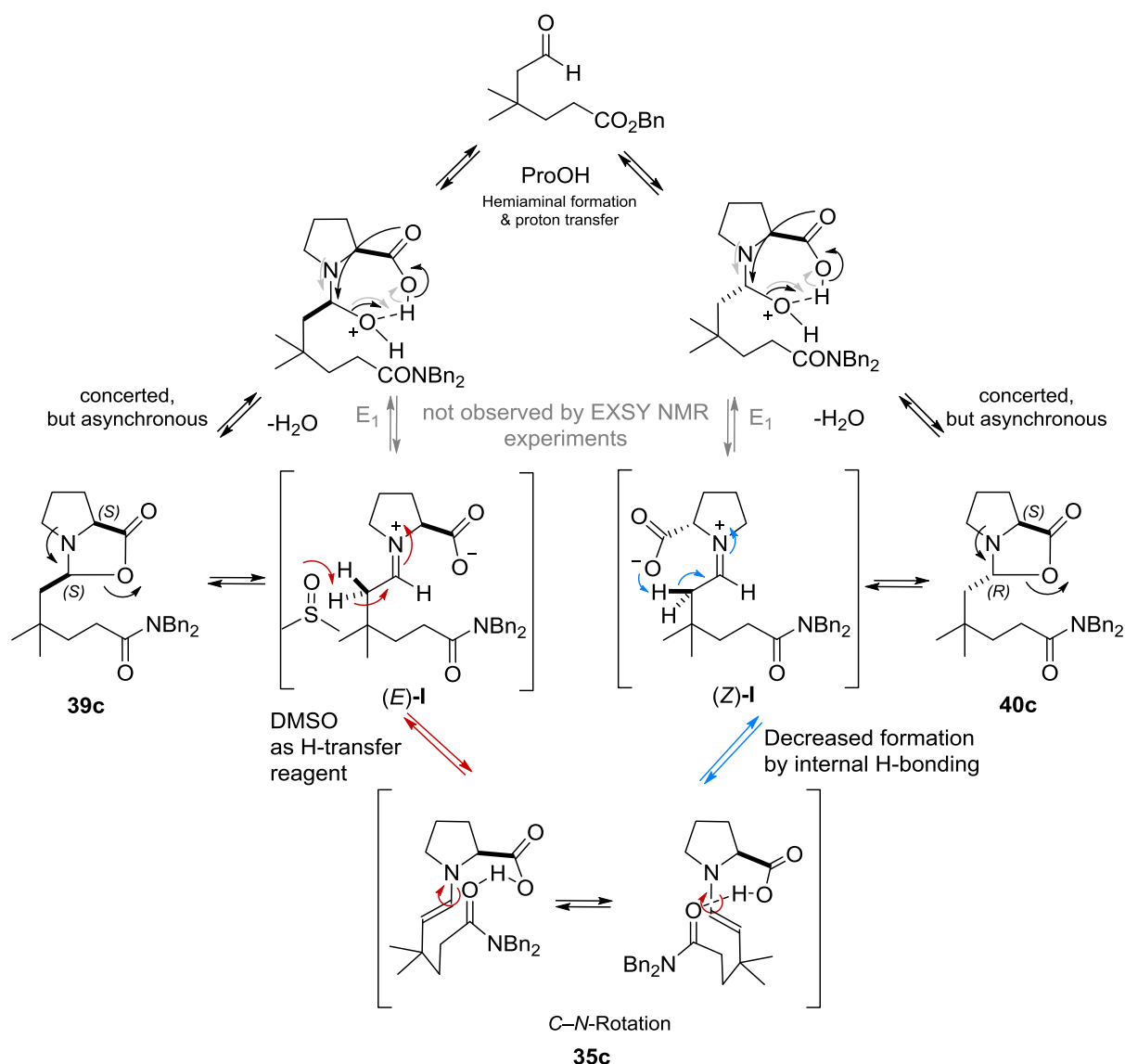


Scheme 4.3: Synthetic route for the synthesis of aldehydes with an amide as H-bond acceptor. Conditions: a) *m*CPBA, CH₂Cl₂, 16h; b) Bn₂NH, AlCl₃, DCM; c) DMP, CH₂Cl₂.

This substrate was tested in the reaction with L-proline (Table 4.1, entry 3). Compared to the previous results for the sulfones and sulfoxide, we observed a significant increase of the enamine : oxazolidinone ratio from 1:4 to 14:11. Worth mentioning is that only the *exo* oxazolidinone **40c** changed its overall amount, but not the *endo* species **39c**. To confirm that this increase is a result of hydrogen bonding and not from the increased sterical effects at the β-position, we conducted an experiment with 3,3-dimethyl butyraldehyde **41**. Also in this case we could observe an increased enamine : oxazolidinone ratio (9:16), which was still lower than the previous result though. In fact it seems that the observed increase of the stability is resulting from the internal hydrogen bond acceptor. To find an explanation for these observations a more detailed look into the mechanism of the enamine formation has to be considered. From NMR investigations by *Gschwind*^[35] it is already known, that formation of the enamine and oxazolidinones occurs via a different intermediate. One plausible mechanism that has not been discussed in her manuscript is that oxazolidinone formation from the aldehyde occurs via a rearrangement pathway, whereas the iminium pathway, which leads to the enamine, is an elimination type reaction (Scheme 4.4). Two different iminium ions (*E*)-I

Results and Discussion

and (Z)-I can be formed from the *exo*- and the *endo*-oxazolidinones which could isomerize to the enamine using an internal or external H-transfer reagent.^[33] The intramolecular hydrogen bond acceptor that was introduced with the amide might block the formation of (Z)-iminium species (Z)-I by intramolecular hydrogen bonding, which decreases the overall concentration of **40c**. In the other pathway the hydrogen bond acceptor or the solvent could act as a hydrogen transfer reagent and it is not influencing the rate of oxazolidinone formation. The concentration of enamine would still be increased in the equilibrium. Overall the equilibrium between these species is not influenced by water as it has been shown by *Gschwind* and the proposed cycle fits well to their observations.

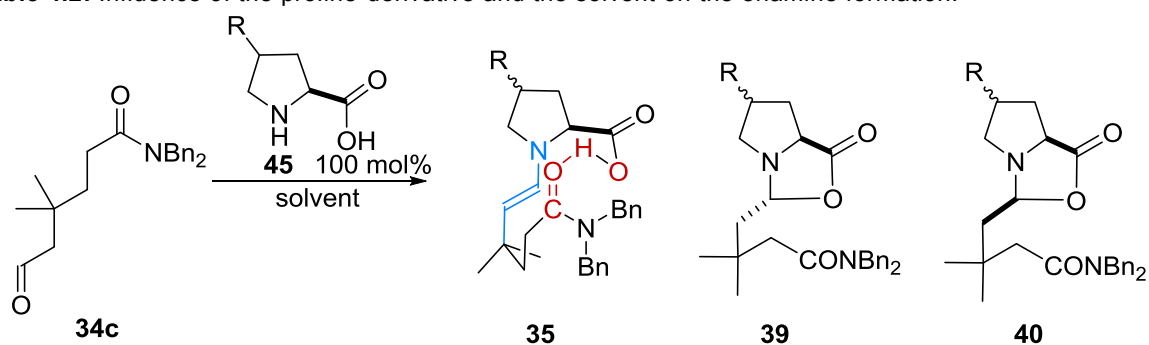


Scheme 4.4: Enamine and oxazolidinone formation via (E)- and (Z)-iminium species I.

After these initial results we were wondering, whether the solubility of the proline derivative might have an influence on this reaction and if the enamine concentration could be further increased in solution. Therefore we tested L-proline derivatives, which were substituted in the 4' position (Table 4.2, entries 1–3). Interestingly, the substitution

had almost no influence on the equilibrium between the intermediates, but it had an influence on the overall intermediate concentration. With the fluorine containing derivative a decreased overall amount in solution was observed whereas the OTBS derivative **45b** generated high intermediate concentrations. In the cases of high intermediate concentrations, the COOH-signal could be detected ($\delta = 12.39$ ppm, broad). Unfortunately the chemical shift was very similar compared to a free enamine without hydrogen bond acceptor in solution ($\delta_{\text{COOH}} = 12.56$ ppm).² This could be explained by using DMSO as solvent that has similar acceptor properties as the amide.^[106,107] In addition, the acidic proton is very dynamic in its electronic environment. It transforms into the aliphatic proton of the oxazolidinones, the acidic proton of the enamine and free proline and water within the NMR timescale. This exchange broadens its NMR signal.

Table 4.2: Influence of the proline-derivative and the solvent on the enamine formation.



Entry	R	Solvent	Ratio 35 : 39 : 40	Ratio Aldehyde : Intermediates ^a
1	H 8	DMSO- <i>d</i> ₆	56: 17 : 27	26 : 74
2	<i>cis</i> -F 45a	DMSO- <i>d</i> ₆	56 : 18 : 26	60 : 40
3	<i>trans</i> -4-OTBS 45b	DMSO- <i>d</i> ₆	56: 17 : 27	18:82
4	45b	CDCl ₃	No observed	100:0
5	45b	CD ₂ Cl ₂	0 : 42 : 58	87 : 13

^a Determined 5 min after mixing the reagents

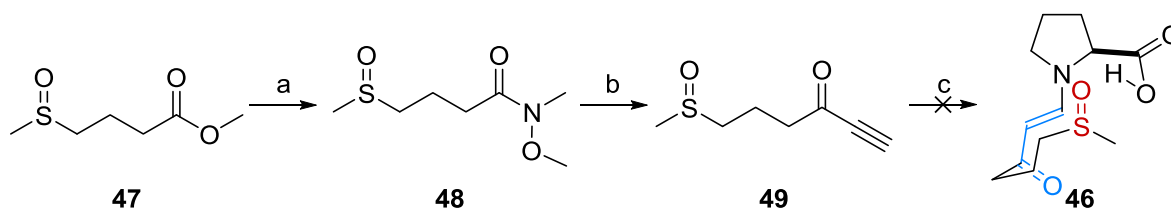
² The shift was determined by the reaction of phenylacetaldehyde (30 μ mol) and L-proline (30 μ mol) in DMSO-*d*₆ (0.6 mL).

In order to circumvent this problem, we attempted to observe the enamine in absence of the solvent as additional hydrogen bond donor. Therefore we had chosen CH_2Cl_2 and CHCl_3 as solvents, that are known as suitable solvents for aldol condensations.^[110] Chloroform did not yield any observable enamine intermediates. Dichloromethane was able to dissolve all the catalyst, but the concentration of potential oxazolidinone species was still rather low and the formation of enamine intermediates could not be observed at all.

At this point we decided to modify our system towards further stabilization of the enamine intermediates and suppression of oxazolidinone formation.

4.1.1.2 Synthesis of Proline-Derived Enaminones as Stable Transition State Analogues

Our group previously reported the formation of stable proline-derived enamines (see chapter 0 on page 5). In parallel to our initial NMR investigations, *D. Bock* investigated the synthesis of enaminone **46** with an internal H-Bond acceptor^[37]:



Scheme 4.5: Synthesis towards proline derived enamines bearing an internal sulfone as hydrogen bond acceptor^[37], conditions: a) AlMe_3 , toluene, $-10\text{ }^\circ\text{C}$, $\text{MeNHOMe}\cdot\text{HCl}$; b) ethynylmagnesium bromide, THF, $-78\text{ }^\circ\text{C}$ c) L-proline, 1N NaOH, then HCl (pH = 3).

The three-step route (Scheme 4.5) had several disadvantages. On the one hand, the starting material **47** of the synthesis was expensive and had only a few suppliers. The Grignard addition to the Weinreb amide **48** gave the desired alkyne **49** only in low yields. Furthermore, Michael addition with proline did not yield the desired product under the conditions that had been reported previously.^[34]

At this point, we decided to combine our results and designed a new model to mimic the enantiodetermining transition state of proline-catalyzed enol-*exo* cyclisations (Figure 4.1). The desired structure **50** contains an amide as hydrogen bond acceptor and an enaminone as stable enamine derivative. In addition, we envisioned to force the enaminone in a cyclic conformation by introducing a cyclohexane with *trans*-substitution in 1,2 position.

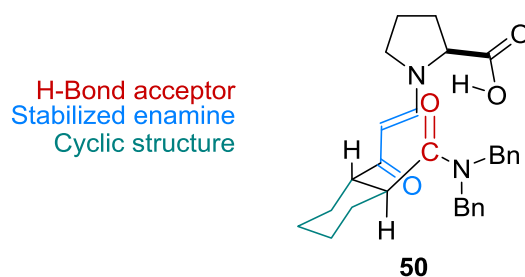
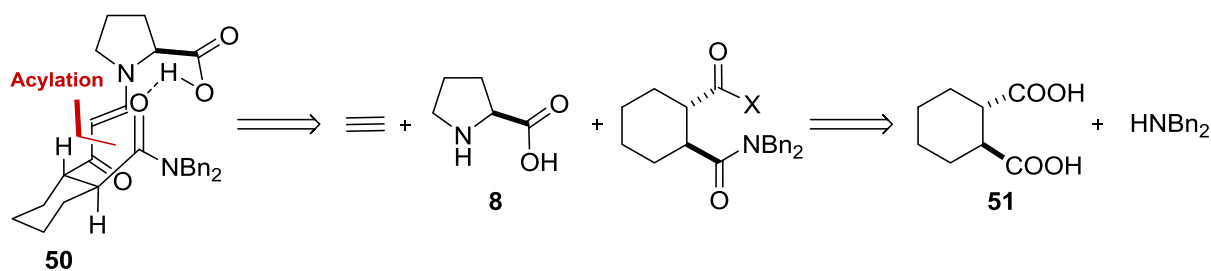


Figure 4.1: Newly designed target structure for the proline catalyzed enol-exo aldol condensation.

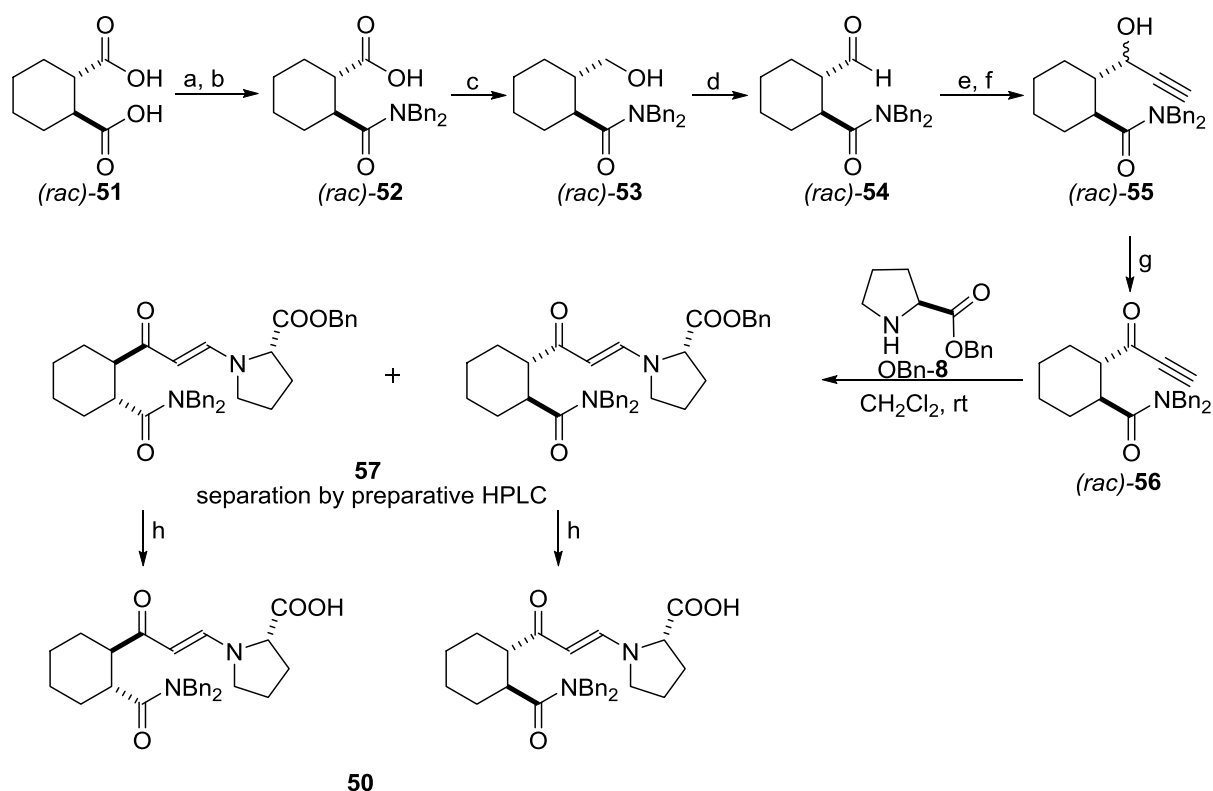
Retrosynthetic analysis of the target structure revealed the following conclusions (Scheme 4.6): The proline derived enaminone could be introduced in the last step through a Michael reaction of proline to the corresponding alkynone. The alkynone could be synthesized via a Grignard addition to a Weinreb amide, as used in the initial experiments,^[37] a Friedel–Craft acylation of acetylene or an alkyl lithium reagent. All potential carbonyl precursors can be traced back to *trans*-1,2-cyclohexanedicarboxylic acid **51**.



Scheme 4.6: Retrosynthetic analysis of the synthesis of transition state analogue **50**.

The dicarboxylic acid **51** was converted with acetic anhydride as dehydrating agent to the corresponding cyclic anhydride, which was quenched without workup to obtain the corresponding amide **52** (Scheme 4.7). The carboxylic acid was then further converted via a selective two-step reduction and oxidation sequence into the corresponding aldehyde **54**. $\text{BH}_3 \cdot \text{SMe}_2$ as reducing agent enabled the selective reduction of the carboxylic acid. Other reducing procedures involving DIBAL-H or LiAlH_4 could have potentially also reduced the amide. The aldehyde **54** was then reacted with TMS-acetylene and *n*-BuLi and yielded the propargyl alcohol **55** after deprotection. Oxidation with manganese(IV) oxide gave the alkynone **56**. As a direct activation and acylation of carboxylic acid **52** with TMS-acetylene did not furnish the desired product, the longer route was chosen.

Results and Discussion



Scheme 4.7: Synthesis of transition state analogue **50**, conditions: a) Ac_2O , reflux; b) Bn_2NH , CH_2Cl_2 ; c) $\text{BH}_3 \cdot \text{SMe}_2$, THF; d) DMP, CH_2Cl_2 ; e) TMS-Acetylene, *n*-BuLi, THF, -78°C to rt; f) K_2CO_3 , MeOH; g) MnO_2 , CH_2Cl_2 ; h) H_2 , Pd/C, EtOAc.

The next step of the synthesis was the Michael addition of proline to the alkyne. In order to understand the previously unsuccessful synthesis of the enaminone,^[37] we decided to investigate this transformation with acetylacetylene. In situ NMR studies revealed that under basic conditions the enaminone formation was proceeding well, but the product decomposed upon acidic workup. Therefore we decided to use a protected proline derivative which could be protected under basic conditions and be deprotected under neutral ones. Thus, a benzyl ester protection seemed suitable. The synthesis of the protected enaminones **57** with L-proline-benzyl ester **OBn-8** from alkyne **(rac)-56** proceeded smoothly without addition of base. The two obtained diastereomers **57** could not be separated via column chromatography and separation via preparative HPLC was necessary. The assignment of individual diastereomers by NMR was rather difficult due to a broadening of all the NMR signals of these compounds. With these compounds in hand, we raised the question, if the deprotection of the benzyl group will improve the sharpness of the NMR signals. After deprotection of enaminones **57**, we obtained two different diastereomers of the target molecule **50**. Unfortunately NMR characterization of the two diastereomers was still impossible, even at lower temperatures (Figure 4.2, Figure 4.3). Chloroform was chosen as solvent again, due to its ability to catalyze proline type aldol reactions. Other solvents, as for instance DMSO or CH_3CN , are also

good solvents for aldol reactions, but they are also hydrogen bond acceptors and could disturb the formation of the desired H-bond. The possibility to average all the broad signals by heating was not considered, since high temperatures break hydrogen bonds.

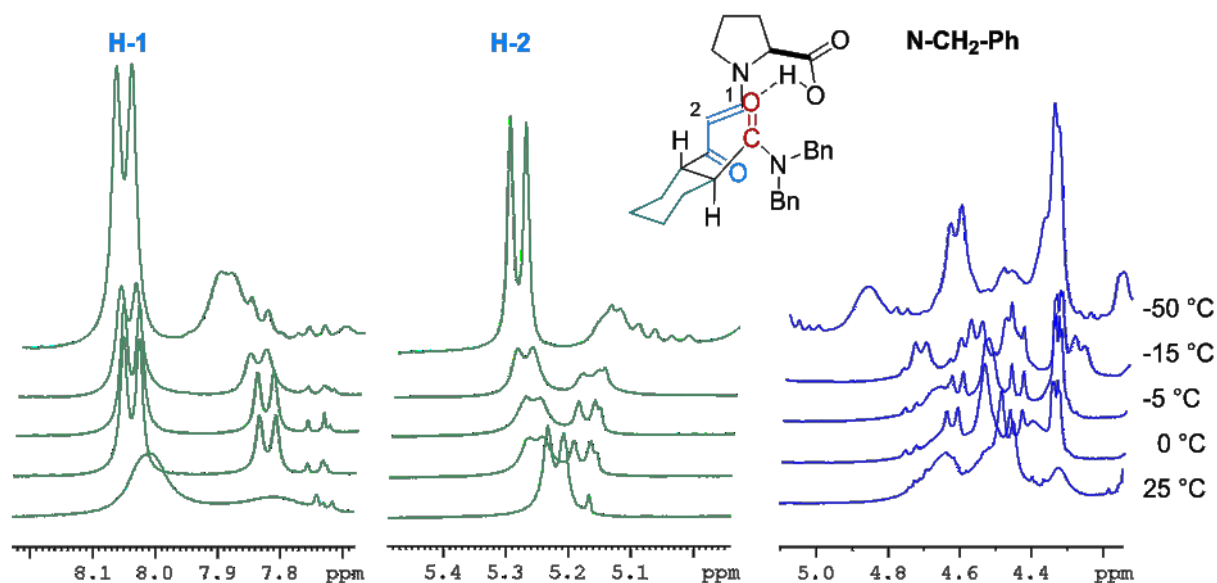


Figure 4.2: ^1H NMR spectrum of diastereomer I of **50** in CDCl_3 at various temperatures.

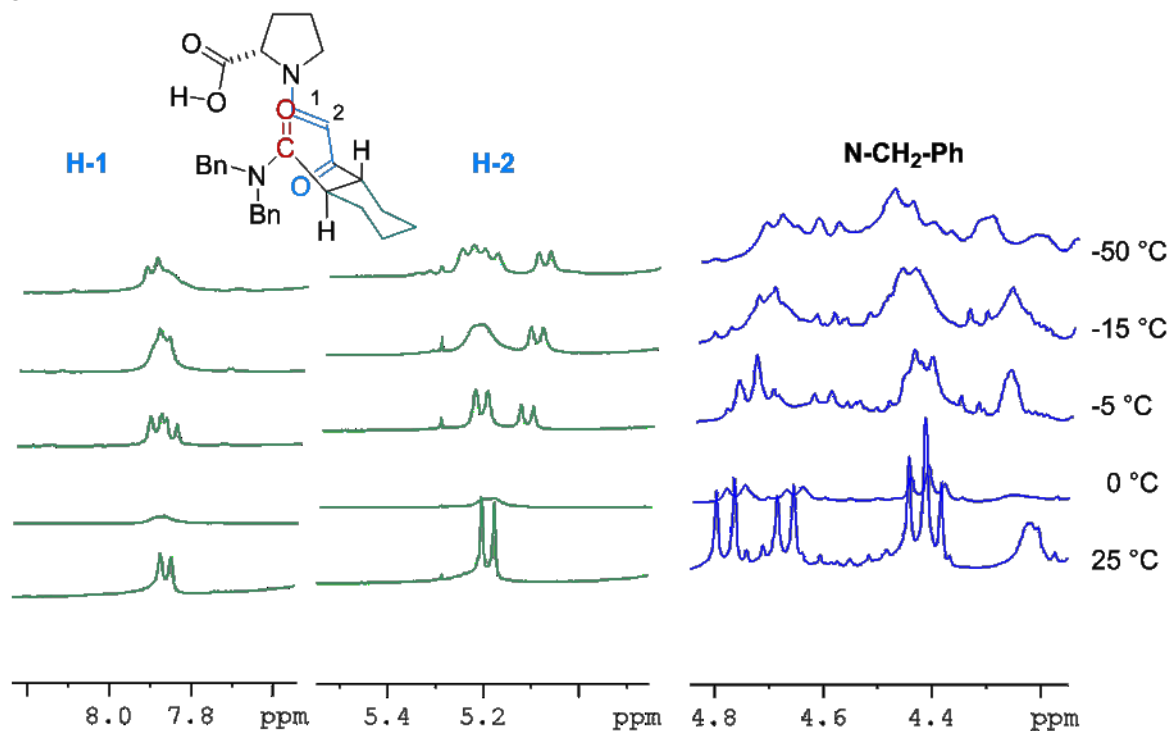


Figure 4.3: ^1H NMR spectrum of diastereomer II of **50** in CDCl_3 at various temperatures.

Interestingly, when we compared the acidic region (10–20 ppm) of the ^1H NMR spectrum (Figure 4.4), one diastereomer showed several broad proton resonances whereas the other one did not. This could indicate that one diastereomer is in the desired conformation and is forming the desired hydrogen bond whereas the other one is not, as we expected from our model.

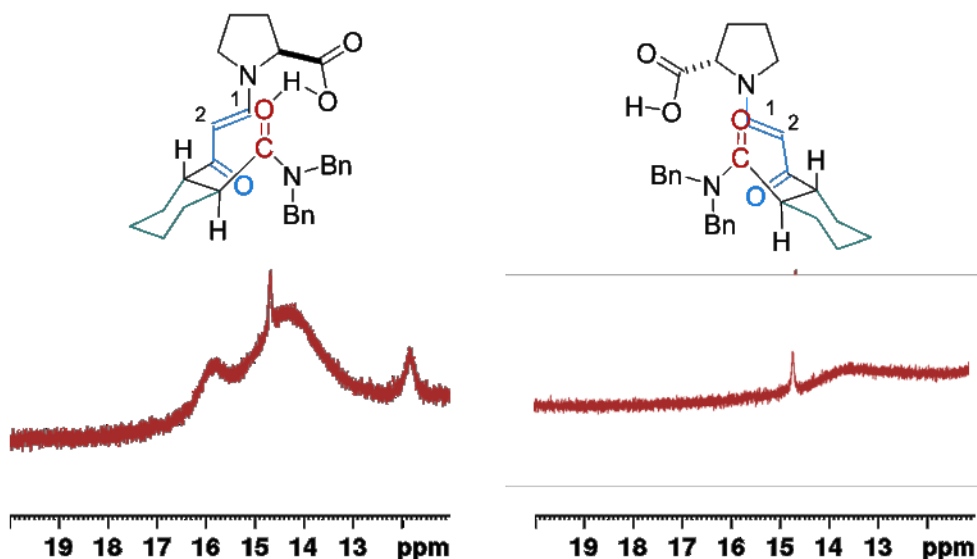
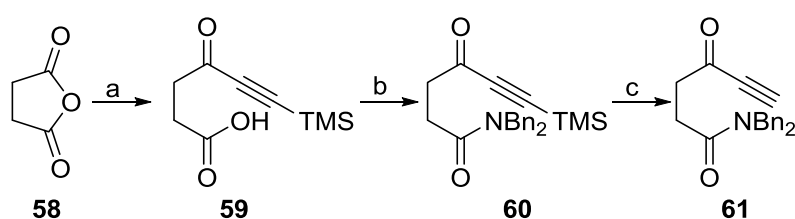


Figure 4.4: Acidic region of the ^1H NMR spectrum of the two different diastereomers **50** at $-50\text{ }^\circ\text{C}$.

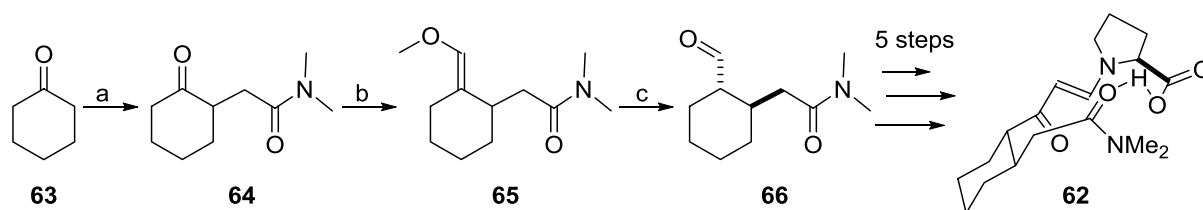
Unfortunately, all attempts to crystallize these compounds to confirm our NMR results were unsuccessful.

In parallel to the six-step synthesis from an anhydride towards the alkynone precursors we have also developed a shorter three-step synthesis (Scheme 4.8). In this synthetic route the introduction of the functional groups was switched. In the first step, the TMS protected alkynone **59** could be introduced by a Friedel–Craft type acylation of bis(TMS)acetylene with anhydride **58** in the presence of AlCl_3 as catalyst. The yields were only moderate to good, and for anhydride with substituents in the α -position, as for instance in our initial synthesis, no product was obtained. The further amidation and deprotection towards the alkynones **61** proceeded smoothly with overall good yields.



Scheme 4.8: A shorter synthetic route to alkynones as precursors for enaminoxones with internal H-bond acceptor. Conditions: a) AlCl_3 , bis(TMS)acetylene, DCM, $0\text{ }^\circ\text{C}$; b) DCC, DMAP, Bn_2NH ; c) Borax, MeOH.

Another potential route towards transition state analogues **62** of enolexo aldolisations can be started from cyclohexanone **63**. After alkylation with the desired H-bond acceptor and a C1 elongation via Wittig reaction, the precursor aldehyde **66** was obtained. Further five-steps towards our previously reported route would lead to another transition state analogue that is supposed to mimic the transition state for the formation of a six-membered ring.



Scheme 4.9: Synthesis of the potential transition state analogue precursor **62**; Conditions: a) LDA, $\text{BrCH}_2\text{CONMe}_2$, $-78\text{ }^\circ\text{C}$ to rt; b) $[\text{MeOCH}_2\text{PPh}_3]\text{Br}$, KO^tBu , THF; c) 10% HCl, DCM.

We wondered, which rotations in the enaminone **67** are responsible for the broadening of the NMR signals. In previous steps the other functional groups have been shown not to broaden the NMR signal. A closer look at the enaminone structure, revealed that it has one C–C and one C–N bond that have a hindered rotation due to their resonance structure and so they can potentially cause different rotamer signals on NMR timescale in analogy to amides:

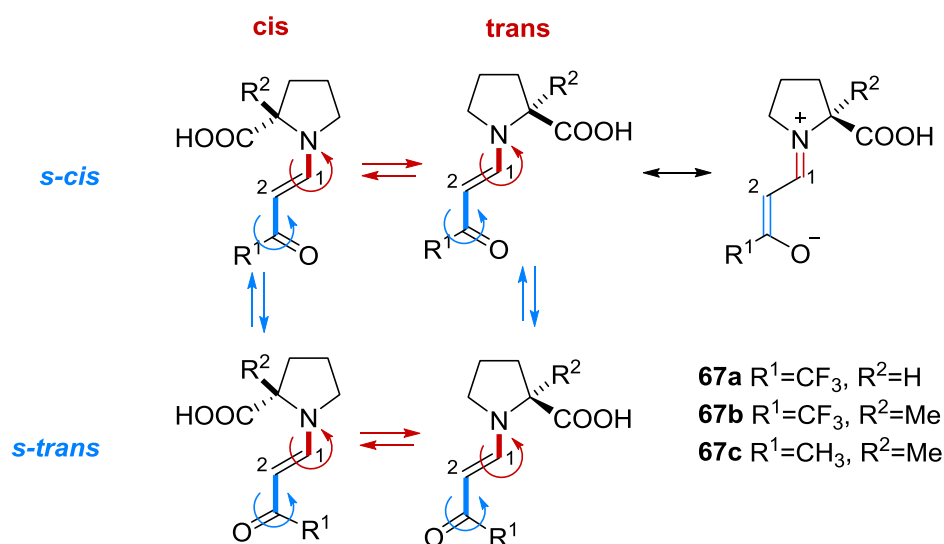


Figure 4.5: Bond rotations of enaminones that could cause 4 different rotamers.

Concerning the rotation around the C–N-bond, a *cis*- and *trans*-conformation are possible. NMR measurements by *Gschwind* have shown,^[35] that the major conformer of proline derived enamines are mainly present as the *trans*-conformer. However, there can be still small contributions coming from the *cis*-conformer, as it has been shown by initial NMR studies by *Mello*^[36], which were the basis for the X-ray structures published by our group. They reported a ratio of 85:15 between the *trans* and the *cis* isomer. When we introduced a methyl group in the α -position of the proline, the corresponding enaminone **67b** was exclusively present in the *trans*-form. In addition the electron withdrawing CF_3 group seemed to influence the system by increasing the iminium character, a fact which has already been seen by comparison of the X-ray structures with the transition states calculated by *Houk*. The *s-trans* form seemed to be the energetically most favored

Results and Discussion

conformer in the solid state and also in solution as we have detected with HOE (heteronuclear Overhauser effect) measurements. When we exchanged the CF_3 of **67b** to a CH_3 group the NMR signals of this new compound **67c** were still broadened (Figure 4.6). On the one hand this might be explained by the hindered rotation around the C–CO bond, which in contrast to the CF_3 -variant has two more equally contributed conformers, on the other hand the higher basicity of the nitrogen could lead to an exchange between the zwitterionic and the neutral form of the enaminone.

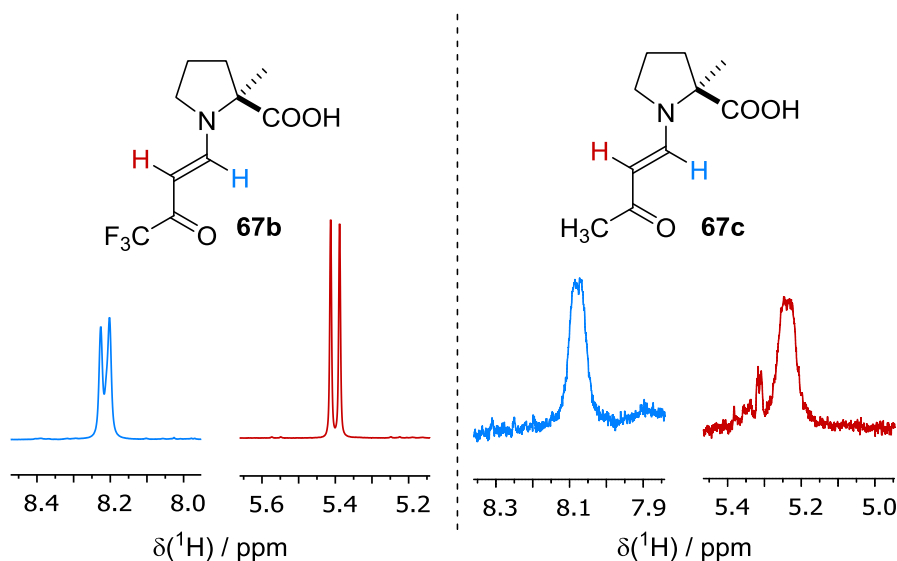


Figure 4.6: Comparison of the ^1H NMR signals of **67b** and **67c**.

These results lead us to design a new target structures, to further advance the transition state analogue (Figure 4.7). Additionally, to the previous functional groups, the introduction of a methyl group in the α -position of the proline is necessary. Furthermore, the electron density of the enaminone has to be tuned, as for instance by introducing an electron withdrawing group in the α -position of the enaminone-carbonyl.

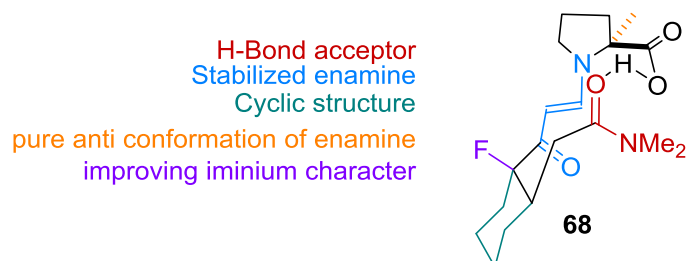


Figure 4.7: Further optimized target structure for the proline catalyzed enol-exo aldol condensation.

Unfortunately, this structural motif requires various functional groups in order to bring it into the desired conformation. This does not agree with our concept of having a simple transition state analogue.

We were wondering if we could improve the rotational problems of the enaminone by simply using a cyclic enaminone, which cannot freely rotate and are, according to our previous reports,^[34] stable. Therefore, we envisioned a transition state analogue for the enolendo cyclisation which contains a enaminone derived from an 1,3-cyclohexanedione with a structure seen in the following figure:

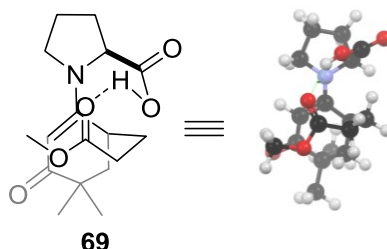


Figure 4.8: Left: Target structure for a potential enol-exo transition state model; right: 3D model generated with Chem3D.

After some optimization we found a very short and efficient two step route for the synthesis of the desired analogue precursor **70** (Figure 4.9). The precursor was synthesized via a Baylis-Hillman type dimerization of methyl acrylate **71**. The obtained product **72** was used in a Michael reaction, followed by a Dieckmann condensation to form the desired 1,3-diketone **70** in good yields. The geminal dimethylgroups of this substrate are crucial for the selectivity of the enaminone formation. If they are not present, the enamine formation occurs on the less hindered ketone.

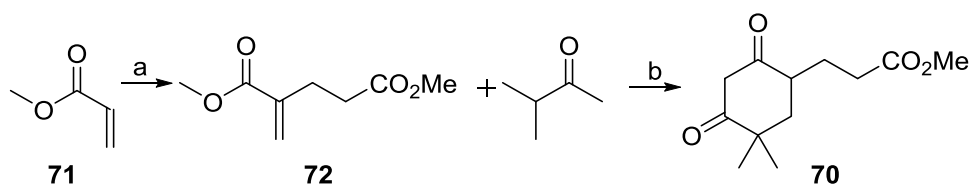


Figure 4.9: A 2-step protocol for the synthesis of cyclic enaminones bearing an internal hydrogen bond acceptor; Conditions: a) $P(\text{oct})_3$, 66%; b) $\text{KO}t\text{Bu}$, THF, 60%.

With this substrate in hand, we investigated the enamine formation. As initial conditions we had chosen the reported ones of our group.^[34] Unfortunately, we could not observe the desired product after heating for several hours at 60 °C in methanol. Other reported conditions to form proline derived cyclic enaminones also failed,^[111] mainly the decarboxylated product **73** was obtained. This indicated that the desired product **70** might be formed, but it decomposed under the reaction conditions due to the additional activation by the internal hydrogen bond acceptor, that can act as a base.

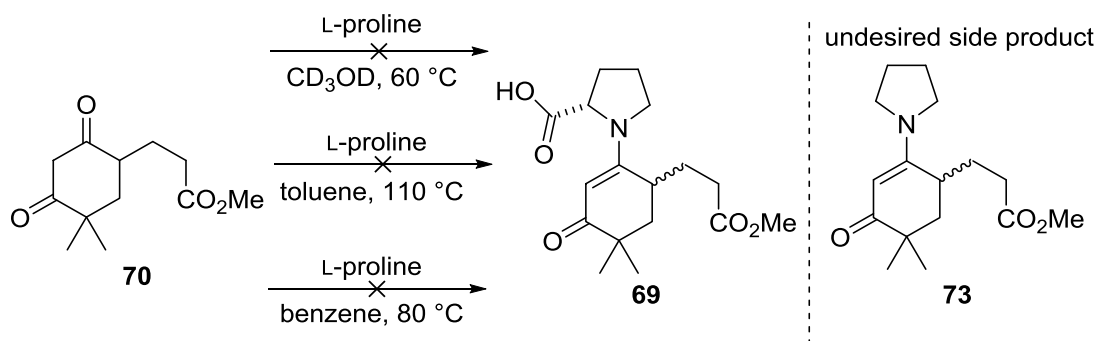


Figure 4.10: Reaction conditions towards proline-derived enaminone formation **69** from diketone **70**.

4.1.1.3 Synthesis of Proline-Derived Aryl Amines as Stable Transition State Analogues

Inspired by our previous investigations of cyclic stabilized enamine derivatives, we had the idea to utilize an aryl amine as a stabilized enamine derivative. Therefore, we designed a model compound that contains the proline derived aryl amine, a hydrogen bond acceptor and additional substituents to stabilize a cyclic conformation by a Thorpe–Ingold type effect. The latter can be achieved efficiently by a sulfone or a quaternary carbon with two geminal methyl groups (Figure 4.11).

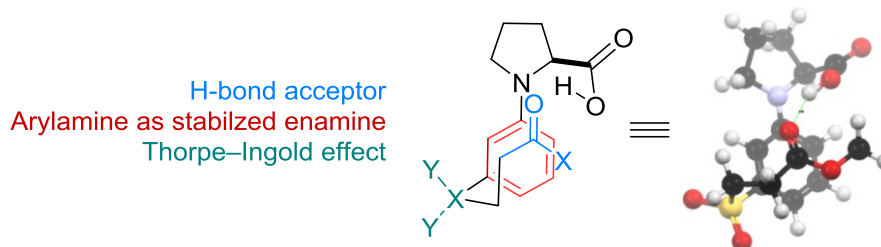


Figure 4.11: Left: target Structure for an aryl amine derived transition state analogue; right: 3D model generated with Chem3D.

We decided to synthesize molecule **74** with an aliphatic aldehyde as hydrogen bond acceptor and a quaternary carbon that bears two geminal methyl groups to favor a cyclic conformation of the molecule. Even though the aldehyde is a good electrophile, we assumed that it would not be attacked by the aryl amine, due to its low enamine type nucleophilicity.

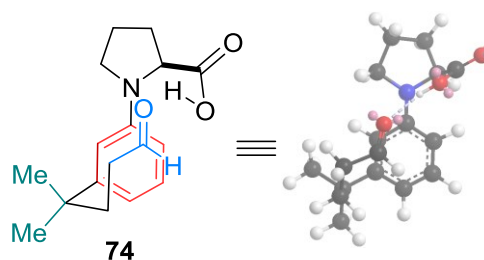
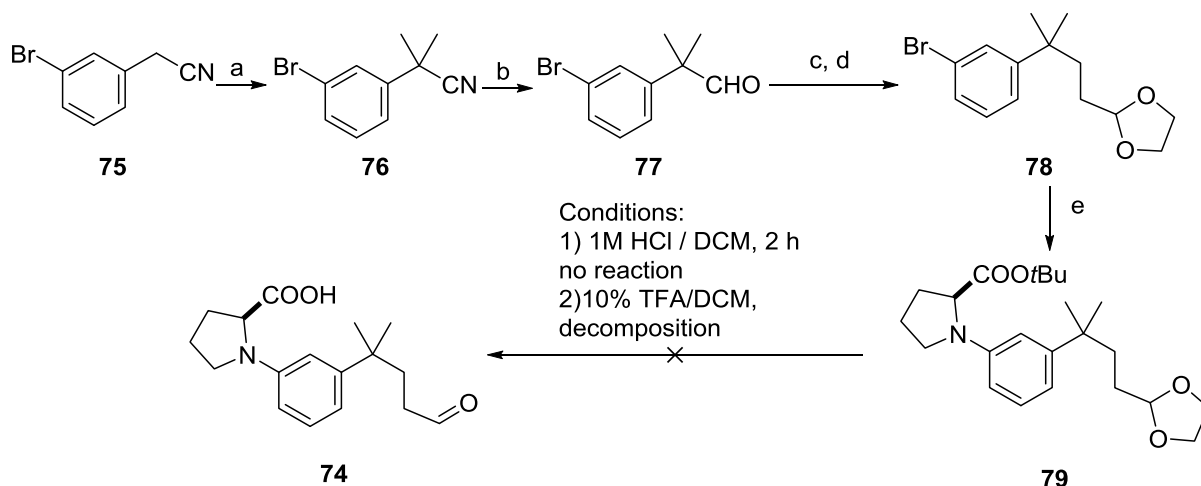


Figure 4.12: Left: Initial target structure with an aldehyde as hydrogen bond acceptor and a quaternary carbon with two geminal methyl groups; right: 3D model generated with Chem3D.

Our initial synthetic route started with the α -dimethylation of 3-bromophenylacetonitrile **75** with excellent yield (99%). After reduction of the nitrile **76** to the corresponding aldehyde **77**, the acetal protected aldehyde was introduced by a Wittig reaction. After a reduction with hydrogen and Pd/C as catalyst the precursor for the aryl amine **78** was obtained in acceptable yields. After testing several reaction conditions with 5-bromo-*meta*-xylene as model substrate, we found that the coupling of *O*-Boc-protected proline in a Buchwald–Hartwig amination to obtain the desired protected target molecule **79** was possible. Unfortunately, the product could not be separated by column chromatography from the dehalogenated starting material as side product. *O*-benzyl-proline did not yield the desired product due to debenylation under the reaction conditions. Interestingly, the dimeric proline anhydride was the main product in some cases. With the protected target molecule **79** in hand, we submitted it to different acidic deprotection conditions, which unfortunately only lead to decomposition of the starting material.



Scheme 4.10: Synthetic route towards transition state analogue **74**; Conditions: a) MeI, THF, KO^tBu, –50 °C, 99%; b) DIBAL, CH₂Cl₂; c) [(OCH₂CH₂O)CHCH₂PPh₃]⁺Br⁻, KO^tBu, THF, 10 d, 45%; d) H₂, Pd/C, EtOAc, 80%; e) L-H-Pro-O^tBu, Pd₂(dba)₃, RuPHOS, toluene, 80 °C, 13 h, 10%.

Disenchanted by these results, we modified our target structure in order to make the aryl amine less electron-rich and so more stable against stronger acidic conditions (Figure 4.13).

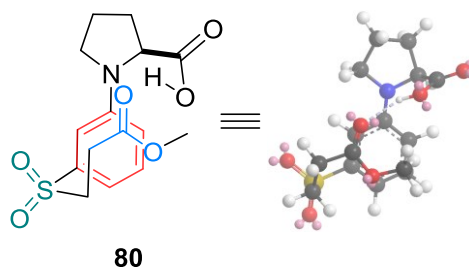
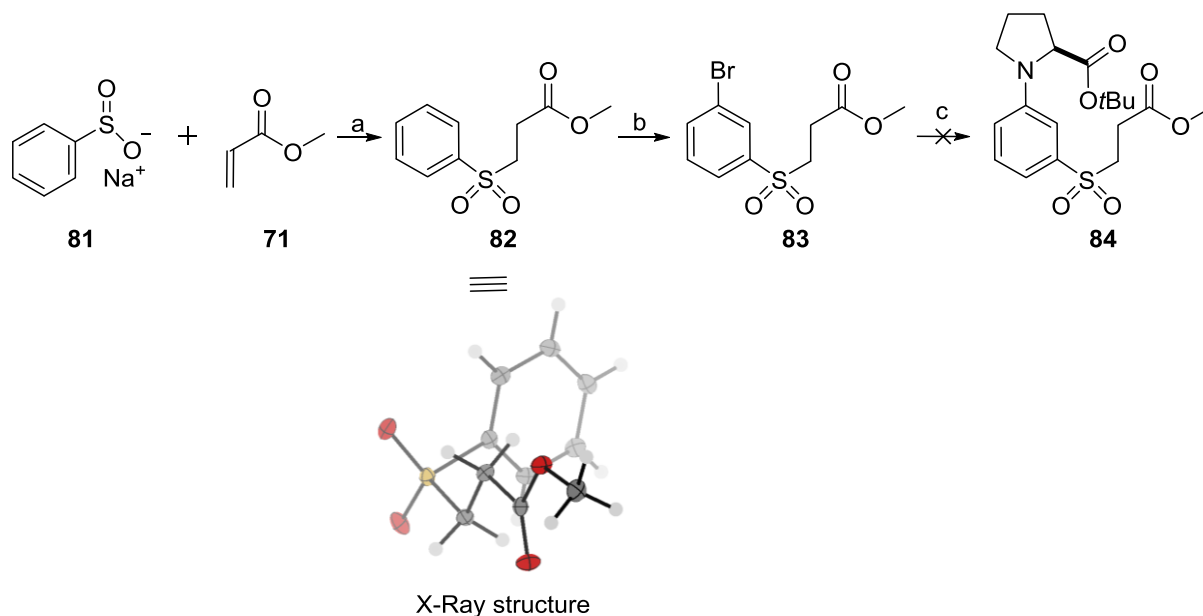


Figure 4.13: Left: Modified target structure **80** with an ester as hydrogen bond acceptor and a sulfone as Thorpe–Ingold initiator; right: 3D model generated with Chem3D.

Instead of the geminal methyl groups, we decided to use a sulfone, which on the one hand should introduce a Thorpe–Ingold like effect and on the other hand reduce electron density in the aromatic π -system. As hydrogen bond acceptor we initially chose an ester since the starting material were commercially available. The introduction of the hydrogen bond acceptor was achieved by a Michael addition of benzene sulfonic acid **81** to methyl acrylate **71** (Scheme 4.11). The product **82** was obtained in good yields and we were able to obtain a single crystal. As we envisioned, the structure nicely shows the preformation of a cyclic structure. Following bromination of the compound gave the *meta*-substituted product **83** with moderate yields. Unfortunately, the following Buchwald–Hartwig coupling was not successful. The instability of the sulfone led to a retro Michael reaction under the basic reaction conditions required for the coupling.



Scheme 4.11: Synthesis towards transition state analogue **84**. Conditions: a) 0.25 M HCl, 70 °C, 13 h; b) H₂SO₄/H₂O (1:1), NBS, then MeOH. 35%; c) L-H-Pro-*Ot*Bu, Pd₂(dba)₃, RuPhos, toluene, 80 °C.

In order to suppress the retro Michael addition we decided to introduce a quaternary carbon center in the α -position of the hydrogen bond acceptor (Figure 4.14).

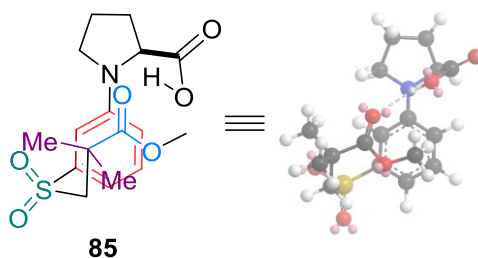
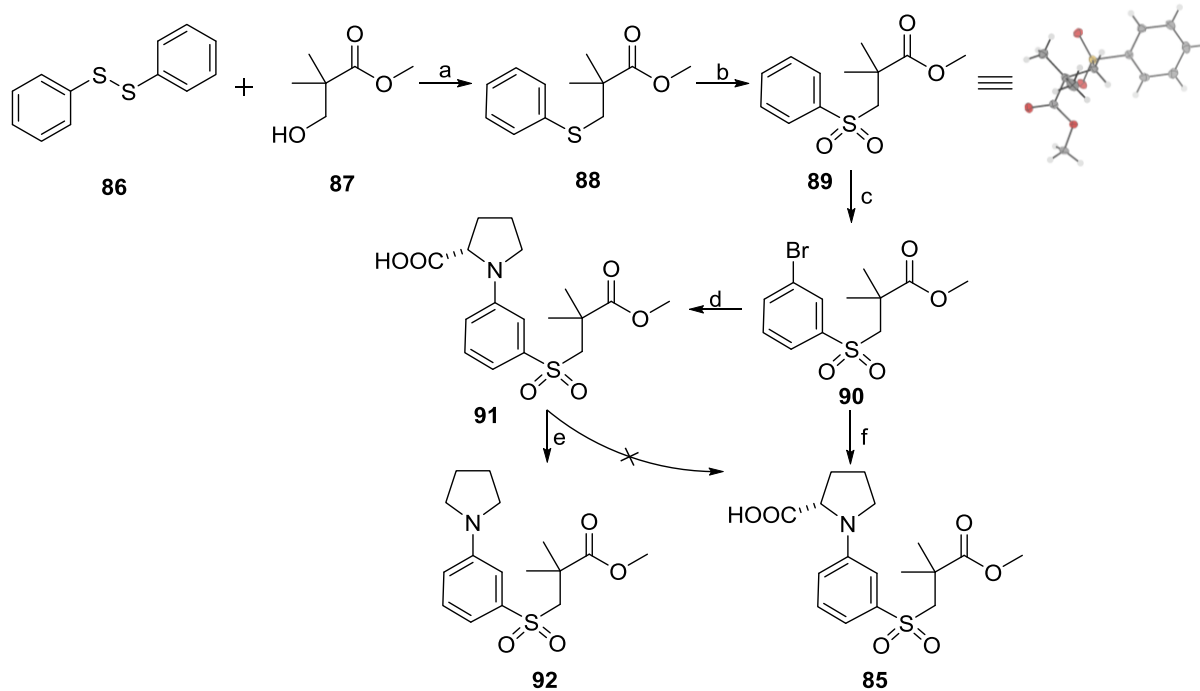


Figure 4.14: Left: Modified target structure **85** with an ester as hydrogen bond acceptor and a sulfone as Thorpe–Ingold initiator and a quaternary carbon center in α -position of the hydrogen bond acceptor; right: 3D model generated with Chem3D.

We started the synthesis with a thioether formation by nucleophilic substitution using 2,2-dimethyl-3-hydroxypropanoic acid methyl ester **87** and dibzenzenesulfide **86**. After oxidation of thioether **88** with oxone, sulfone **89** was obtained with moderate yields. Similar to the previously synthesized sulfone **82** we could obtain a single crystal of sulfone **89**. In contrast to the previous molecule, sulfone **89** is now present in an undesired conformation that would not form the hydrogen bond interaction after amination. The aryl ring was brominated in *meta* position and following re-esterification gave the coupling precursor **90**. The separation from residual starting material was not possible by preparative thin layer chromatography. Since no side reactions of the residual starting material were expected in the next step, crude compound was used. The coupling of the proline-*tert*-butyl ester was achieved with moderate yields. Unfortunately the separation from sulfone **89** was still not possible by preparative thin layer chromatography at this stage. To see whether the deprotection of **91** is working under acidic conditions, we treated the mixture to with 50% TFA in CH_2Cl_2 . To our disenchantment the amino acid decarboxylated under the reaction conditions and so only the decarboxylated product **92** could be observed. At this point, we were wondering if the direct proline coupling via Ullmann-type coupling with the precursor **90** was possible. Previous tests of these conditions yielded complex reaction mixtures. To our delight, we could obtain the desired product **85**, although the yields were relatively low (<10%).



Scheme 4.12: Synthesis of transition state analogue **85**; conditions: a) $\text{P}(\text{oct})_3$, DMF, 70%; b) Oxone, MeOH/THF/H₂O (1:1:1), 36%; c) NBS, H₂SO₄/H₂O (1:1), 3 h, then excess MeOH, 1 h, 60% conversion; d) L-H-Pro-OfBu, $\text{Pd}_2(\text{dba})_3$, BINAP, toluene, 110 °C, full conversion; e) TFA/CH₂Cl₂ (1:1); f) L-proline, DMF, CuI KOtBu, 100 °C, 8%.

Nevertheless we were excited about the structure of the obtained compound **85** in solution. When we analyzed the NMR data at room temperature in CD₂Cl₂, we found that the compound has relatively free rotation around the C–N bond. At low temperature (-90 °C) we found that the aryl amine is preferably present in the desired *trans*-conformation. Unfortunately, we could not detect a sharp signal of the acidic proton that would help us to determine hydrogen bond formation. In fact, the broadening shows, that a fast exchange of the acidic proton is still present, which would be suppressed in presence of a strong H-bond. Furthermore, we found that the main conformation of the side chain is similar to the formation, which we observed in the crystal structure of **89**, indicating the molecule is mainly not in its cyclic form. At lower temperature we could observe a second, but less populated conformer. During the NOE analysis we found also, that it is preferentially in the *trans* conformation. Also the other observed NOEs were similar to the main compound.

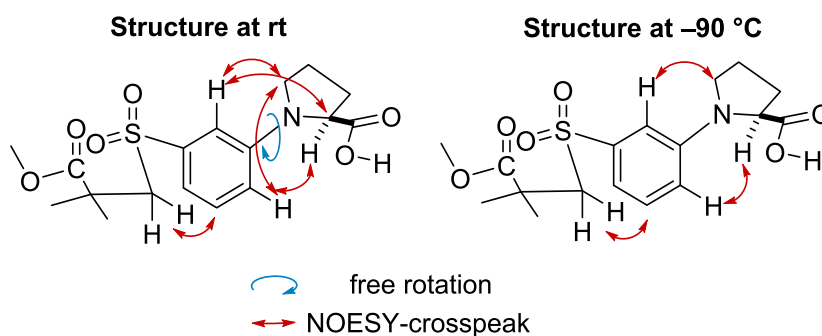


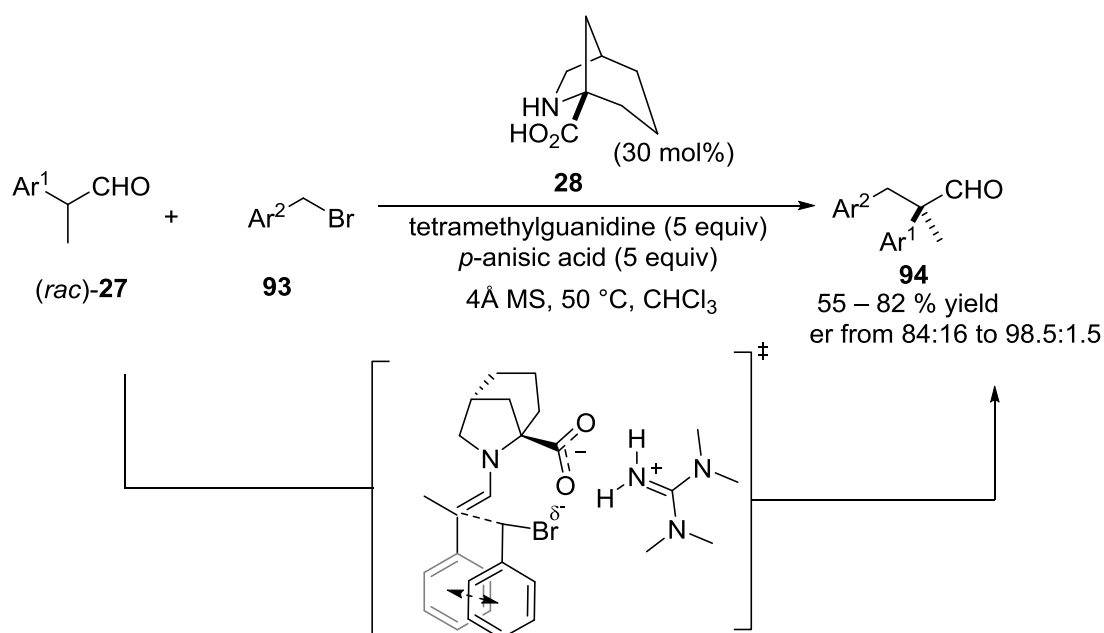
Figure 4.15: Relevant NOE contacts of **85** at room temperature and $-90\text{ }^{\circ}\text{C}$ with important structural information.

In analogy to our previous results of enamine systems, the two stable conformers might be present in solution as a zwitterionic and non-zwitterionic form. In the calculated transition states by *Houk* it was initially found, that there is no hydrogen bond interaction with the nitrogen present. The *N*-protonated form of the enamine might simply not be reactive. In most of our synthesized systems this hydrogen bond interaction is still present, at least in small amounts. This might disturb the formation of our envisioned hydrogen bond and is broadening the NMR signals. To overcome this, the basicity of the nitrogen has to be reduced further by introducing strong electron withdrawing groups in the enamine system. Additionally, a lower basicity of the nitrogen might increase the stability under acidic conditions that have been shown to be problematic in our synthetic routes. Stronger H-bond acceptors might also help to observe the elusive H-bond interaction.

4.1.2 Enamine Intermediates in the α -Benylation of α -Branched Aldehydes

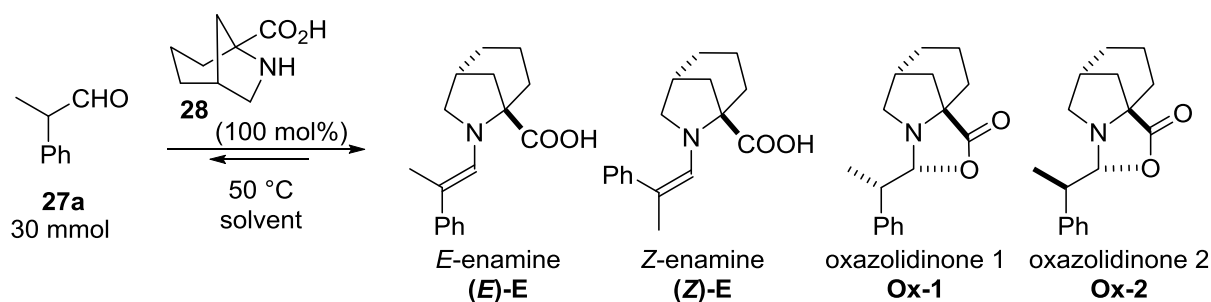
These studies were conducted in cooperation with Dr. Anna Lee and Dr. Manuel van Gemmeren. The other authors of our manuscript are also thanked for their contributions [112]

Recently, our group developed a protocol for the catalytic asymmetric α -benzylation of aldehydes (Scheme 4.13).^[112] By using the sterically demanding proline derived catalyst **28** in a buffer system, racemic α -branched aldehydes **27** are converted in a dynamic kinetic asymmetric transformation with benzyl bromides **93** to the benzylated products **94** bearing a quaternary stereogenic center in good yields and high enantioselectivities.



Scheme 4.13: The catalytic asymmetric α -benzylation of aldehydes

The use of a buffer mixture containing a strong base and weak carboxylic acid is essential for the yields and enantioselectivities of the reaction. In order to understand the influence of the additives, the formation of enamine and oxazolidinone intermediates was studied. The direct comparison of the common solvent for proline catalyzed aldol reactions, DMSO, and the best solvent for the α -benzylation, chloroform, revealed a significant difference in the amount of intermediate species in solution (Table 4.3).

Table 4.3: Enamine and oxazolidinone formation in the presence of catalyst **28** and aldehyde **27a**.

#	solvent	ratio	ratio intermediates
		aldehyde : intermediates	(<i>E</i>)- <i>E</i> : (<i>Z</i>)- <i>E</i> : <i>Ox</i> -1 : <i>Ox</i> -2
1	DMSO- <i>d</i> ₆	18 : 72	26 : 5 : 24 : 27
2	CDCl ₃	98 : 2	0 : 0 : 1 : 2

In DMSO we could observe the formation of (*E*)- and (*Z*)-enamine intermediates. In contrast to this no enamine intermediates were observed in chloroform. The formation of oxazolidinones could be detected in both solvents. These results are in agreement with our previous results presented in the last chapter and also with the trend reported by *Gschwind* and co-workers^[35] that polar aprotic solvents increase the observable enamine concentration.

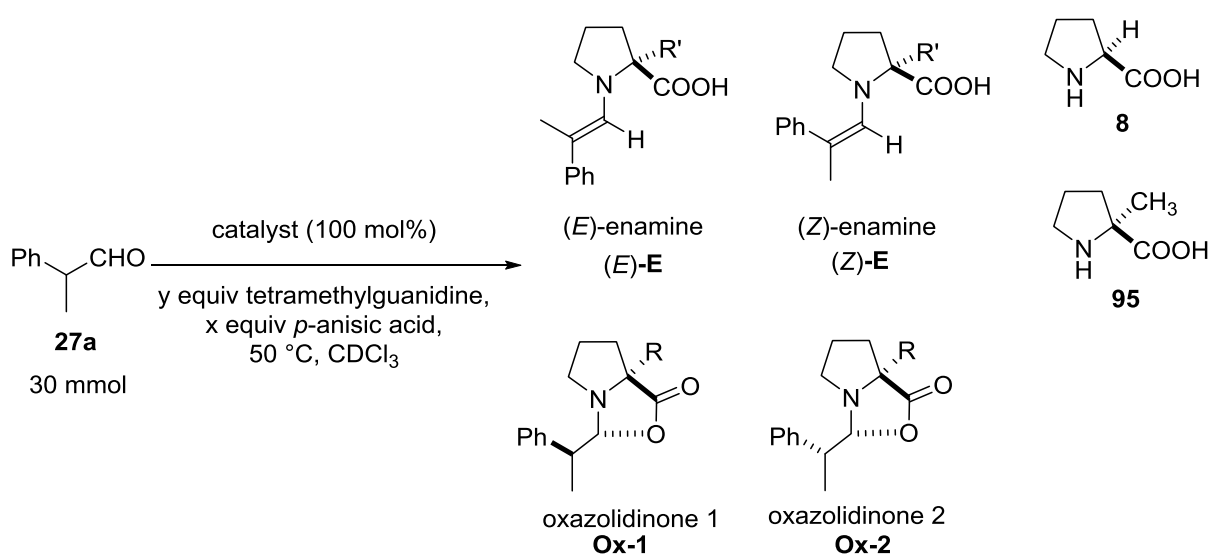
Interestingly, when branched aldehydes were used we observed a slower exchange in EXSY of the intermediate species in DMSO compared to unbranched aldehydes. At room temperature we could not observe the exchange between the intermediates ($t_{\text{mix}} = 1$ s). However, when we increased the temperature to 50 °C or 80 °C the exchange process between the intermediates became faster and the EXSY cross-peaks visible. Interestingly, the two major oxazolidinones are formed, where one has a more intense exchange peak to the (*E*)-enamine and the other to the (*Z*)-isomer. Also two minor oxazolidinone species were detected, which probably correspond to the *endo*-oxazolidinones forms. No crosspeaks between those and the enamine intermediates could be detected.

Under optimized reaction conditions a buffer was used. We conducted several experiments in the presence of various equivalents of the additives and different proline derivatives in chloroform. The first effect that was directly observed was the increased solubility of the catalyst upon increasing amounts of additives. Without additives, the catalysts were almost insoluble in chloroform. Upon addition of one equivalent of aldehyde to these different mixtures, we investigated the influence on the formation of enamine and oxazolidinone intermediates (Table 4.4). With an increasing amount of acid

Results and Discussion

in solution, the formation of oxazolidinone intermediates was accelerated and we could observe a higher concentration in solution. In contrast to this, the addition of a base leads to an increased concentration of enamines and oxazolidinones. This observation is in accordance with the previous experimental observations, where the addition of a base was found to be crucial for the reactivity. Without the addition of a base the reaction is not proceeding and we also could not observe the enamine as the proposed reactive intermediate. For comparison we also studied the equilibria in the presence of the weaker bases Et₃N and 2,6-lutidine (Table 4.4, entries 14 and 15). Interestingly, these bases were inactive in the reaction and we also could not observe the formation of enamines in our NMR experiments.

Table 4.4: Equilibria between catalysts and aldehyde **27a** in CDCl₃ with the addition of various equivalents of additives



entry	x	y	catalyst	ratio	
				aldehyde : intermediates	(E)-E : (Z)-E : Ox-1 : Ox-2
1	0	0	8	> 99 : 1	-
2	0	1	8	74 : 26	46 : 5 : 0 : 0
3	1	0	8	71 : 29	0 : 0 : 5 : 4
4	1	1	8	87 : 13	4 : 1 : 4 : 4
5	2	2	8	89 : 11	5 : 1 : 6 : 5
6	5	5	8	84 : 16	9 : 2 : 2 : 2
7	0	0	95	> 99 : 1	-
8	0	1	95	86 : 14	6 : 1 : 19 : 17
9	1	0	95	92 : 8	0 : 0 : 21 : 19

10	1	1	95	82 : 18	0 : 0 : 18 : 19
11	2	2	95	76 : 24	6 : 1 : 125 : 136
12	5	5	95	80 : 20	1 : - : 12 : 13
13 ^a	0	1	95	> 99 : 1	-
14 ^b	0	1	95	> 99 : 1	-
15	0	0	28	98 : 2	0 : 0 : 1 : 2
16 ^c	1	0	28	96 : 4	0 : 0 : 1 : 1
17 ^c	0	1	28	84 : 16	19 : 6 : 21 : 28
18 ^c	1	1	28	93 : 7	0 : 0 : 3 : 4
19 ^c	2	2	28	89 : 11	3 : 1 : 7 : 8
20 ^c	5	5	28	88 : 12	12 : 1 : 14.5 : 17

^a Et₃N was used as a base.

^b 2,6-Lutidine was used as a base.

^c Errors in the integration due to overlap of broad polar protons, ¹³C satellites or the low concentration of the species are possible .

After we had conducted all the experiments, the role of the intermediates became clear. The base is solubilizing the catalyst and therefore forming an ion pair in solution. In addition, the stability of the enamine intermediate by forming the corresponding enamine-carboxylate is increased. These results are in agreement with previous reports by *Gschwind* et al., who have nicely shown, that stronger bases stabilize enamine carboxylates.^[113] In addition, *Blackmond* and coworkers have studied the intermediate formation with the same aldehyde and a DBU-proline salt and came to similar conclusions.^[40]

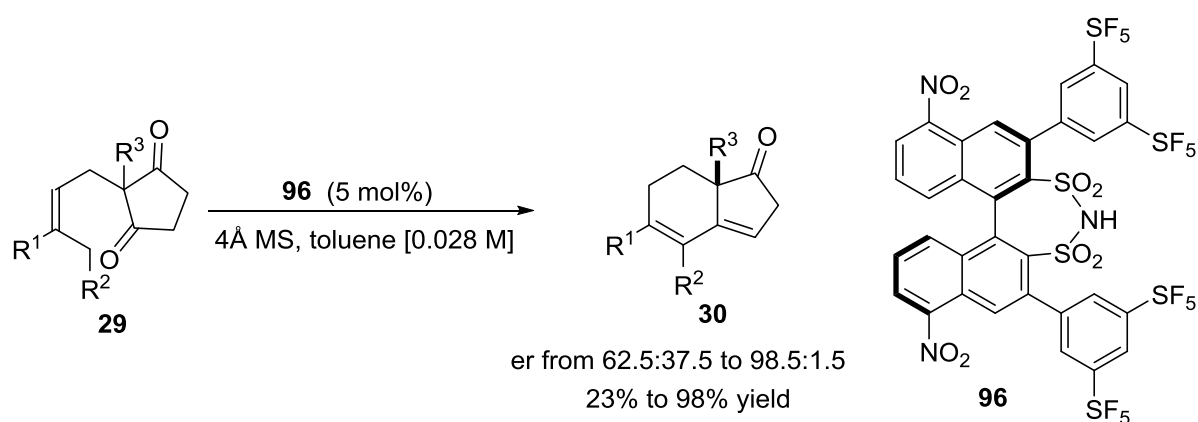
The acid additive has mainly two roles. It accelerates oxazolidinone formation, but also prevents the formation of undesired side products as strongly basic conditions lead to salt formation of the catalyst. The addition of the alkylating reagent alkylates and thereby deactivates the catalyst. The alkylated catalyst has been observed by GC-MS even under optimized conditions. Furthermore, formation of *p*-anisic acid benzyl ester indicates possible esterification of the catalyst although *N*-alkylation is also possible. The addition of acid might reduce the *N*-nucleophilicity by simple protonation. Strongly basic conditions are known to accelerate enol alkylation^[114] The acid might prevent non-enantioselective side pathways, by changing the pH. In summary we can conclude that the proposed enamines under the reaction conditions can be observed and that the additives are acting as a well-adjusted buffer system that is preventing unwanted side pathways.

4.2 Disulfonimides as Brønsted- and Lewis-Acid Catalysts

4.2.1 Reaction Monitoring of the Asymmetric Torgov Cyclisation

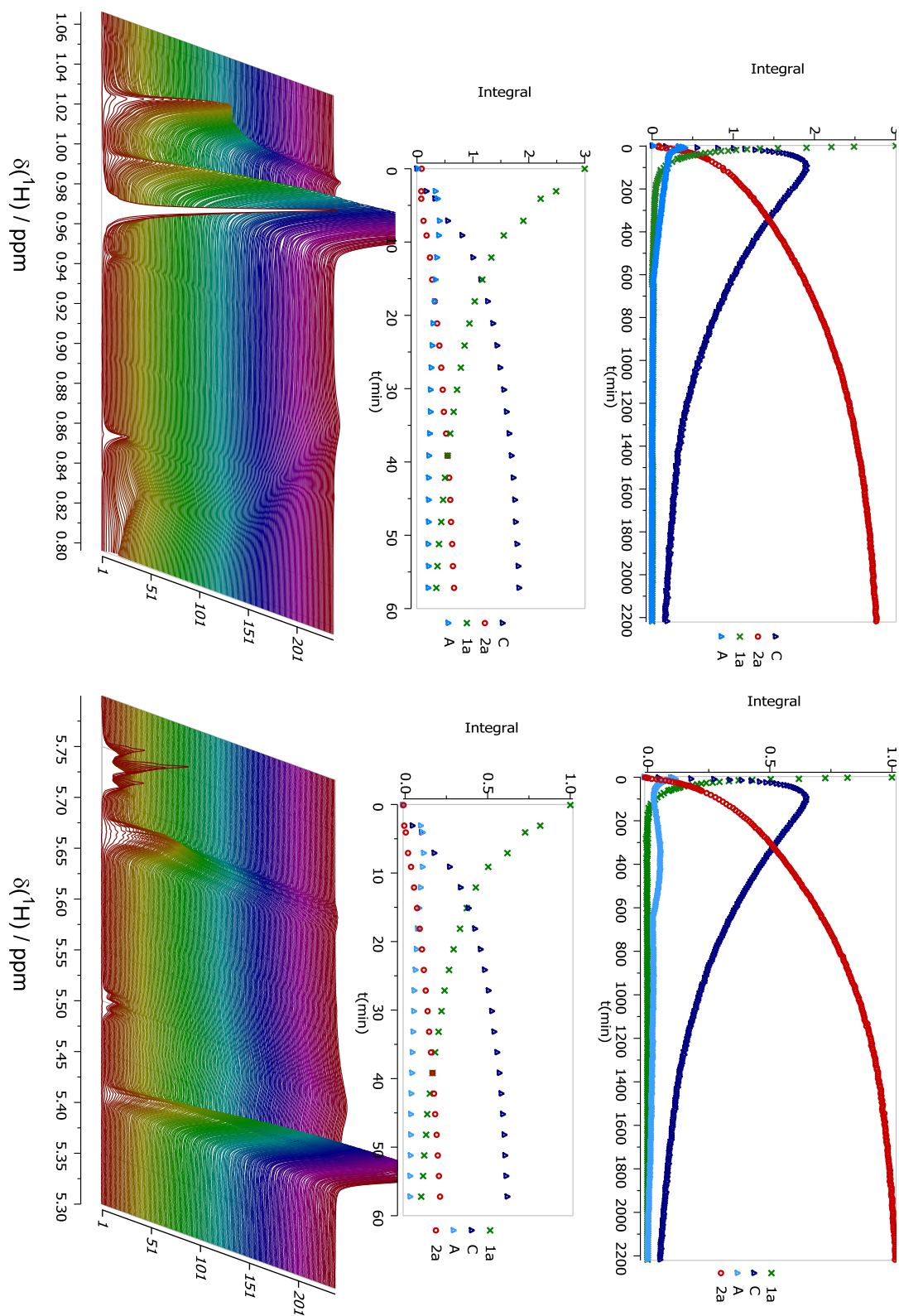
This chapter describes an NMR kinetic study that has been conducted during the development of the asymmetric Torgov cyclisation. The development of the reaction was mainly performed by Dr. S. Prévost, Dr. N. Dupré, Dr. Q. Wang and Dr. V. Wakchaure.

Recently the first highly enantioselective Torgov cyclisation was developed in our group, utilizing a highly acidic disulfonimide **96** to provide facile access to several enantioenriched tri- and tetracyclic dienes.^[60]



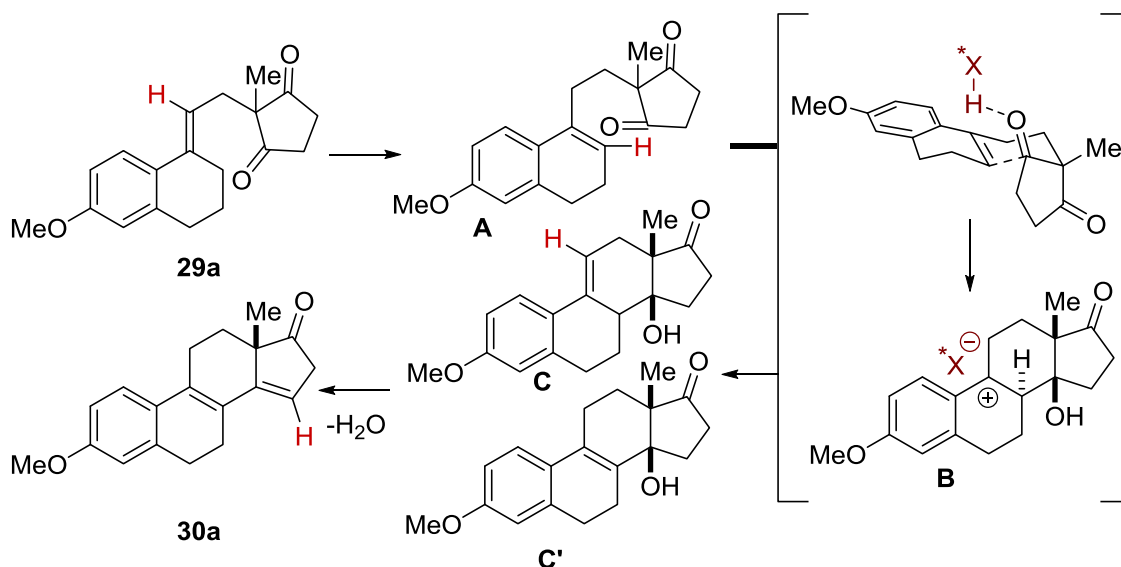
Scheme 4.14: The Brønsted acid catalyzed asymmetric Torgov cyclisation.

To obtain a better mechanistic insight, we conducted the reaction in an NMR tube and monitored its course over time by ¹H NMR (Scheme 4.15). In order to perform this cascade in an NMR tube we slightly modified the optimized conditions. The reaction was conducted at slightly higher temperatures (0 °C), in the absence of molecular sieves and with a lower catalyst loading to compensate the higher reaction temperature.



Scheme 4.15: Kinetic NMR data for the reaction of **29a** with 1.5 mol% of cat. **96** in toluene- d_8 .

Immediately after adding the catalyst **96** to the reaction mixture, a new olefinic proton signal ($\delta_{\text{H}} = 5.5$ ppm) was observed, which we assigned to the isomerized product **A** and which is also present in our proposed catalytic cycle (Scheme 4.16).



Scheme 4.16: Proposed mechanism of the Torgov cyclisation.

In parallel also two other signals are observable. These signals belong to alcohol **C** ($\delta_{1H} = 5.67$ ppm) and the product **30a** ($\delta_{1H} = 5.41$ ppm). After 60 min under the reaction conditions, almost all of the starting material was converted either to the cyclized intermediates or further to product. Subsequently the intermediate **C** is slowly converted into the product. These observations are consistent with the experimental observations during the development of the reaction. In order to achieve a faster product formation, a temperature gradient was applied. A lower reaction temperature (-40 °C) was applied for the cyclisation. Afterwards the reaction temperature was increased to -10 °C to accelerate the elimination step. A further raise of temperature could not be applied, due to the decreased enantioselectivity of the product possibly through a retro ene reaction.

In our NMR experiments we could not observe the formation of the rearranged intermediate **C'**. This indicates, that the acid-catalyzed isomerization of the double bond from **C** to **C'** and not the elimination of water is the rate determining step of the reaction.

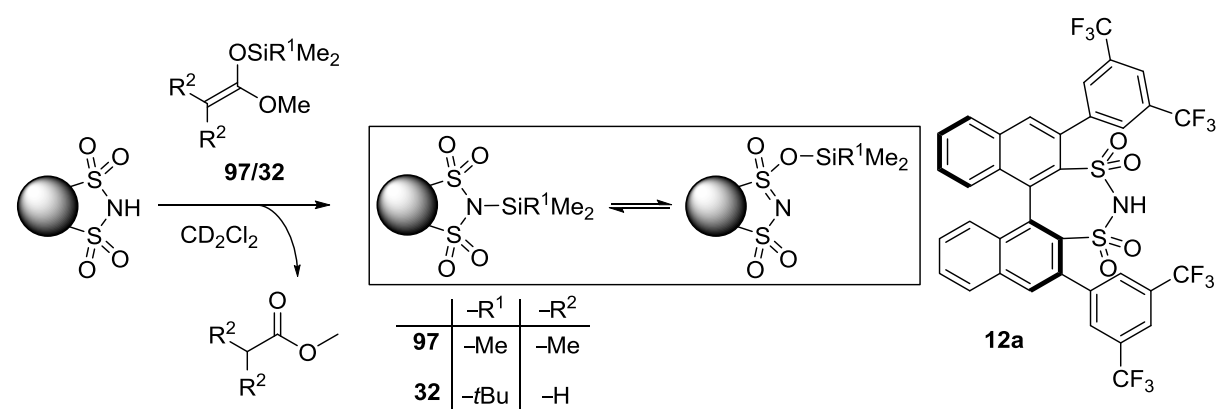
4.2.2 Silylation Trends of Disulfonimides

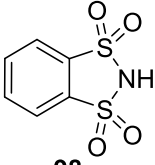
These experiments were conducted together with Dr. Z. Zhang. Previous investigations in our group were conducted by F. Lay.

Chiral disulfonimides (DSIs) are precursors for powerful chiral Lewis acids. Under the reaction conditions DSIs are silylated by silyl enol ethers by protonation and silicon transfer. One advantage of this methodology is the self-healing ability of the catalyst that can be re-silylated after it is quenched by small amounts of water in the reaction.

The silylation of a DSI can lead to two different species, either by *N*- or *O*-silylation (Table 4.5). Both species have been characterized by NMR spectroscopy in solution for flexible disulfonimides, as for instance triflimide (**99**, (CF₃SO₂)₂NH).^[115,116] In order to understand the silylation behavior of conformationally fixed disulfonimides, as is the case for BINOL derived DSIs, further NMR experiments were conducted. Therefore two catalysts were chosen as representatives of this class. These catalysts were titrated with different silyl ketene acetals until the signal of the acidic proton completely disappeared.

Table 4.5: Comparison of the silylation of various DSIs



Entry	Silylating agent	DSI	Ratio <i>N</i> : <i>O</i> ^a	$\delta^{29}\text{Si}$ (ppm)	
				<i>O</i>	<i>N</i>
1	97	3,5-CF₃-C₆H₄-DSI	1:3	40.38	24.89
2	32	12a	1:10	42.49	28.25
3	97		>99:1	-	21.81
4	32	98	1:2	43.86	28.95
5 ^{[115],b}	(Me₃Si)₂NH	(CH ₃ SO ₂) ₂ NH	-	39.72	22.61

Results and Discussion

6 ^[116]	HSi <i>t</i> BuMe ₂	99	<1:99	-	-
7 ^[117]		(CF ₃ SO ₂) ₂ NTMS			55.9

^a The ratios were determined by ¹H-NMR, ^b CDCl₃ was used as the solvent.

Upon silylation two different sets of signals between 0.8 and –0.5 ppm appeared in the ¹H-NMR spectrum, which can be assigned to two different silyl groups. Additionally two separate sets of aromatic NMR signals appeared. The silyl groups were further characterized by ¹H-²⁹Si-HMBC (Figure 4.16). This method was the most suitable for these studies, because the corresponding ²⁹Si NMR shifts could be obtained in short times and directly correlated to the species. Other possible NMR measurements, as for instance ²⁹Si-INEPT or ²⁹Si-DEPT showed various other signals from different silylethers, which were generated upon in situ silylation or excess of starting material. Assignment of the correct shift in this case is more difficult. Additionally these experiments are also less sensitive compared to the 2D measurement due to the direct measurement of ²⁹Si. The obtained ²⁹Si chemical shifts are in good agreement with a previously reported example.^[115] We have also investigated the silylation behaviour of (biaryl)-hydroxy-acid (HYDRA) catalysts **16**.^[73] Unfortunately, upon excess of silyl enol ethers in our measurement, they were partially silylated on the Brønsted acidic OH-moiety and mixtures became very complex.

A general trend that is observed in our studies is the preference of the silicon towards O-silylation with increasing sterical demand of the silyl group. This result is in good agreement with previous work by *Simchen* and *Jonas*, who described this trend for the silylation of triflimide with HSi*t*BuMe₂.^[116] The ratio of *N*-TMS-**12a** and *O*-TMS-**12a** was determined to be 1:3 based on the ¹H-NMR-signal of the BINOL-Backbone. In contrast to this, the ratio of *N*-TBS-**12a** and *O*-TBS-**12a** was determined to be 1:10. The proton signal of the TMS group in *O*-TMS-**12a** was very broad indicating a fast exchange of the TMS group in the two possible diastereomeric structures of *O*-TMS-**12a**. In contrast to this, *O*-TBS-**12a** showed two distinguishable diastereotopic methyl signals and so just one diastereomer was preferably formed. The *N*-silylated forms of the catalyst did not lead to diastereomeric methyl group signals due to the C₂-symmetry of these species.

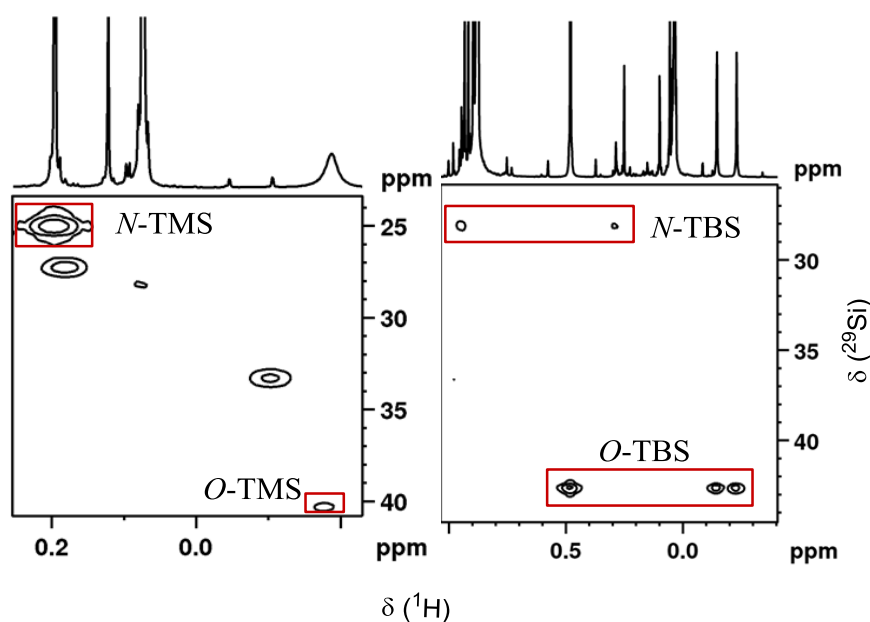


Figure 4.16: ^{29}Si -HMBC spectra of in situ silylated DSI; left: ^{29}Si -cross signals of O- and N-TMS **12a**, right: ^{29}Si -crosssignals of O- and N-TBS **12a**.

In order to show the silatropy and the equilibria between different silylated species, we conducted 2D-EXSY measurements (Figure 4.17). In all of the investigated substrates we observed an EXSY cross peak between the different silyl signals. This showed nicely, that the two distinguished species are indeed interconverting into each other. This fact has originally been investigated and shown in variable temperature measurements.^[115]

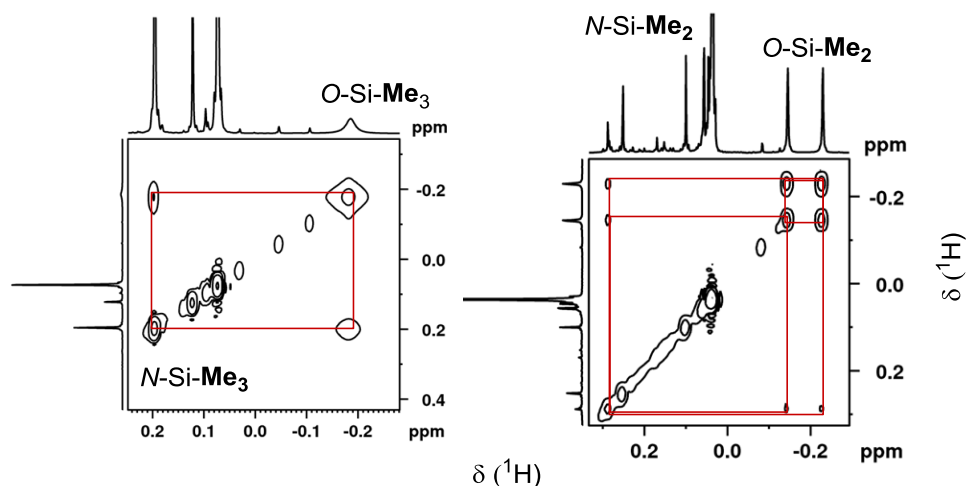


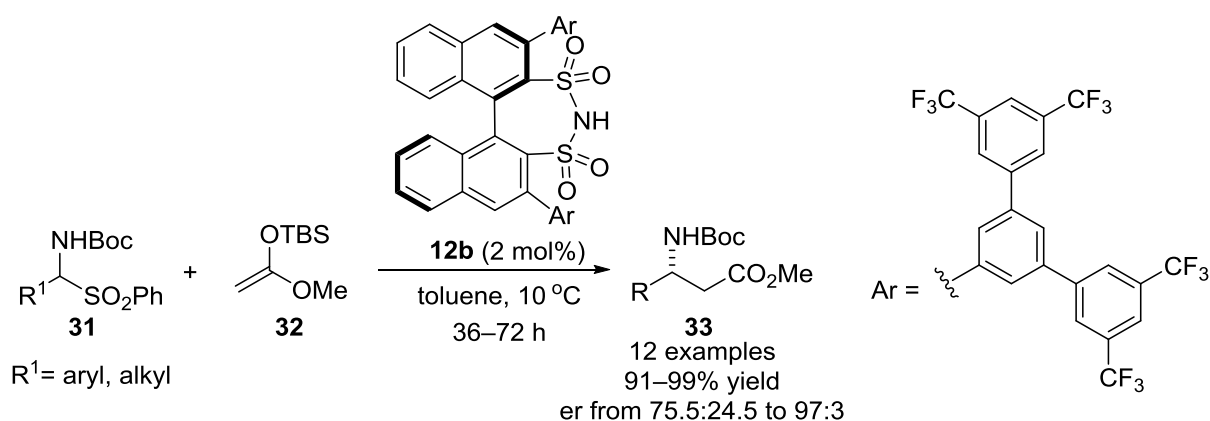
Figure 4.17: 2D-EXSY-spectra; left: Exchange of O- and N-TMS **12a**, right: Exchange of O- and N-TBS **12a**.

The fast exchange between the silyl species is explained by the fact that the oxygen–/nitrogen–silicon bond is rather weak. This increases the cationic character of the silicon. By comparing the ^{29}Si chemical shifts and structural preferences of the silicon it is still rather difficult to conclude a concept about the potentially more Lewis acidic sites of the silylated catalyst.

4.2.3 Intermediates and Reaction Profiles of the DSI catalyzed Synthesis of β^3 -Amino Esters from *N*-Boc-Amino Sulfones

These experiments were conducted in collaboration with Dr. Q. Wang.

Recently our group developed a protocol which applied asymmetric counteranion-directed catalysis (ACDC) for the first asymmetric Mannich reaction catalyzed by an organic Lewis acid using silyl ketene acetals, directly from *N*-Boc-amino sulfones (Scheme 4.17). The catalyst **12b** gave the desired products in excellent yields and enantioselectivities. Our new protocol had several advantages compared to the previous reported^[118]: commercially available ketene acetals could be used, the *N*-Boc-amino sulfones **31** are more stable than previously applied *N*-Boc-imines and one step could be saved. In addition, the reaction could be easily monitored by homogenization with conversion, only a low catalyst loading was necessary and the products were easy to recrystallize.



Scheme 4.17: DSI catalyzed synthesis of β^3 -amino esters from *N*-Boc-amino sulfones.

During the development of the reactions, we became interested in the reaction intermediates. In the usual protocol the reaction mixture is immediately quenched on silica, purified and the corresponding *N*-Boc-imines are obtained as products. Initial IR-investigations by Dr. Q. Wang showed that prior to work-up, other products are present in the mixture. Before we were able to follow the reaction by NMR we had to slightly change the reaction conditions again in order to have optimal conditions for our NMR measurements. The solvent had to be changed from toluene to chloroform to ensure a homogenous solution during the reaction, since heterogeneous reactions are usually harder to investigate. If heterogeneous reactions shall be monitored, a system for online NMR monitoring is necessary. Although the enantioselectivity might change during the reaction, the overall mechanism should still be similar. Our first investigation aimed to determine the structure of the products. After the reaction proceeded we observed two

different main products *N*- and *O*-TBS-**33** in a ratio of ~ 6:1 at 4.85 ppm and 5.00 ppm (Figure 4.18). Other two side products *N*- and *O*-TBS-**100** were generated in the same ratio together with equimolar amounts of *iso*-butene **101**. These side products can be explained by an elimination of *iso*-butene upon activation by residual amounts of Brønsted acid in solution. The generated *N*-carbamic acid is then in situ silylated prior to decarboxylation. However under the optimized reaction conditions in toluene these side products could not be observed. In our experiments, they were just generated in the initial period of the reaction and might be generated by small amounts of residual Brønsted acid in solution.

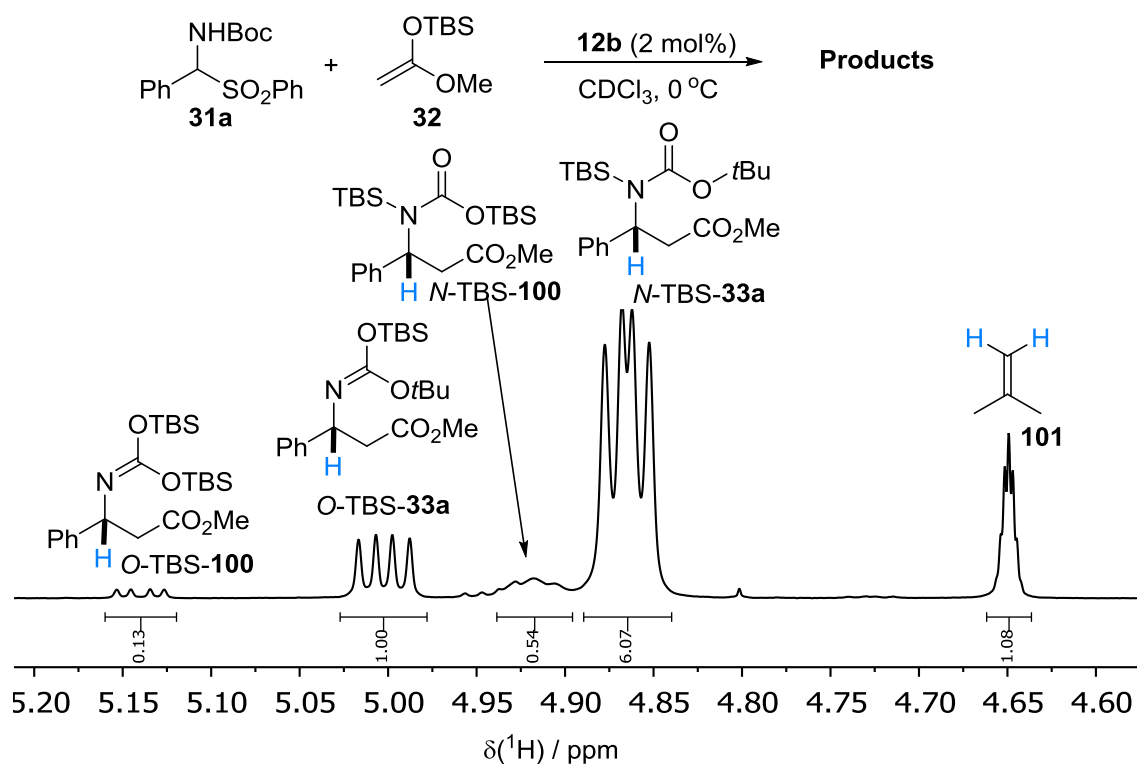


Figure 4.18 $^1\text{H-NMR}$ spectrum of the CHN signals of the reaction mixture (at 20°C). The reaction was performed at 0°C.

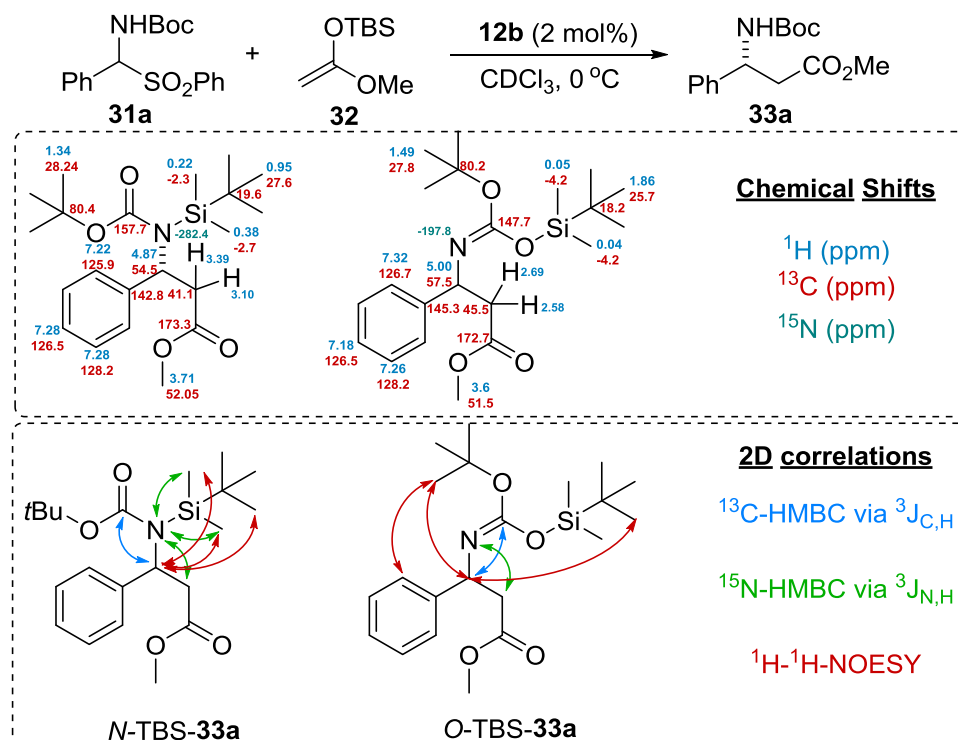


Figure 4.19: NMR data of the reaction intermediates.

The intermediates were analyzed in situ by standard 2D-NMR methods (^1H - ^{13}C -*edited*-HSQC, ^1H - ^{13}C -HMBC ^1H - ^{15}N -HMBC, ^1H - ^1H -COSY, ^1H - ^1H -NOESY). With the spectra in hand, we were able to assign the atoms and to determine the structure of these intermediates. The assigned chemical shifts and some important 2D-correlations are presented in Figure 4.19. To our surprise the NMR data suggests two different regioisomers, in analogy to the regioisomers observed for the silylation of the DSI catalysts in the previous chapter. The CH-N NMR signal of *N*-TBS **33a** and the methylene protons are broadened due to the amide rotation of the Boc-group. In contrast to this the NMR signals of the CH-N in *O*-TBS **33a** are sharp because no rotamer formation is possible in this case. In addition the Me_2Si -group of *N*-TBS **33a** shows a cross peak in the ^{15}N -HMBC spectrum to the nitrogen nucleus indicating that the silyl group is indeed attached to a nitrogen. In the other isomer, no crosspeak is observed. Comparing the ^{15}N shifts of these two isomers showed, that they are significantly different (*N*-TBS -282.4 ppm vs. *O*-TBS -197.8 ppm), which finally proves the different electron density on the nitrogen. We were also interested, if these two species have a silatropic equilibrium. At 0°C no fast exchange could be detected. When we kept the sample some time at room temperature, only the major regioisomer *N*-TBS **33a** could be observed. This proves a slow equilibration towards the thermodynamically more stable isomer.

After determination of the intermediate formation, we became interested in the course of the reaction. Therefore we conducted the reaction again in an NMR tube and this time we acquired proton NMR spectra in constant time intervals. The result of this NMR kinetic investigation is shown in Figure 4.20. The obtained NMR data is in good agreement with our proposed reaction mechanism (Scheme 4.18). At the beginning of the reaction we can observe a rapid formation of a new species. Interestingly, the catalyst rapidly silylates sulfone **31a** to the corresponding *N*-silyl derivative TBS-**31a**, which CHN signal appears at 5.62 ppm as a singlet (cycle I). A small but detectable quantity of *N*-Boc-imine **101** ($\delta_{\text{CHN}} = 8.75$ ppm) is then generated via a slow and apparently rate determining elimination of PhSO₂TBS from silylated sulfone **31a**, initiating catalytic cycle II. The rate of this step might be influenced by the electronic properties of the sulfones. Reactions with more electron rich sulfones proceeded much faster during our studies and they had almost no influence on the enantioselectivity. The free imine is activated by the catalyst through an ion pair formation (**A**), which together with the ketene acetal **32** then assembles transition state **B** that leads to the two different silylated products and the regeneration of the catalyst.

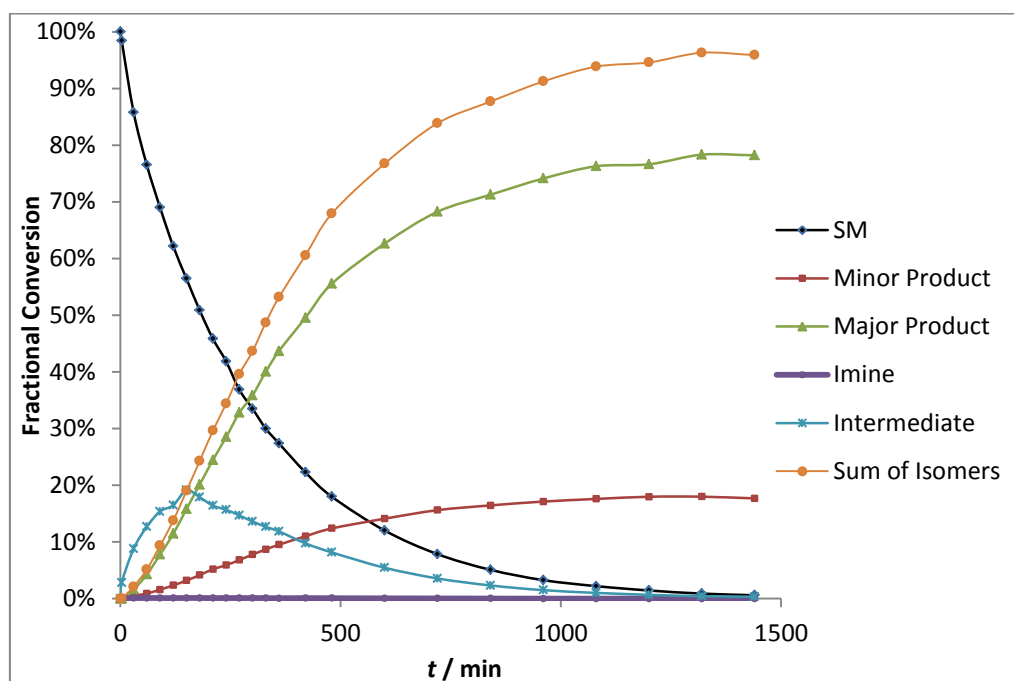
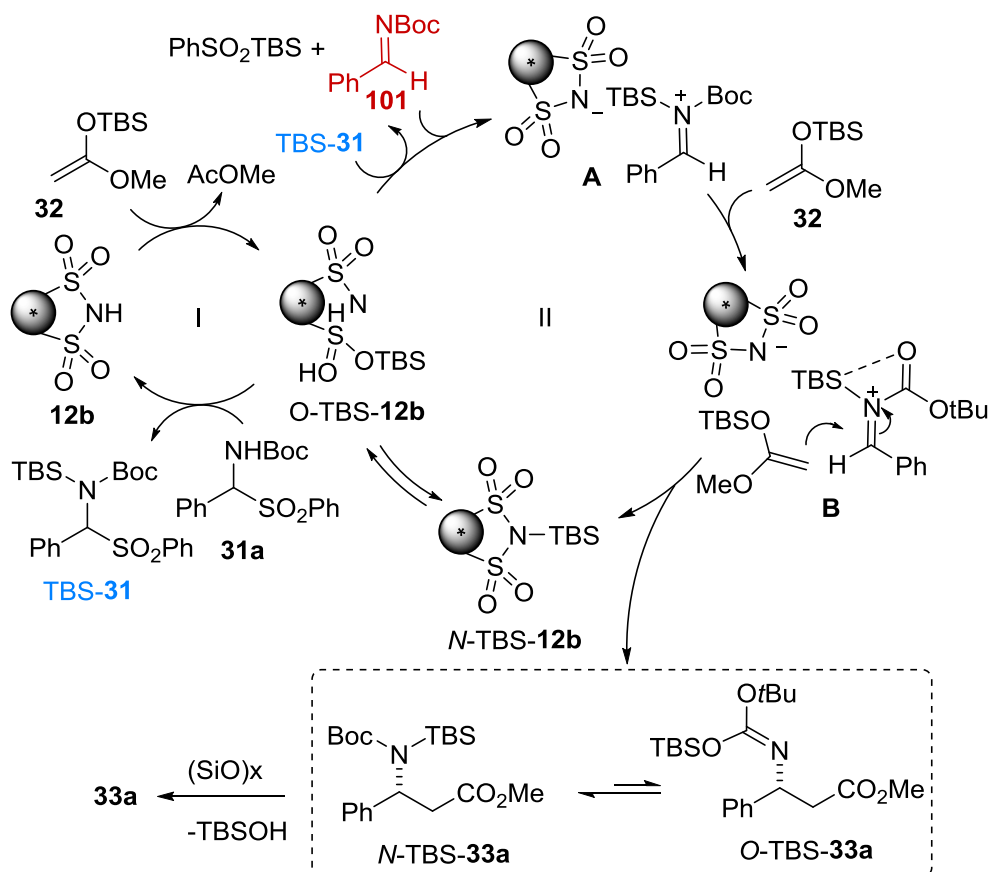


Figure 4.20: Kinetic NMR data of the reaction of substrate **31a** with silyl ketene acetal **32** and 2 mol % of catalyst **13b** in CDCl₃ at 0 °C.



Scheme 4.18: Proposed mechanism for the DSI catalyzed formation of β^3 -amino esters from *N*-Boc amino sulfones.

When the reaction was monitored until all the silyl ketene acetal **32** was converted or quenched by water, all the species **TBS-33a** and **TBS-100** were converted into the new silylated species **102**. This proves that Brønsted acid is responsible for the formation of isobutene and the importance of an excess of silyl ketene acetal in solution.

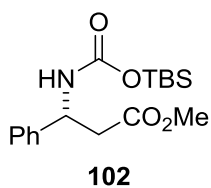


Figure 4.21: Desilylated product **102** formed upon desilylation and deprotection by Brønsted acid **13b**.

4.3 Unexpected Carbene Intermediates in the *Trans*-Hydrogenation of Internal Alkynes

This part of the PhD thesis was performed in the NMR Department of the Max-Planck-Institut für Kohlenforschung under supervision of Dr. Christophe Farès. After our preliminary investigations we initiated a collaboration with the group of Prof. Dr. A. Fürstner. To further understand and explain our results a collaboration with the computational group of Prof. Dr. W. Thiel was started. The results obtained from this joint interdisciplinary venture and the involved colleagues will be mentioned in the corresponding subchapters.

4.3.1 Parahydrogen Enrichment

Before conducting initial experiments on the *trans*-hydrogenation of terminal alkynes, enriched $p\text{H}_2$ was required. Therefore, we initially tried to enrich the *parahydrogen* to 50% by using a simple autoclave filled with activated charcoal and commercial hydrogen that was cooled with liquid nitrogen (Figure 4.22). Usually the enrichment of

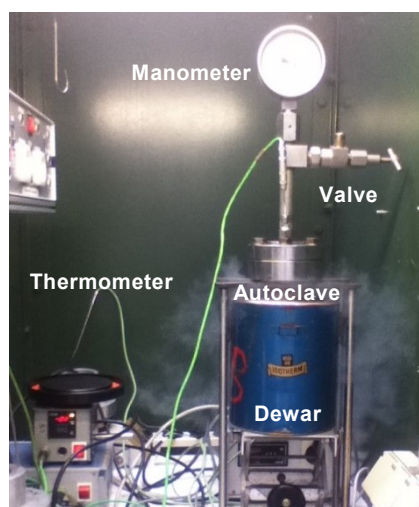


Figure 4.22: Autoclave for $p\text{H}_2$ enrichment

parahydrogen is determined by Raman spectroscopy^[119] or thermal conductance measurements^[120]. The ratio can also be determined directly by $^1\text{H-NMR}$ by comparing thermal hydrogen (25% *para*) to the enriched sample.^[121] Due to the missing equipment, we decided to determine the enrichment chemically. If we enriched hydrogen, the hydrogenation of phenylacetylene in the presence of Wilkinson's catalyst (10 mol%) should lead to a strong signal enhancement of the styrene and ethylbenzene signals as shown previously by Eisenberg *et al.*^[81] The initial results were non-satisfying. The problem of the autoclave was a insufficiently cooling of the gas in the

reactor, so that we decided to build a U-shaped tube with better surface-to-volume ratio, similar to the experimental setup reported by Bargon before (Figure 7.1, page 134). The higher outer surface of the tube allowed the sufficient cooling of the inner part of the tube. With the help of the workshops of our institute the tube was produced and the obtained results for our test reaction were promising, but further optimization was required. Therefore, the activated charcoal was mixed with Fe_2O_3 . The new catalyst mixture did not improve the results. After reducing the catalyst loading to 1 mol% and using high pressure NMR tubes, satisfactory results were finally obtained (Figure 4.23).

Results and Discussion

Higher catalyst loadings seemed to promote the relaxation of the hydrogen, so that the observed signals were less intense.

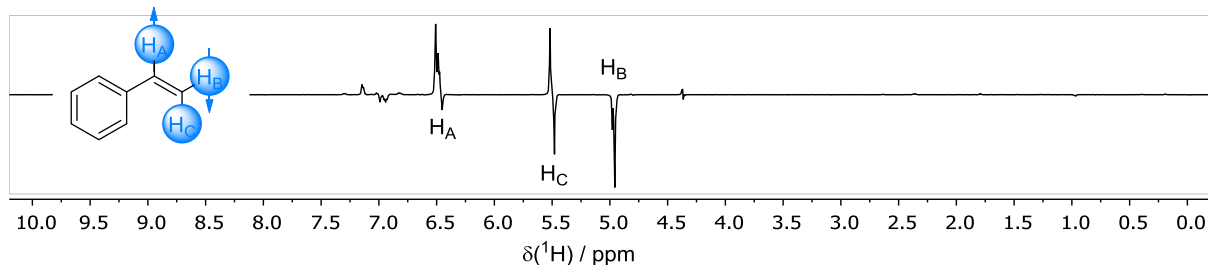


Figure 4.23: ^1H -PHIP-NMR spectrum for the hydrogenation of phenylacetylene with $\text{Rh}(\text{PPh}_3)_3\text{Cl}$ in C_6D_6 as a test reaction for the *parahydrogen* enrichment.

At a later stage of our studies, we started to use a *parahydrogen* generator, on loan from Bruker Biospin, which is able to enrich $p\text{H}_2$ up to 92%. The use of this hydrogen will be mentioned in the corresponding schemes.

4.3.2 Initial Experiment on the *Trans*-Hydrogenation of Internal Alkynes

After establishing the *parahydrogen* enrichment and measurement conditions, we were interested in determining, if the *trans*-hydrogenation protocol published by *Fürstner* and his coworkers^[100] is proceeding via a similar mechanism as the previously reported reaction by *Bargon et al.*^[94] If this was the case, the hydrogen atoms in the product would originate from the same hydrogen molecule and a strong signal enhancement of the alkene signals of the product would be detected. As a starting point we used the reported conditions, 2-hexyne **22a** as the substrate and 5 bar of hydrogen pressure under ALTADENA conditions. The NMR tube was loaded with *parahydrogen*, shaken for 30 s and then transferred into the magnet and a spectrum was acquired. As expected, we observed a hyperpolarization of the *trans* signals at around 5.3 ppm (Figure 4.24). Other product signals in the aliphatic region of the ^1H spectrum were also strongly enhanced. This is explained by the magnetization transfer of the strongly coupled spins at low field before transferring the sample into the higher field. Unfortunately, we could not observe any other hyperpolarized signals in the hydride region, in agreement with the previous results by *Bargon.*^[94]

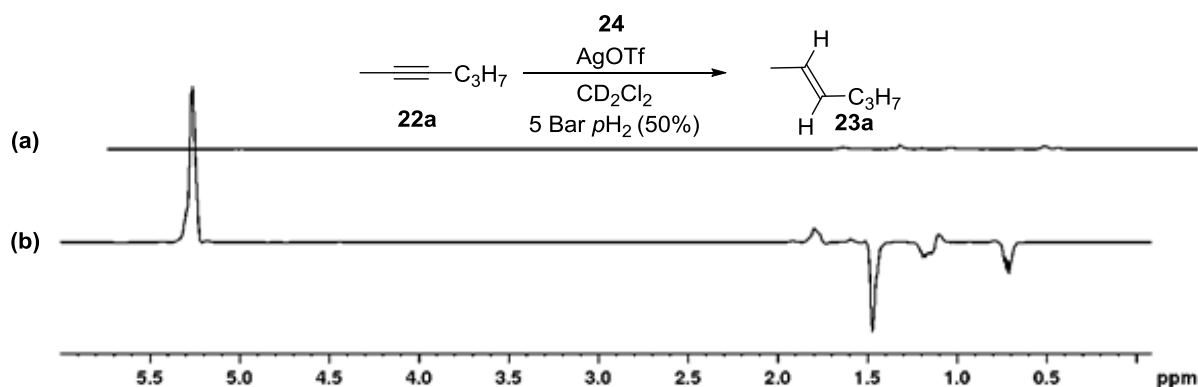


Figure 4.24: Comparison of the spectra at thermal equilibrium (a) and the PHIP-spectrum under ALTADENA-conditions (b).

Bargon explained this observation with the high symmetry in the intermediates and the resulting chemical equivalence of the hydrogen atoms in the intermediate (see Scheme 2.10 on page 20). In order to break the symmetry of intermediates, a chiral substrate or counter anion could be introduced for inducing diastereotopicity on the hydrogen atoms and thus, strongly enhanced hydride signals of the intermediate would be observable. This methodology is inspired by the ACDC (Asymmetric Counteranion-Directed Catalysis) concept^[122] first introduced by *List* and his coworkers, which in a variety of cases has been shown to induce chirality during reactions. Unfortunately, we could not observe enhanced signals of hydride intermediates during these experiments. On the one hand this can be explained by an inexistence of these intermediates, but also by their potential short lifetime, a broadening of the hydride signals due to a paramagnetic Ru^{III} species in the mixture or a low induced diastereotopicity on the protons.

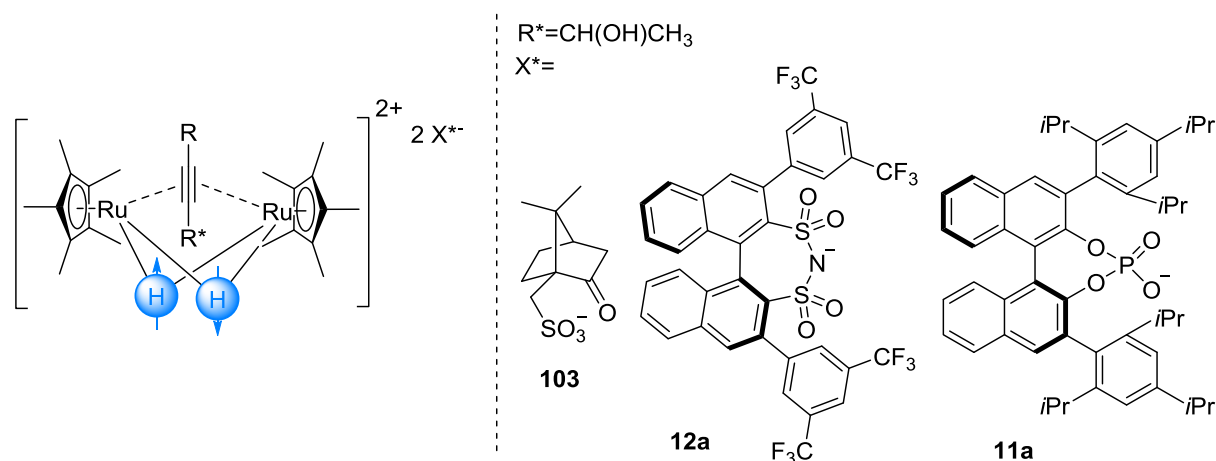


Figure 4.25: Opportunities for the induction of diastereotopicity by either chiral substrates or counter anions.

In all reactions tested so far, no enhanced intermediate signals could be observed. Interestingly, we could observe several non-hyperpolarized hydride signals at around -7.0 ppm and -8.5 ppm at higher conversions (Figure 4.26) in the reaction of 2-hexyne

22a that were still present after the full conversion of the starting material. These signals are not the same as previously described by *Fürstner*.^[100] The low field signals are triplets, indicating a coupling to two protons, whereas the corresponding high field signals are multiplets or pentets showing, that another non-hydride species is part of the complex. After integration of those signals it can be concluded that three different hydride complexes in a ratio of 1:2.5:1.2 are formed. Each hydride complex contains several hydride species in a ratio of 1:2 or 2:2:2, which hints to a dimeric nature of the complex. In order to further characterize these species we conducted 2D NOESY and COSY measurements (Figure 4.27) in order to potentially detect some involved ligands. In the COSY spectrum it clearly can be seen that the low field hydrides around -7 ppm couple to one or two different hydride species at higher field. In addition, the high field hydrides are coupled to a signal in the aliphatic region at around 1.2 ppm. A further, unambiguous characterization of this signal was hardly possible due to a high overlap of other species. It can either be a normal aliphatic signal or an olefinic CH, which is strongly shifted due to π -interactions of the double bond with the ruthenium. The characterization of the carbon correlations via HMBC spectra did not give any cross signals due to the low concentration of this species in solution. The NOESY spectra gave some further structural information about the complex. The coupling hydrides are spatially close to each other. In addition, the low field hydrides are in proximity to the Cp* and another aliphatic signal, which could be an aliphatic signal close to a sp^2 carbon. The high field hydrides are in proximity to at least two different aliphatic signals.

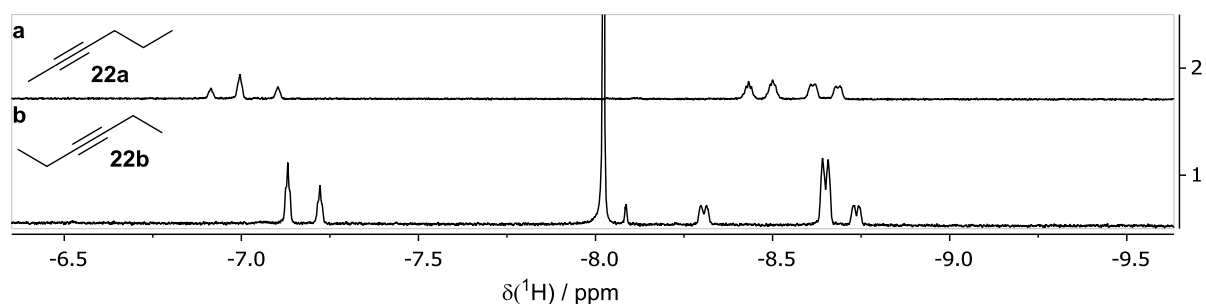


Figure 4.26: Comparison of the observed hydride signals with 2-hexyne **22a** (a) or 3-hexyne **22b** (b) as substrates for the hydrogenation.

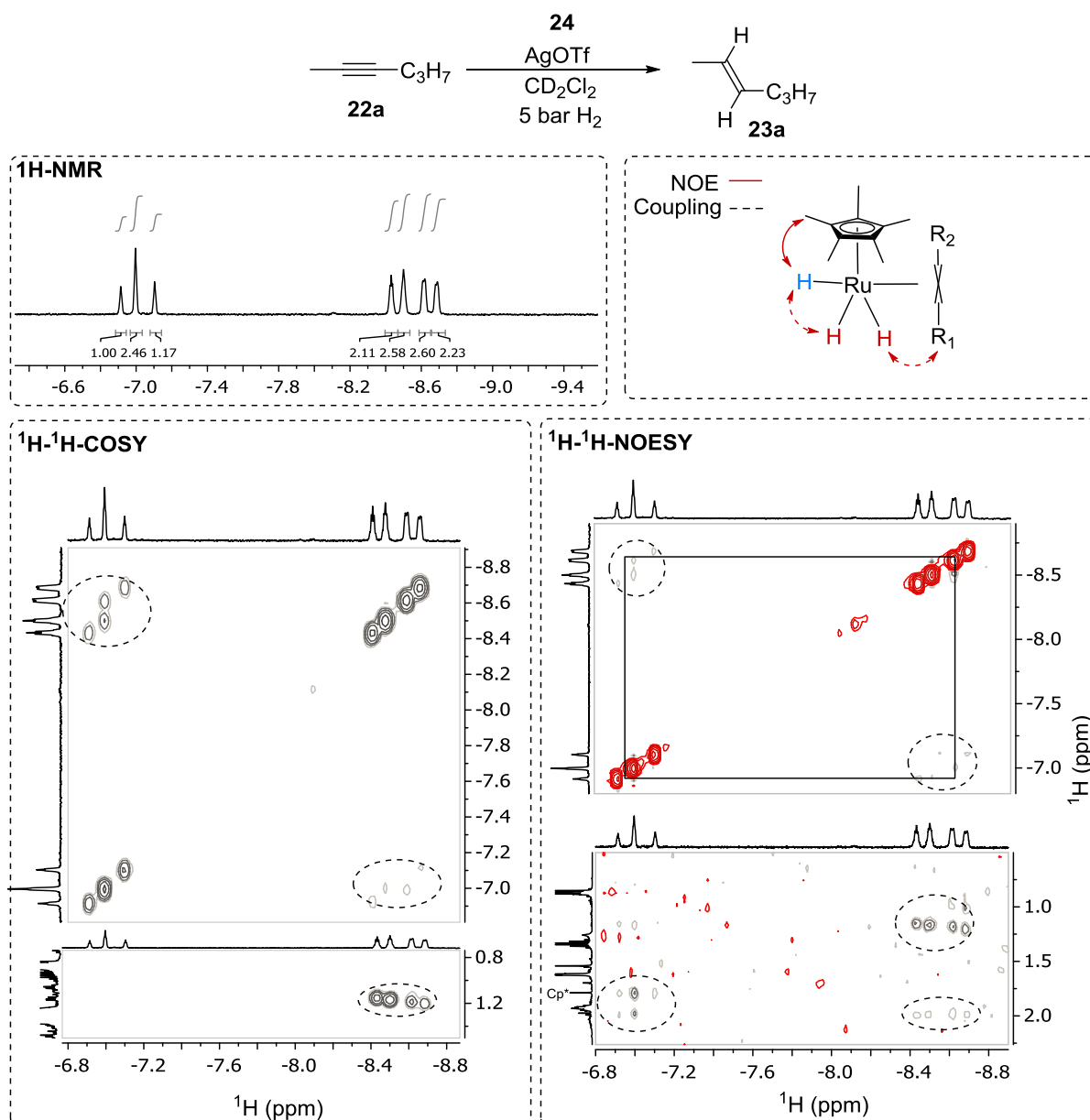


Figure 4.27: Observed hydride species after the hydrogenation of **22a** with $\text{Cp}^*\text{Ru}(\text{cod})\text{Cl}$ **24** and AgOTf.

With these results in hand a structure proposal is not conclusive. In order to determine if the alkyne or a derived product/isomer is part of this complex, we conducted the reaction in the presence of the symmetrical 3-hexyne **22b** (Figure 4.26). Interestingly, two different hydride signals were generated, showing similar cross peaks in the 2D NMR spectra as complexes derived from 2-hexyne **22a**. In addition, the hydride species previously reported by *Fürstner* are also visible in this case.

In literature, several different ruthenium hydride complexes with a Cp^* ligand have been described (Figure 4.28). However the described polyhydride complexes are highly symmetric resulting in a single proton signal, which is in stark contrast to our observations. However, the hydride chemical shift of complex **107** is close to ours and could provide a structural hint.

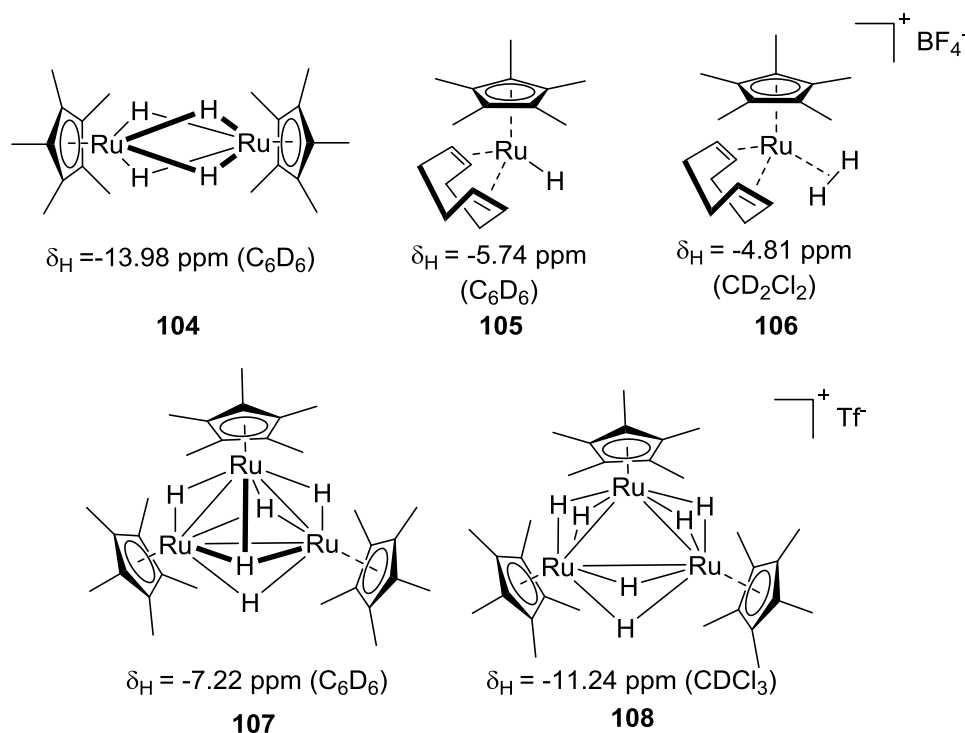


Figure 4.28: Characterized RuCp^* hydride/hydrogen complexes that could be formed during the reaction by *Suzuki*^[123–125] and *Lau*.^[126]

In order to determine the structure of the intermediate, we took a closer look on the previously reported hydride signals by *Fürstner*^[100] at -4.96 , -8.02 and -13.42 ppm during the hydrogen treatment of $\text{Cp}^*\text{Ru}(\text{cod})\text{Cl}$ **24** and AgOTf in CD_2Cl_2 . To our surprise we could observe an additional hydride signal at -13.28 ppm, which has not been reported before. In contrast to *Fürstner* we found some literature evidence, that the signal at around -8.00 ppm could be assigned to the bridged penta-hydride trimer, but the shift does not fit exactly. One explanation could be the solvent dependency of the shifts.

For further characterization of these species a 2D NOESY experiment was conducted. Interestingly, three of the four hydride species showed an EXSY cross peak, which indicates that they are interconvertible. All the hydride signals showed cross peaks to the methyl groups of the Cp^* ligand at around 1.8 ppm. With the NOE cross peaks, it was possible to assign the corresponding Cp^* ligands. The integration revealed that the overall ratio in the symmetric complex is $\text{Cp}^*:\text{H} = 4:5$ and for the asymmetrical complex $\text{Cp}^{*1}:\text{Cp}^{*2}:\text{H}_\text{A}:\text{H}_\text{B}:\text{H}_\text{C} = 2:1:1:1:2$.

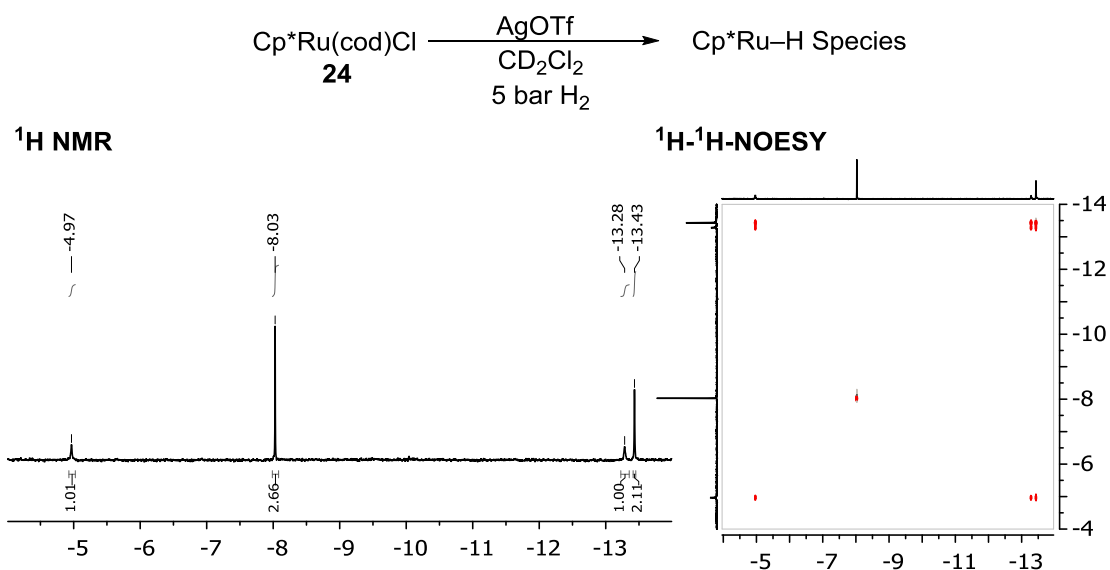


Figure 4.29: ^1H -NMR and ^1H - ^1H -NOESY spectra of $\text{RuCp}^*(\text{cod})\text{Cl}$ and AgOTf under reductive conditions at room temperature.

At this point, the sample was cooled to suppress the interconversion of the hydride signals. Therefore the sample was cooled to $-40\text{ }^\circ\text{C}$. To our surprise three new hydride species appeared at -9.51 , -10.48 and -10.77 ppm. The structure of these could be similar to the literature-known trimeric hexahydride complex **107**. In the 2D-NOESY spectra the exchange process was suppressed as expected, so that we could now confirm the close spatial arrangement of the hydrides in the complex with the three signals.

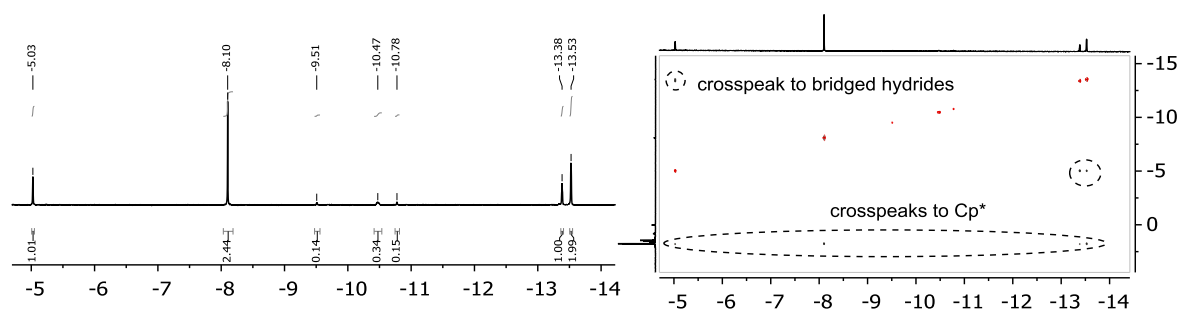


Figure 4.30: ^1H -NMR and ^1H - ^1H -NOESY spectra of **24** and AgOTf under reductive conditions at $-40\text{ }^\circ\text{C}$.

With our observations, we could make a coherent prediction for the observed signals based on a comparison with literature known complexes and on our results from the NMR measurements (Figure 4.31). The signal at -8.02 ppm could belong to a tetrameric ruthenium complex **109** that is bridged by several hydrogen atoms. The other complex has to be an asymmetric species such as **110**, having at least three μ_2 -bridged hydrogens, that have signals at around -13.5 ppm. The other signal can be derived from either a hydride or formally a hydrogen molecule, trapped by two ruthenium trimers. It should be mentioned that all the proposed structures are only speculative based on the

Results and Discussion

NMR correlations. Only X-ray structural analysis could give the final solution. NMR measurements in general do not deliver information about other ligands, as for instance chloride ions, that are invisible due to their quadrupole properties or are simply NMR inactive.

To figure out whether these hydride clusters are catalytically active species or not, we prepared the cluster mixture in situ in the NMR tube, to see its formation. After the release of hydrogen pressure and the addition of 2-hexyne **22a**, the hydride complexes were still present in solution without significant change of concentration. At lower temperatures we observed, that the signals at around -10 ppm disappeared when an atmosphere of argon was used. Additionally, a product formation of **23a** could not be observed. The complexes did not seem to release hydrogen for the product formation and are therefore not catalytically active.

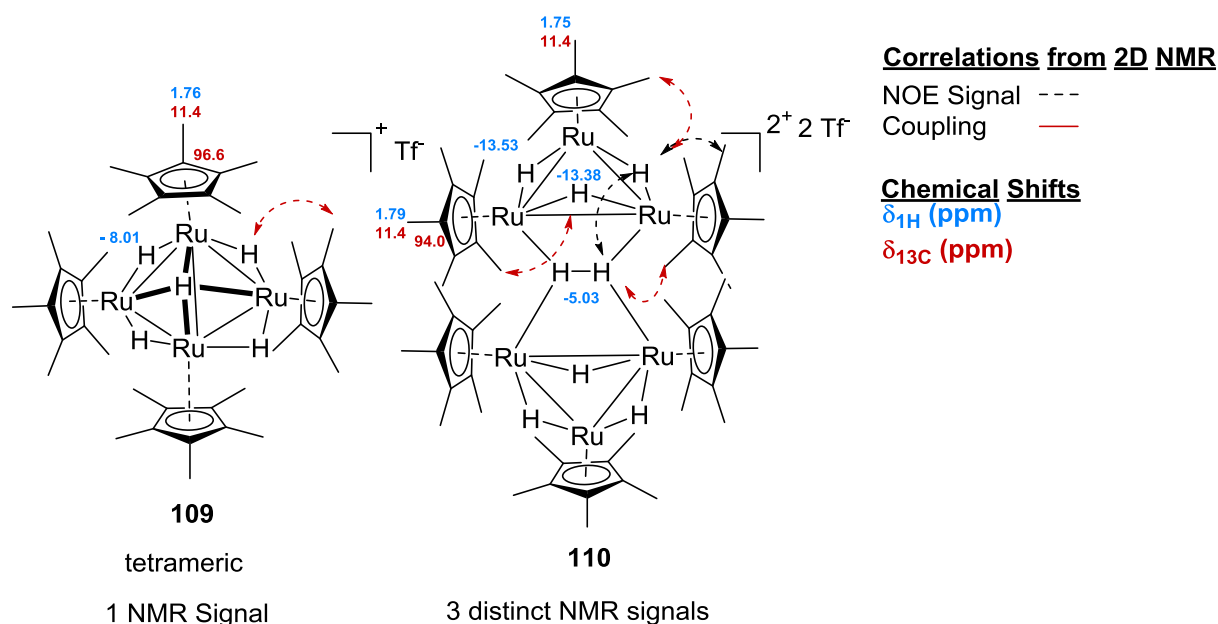


Figure 4.31: Structural proposals for the observed hydride species based on literature comparisons with assigned chemical shifts at -40 °C in CD_2Cl_2 .

After exchanging the argon atmosphere to hydrogen, product formation was observed, indicating that the catalytically active hydride species, such as for instance a monomeric ruthenium hydride, has never been detected in our measurements. Interestingly, also the previously described hydride signals can be obtained during the reaction. This again shows that the formed complex might contain one or more olefinic ligands. One possible solution is shown in Figure 4.32 which is based on the idea, that the cationic catalyst species might accelerate the dimerization of the alkyne leading to two different regioisomers. This would give a possible explanation for appearance of several different hydride species.

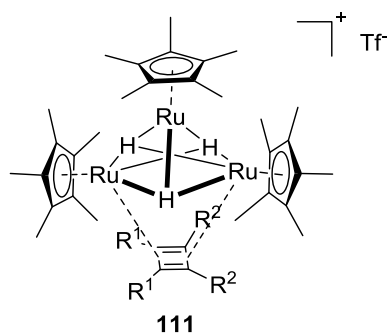


Figure 4.32: Possible hydride complex formed during the hydrogenation of internal alkynes with RuCp*(cod)Cl and AgOTf in CD₂Cl₂.

At this point, we started to collaborate with Dr. M. Fuchs from the group of Prof. Dr. Fürstner to further investigate these results. Due to its preorganization by coordination of the alcohol via hydrogen bonding to the chloride ligand of the ruthenium catalyst Cp*Ru(cod)Cl **24** 1-(1-propyonyl)cyclohexanol **112a** was chosen as the next substrate for our investigation.^[103]

4.3.3 Observation and Characterization of (Metastable) Carbene-Intermediates

During the reaction of 1-(1-propyonyl)cyclohexanol **112a**, we could observe hyperpolarization on the generated *trans* product (Figure 4.33). Also this time, no hyperpolarized signals have been observed in the hydride region of the ¹H-NMR spectrum. Moreover, only a proton low field chemical shift of –1.14 ppm was observed in this region. This signal can be assigned to the alcohol of the starting material coordinated to the catalyst.

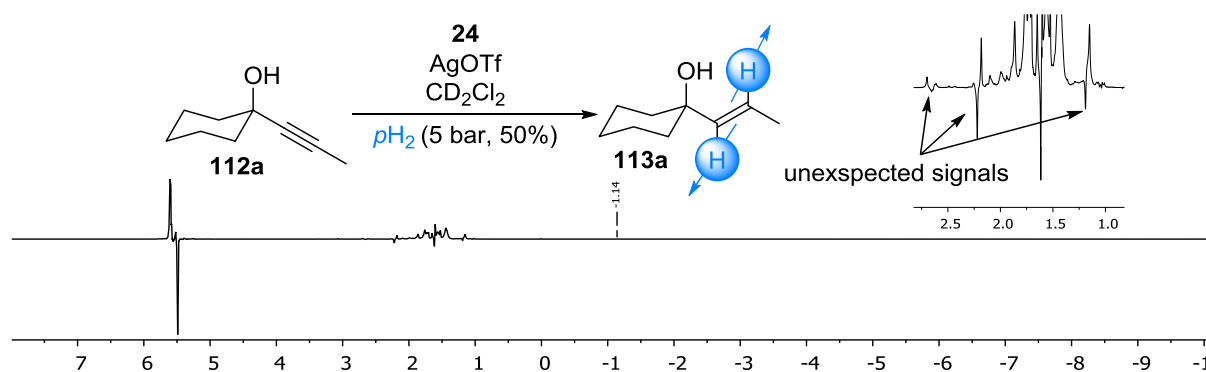
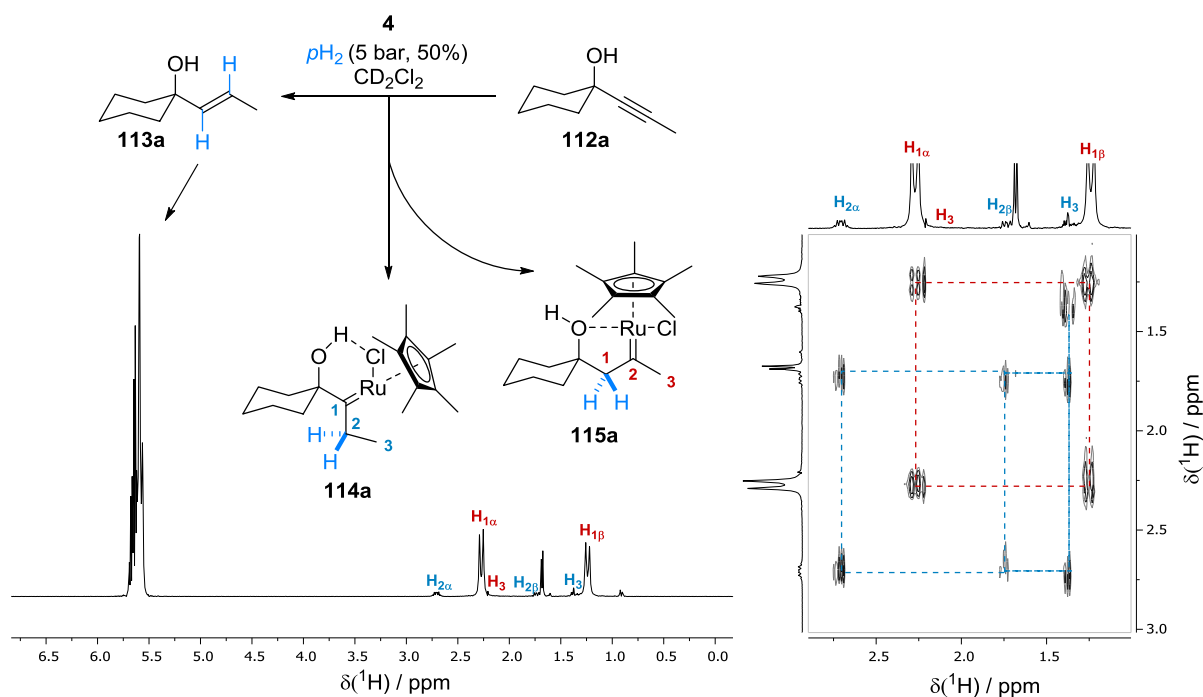


Figure 4.33: ¹H-PHIP NMR spectrum during the hydrogenation of **112a** with 5 bar of enriched pD₂.

To our big surprise we observed new, additional antiphase signals at 2.64 (dq), 2.20 (d) and 1.16 ppm (d), which had the opposite intensities of the usual antiphase pattern, indicating negative coupling constants of the coupled protons. In general only geminal protons can have negative coupling constants of this magnitude.^[127] The signals belong to two distinct species. The two doublets have a coupling constant of ~ –19 Hz, whereas the third signal is coupled to another undetectable proton with –14 Hz. In

Results and Discussion

monounsaturated five-membered rings, a geminal coupling is usually around -19 Hz. Taking this into account and with the structure of the starting materials in mind, the only explanation for the observed doublet would be the formation of a ruthenium carbene species from the alkyne with a formal geminal hydrogenation. The other observed hyperpolarized signal might come from the corresponding regioisomer, which is coupling to a methyl group (Scheme 4.19). The diastereotopicity of these protons is easily explained by the chiral ruthenium center in this structure and the ring formation. Similar carbene structures are known from the *Hoveyda-Grubbs* catalyst used in olefin metathesis^[128]. Usually these carbenes are benzylidene-derived, whereas in our case we would have generated an alkylidene derivative. To further characterize these intermediates, we applied the OPSY (Only *Parahydrogen* SpectroscopY)-filter developed by *Duckett et al.*^[129,130] in our further NMR measurements to selectively detect only hyperpolarized NMR signals. The acquired spectra after the measurement can be found in Scheme 4.19.



Scheme 4.19: Left: ^1H -OPSY-NMR spectrum (magnitude mode) of **112a** acquired during the hydrogenation with $p\text{H}_2$ (50%); right: aliphatic region of the ^1H -OPSY-COSY spectrum confirming the coupling between the observed signals.

With this technique it is possible to suppress the overlapping signals of the substrate and product almost completely and all of the previously observed peaks are much better resolved. Also the missing coupling partner of the other hyperpolarized signal is now observed in the spectrum. In addition, we could determine the relative ratio the regioisomers (**114a**:**115a** = 1:10). In order to show the connectivity of the hyperpolarized signals we acquired a ^1H - ^1H -OPSY-COSY spectrum. It clearly confirms the previous

results from the coupling constants. For the further characterization, other PHIP versions of 2D spectra (e.g. OPSY-HMBC) of these intermediates were measured, but probably due to the fast relaxation of the hyperpolarization during longer delays and acquisition, no cross peaks were obtained. With the ^1H -OPSY-NMR spectrum in hand, we simulated the magnitude NMR spectra for an exact determination of the coupling constants of the minor regioisomer (Figure 4.34).

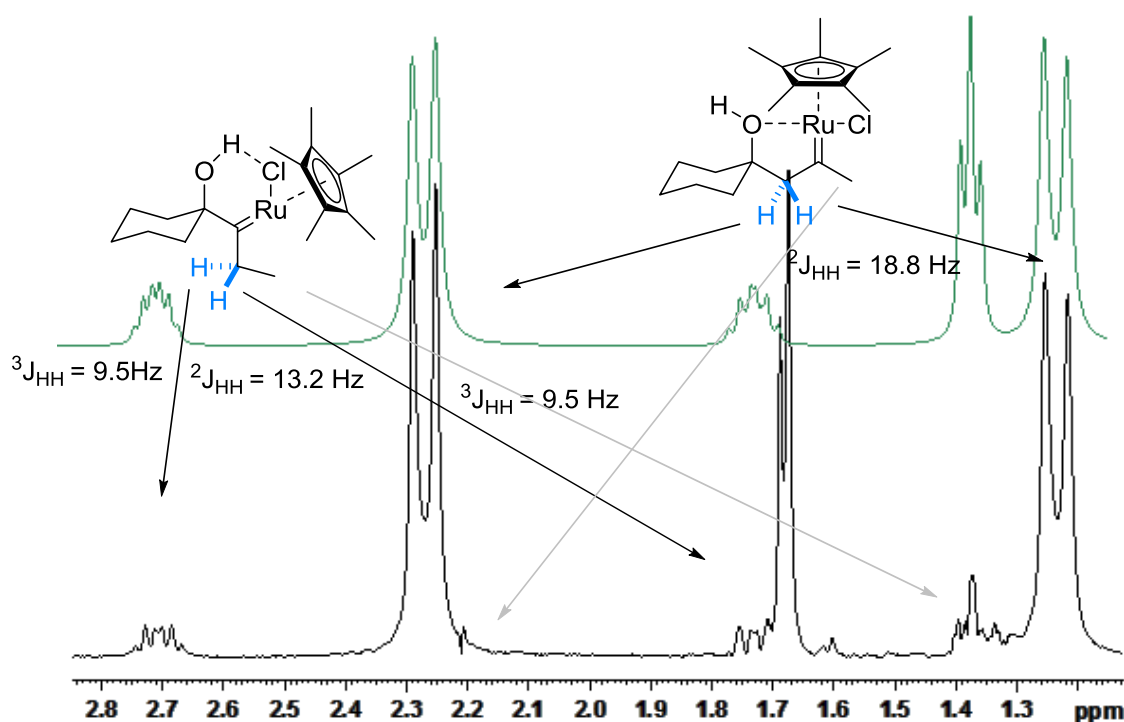


Figure 4.34: Comparison of the acquired ^1H -OPSY-Spectrum (black) and the simulated spectrum (green).

To our delight, the chemical shifts and the coupling constants are in a good agreement with our proposed structures. The electronic environment of the α -position of a carbene is similar to the ones next to other sp^2 carbon centers, as for instance of alkenes, ketones and aldehydes. The reason for the big difference of the two diastereotopic protons can be explained by an anisotropic effect of the $\text{Ru}=\text{C}$ bond, which shields the protons in plane with the bond and deshielding the ones out of it. The question about the role of this observed species remains open. After several attempts, EXSY measurements did not show any chemical exchange to the observed product. However, no carbene species were observable after full conversion, indicating that this species might be an intermediate of the reaction or from an off cycle equilibrium.

The hydroxyl group of the substrate is the key to the increased lifetime of this carbene intermediate. Due to the coordination to the ruthenium it is saturated and therefore fulfills the 18-electron-rule for carbene **115a**. However, in the other regioisomer **114a** the weak hydrogen bond of the hydroxyl group to the chloride improves its donor abilities. We were wondering if we could combine these two effects to by inserting an additional

Results and Discussion

alcohol function in the starting material. When we used 2,5-dimethyl-3-hexyne-2,5-diol **116a** as a substrate only 2 doublets could be observed in the ^1H -OPSY-NMR spectrum at 2.08 and 2.65 ppm (Figure 4.35). No hyperpolarized *trans*-product was observed. Over the course of the reaction the concentration of this species increased and we were able to observe this species even without the use of hyperpolarization methods. With this observation we were able to characterize the generated species with the common dataset for organic species. As predicted previously a cross peak of the geminal hydrogen signals in the HMBC to a ^{13}C signal with a chemical shift of 335.6 ppm was observed, which finally proved the carbene formation. We were able to fully characterize the carbene intermediate by various NMR methods (Scheme 4.20).

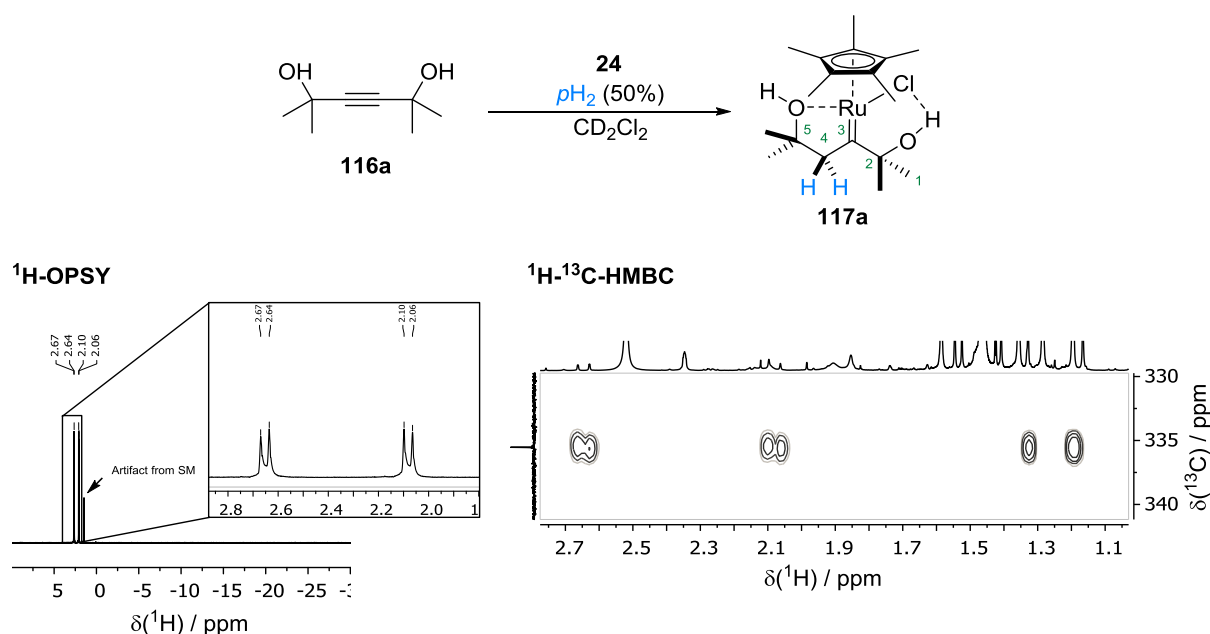
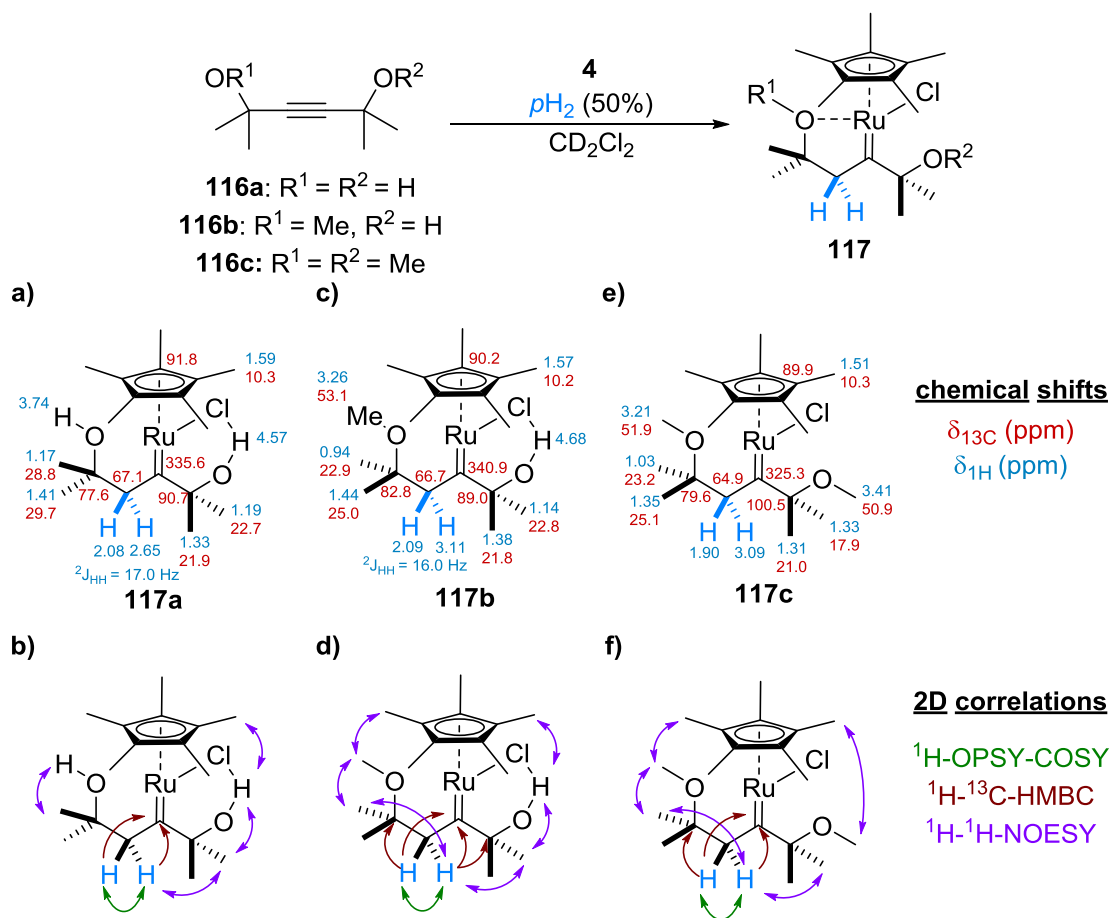


Figure 4.35: Left: ^1H -OPSY-NMR spectrum acquired during the reaction. right: ^1H - ^{13}C -HMBC spectrum of the reaction mixture showing the cross peaks to the carbene.

Upon comparison of the proton chemical shifts of the alcohol at C-2 and the alcohol at C-5, the proton OH-2 is much more deshielded (4.57 ppm vs. 3.76 ppm). This indicates a hydrogen bond interaction of the alcohol with the chlorine of the catalyst as we expected before. Besides the carbene we also observed the formation of the hydrogenated product with a low *E/Z* ratio of almost 1:1. The signals were not hyperpolarized, which could indicate either the involvement of an additional hydrogen molecule or the very slow conversion from the carbene to the corresponding products.

These results indicate that the carbene species is rather stable. In parallel, the free alcohol was protected in order to transform the corresponding oxygen into a better electron donor that might further stabilize the carbene. The formation of carbenes from a

mono- and dimethylated diol proceeded as smoothly as in the free diol and we could characterize the carbene species from all three substrates (Scheme 4.20)



Scheme 4.20: Chemical shift assignment of the in situ prepared carbenes **117** and important correlations obtained from 2D NMR data.

Interestingly the doubly protected diol **117c** was not converted into hydrogenated product at all, which might be explained by the high stability of the carbene species. The mono protected diol **117b** resulted in only one regioisomer of the carbene. This regioisomer has profited from several advantages: on the one hand the better donor properties of the OMe group, that donates electrons into the free coordination site of the ruthenium and on the other hand from the free hydroxyl group that generates a weak hydrogen bond to the chloride. This hydrogen bond is important for the preorganization of the complex before hydrogenation and it has recently been shown by the *Fürstner* group that this interaction has a directing effect on the *trans* addition of different hydrometalation reactions, which we also observe in this case.^[103]

Results and Discussion

To our pleasure the carbene **117b** was crystallized by *Dr. M. Fuchs* and the X-ray analysis could confirm our NMR structures (Figure 4.36). The C1-Ru1 bond length in the solid state is slightly longer (1.88 Å) than the ones of the PhCH= Ru bond in known *Grubbs* carbene (1.79 to 1.85 Å)^[131] The etheric oxygen O1 as electron donating ligand is confining the ruthenium in a cyclic structure as we have already concluded from our NMR analysis. Additionally, this coordination prevents the rotation of the C1–C2 bond that might lead to a 1,2-hydride shift, which would explain the product formation. Also the attractive interaction between the OH and the chloride ligand can be seen in the X-ray structure although the interaction is not strong.

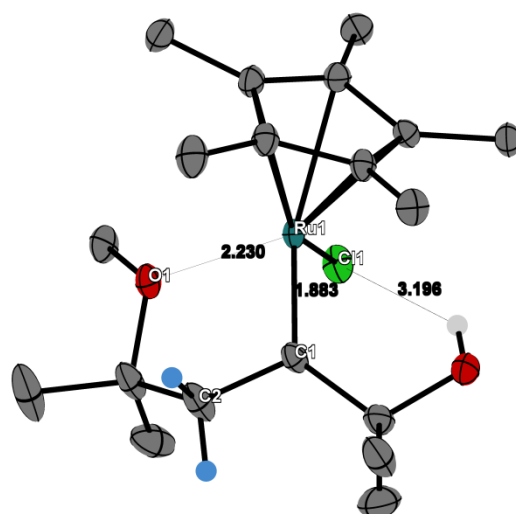


Figure 4.36: Structure of carbene **117b** in the solid state. Anisotropic displacement parameter shown at 50% probability level and hydrogen atoms, except the two transferred protons from the hydrogen and the OH are removed for clarity.

4.3.4 The Role of the Carbene Intermediates in the Catalytic Cycle

After the final confirmation of our proposed carbene species by X-ray analysis, we were interested in the role of these species in the catalytic cycle. Our previous results already indicated that they might be intermediates, but their exact role was not clear. The previous EXSY studies with the propargyl alcohol **112a** were not successful. We were wondering, if we can tune the rate of product formation by increasing the donor abilities of the alcohol by methylation. The experiments with the diols had already shown that this modification increased the stability of the carbenes. Indeed, when performing the reaction with 1-OMe-1-propynyl-cyclohexane **112b** we could observe the formation of the regioisomer that is stabilized via the coordination of the ether group to the ruthenium. It is worth mentioning the fact that the olefinic product was not hyperpolarized also in this case. To see whether this time it was possible to track the fate of the intermediate, we measured an EXSY spectrum. To suppress the signals that are arising from Boltzmann polarization (Figure 4.37), we inserted an OPSY filter in the EXSY/NOESY pulse sequence. To the best of our knowledge the application of this methodology has not been reported before. To our delight, the *trans*-formation rate was on the EXSY timescale of 300 ms. When increasing the mixing time to 1 s or longer, no signals could be detected anymore. As it can nicely be seen in the spectrum (Scheme 4.21) the hydrides of the carbene are transformed into several new species, as well as into the *trans*-product. We could only observe the transformation of geminal protons to the olefinic α -position of the quaternary carbon of **113b**. The other exchange peak could not be detected. On the one hand this could indicate that a second hydrogen molecule has to be involved for the product formation, but it could also simply be lost in the noise due to the splitting of the signal. Interestingly we also observed a small EXSY cross peak to the *cis*-product. The involvement of a hydrogen exchange reaction is also supported by the observation of the EXSY cross peak to free hydrogen. Due to its symmetry this usually cannot be hyperpolarized, but it can be enhanced if the intermediate is enhanced. The last two, no less interesting exchange peaks that were observed are the formation of the isomerization product **119b** and the formation of an aliphatic species that fits to the reduced product **120b**.

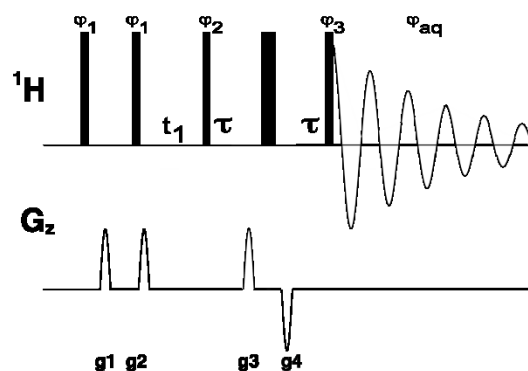
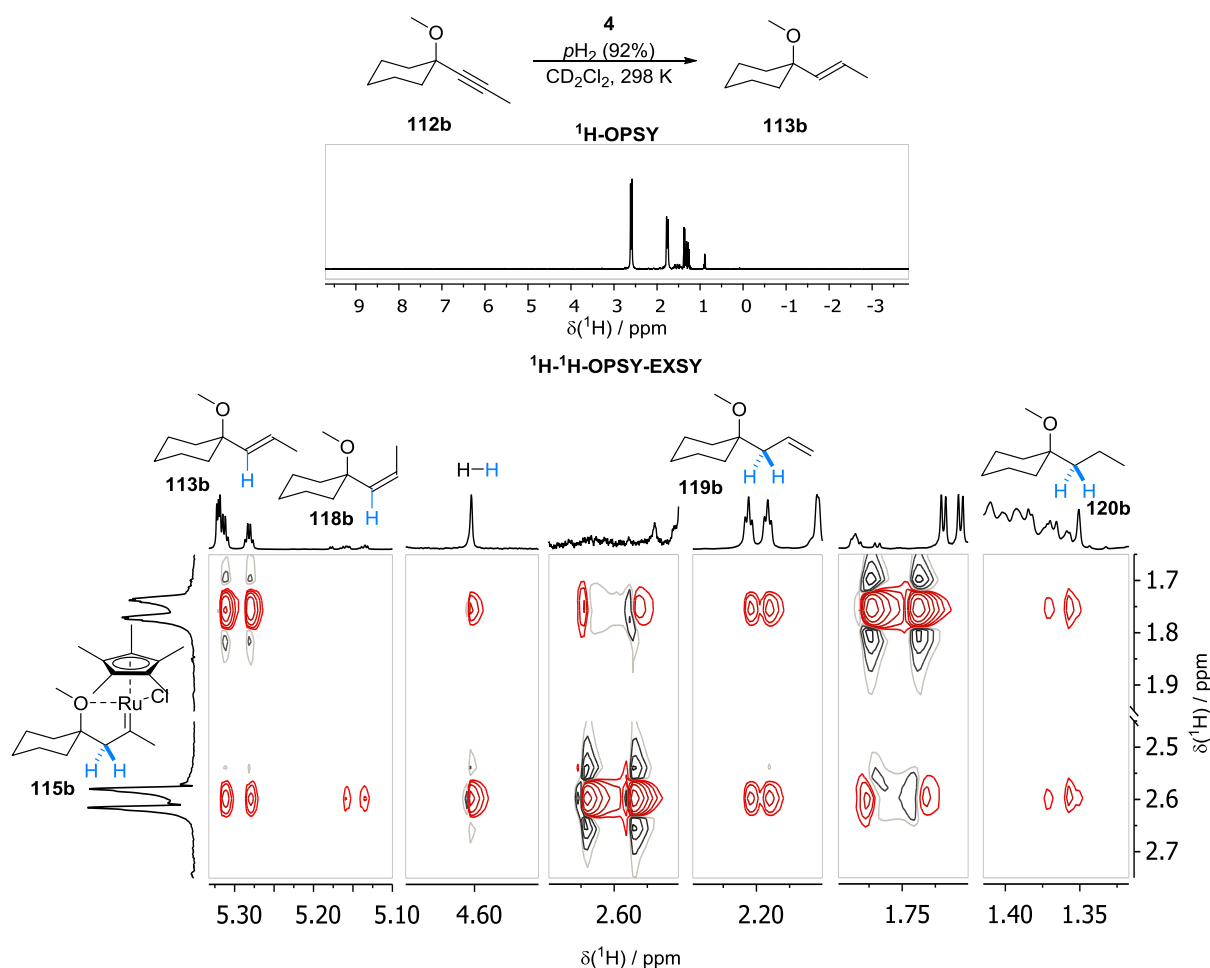


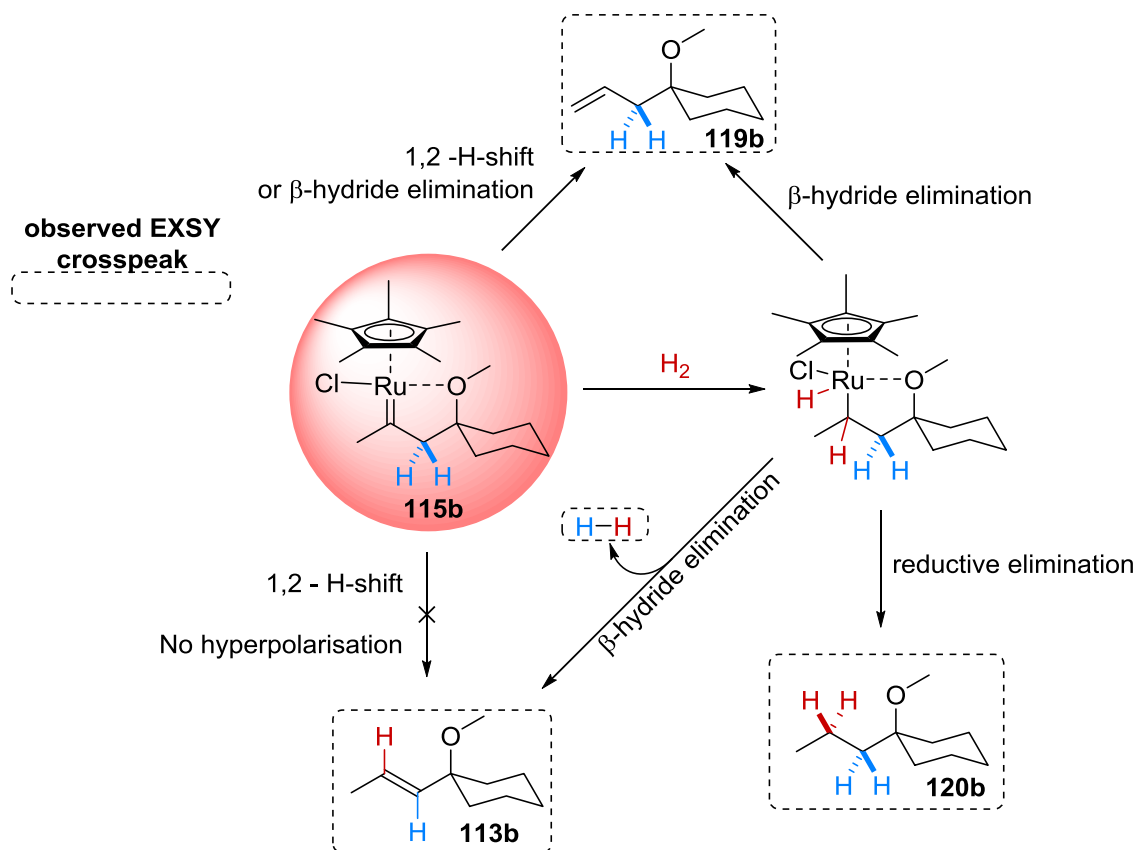
Figure 4.37: NOESY/EXSY with OPSY-*d*-Filter (OPSY-*d*-EXSY): Black thin bars represent 90° pulses and thick bars represent 180° pulses. Pulses are applied with x-phase unless the phase is indicated above the bar. Phase cycle: $\varphi_1 = [x, -x]$, $\varphi_2 = [(x)_8 (-x)_8]$, $\varphi_3 = [x, x, -x, -x, y, y, -y, -y]$, $\varphi_{aq} = [x, -x, -x, x, y, -y, -y, y, -x, x, x, -x, -y, y, y, -y]$. Half-sine 1 ms gradients were used with gradient ratio $g1:g2:g3:g4 = 10:20:4:-4$, and were each followed by a 0.2 ms recovery delay. The chemical exchange mixing time is represented by 2τ .



Scheme 4.21: Selected slices of the ^1H -OPSY-NOESY spectrum showing EXSY crosspeaks; top projection: ^1H spectrum at high conversion of **112b**; left projection: ^1H -OPSY NMR-spectrum of the reaction.

Overall we can conclude that the carbene species is indeed an intermediate of the reaction that is entering different pathways that lead to different, mainly unwanted side

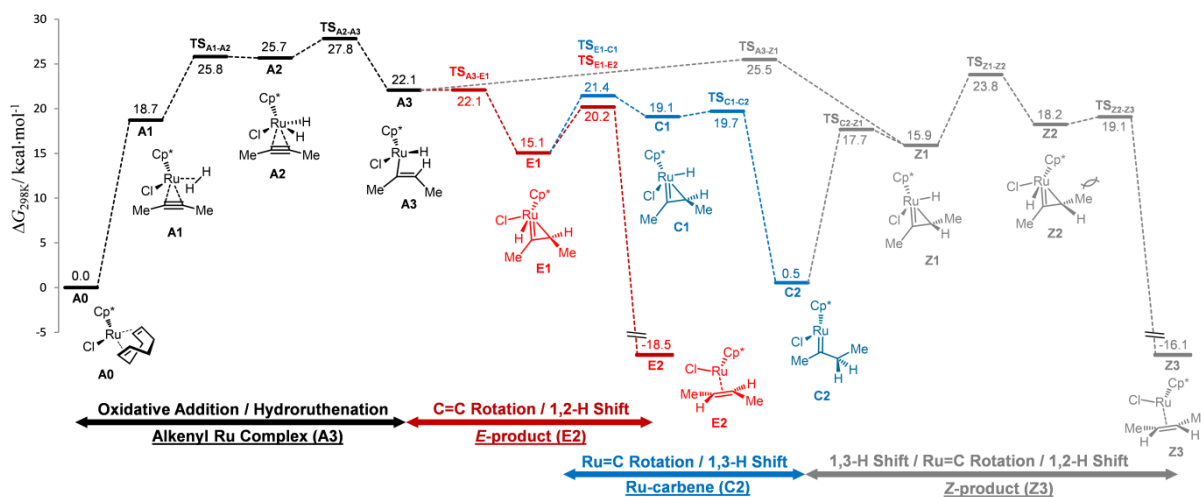
products. A conclusive mechanism that explains the observed correlations is shown in Scheme 4.22.



Scheme 4.22: Possible pathways of the carbene explaining the observed exchange peaks. Blue atoms show the fate of the hyperpolarized hydrogens of **115b**.

At this point we started a collaboration with Dr. L. M. Wolf and Dr. P. Gupta from the group of Prof. Dr. W. Thiel to further help us understanding the formation and the fate of these carbene intermediates. That data including the schemes that are presented here were kindly provided by them.

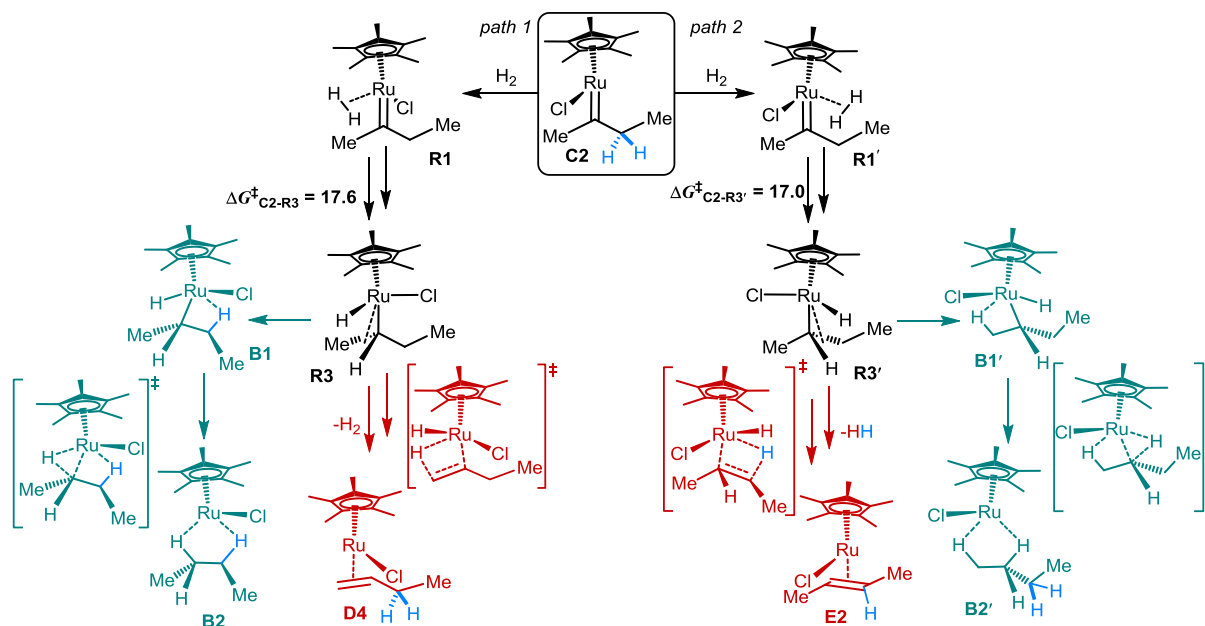
Detailed computational studies were carried out at the M06/def2-TZVP/SMD(CH₂Cl₂)/M06/def2-TZVP level of DFT. As calibration point for the calculations, carbene **117b** was chosen due to the known reactivity and molecular structure. After the validation, a more detailed computational analysis was started by using the simplest internal alkyne 2-butyne as the substrate (Scheme 4.23). Starting from the free catalyst Cp^{*}Ru(cod)Cl **24** (= **A0**), complex **A1** is formed upon alkyne binding and coordination of the hydrogen molecule via its σ -bond. This finding is in a good agreement with previous observations, that [Cp^{*}Ru(H₂)(cod)]OTf can act as *trans*-selective hydrogenation catalyst.^[100] After activation of the dihydrogen bond, the short lived dihydride complex **A2** is formed, which is transferring one hydrogen via the low-lying transition state **TS_{A2-A3}** ($\Delta G^\ddagger = +2.1 \text{ kcal}\cdot\text{mol}^{-1}$) to the alkyne.



Scheme 4.23: Free energy profile for the hydrogenation of 2-butyne with complex **24** (**A0**) at 298 K; computed structures of pertinent intermediates.

After the formation of the η^1 -vinyl complex **A3**, two different pathways are opened. A rotation around the C_α - C_β axis of **A3** (TS_{A3-Z1}) opens the pathway to the formation of *Z*-alkene. The activation barrier for this rotation is around $3.4 \text{ kcal}\cdot\text{mol}^{-1}$. Ruthenacyclopropene **E1** can be formed by an almost barrier-less rotation around the C_α - C_β axis (TS_{A3-E1}) in the other direction. After reductive elimination via TS_{E1-E2} , *E*-2-butene is formed. This transformation is strongly exergonic ($\Delta G = -33 \text{ kcal}\cdot\text{mol}^{-1}$) and therefore irreversible.

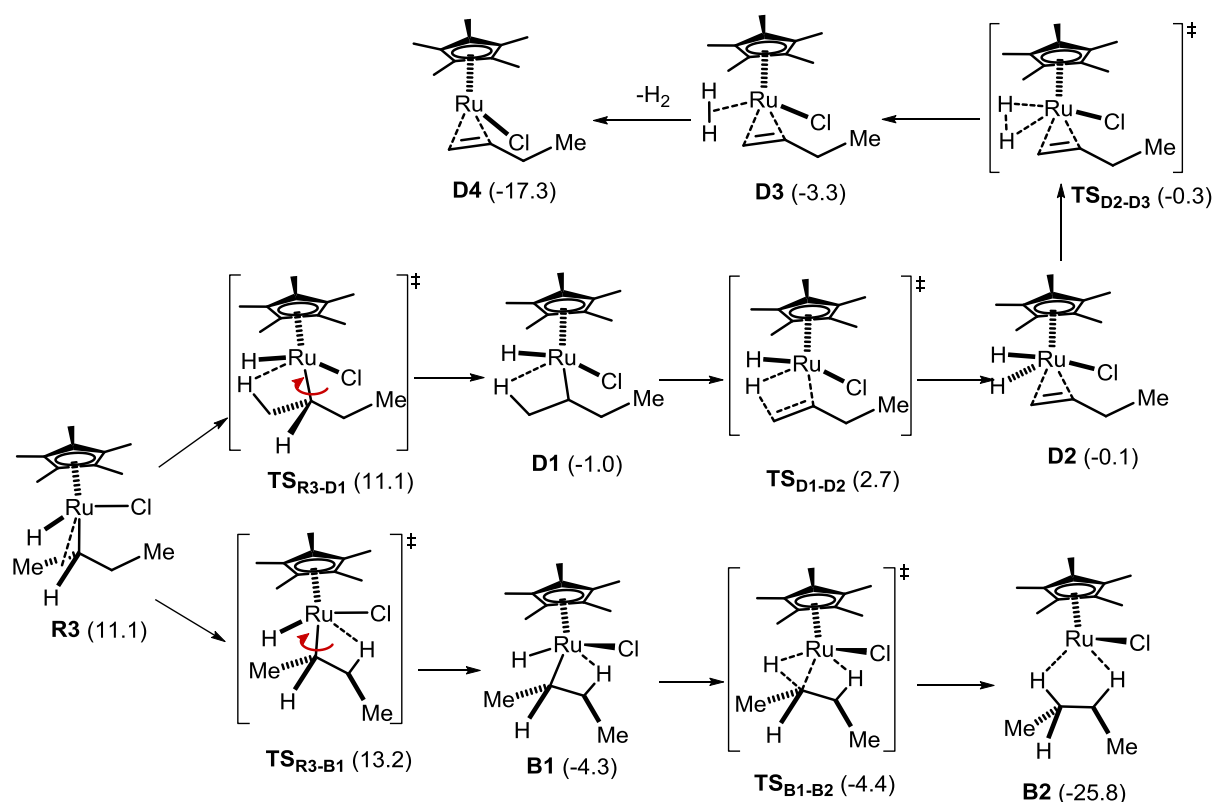
The high observed *E*:*Z* ratios in the experiments is well explained by the energy difference of TS_{A3-E1} and TS_{A3-Z1} in the calculations. During the computations it was found that the ruthenacyclopropene **E1** can convert into the carbene species **C2** upon rotation around the Ru- C_α bond. The transition state TS_{E1-C1} is only $1.2 \text{ kcal}\cdot\text{mol}^{-1}$ higher in energy, than TS_{E1-E2} that leads to **E2**. Overall the carbene formation is also exergonic ($\Delta G = 14.6 \text{ kcal}\cdot\text{mol}^{-1}$). If we now consider, that a -OR substituent coordinated to the ruthenium result in a stabilization of around $7 \text{ kcal}\cdot\text{mol}^{-1}$ by making it an 18 electron complex, it becomes reasonable that carbenes like **115** or **117** are stable enough for spectroscopic characterization or isolation. Additionally these calculations are in good agreement with our PHIP-NMR data that the geminal protons in the C_β position of the carbene derive from a single hydrogen molecule.



Scheme 4.24: Computed fate of the carbene formed by *geminal* hydrogenation upon addition of a second H_2 molecule; the blue hydrogen atoms show the fate of the carbene hydrogen atoms; Gibbs free energies in units of $\text{kcal}\cdot\text{mol}^{-1}$.

The fact that the 16-electron carbene species **C2** is capable of binding and accepting a second hydrogen molecule was of high importance for understanding the different product formation. The formation of the products by a 1,2-hydride shift was ruled out based on a high predicted energy barrier ($\Delta G(\text{TS}_{\text{C2-E2}}) = +25.6 \text{ kcal}\cdot\text{mol}^{-1}$). The energy barriers that are associated with the hydrogen adducts are by more than $3 \text{ kcal}\cdot\text{mol}^{-1}$ lower in energy than the reverse reaction directly from **C2** back to **E1** ($\Delta G(\text{TS}_{\text{C2-E1}}) = +20.9 \text{ kcal}\cdot\text{mol}^{-1}$). The product formation depends on the side from which the additional hydrogen molecule is coordinating to the ruthenium center.

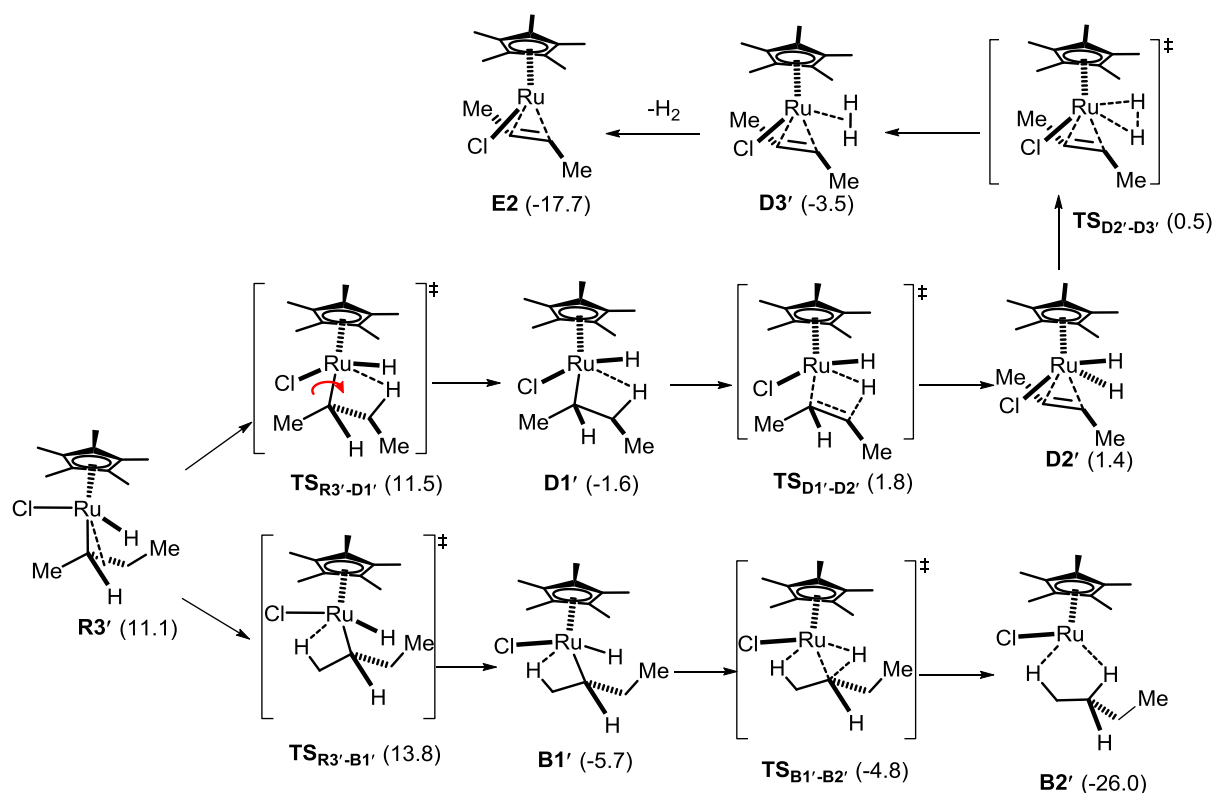
When the hydrogen is coordinating from the side of the methyl group (Scheme 4.24, path 1; Scheme 4.25) complex **R1** is formed, which further evolves to the ruthenium alkyl complex **R3**, which is stabilized by an α -agostic interaction. A further barrierless rotation around the $\text{C}_\alpha\text{-Ru}$ bond changes the agostic binding site to the methyl C-H (**D1**). This opens the doors to the isomerized product 1-butyne (**D4**). Keeping our experimental observations in mind, this pathway from the carbene to the observed isomerized product **119** is in good agreement with our NMR experiments.



Scheme 4.25: Detailed mechanism for the conversion of **R3** to the saturated (**B2**) and isomerized (**D4**) products. Values in parenthesis are Gibbs free energies in units of $\text{kcal}\cdot\text{mol}^{-1}$.

The rotation around the C_α -Ru bond can also lead to an agostic interaction with the internal methylene group (**B1**) via relatively low energy barrier ($\Delta G(\text{TS}_{\text{R3-B1}}) = +2.1 \text{ kcal}\cdot\text{mol}^{-1}$). This species **B1** can convert further after a reductive elimination to the overreduced butane. These results are also in good agreement with our NMR observations.

In analogy to path 1, the hydrogen molecule can also coordinate at the ethylene side chain on the ruthenium center (**R1'**) (Scheme 4.24, path 2; Scheme 4.26), that also leads to a complex with an agostic C_α -H-interaction **R3'**. The two reaction pathways arising from there are analogous to the ones of **R3**. One pathway converts **R3'** to the alkane, the other one to the desired *trans*-2-butene. Worth mentioning is that the protons in the *trans*-product originate from two different hydrogen molecules, which could explain the missing hyperpolarized PHIP signal in the formation of **113b** from carbene **115b**. Additionally, the released hydrogen molecule has two different parents. This also would explain the observed exchange cross peak to the free hydrogen molecule in solution.



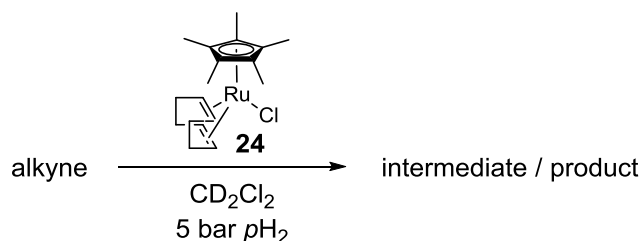
Scheme 4.26: Detailed mechanism for the conversion of **R3'** to the saturated alkane (**B2'**) and the *trans*-alkene (**E2**) products. Values in parenthesis are Gibbs free energies in units of $\text{kcal}\cdot\text{mol}^{-1}$.

In summary the theoretical calculations are in excellent agreement with our NMR observations from the EXSY NMR data and they were very helpful and necessary to understand the formation and fate of the carbenes. Both experimental and computational results have shown that the carbenes are indeed intermediates of the catalytic cycle, but they open pathways that lead to unwanted side reactions such as overreductions and isomerisations. A suppression of the carbene formation might result in higher reaction yields and fewer by-products.

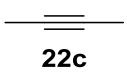
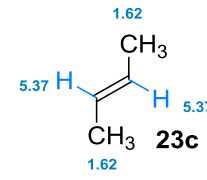
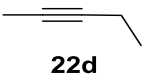
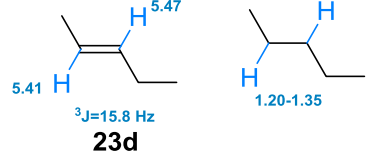
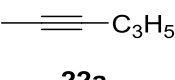
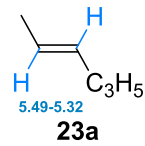
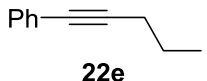
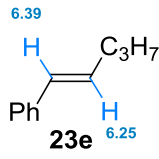
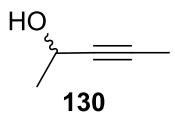
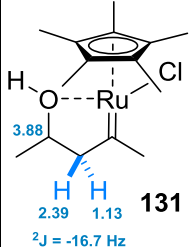
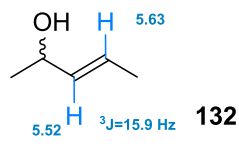
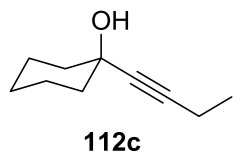
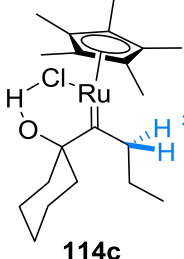
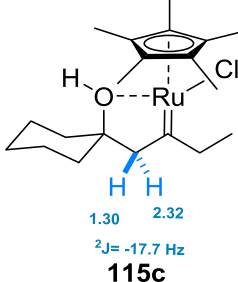
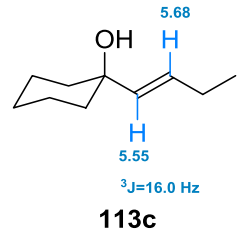
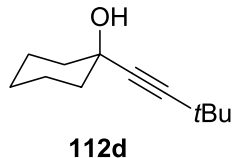
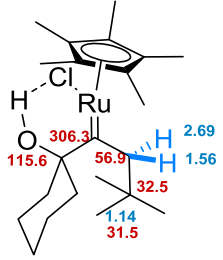
4.3.5 Characterization of Other Carbenes

After our discovery of the carbene intermediates we were wondering if other alkynes lead to detectable carbene intermediates. Therefore we tested a variety of different substrates in the reaction (Table 4.6):

Table 4.6: Overview of different substrates tested for carbene formation.^a



entry	alkyne	carbene intermediate	product
1	<p>122</p>	<p>123 3.65 ppm</p>	<p>no hyperpolarization due to the high symmetry of the product, low <i>E/Z</i> ratios and yields, side product:</p> <p>124</p>
2	<p>125a</p>	<p>126a broad signals 2.20 2.50 ²J=25 Hz</p> <p>127a 0.92 1.61 2.24</p>	<p>128a 6.94 1.86 ³J = 15.3 Hz</p>
3	<p>125b</p>	<p>Not observed</p>	<p>128b 7.11 1.92 5.85 ³J=15.5</p> <p>129b 6.51 5.80 1.92 ³J=11.2</p> <p><i>E/Z</i> = 50:50</p>

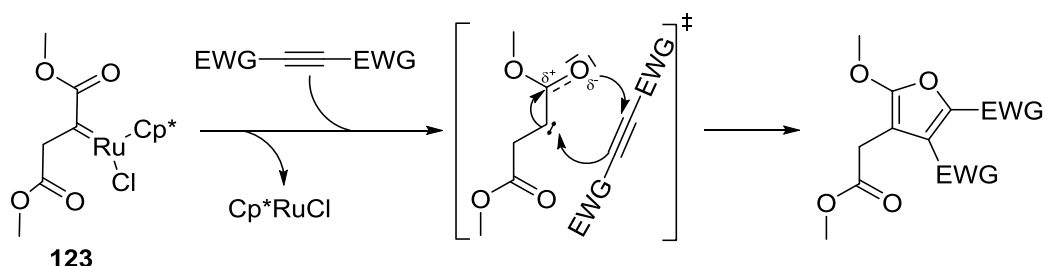
4 ^b	 22c	Not observed ^b	 23c	
5	 22d	Not observed ^b	 23d	
6	 22a	Not observed ^b	 23a	
7	 22e	Not observed ^b	 23e	
8	 130	 131	Complex signal mixture ^b	 132
9	 112c	 114c	 115c	 113c
10	 112d	 114d stable	Very slow at rt	

^a Values in blue represent ¹H-chemical shifts in ppm, red values ¹³C-chemical shifts in ppm, blue protons indicate strong hyperpolarized signals ^b (*E*)-alkenones and potential carbene intermediates with $J \approx 25$ Hz could be detected and may originate from an impurity of the starting material.

Results and Discussion

Dimethyl acetylenedicarboxylate (Table 4.6, entry 1) should yield the highly symmetrical dimethyl fumarate. To our surprise the desired product was not formed, instead we observed a hyperpolarized signal at $\delta_{\text{H}} = 3.65$ ppm. This was assigned in analogy to the previous results to carbene **117** with an ester function in the 3-position. This species might be very reactive and indeed we could characterize a tetrasubstituted furan **124** which carries the 2 geminal hydrogenated protons as the main product. Formally this reaction can be seen as a 1,3-dipolar cycloaddition of a carbene and alkyne (Scheme 4.27). Unfortunately the desired dimethylfumarate was generated in a low *E/Z* ratio of almost 1:1 and in low amounts. Interestingly, as another byproduct hexamethyl mellitate was observed, which was generated by trimerisation of the starting material.

Methyl tetrolate **125a** (Table 4.6, entry 2) yielded also 2 different hyperpolarized species, which were assigned in analogy to the known carbenes. Worth mentioning is that the signals of the carbene, that is forming upon coordination a five membered ring has an unusual large Ru-C coupling constant of -25 Hz. Similar coupling constants are known from cyclopentadiene derivatives, with a planar π -system.^[127] However the reason for the broadening is not clear yet, but it might accounted for the short lifetime of these species.



Scheme 4.27: Formal 1,3-dipolar-cycloaddition of the carbene intermediate **123** to an activated alkyne.

In contrast to this, tetrolic acid **125b** (Table 4.6, entry 3) does not yield any observable intermediates and the *E/Z* ratio in the olefinic products is 1:1. We could not figure out by EXSY measurements, if the *trans*-product is formed first and then isomerizes to the *cis* product or if both are formed simultaneously from the catalytic cycle. The substrate, which was used for the theoretical calculations, 2-butyne **22c**, was also investigated. Unfortunately we could not observe any carbene intermediate, but the *E/Z* ratio in the product was very high as also predicted by computation. Although the olefinic protons are chemically identical, the product is still hyperpolarized due their magnetic inequivalence. Worth mentioning is that we could observe a hyperpolarized signal at the beginning of the reaction, which could have its origin in 2-butyne. 2-Pentyne **22d**, as a slightly larger alkyne (Table 4.6, entry 5), yielded hyperpolarized *E*-product **23d**, but the signals of the overreduced product were enhanced. Interestingly, also here *trans*-3-pentene-2-one was observed as a hyperpolarized side product as well as the

corresponding intermediate with the strong J coupling (~ 25 Hz) (Figure 4.38). At higher conversions of the starting material, these signals are no longer observed, which is indicating a complete conversion of these more reactive impurities. These side products have also been observed in other substrates (Table 4.6, entries 6,7,8). The origin of these species is not clear yet, but presumably is based on an impurity in the starting material, which could not be detected by NMR before.

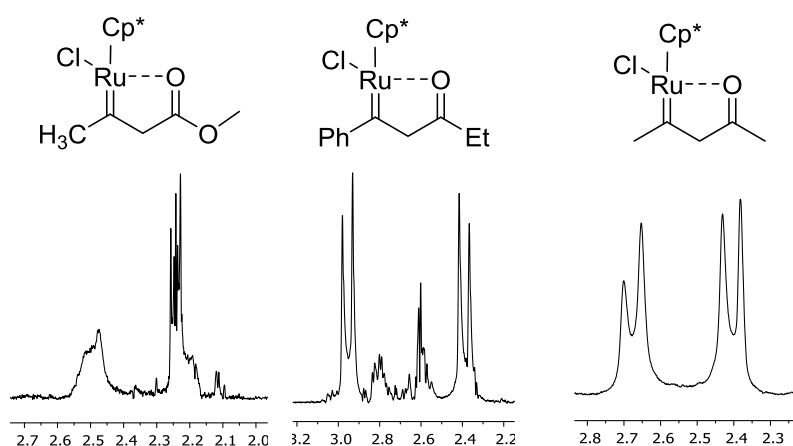
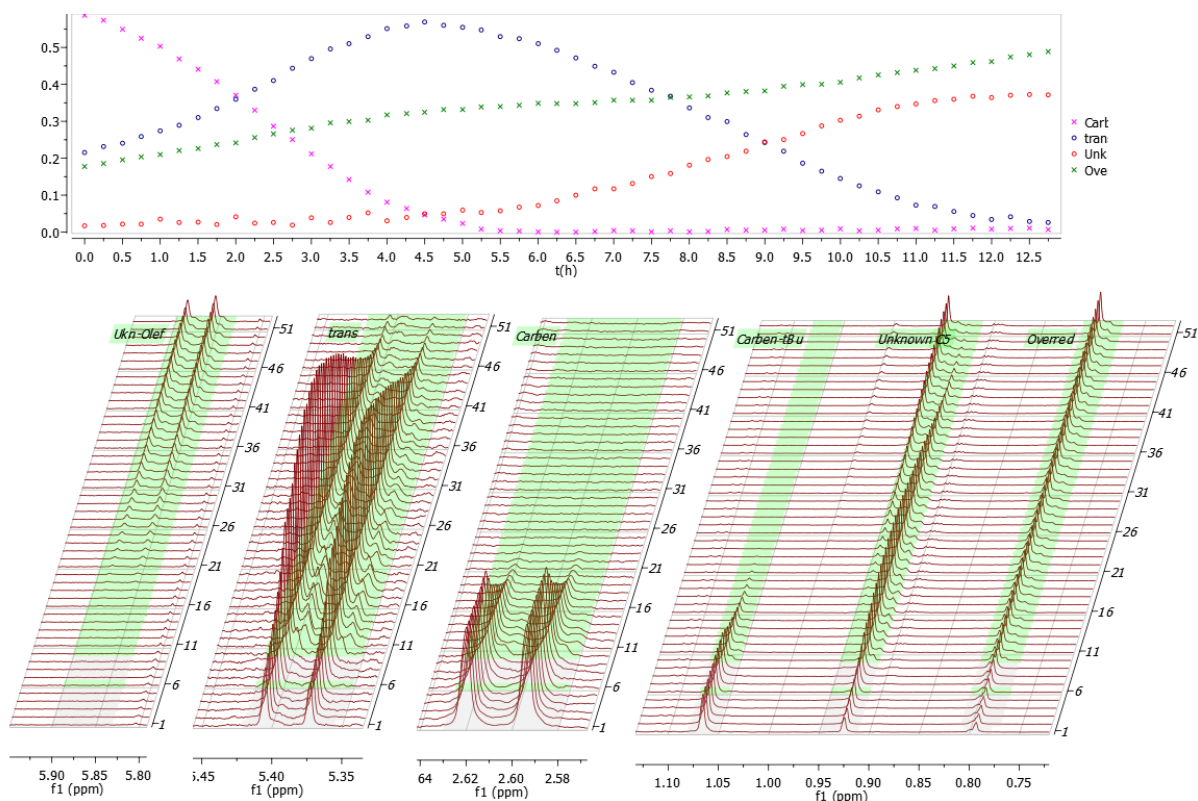


Figure 4.38: Various observed J couplings with a size of around 25 Hz and the structure of the corresponding carbene.

We were also interested if carbenes can be generated from a chiral, secondary alcohol (Table 4.6, entry 8). Therefore 3-pentyn-2-ol **130** was chosen as substrate. Indeed carbene intermediates could be obtained, but the mixture is complex and therefore hard to analyze due to the big overlaps of different hyperpolarized signals. The 2D-OPSY-COSY spectra hinted at the occurrence for at least two different carbene intermediates that couple to a secondary alcohol, which could be explained by the formation of two diastereomeric proximal carbenes. In further studies, we were interested in the influence of sterics on the carbene formation (Table 4.6, entry 9 & 10). With an increasing chain length from methyl to ethyl, the ratio of the carbene regioisomer ratio (1,2-hydroxycarbene **114** : 1,3-hydroxycarbene **115**) changes significantly from 1:10 to 5:1. The relatively small increase of steric bulk leads to a preferred addition of hydrogen occurring preferentially from the other side of the ruthenium. After this result, we were wondering if an even bulkier chain would further follow this trend. Indeed, when we exchanged the ethyl by a *tert*-butyl group, only the 1,2-hydroxycarbene **114d** was detected. To our big surprise the lifetime of this carbene intermediate was long enough for an NMR characterization and only small amounts of product were observed. In agreement with the previous result, we could determine the carbene chemical shift with $\delta(^{13}\text{C}) = 306.3$ ppm, although it is shifted towards higher field by 30 ppm compared to the diol derived carbenes. With this stable carbene in hand, we wondered, if the product

Results and Discussion

formation could be achieved by increasing the temperature. Indeed, when heating the mixture to 60 °C the carbene decomposed and formation of desired *trans*-product, but also over reduced alkane was observed. At high conversions of the carbene, the formation of various hydride complexes was observed in the high field region (broad signal at -5.10 and -7.15 ppm) and the signals of the *trans*-product were also shifted. Overall this experiment gave us a second independent proof, that the carbenes are indeed intermediates and not a dead end of the reaction.

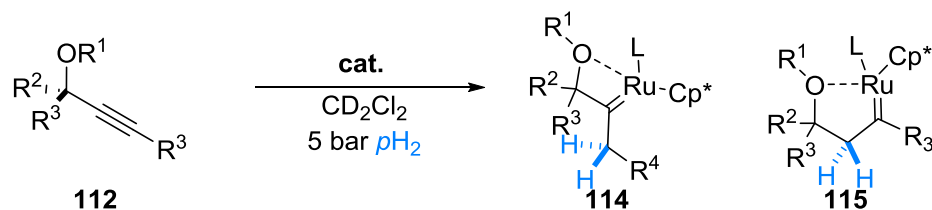


Scheme 4.28: ^1H NMR kinetic profile for the decomposition of the carbene intermediate **114d**.

4.3.6 Influence of the Catalyst on the Carbene Formation

Fürstner and coworkers recently pointed out the influence of a preorganization of the substrate by a hydrogen bond to the chlorine ligand of the catalyst.^[103] We were interested, if the choice of the catalyst has an influence on the observed carbene intermediate ratio. From previous studies we knew that a cationic catalyst species in general has a higher turnover number, but it leads to a higher amount of isomerization, whereas neutral catalysts lead to less isomerization, but to a higher amount of overreduction.

In our studies we used two different catalysts $\text{Cp}^*\text{Ru}(\text{cod})\text{Cl}$ (**24**) and the $[\text{Cp}^*\text{Ru}(\text{CH}_3\text{CN})_3]\text{PF}_6$ (**133**) and compared the outcome on of carbene intermediates and the occurrence of enhanced product signals. The results are summarized in Table 4.7:

Table 4.7: Observed carbene isomer ratios with different substrates and catalysts.

entry	alkyne	isomer ratio ^a 115: 114		hyperpolarized product signals	
		24	133	24	133
1*		10:1	3:2	yes	yes
2		99:1	14:1	No	yes
3		<1:99	1:1	yes (at higher temperatures)	no

^a The isomer ratio was determined by integrating the corresponding signals in the ¹H-OPSY spectra after magnitude processing.

In all the substrates we tested, the cationic complex **133** was less selective with respect to the carbene intermediate ratio. In general, the carbene is preferentially formed on the less sterically hindered position of the alkyne. When both sides have similar steric demand (Table 4.7, entry 3), hydrogen bonding has an enormous influence on the selectivity of the carbene formation. It seems that a hydrogen bond interaction between the chloride, which was observed in the X-ray structure, is responsible for the preference of the carbene formation on the proximal position (**114**). If this hydrogen bond interaction is removed by protection and the donor ability of the oxygen is increased, the preference shifts clearly towards the distal position (**115**) is clearly preferred. Interestingly the influence on the neutral catalyst is again much bigger compared to the cationic one. One might explain this by an additional higher flexibility of the binding site of **133**.

5. Summary

5.1 Transition State Analogues for Proline Catalyzed Aldol reactions

In the beginning several aldehydes **34** bearing an intramolecular hydrogen bond acceptor were synthesized. These aldehydes **34** were in situ reacted with proline to observe the formation of proline derived enamines **35**. Substrate **34c** showed a big increase of observable enamine intermediates in solution. Attempts to increase the observable amount even more by using a better soluble proline derivative were successful (Figure 5.1). By changing to unpolar solvents, this intermediate **35c** should be characterized to enable an undistinguishable observation of the intramolecular hydrogen bond, which unfortunately proved unsuccessful.

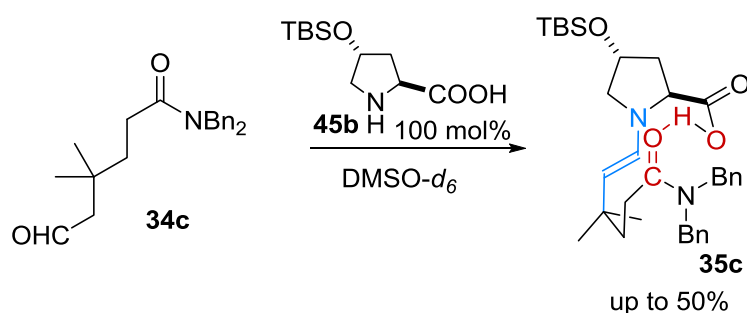


Figure 5.1: Stabilizing enamines by intramolecular H-bonding in DMSO and a modified proline.

To circumvent oxazolidinone formation and to enable a higher stability of the enamines, several attempts towards the synthesis of proline derived enaminones bearing an intramolecular hydrogen bond acceptor were made. The synthesis of two diastereomeric enaminones **50** was successful. Unfortunately a detailed characterization by NMR or X-Ray was not possible due to several stable rotamers of these species at various temperatures. The synthesis of rotational hindered enaminones **69** did not yield the desired products (Figure 5.2).

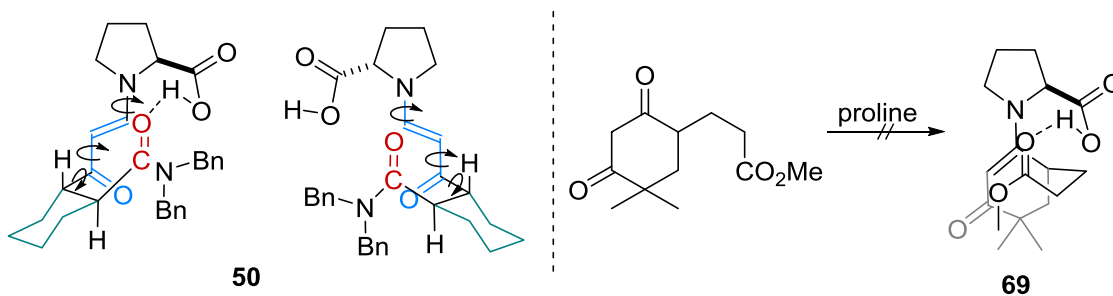


Figure 5.2: Attempts towards stable enaminones with intramolecular hydrogen bond acceptor.

Another attempt towards stable enamine derivatives with an intramolecular hydrogen bond acceptor was established by the synthesis of the proline derived aryl amine **85**.

The compound was analyzed by NMR at ambient and low temperatures. The structure was found to be in another conformation than the desired one (Figure 5.3).

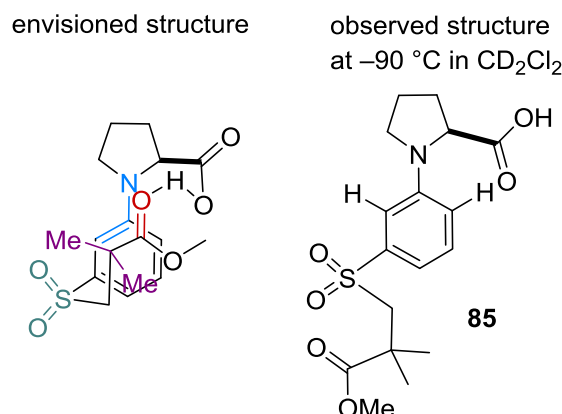


Figure 5.3: Proline derived aryl amines as transition state analogues.

5.2 NMR Studies of Organocatalytic Reactions

During this PhD work various recently developed organocatalytic reactions have been studied by NMR. We could show that enamines, which are the proposed reactive intermediates in the α -benzylation of α -branched aldehydes, are present in solution under the reaction conditions. The role of the base and acid additives in the reaction has been studied. Without the addition of the additives, no enamine species could be observed in solution.

In further studies the silylation behavior of in situ silylated disulfonimides was studied by $^1\text{H-NMR}$, $^1\text{H-}^{29}\text{Si-HMBC}$ and EXSY measurements. The formation of an *N*- and an *O*-silylated species was previously studied for simple, open disulfonimides by Blaschette^[115] and Simchen.^[116] With our experiments it could be shown that the increased bulk of the silicon species increases follows the trend in the case of DSIs and prefers *O*-silylation upon higher steric bulk. The chemical exchange between both species could be shown by EXSY experiments.

Furthermore NMR studies were conducted to study the course of reaction of both the DSI-catalyzed Torgov cyclisation and the synthesis of β_3 -amino esters from *N*-Boc-amino sulfones. The results were in good agreement with the proposed mechanism for these reactions. As products prior to workup of the Mukaiyama–Mannich reaction two different *N*- and *O*-silylated products could be characterized in analogy to the observed silatropic behavior of the DSIs.

5.3 Carbenes as Intermediates in the *Trans*-Hydrogenation of Internal Alkynes

Recently the group of *Fürstner* reported a new protocol for the catalytic *trans*-hydrogenation of internal alkynes with [RuCp*]-complexes. The reaction was investigated by *parahydrogen* induced polarization (PHIP). The reaction with 2-hexyne showed the occurrence of hyperpolarized product signals and thereby proved the pairwise transfer of hydrogen atoms to the alkyne substrate in accordance to the similar protocol previously reported by *Bargon*.^[94] While using 1-propynyl-1-cyclohexanol as the substrate new intermediates in the aliphatic region of the ¹H-NMR spectrum were observed. The use of an OPSY filter yielded a clear spectrum showing only the hyperpolarized signals. The observed intermediates were proposed as carbenes that were formed by a formal *geminal* hydrogenation. To further stabilize the carbene intermediates a second alcohol was introduced. Under reaction conditions stable carbenes were observed could be characterized by conventional NMR methods. For complex **117b** an X-ray structure was obtained, that confirmed the NMR data.

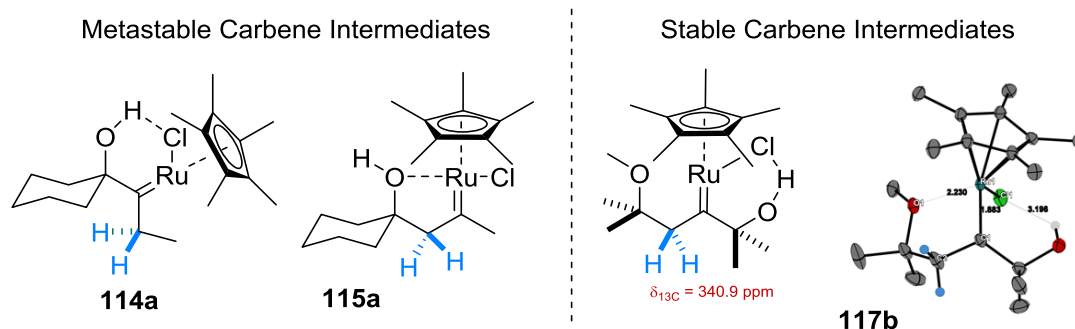
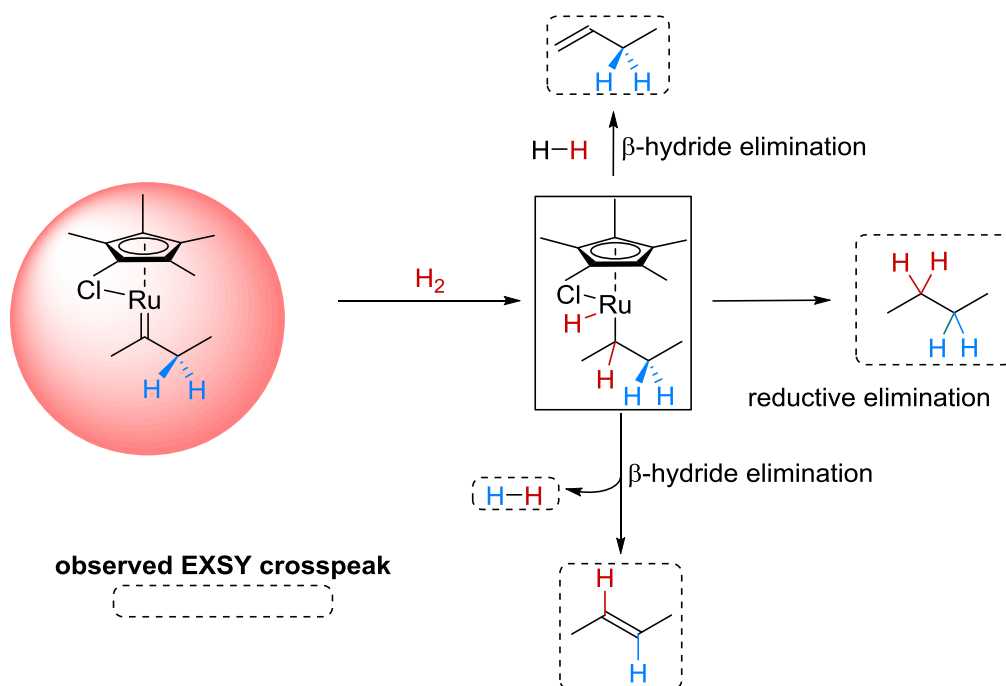


Figure 5.4: Observed and characterized carbenes by NMR and X-ray.

To determine the role of these carbene intermediates ¹H-¹H-OPSY-EXSY experiments were conducted. One substrate (1-propynyl-1-methoxycyclohexane) enabled the observation of the fate of the carbene intermediate. It was found, that the carbene intermediate leads to several isomerized and overreduced side products, but also the desired *trans*-alkene. DFT calculations were performed and supported these observations nicely (Scheme 5.1).



Scheme 5.1: Fate of carbene intermediates analyzed by EXSY-NMR and DFT calculations.

Overall the carbene observations and DFT calculations enabled a conclusive model of side product formation in the *trans*-hydrogenation of internal alkynes.

6. Outlook

6.1 New and Advanced Proline Catalyzed Aldol Enamine Transition State Models

Studies towards the synthesis of a stable transition state analogue were not successful until today. The results have shown the desired conformation is less stable than other conformers. Their formation has to be suppressed in new models. The stabilization by a hydrogen bond is usually in the range of $5 \text{ kcal}\cdot\text{mol}^{-1}$. The desired conformer has to be designed to be the minimal energy conformer including the hydrogen bond energy. To find this lowest energy conformer computational studies have to be included in the process of designing potential analogues. As stable enamine analogues electron deficient enaminones, vinylogous sulfonamides or aryl amines are valuable. Amides have been shown to be hydrogen bond acceptors. Potential advanced structural motifs are shown in Figure 6.1.

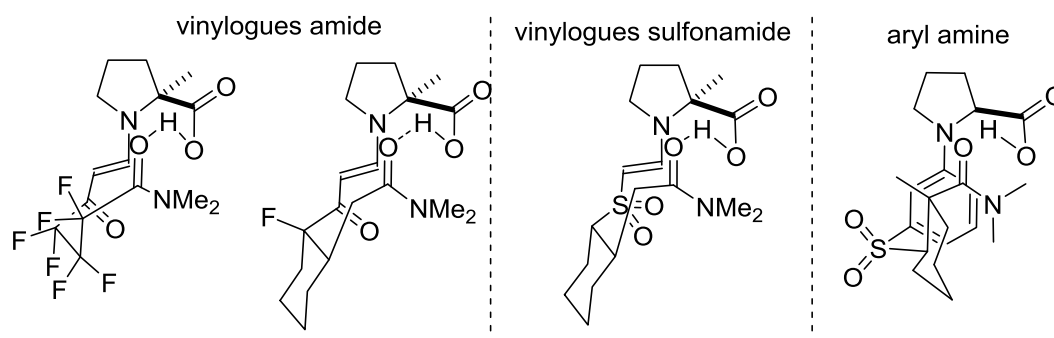


Figure 6.1: Potential structures of advanced transition state analogues.

The synthesis towards the electron deficient vinylogous amide could be performed, by adding one additional α -fluorination step in the presented successful synthesis.

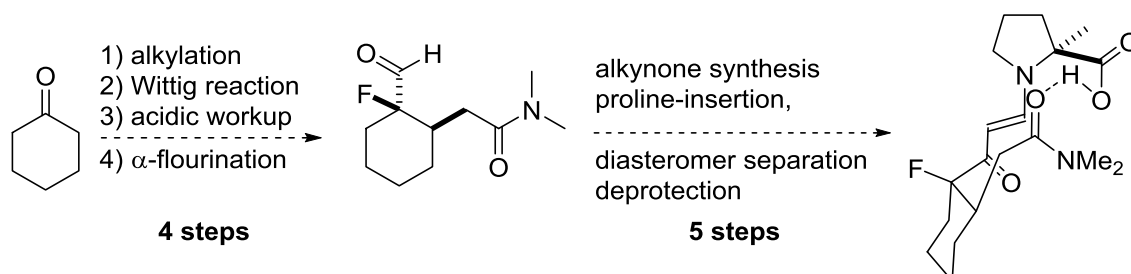


Figure 6.2: Potential synthetic route for an electron deficient enaminone.

6.2 Further NMR Studies of Brønsted Acid Catalyzed Reactions and their Intermediates

In this Ph.D. work it could be shown, that NMR is a versatile method for studying the enamine formation, course of DSI catalyzed reactions or the silatropy of DSIs. Recent NMR studies of our group could also show the application of kinetic NMR studies in other Brønsted acid catalyzed reactions.

NMR investigations by various methods, as for instance diffusion (DOSY) measurements or a job plot analysis, together with *M. Monaco* enabled the characterization of hetero-dimer complexes of phosphoric acids with carboxylic acids (Figure 6.3).

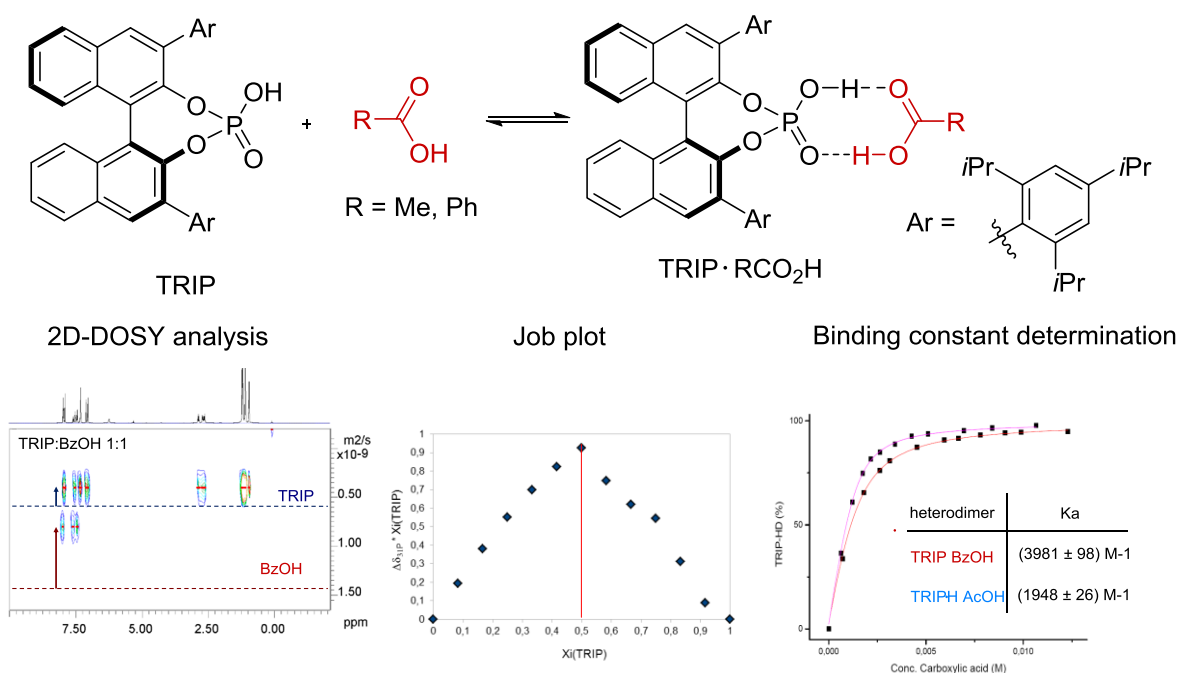


Figure 6.3: Characterization of hetero-dimeric Brønsted acid complexes by NMR.

After initial investigations these hetero-dimeric complexes could be applied in the desymmetrisation of *meso*-aziridines and *meso*-epoxides affording protected 1,2-amino alcohols or 1,2-diols in excellent yields and enantioselectivities.^[132–134] Additionally an NMR-kinetic analysis allowed us to follow the course the reaction and to determine the ring opening reaction to be first order in epoxide concentration.^[135]

More recently a covalent intermediate with an imidodiphosphate catalyst could be detected and characterized in the asymmetric intramolecular carbonyl ene reaction of alkenyl aldehydes (together with *L. Liu*).^[136] Furthermore we were able to follow the course of the reaction by NMR and to determine the role of this covalent intermediate. The recovery of the catalyst via elimination was found to be rate determining.

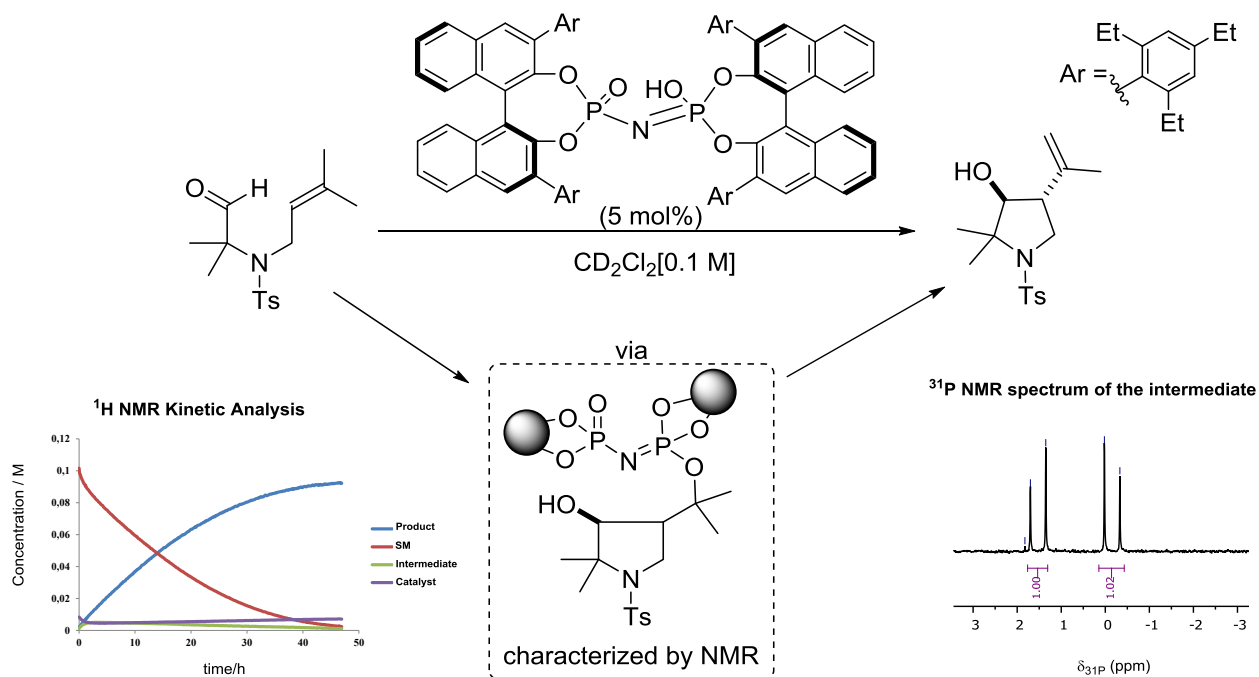
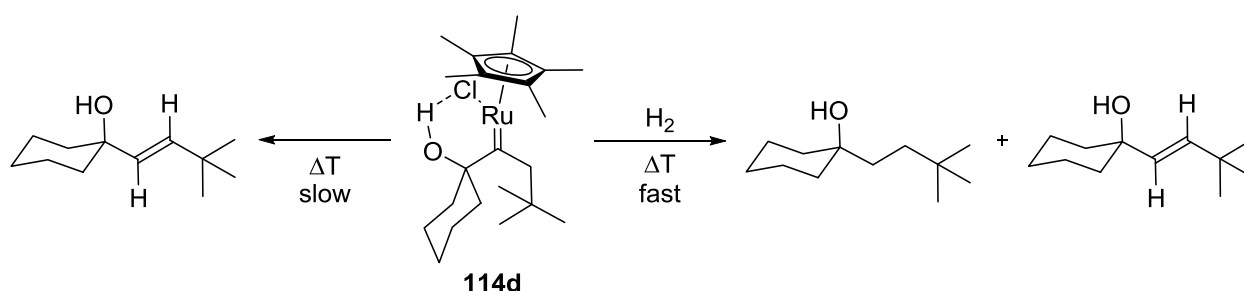


Figure 6.4: NMR studies in the intramolecular carbonyl ene reaction of alkenyl aldehydes.

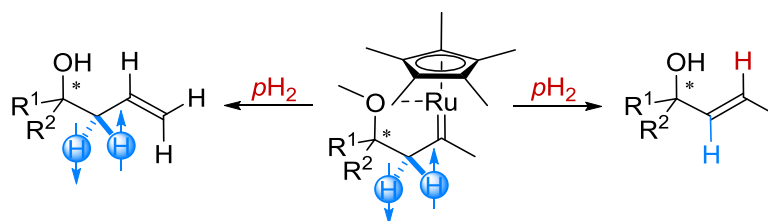
6.3 Carbene Intermediates

Detailed NMR studies have shown the formation of carbene intermediates during the stereoselective *trans*-hydrogenation of internal alkynes. DFT calculations have found that an additional hydrogen molecule is necessary to activate the carbene. In order to confirm this experimentally, several experiments can be conducted. On the one hand a stable ruthenium species, as for instance **114d**, can be synthesized and its conversion can be studied in the presence or in the absence of hydrogen. From the computations a slow conversion to the desired product would be expected in the absence of hydrogen, whereas the formation of the desired and the overreduced product would be faster in the presence of hydrogen (Scheme 6.1).



Scheme 6.1: Conversion of the carbene in the presence or absence of hydrogen.

On the other hand, the inclusion of a second hydrogen molecule can be studied by a carbene intermediate with an additional stereocenter. Assuming that both isomerized and desired product are formed with similar rates and fast enough, the desired *trans* product would not show hyperpolarized signals, whereas the isomerized product would show two hyperpolarized, diastereotopic signals.



Scheme 6.2: Observation of isomerized hyperpolarized products.

Developments towards carbene suppression by optimizing the catalyst would suppress the undesired side product formation and makes the *trans*-hydrogenation protocol even more selective. The development of new transformations that are applying the carbene as a reactive intermediate towards an intramolecular metathesis reaction might also be envisioned.

7. Experimental Section

7.1 General Remarks

Solvents and Reagents

All solvents used in the standard procedures were purified by distillation. The absolute solvents were dried by distillation over an appropriate drying agent in the technical department of the institute and stored in conical shoulder bottles with an gas tab adapter under argon atmosphere or directly purchased from the Sigma-Aldrich and used as received. Commercial reagents were obtained from various sources and used without further purification.

Inert Gas Atmosphere

Air and moisture sensitive reactions were conducted in flame dried flasks under an atmosphere of argon (Air Liquide, >99.5% purity).

Thin Layer Chromatography (TLC)

If possible reactions were monitored by thin layer chromatography on silica gel or aluminum oxide recoated plastic sheets (0.2 mm, Macherey-Nagel). Visualization was accomplished by irradiation with UV light at 254 nm and different staining reagents:

Phosphomolybdic acid (PMA) stain: PMA (10 g) in EtOH (100 ml).

KMnO₄-Stain: NaOH_{aq.} (10%, 1.25 mL) was added to a solution of KMnO₄ (1.5 g) and K₂CO₃ (10 g) in H₂O (200 mL).

2,4-DNP-Stain(Selective for Aldehydes/Ketones): 2,4-dinitrophenylhydrazine (12 g) + conc. H₂SO₄ (60 ml) + H₂O (80 ml) + EtOH (200 ml).

Column Chromatography

Column chromatography was performed under elevated pressure on silica gel (60, particle size 0.040-0.063 mm, Merck)

GC-MS

GC-MS analyses were recorded on one of two Agilent Technologies GC systems: System 1: Agilent Technologies 6890N Network GC System equipped with a 5973 Mass Selective Detector; System 2: Agilent Technologies 7890A GC System equipped with a 5975C VL MSD mass selective detector (70 eV). Both systems were equipped with a

Experimental Section

Gerstel Multi-Purpose Sampler MPS2 and a Macherey-Nagel Optima 5 column (30 m length, 0.25 mm diameter).

Nuclear Magnetic Resonance Spectroscopy (NMR)

Standard proton and carbon NMR spectra for the synthetic procedures were recorded on Bruker AVIII-500 MHz spectrometer in deuterated solvents at room temperature (296 K / 298 K) with the standard Bruker parameters. Proton chemical shifts are reported in ppm (δ) relative to tetramethylsilane with the residual solvent signal employed as the internal standard (DMSO- d_6 , δ 2.50 ppm; CD_2Cl_2 , δ 5.32 ppm; $CDCl_3$, δ 7.24 ppm).^[137] The ^{13}C -data was referenced indirectly to the referenced proton frequency with the Ξ -scale^[138,139] Data are reported as follows: chemical shift, multiplicity (s = singlet, d = doublet, t = triplet, q = quartet, m = multiplet), coupling constants (Hz), integration and assignment.

The methodologies for special NMR measurements (e.g. kinetic studies, PHIP experiments) are described in the respective subsections.

Mass spectrometry (MS)

Mass spectra were measured on a Finnigan MAT 8200 (70 eV) or MAT 8400 (70 eV) by electron ionization, chemical ionization or fast atom/ion bombardment techniques. Electrospray ionization (ESI) mass spectra were recorded on a Bruker ESQ 3000 spectrometer. High resolution mass spectra were obtained on a Finnigan MAT 95 or Bruker APEX III FT-MS (7 T magnet). All masses are given in atomic units/elementary charge (m/z).

X-Ray Crystallography

The X-ray structure analyses were conducted at the X-ray service department of the MPI für Kohlenforschung. After data collection, the structures were resolved by the J. Rust & Prof. Dr. C. W. Lehmann.

The X-Ray single crystal diffraction data was collected on a Bruker AXS X8 Proteum diffractometer with a 'MONTEL graded multilayer optic' as monochromator on a 0.2 x 2 mm² focused rotating anode. The software packages used for data collection and structure refinement consisted of SHELXS-97 (Sheldrick, 2008) and SHELXL-97 (Sheldrick, 2008).

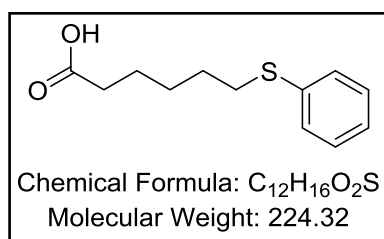
7.2 In Situ Observation of Enamines with an Intramolecular H-Bond Acceptor

The reactions presented here have not been optimized. The most reactions have been conducted only once in order to verify if the desired target structure can be synthesized.

7.2.1 Aldehyde Synthesis

5-(Phenylthio)hexanoic acid (134)

To a solution of 5-bromopentanoic acid (1.00 g, 5.15 mmol) in EtOH (25 mL) aq. NaOH (1 M, 1 mL) was added and cooled to 0 °C. Afterwards sodium thiophenolate (0.91 g, 6.85 mmol) was added and stirred for 2 h. Then the solution was warmed up to rt and stirred overnight. After TLC analysis showed full consumption of the SM, EtOH was removed under reduced pressure. The residue was dissolved in 1M NaOH solution and washed with EtOAc (2x). The aqueous phase was acidified with 10% HCl to pH=3 and extracted with EtOAc (3x). The combined organic layers were washed with sat. aq. NaHCO₃ and brine. Afterwards the solution was dried over MgSO₄*H₂O and the solvent was removed under reduced pressure. After FC (14% Hexanes / EtOAc) the product was obtained as a white solid (1.66 g, 85%).



¹H NMR (¹H NMR (500 MHz, CDCl₃) δ 11.58 (bs, 1H, COOH), 7.35 (d, *J* = 7.8 Hz, 2H, *o*-C_{arom}H), 7.30 (t, *J* = 7.9 Hz, 2H, *m*-C_{arom}H), 7.20 (t, *J* = 7.4 Hz, 1H, *p*-C_{arom}H), 2.94 (t, *J* = 7.3 Hz, 2H, CH₂S), 2.38 (t, *J* = 7.5 Hz, 2H, CH₂COOH), 1.75 – 1.64 (m, 4H, 2x CH₂-CH₂-X), 1.56 – 1.46 (m, 2H, CH₂-CH₂-CH₂).

¹³C NMR (126 MHz, CDCl₃) δ = 180.2, 136.7, 129.1, 128.9, 125.8, 76.9, 33.9, 33.4, 28.8, 28.2, 24.2.

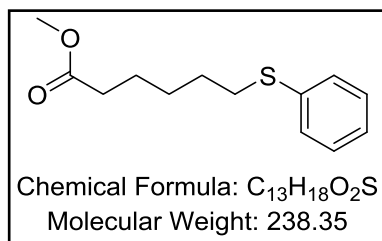
The NMR data is in good agreement to those previously reported.^[140]

MS (EI) m/z: 224 (57%, M⁺), 123 (34 %), 110 (100%, PhS⁺)

HRMS (ESI-neg) m/z (M-H): calcd: 223.079825 found: 223.079668

Methyl 5-(phenylthio)hexanoate (37)

Thioether **134** (1.6 g, 7.14 mmol) was dissolved in 15 mL MeOH. Then 4 drops of conc. H₂SO₄ were added and stirred for 1 h at 40 °C. The reaction was quenched with sat. aq. NaHCO₃ (10 mL) and the aqueous phase was extracted with EtOAc (3x 25 mL). The combined organic layers were washed with Brine, dried over MgSO₄ and the solvent was removed under reduced pressure to give the product as a colorless liquid (quant). No further purification was necessary.



¹H NMR (500 MHz, CDCl₃) δ 7.34 – 7.30 (m, 2H, *o*-C_{arom}H), 7.30 – 7.25 (m, 2H, *m*-C_{arom}H), 7.19 – 7.14 (m, 1H, *p*-C_{arom}H), 3.66 (s, 3H, OCH₃), 2.92 (t, J = 7.4 Hz, 2H, CH₂S), 2.31 (t, J = 7.5 Hz, 2H, CH₂COOMe), 1.71 – 1.60 (m, 4H, 2x CH₂-CH₂-X), 1.51 – 1.39 (m, 2H, CH₂-CH₂-CH₂).

¹³C NMR (126 MHz, CDCl₃) δ = 174.2, 136.8, 129.2, 129.0, 125.9, 51.7, 34.0, 33.5, 28.9, 28.4, 24.6.

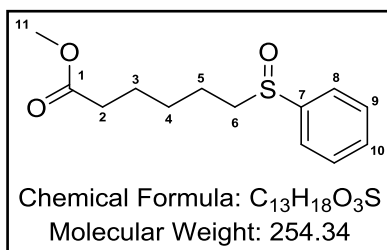
MS (EI) m/z: 238 (61%, M⁺), 123 (37%), 110 (100%, PhS⁺), 97 (36%), 69 (40 %)

HRMS (ESI-pos) m/z (M+Na): calcd: 261.091974 found: 261.091943

General Procedure for the Oxidation of Thioethers 37

Methylester **37** (400 mg, 1.7 mmol) and (PhO)₂POOH (8.5 mg, 0.2 mmol) were suspended in hexanes (20 mL) and aq. H₂O₂ (35%, 230 μL) was added. After 4 h TLC analysis indicated full consumption of the SM and the reaction mixture was quenched with sat. aq. Na₂S₂O₅. The mixture was diluted with EtOAc (20 mL) and sat. aq. NaCO₃ (20 mL). The phases were separated and the aq. phase was extracted with EtOAc (3x 20 mL). The combined organic phased were washed with brine, dried over MgSO₄ and the solvent was removed under reduced pressure. After FC (11 % to 66% EtOAc / hexanes) the desired products could be obtained.

Methyl 5-(phenylsulfinyl)hexanoate (38a)



Yield: 325 mg, colorless oil

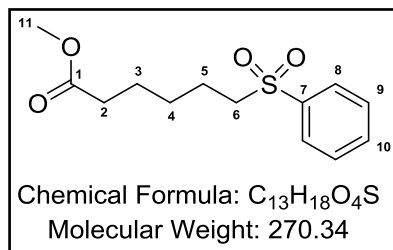
Rf (50% EtOAc / Hexanes) = 0.2

¹H NMR (500 MHz, CDCl₃) δ = 7.61 (dd, J=7.8, 1.7, 2H, H-8), 7.57 – 7.46 (m, 3H, H-9, H-10), 3.66 (s, 3H, H-11), 2.79 (t, J=7.7, 2H, H-6), 2.30 (t, J=7.4, 2H, H-2), 1.85 – 1.73 (m, 1H, H-5'), 1.69 – 1.59 (m, 3H, H-3, H-5''), 1.53 – 1.36 (m, 2H, H-4).

MS (EI) m/z: 254 (3%, **M⁺**), 223 (16%, **M-OMe**), 129 (57%, **M-SOPh**), 97 (55%), 69 (100%)

HRMS (ESI-pos) m/z (M+Na): calcd: 277.086886 found: 277.087023

Methyl 5-(phenylsulfonyl)hexanoate (**38b**)



Yield: 85 mg, colorless oil

R_f (50% EtOAc / Hexanes) = 0.6

¹H NMR: (500 MHz, CDCl₃) δ = 7.84 (d, *J*=7.5, 1H, **H-8**), 7.62 – 7.57 (m, 1H, **H-10**), 7.55 – 7.48 (m, 1H, **H-9**), 3.58 (s, 1H, **H-11**), 3.06 – 2.98 (m, 1H, **H-6**), 2.21 (t, *J*=7.4, 1H, **H-2**), 1.71 – 1.62 (m, 1H, **H-5**), 1.53 (p, *J*=7.3, 1H, **H-3**), 1.34 (m, 1H, **H-4**).

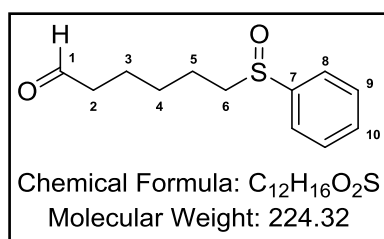
MS (EI) m/z: 270 (7%, **M⁺**), 239 (27%, **M-OMe**), 197 (41%, **M-CH₂COOMe**), 143 (81%), 129 (73%), 97 (67%), 69 (100%).

HRMS (ESI-pos) m/z (M+Na): calcd: 293.081802 found: 293.081947

General Procedure for the Reduction of Esters **38**

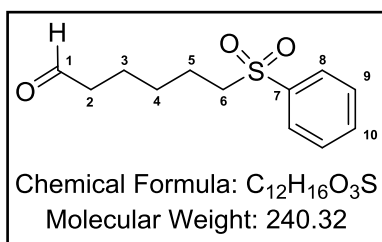
The ester **38** (0.28 mmol) in CH₂Cl₂ was cooled to -78 °C and DIBAL-H (1 M in Toluene, 0.3 mL, 0.30 mmol) was slowly added. The solution was quenched with 10% HCl. After extraction of the aq. phase with CH₂Cl₂ the combined organic layers were washed with brine and dried over MgSO₄. The solvent was removed under reduced pressure and the product was purified by prep. TLC (50% EtOAc in hexanes).

5-(Phenylsulfinyl)hexanal (**34a**)



¹H NMR (500 MHz, DMSO-*d*₆) δ = 9.63 (t, *J*=1.6, 1H, **H-7**), 7.69 – 7.62 (m, 2H, **H-8**), 7.62 – 7.47 (m, 3H, **H-10**, **H-9**), 2.94 (ddd, *J*=13.3, 9.3, 6.1, 1H, **H-6'**), 2.75 (ddd, *J*=13.3, 9.6, 4.9, 1H, **H-6''**), 2.39 (td, *J*=7.2, 1.6, 2H, **H-2**), 1.68 – 1.56 (m, 1H, **H-5'**), 1.50 (p, *J*=7.1, 2H, **H-3**), 1.46 – 1.27 (m, 3H, **H-4**, **H-5''**).

5-(Phenylsulfonyl)hexanal (34b)



¹H NMR (500 MHz, DMSO-*d*₆) δ = 9.61 (d, *J*=1.6, 1H, **H-1**), 7.93 – 7.85 (m, 2H, **H-8**), 7.79 – 7.73 (m, 1H, **H-10**), 7.70 – 7.61 (m, 2H, **H-9**), 3.33 – 3.24 (m, 2H, **H-6**), 2.36 (td, *J*=7.2, 1.6, 2H, **H-2**), 1.59 – 1.38 (m, 4H, **H-3**, **H-5**), 1.35 – 1.22 (m, 2H, **H-4**).

¹³C NMR (126 MHz, DMSO-*d*₆) δ = 203.7 (**C-1**), 139.5 (**C-7**), 134.2 (**C-10**), 129.9 (**C-9**), 128.1 (**C-8**), 54.8 (**C-6**), 43.0 (**C-2**), 27.4 (**C-4**), 22.6 (**C-3**), 21.4 (**C-5**).

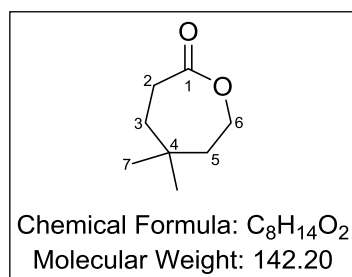
MS (EI) m/z: 55 (100%, **CHOCHCH⁺**), 143 (84%, **PhS⁺(OH)₂**), 77 (81%, **Ph⁺**), 197 (42%, **M-CH₂CHO**)

HRMS (ESI-pos) m/z (M+Na): calcd: 263.071233 found: 263.071294

5,5-Dimethyloxepan-2-one (43)

The compound was synthesized in analogy to a literature procedure.^[141]

*m*CPBA (957 mg, 5.55 mmol) was added to a stirred solution of 4,4-Dimethylcyclohexanone (500.0 mg, 3.96 mmol) in 17 mL DCM. After the addition was completed, the reaction was allowed to continue stirring at room temperature for 1 day under a argon. The resulting white suspension then filtered and the filter cake washed with DCM. The filtrate washed with 1 M NaHSO₃ (10 mL), sat. NaHCO₃ (3 x 7.5 mL), and Brine (2 x 7.5 mL) and dried over MgSO₄. After the solvent was removed under reduced pressure, the light yellow oil was purified by FC (35% EtOAc / hexanes) to provide the lactone as a clear, colorless liquid (533 mg, 3.75 mmol, 95%).



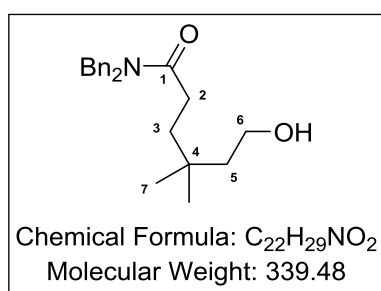
¹H NMR (500 MHz, CDCl₃) δ = 4.22 – 4.17 (m, 2H, **H-6**), 2.63 – 2.56 (m, 2H, **H-2**), 1.67 – 1.61 (m, 2H, **H-5**), 1.59 – 1.51 (m, 2H, **H-3**), 1.01 (s, 6H, **H-7**).

¹³C NMR (126 MHz, CDCl₃) δ 176.2 (**C-1**), 64.8 (**C-6**), 41.9, 35.7, 32.0, 30.0, 28.5.

The NMR data is in good agreement to those previously reported.^[142]

***N,N*-Dibenzyl-6-hydroxy-4,4-dimethylhexanamide (44)**

To a solution of AlCl_3 (952.7 mg, 7.1 mmol) in dry CH_2Cl_2 (1.5 ml), dibenzylamine (5.2 mL, 57.2 mmol) was added slowly at 0°C . After stirring the yellow solution, lactone **43** (508.0 mg, 3.6 mmol) in dry CH_2Cl_2 (1 mL) was added at 0°C dropwise, and the mixture was stirred for 5 h at that temperature. To the suspension H_2O (2.5 ml) was added. After stirring for 30 min the solution was passed through Celite. The layers were separated, and the aq. layer was extracted with CH_2Cl_2 (2x 5 mL). The combined org. layers were dried over MgSO_4 and the solvent was removed under reduced pressure. After FC (5% *i*PrOH / pentane) the product was obtained as colorless oil (741.5 mg, 2.18 mmol, 61%).



$^1\text{H NMR}$ (500 MHz, CDCl_3) δ = 7.37 (m, 2H, $\text{CH}_{\text{arom, meta}}$), 7.37 – 7.23 (m, 3H, CH_{arom}), 7.24 – 7.18 (m, 2H, $\text{CH}_{\text{arom, ortho}}$), 7.18 – 7.13 (m, 2H, $\text{CH}_{\text{arom, ortho}}$), 4.61 (s, 2H, COCH_2N), 4.46 (s, 2H, COCH_2N), 3.68 – 3.64 (m, 2H, **H-6**), 2.41 – 2.35 (m, 2H, **H-2**), 1.70 – 1.63 (m, 2H, **H-3**), 1.49 – 1.44 (m, 2H, **H-5**), 0.87 (s, 6H, **H-7**).

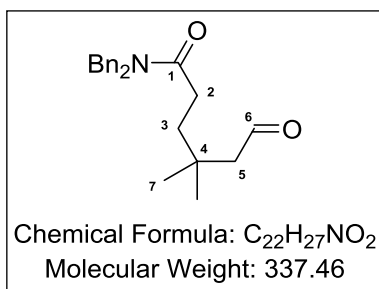
$^{13}\text{C NMR}$ (126 MHz, CDCl_3) δ = 174.2 (**C-1**), 137.4 ($\text{C}_{\text{arom, ipso}}$), 136.7 ($\text{C}_{\text{arom, ipso}}$), 129.0 ($\text{C}_{\text{arom, meta}}$), 128.6 ($\text{C}_{\text{arom, meta}}$), 128.3 ($\text{C}_{\text{arom, ortho}}$), 127.6 ($\text{C}_{\text{arom, para}}$), 127.4 ($\text{C}_{\text{arom, para}}$), 126.3 ($\text{C}_{\text{arom, ortho}}$), 59.6 (**C-6**), 50.1 (N- CH_2 -Ph), 48.4 (N- CH_2 -Ph), 43.9 (**C-5**), 37.4 (**C-3**), 32.0 (**C-4**), 28.3 (**C-2**), 27.2 (**C-7**).

The NMR assignment was supported by ^1H - ^1H -COSY and ed. ^1H - ^{13}C -HSQC measurements.

***N,N*-Dibenzyl-4,4-dimethyl-6-oxohexanamide (34c)**

A solution of alcohol **44** (265 mg, 0.78 mmol) in CH_2Cl_2 (1.0 mL) was added over 2 min to a stirred solution of DMP (397 mg, 0.94 mmol) in CH_2Cl_2 (3.0 mL). After 2 h the homogeneous solution was diluted with Et_2O (10 mL) and poured into sat. aq. NaHCO_3 (10 mL, containing 1.3 g of $\text{Na}_2\text{S}_2\text{O}_3$ per 100 mL). After stirring for 5 min, the phases were separated. The aq. layer was extracted with Et_2O (2x 10 mL) and the combined org. layers were washed with sat. NaHCO_3 and H_2O . After drying over MgSO_4 and removal of the solvent under reduced pressure, the crude product was purified by FC (33% EtOAc in hexanes). The desired aldehyde was obtained as a colorless oil (158.0. 0.47 mmol, 60%).

Experimental Section



¹H NMR (500 MHz, CDCl₃) δ = 9.79 (t, *J*=3.0, 1H, **H-6**), 7.37 (m, 2H, CH_{arom, meta}), 7.35 – 7.27 (m, 4H, CH_{arom}), 7.24 – 7.19 (m, 2H, CH_{arom, ortho}), 7.18 – 7.12 (m, 2H, CH_{arom, ortho}), 4.62 (s, 2H, COCH₂N), 4.46 (s, 2H, COCH₂N), 2.43 – 2.34 (m, 2H, **H-2**), 2.21 (d, *J*=3.1, 2H, **H-5**), 1.81 – 1.75 (m, 2H, **H-3**), 1.01 (s, 5H, **H-7**).

¹³C NMR (126 MHz, CDCl₃) δ = 203.1 (**C-6**), 173.4 (**C-1**), 137.4 (**C_{arom, ipso}**), 136.6 (**C_{arom, ipso}**), 129.0 (**C_{arom}**), 128.6 (**C_{arom}**), 128.3 (**C_{arom}**), 127.7 (**C_{arom, para}**), 127.4 (**C_{arom, para}**), 126.3 (**C_{arom}**), 54.4 (**C-5**), 50.1 (N-CH₂-Ph), 48.5 (N-CH₂-Ph), 37.8 (**C-3**), 33.2 (**C-4**), 28.1 (**C-2**), 27.1 (**C-7**).

GC-MS GC System 1, *t_r* = 18.64 min

MS (GC, EI) *m/z*: 106 (100%, **BnNH⁺**), 91 (59%, **PhCH₂⁺**), 246.2 (16%, **M-Bn**)

HRMS

7.2.2 In Situ Preparation of Enamines

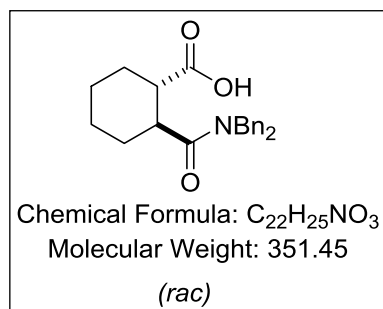
In a standard 5mm NMR tube L-proline (30 μmol) was suspended in the deuterated solvent (0.6 mL). Then the corresponding amounts of additives and aldehyde (30 μmol) were added. After shaking, the sample was transferred to the spectrometer and the NMR-experiments were started.

7.3 Synthesis of Proline Derived Enaminones with an Intramolecular Hydrogen Bond Acceptor

The reactions presented here have not been optimized. The most reactions have been run only once to see, whether the desired target structure can be synthesized and whether it shows the elusive hydrogen bond.

trans-2-(Dibenzylcarbamoyl)cyclohexane-1-carboxylic acid (**52**)

A solution of *trans*-1,2-cyclohexanedicarboxylic acid **51** (2.2 g, 12.8 mmol) was refluxed for 3 h in Ac₂O (50 mL). After removal of the excess acetic anhydride and AcOH under reduced pressure, the solid residue was dissolved in dry CH₂Cl₂ and dibenzylamine (2.7 mL, 14.1 mmol) was added. After stirring for 1h, the solvent was removed under reduced pressure. After washing with pentane (2x) the desired product was obtained as a white solid (3.1 g, 8.8 mmol, 69%).



¹H NMR (500 MHz, CDCl₃) δ = 11.86 (s, 1H, COOH), 7.40 – 7.34 (m, 2H, CH_{arom, meta}), 7.34 – 7.28 (m, 5H, CH_{arom}), 7.24 (m, 1H, CH_{arom, para}), 7.18 – 7.13 (m, 2H, CH_{arom, ortho}), 4.80 (d, J=14.9, 1H, CHHN), 4.59 (d, J=16.6, 1H, CHHN), 4.46 (d, J=16.5, 1H, CHHN), 4.38 (d, J=14.9, 1H, CHHN), 3.10 – 3.02 (m, 1H, CHCO), 2.97 – 2.89 (m, 1H, CHCO), 2.29 – 2.18 (m, 1H, CH_{aliph}), 1.90 – 1.73 (m, 3H, CH_{aliph}), 1.53 (qd, J=13.1, 3.4, 1H, CH_{aliph}), 1.47 – 1.34 (m, 2H, CH_{aliph}), 1.28 – 1.14 (m, 1H, CH_{aliph}).

¹³C NMR (126 MHz, CDCl₃) δ = 181.2, 175.7, 128.8, 128.6, 127.9, 127.7, 127.2, 127.1, 49.8, 47.7, 45.4, 42.3, 29.2, 29.2, 25.5, 25.4.

MS (EI) m/z: 106 (100%, BnNH⁺), 91 (84%, Bn⁺), 351 (18%, M⁺)

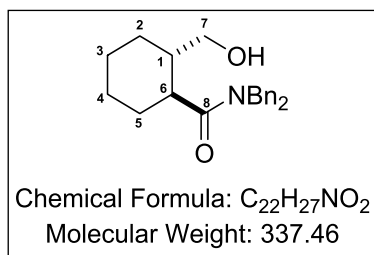
HRMS (ESI-pos) m/z (M+Na): calcd: 374.172661 found: 374.173027

trans-N,N-Dibenzyl-2-(hydroxymethyl)cyclohexane-1-carboxamide (**53**)

To carboxylic acid **52** (2.7 g, 7.7 mmol) in dry THF (50 mL) the borane complex BH₃·Me₂S (0.8 mL, 8.9 mmol) was added at 0 °C and stirred at room temperature overnight. After quenching with H₂O (100 mL), the mixture was extracted with EtOAc (3x 50 mL). The combined org. layers were washed with brine, dried over Na₂SO₄ and the

Experimental Section

solvent was removed under reduced pressure. Purification by FC (5% iPrOH / pentane) gave the desired product as a colorless, viscous oil (2.2 g, 6.7 mmol, 87%).



¹H NMR (500 MHz, CDCl₃) δ = 7.38 (dd, J =8.2, 6.8, 2H, CH_{arom, meta}), 7.34 – 7.28 (m, 3H, CH_{arom}), 7.30 – 7.22 (m, 1H, CH_{arom, para}), 7.24 – 7.19 (m, 4H, CH_{arom}), 4.90 (d, J =14.8, 1H, CHHN), 4.55 (d, J =17.1, 1H, CHHN), 4.46 (d, J =17.1, 1H, CHHN), 4.34 (d, J =14.8, 1H, CHHN), 3.49 (dd, J =10.8, 4.8, 1H, H-7'), 3.45 (dd, J =10.8, 5.5, 1H, H-7''), 2.45 (ddd, J =11.9, 10.3, 3.4, 1H, H-6), 2.18 – 2.07 (m, 1H, H-1), 1.85 – 1.70 (m, 4H, H-3', H-4', H-5', H-2'), 1.59 (qd, J =12.9, 3.2, 1H, H-5''), 1.35 (qt, J =13.0, 3.7, 1H, H-3''), 1.13 (qt, J =13.3, 3.5, 1H, H-4''), 1.04 (qd, J =12.7, 3.3, 1H, H-2'').

¹³C NMR (126 MHz, CDCl₃) δ = 177.1 (C-8), 137.5 (C_{arom, ipso}), 136.9 (CH_{arom, ipso}), 128.9 (CH_{arom}), 128.6 (CH_{arom}), 128.1 (CH_{arom}), 127.6 (CH_{arom}), 127.3 (CH_{arom}), 126.5 (CH_{arom}), 67.2 (C-7), 49.8 (N-CH₂-Ph), 48.3 (N-CH₂-Ph), 43.6 (C-6), 41.5 (C-1), 30.7 (C-5), 28.6 (C-2), 25.7 (C-4), 25.4 (C-3).

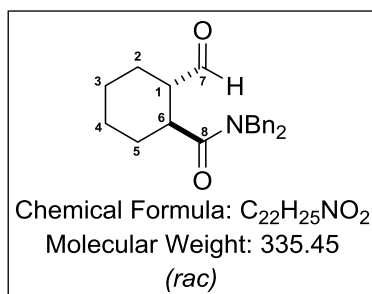
The NMR assignment was supported by ¹H-¹H-COSY and ed. ¹H-¹³C-HSQC measurements.

MS (EI) m/z: 106 (100%, BnNH⁺), 91 (46%, Bn⁺), 246 (25%, M-Bn)

HRMS (ESI-pos) m/z (M+Na): calcd: 360.193398 found: 360.193055

***trans*-N,N-Dibenzyl-2-formylcyclohexane-1-carboxamide (54)**

A solution of alcohol **53** (2.0 g, 5.9 mmol) in CH₂Cl₂ (3.5 mL) was added to a stirred solution of DMP (3.0 g, 7.1 mmol) in CH₂Cl₂ (20 mL). After 2 h the homogeneous solution was diluted with Et₂O (30 mL) and poured into sat. aq. NaHCO₃ (30 mL, containing 7.8 g of Na₂S₂O₃). After stirring for 5 min, the phases were separated. The aq. phase was extracted with Et₂O (2x 50 mL) and the combined org. layers were washed with sat. NaHCO₃ and H₂O. After drying over MgSO₄ and removal of the solvent, the crude product was purified by FC (33% EtOAc in hexanes). The desired aldehyde was obtained as colorless oil (1.5 g, 4.5 mmol, 66%).



1H NMR (500 MHz, $CDCl_3$) δ = 9.71 (s, 1H, **H-7**), 7.43 – 7.36 (m, 2H, $CH_{arom, meta}$), 7.35 – 7.27 (m, 5H, CH_{arom}), 7.29 – 7.22 (m, 1H, $CH_{arom, para}$), 7.16 (m, 1.7, 2H, $CH_{arom, ortho}$), 4.75 (d, $J=14.9$, 1H, $CHHN$), 4.60 (d, $J=16.7$, 1H, $CHHN$), 4.49 (d, $J=16.7$, 1H, $CHHN$), 4.41 (d, $J=15.0$, 1H, $CHHN$), 3.09 (ddd, $J=13.4, 10.2, 3.5$, 1H, **H-1**), 2.80 (ddd, $J=12.4, 10.2, 3.5$, 1H, **H-6**), 2.24 – 2.15 (m, 1H, **H-2'**), 1.91 – 1.73 (m, 3H, **H-3'**, **H-4'**, **H-5'**), 1.51 (qd, $J=12.9, 3.3$, 1H, **H-5''**), 1.40 (qt, $J=12.9, 3.6$, 1H, **H-3''**), 1.13 (qt, $J=13.2, 3.5$, 1H, **H-4''**), 1.07 (qd, $J=13.0, 3.6$, 1H, **H-2''**).

^{13}C NMR (126 MHz, $CDCl_3$) δ = 203.4 (**C-7**), 175.3 (**C-8**), 137.3 ($C_{arom, ipso}$), 136.7 ($C_{arom, ipso}$), 128.9 (CH_{arom}), 128.5 (CH_{arom}), 128.0 (CH_{arom}), 127.6 ($CH_{arom, para}$), 127.2 ($CH_{arom, para}$), 127.0 (CH_{arom}), 52.3 (**C-1**), 49.9 (N- CH_2 -Ph), 47.8 (N- CH_2 -Ph), 40.4 (**C-6**), 29.4 (**C-5**), 25.41 (**C-2**), 25.42 (**C-3**), 25.35 (**C-4**).

The NMR assignment supported by comparison with **53** and by 1H - 1H -COSY and ed. 1H - ^{13}C -HSQC measurements.

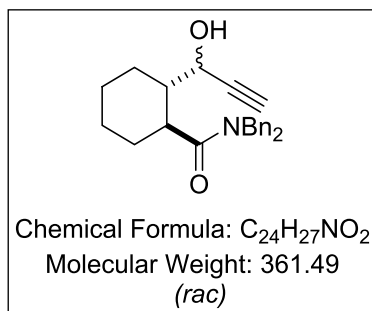
MS (EI) m/z: 106 (100%, $BnNH^+$), 91 (82%), 91 (84%, Bn^+), 244 (70%, **M-Bn**), 335 (34%, M^+)

HRMS (ESI-pos) m/z (M+Na): calcd: 358.177747 found: 358.177510

***trans*-N,N-Dibenzyl-2-(1-hydroxyprop-2-yn-1-yl)cyclohexane-1-carboxamide (**55**)**

To a solution of trimethylsilyl acetylene (0.7 mL, 4.2 mmol) in dry THF (90 mL) at -78 °C, *n*-BuLi (2.5 M in hexane, 1.9 mL, 4.7 mmol) was added dropwise. After stirring for 1 h at -78 °C aldehyde **54** (1.5 g, 4.5 mmol) in THF (10 mL) was added dropwise and the reaction was stirred for additional 30 min at -78 °C and then warmed up to rt in 30 min. Afterwards the mixture was quenched with water and extracted with MTBE (3x 100 mL). The organic layers were combined, washed with brine, dried over $MgSO_4$ and the solvent was removed under reduced pressure. The crude mixture was dissolved in MeOH (50 mL) and K_2CO_3 (1.9 g.) was added and stirred for at rt for 2 h. The crude mixture was filtered through a pad of celite and washed with CH_2Cl_2 . The residue was washed with aq. NH_4Cl and brine and dried over $MgSO_4$. The crude alcohol (1.5 g) was used for the further the next step without further purification.

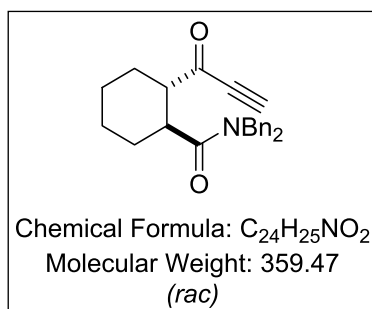
Experimental Section



¹H NMR (500 MHz, CDCl₃) δ = 7.39 – 7.16 (m, 10H, CH_{arom}), 4.87 – 4.75 (m, 1H, CHHN), 4.55 (d, J=16.9, 1H, CHHN), 4.49 – 4.33 (m, 3H, 2 x CHHN, CHOH), 2.53 (ddd, J=12.0, 10.4, 3.4, 1H), 2.39 (d, J=2.2, 1H, CH_{sp}), 2.38 – 2.29 (m, 2H, OH, CH-CHOR), 2.12 (ddd, J=12.5, 5.7, 3.5, 1H), 1.84 – 1.70 (m, 3H), 1.59 – 1.48 (m, 1H), 1.35 (m, 1H), 1.22 – 1.05 (m, 2H).

trans-N,N-Dibenzyl-2-propioloylcyclohexane-1-carboxamide (**56**)

Crude alcohol **55** (1.5 g, 4.5 mmol) was dissolved in CH₂Cl₂ (50 mL) and treated with MnO₂ (5.8 g 67.1 mmol). After stirring at rt for 8 h, the reaction was completed as monitored by TLC analysis. Excess MnO₂ was removed by filtration of the reaction mixture through celite. The filtrate was washed H₂O and brine. After drying over MgSO₄ the product (410 mg, 26%) was obtained.

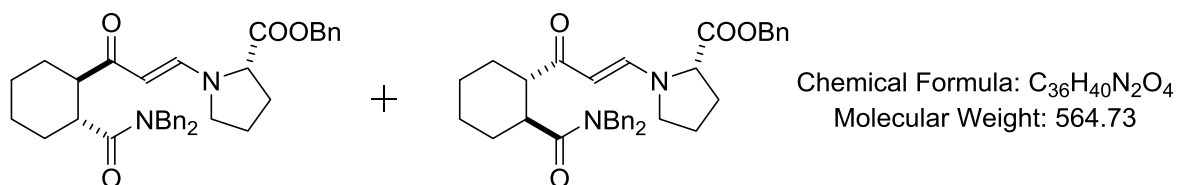


¹H NMR (500 MHz, CDCl₃) δ = 7.42 – 7.36 (m, 2H), 7.35 – 7.28 (m, 5H), 7.24 (d, J=7.4, 1H), 7.16 – 7.11 (m, 2H), 4.78 (d, J=15.0, 1H, CHHN), 4.61 (d, J=16.5, 1H, CHHN), 4.44 (d, J=16.5, 1H, CHHN), 4.30 (d, J=15.0, 1H, CHHN), 3.25 (ddd, J=13.2, 10.1, 3.5, 1H), 3.25 (s, 1H, COCCH), 2.93 (ddd, J=12.5, 10.2, 3.5, 1H), 2.42 – 2.34 (m, 1H), 1.85 (ddt, J=17.3, 13.9, 3.6, 2H), 1.77 (dt, J=13.2, 3.3, 1H), 1.54 – 1.36 (m, 2H), 1.26 – 1.09 (m, 2H).

¹³C NMR (126 MHz, CDCl₃) δ = 189.9, 175.0, 137.3, 136.6, 128.8, 128.6, 128.0, 127.7, 127.2, 79.4, 54.6, 49.8, 47.5, 41.5, 29.2, 28.4, 25.7, 25.4.

Benzyl ((E)-3-*trans*-2-(dibenzylcarbamoyl)cyclohexyl)-3-oxoprop-1-en-1-yl)-L-prolinate (**57**)

L-Proline benzylester (240 mg, 1.17 mmol) was added to alkynone **56** (400 mg, 1.11 mmol) in DCM (20 mL) and stirred for 3h. Then the solvent was removed under reduced pressure. After purification by FC (50% EtOAc/hexanes), the diastomeric product mixture (455 mg, 0.81 mmol, 72 %) was obtained as white, powder.



MS (ESI-pos) m/z: 565.29 (**M+H**)

HRMS (ESI-pos) m/z (M+Na): calcd: 587.288026 found: 587.288171

The diastereomers were separated by prep. HPLC with the following conditions: 250 mm Zorbax Sil 21.2 mm i.d., *iso*-hexane/*i*-ProOH=90:10, 15 mL/min, 308 K.

The first diastereomer (150.8 mg, $t_r = 16.36$ min) was obtained with high purity (99.9 %).

The second diastereomer (223.2 mg, $t_r = 18.01$ min 94% purity) was re-purified with the following conditions: 250 mm Zorbax Sil 21.2 mm i.d., *iso*-hexane/*i*-ProOH=95:5, 15 mL/min, 308 K. Diastereomers II (156.0 mg, $t_r = 46.37$ min) was obtained with a purity of 98.3%.

The dr of the samples was analyzed with an analytical column (100 Interchim XS Strategy Si, 4.6 mm i.d., 81580) and the following conditions: *n*-heptane/*i*-ProOH=90:10, 1.0 mL/min, 308K, UV 220 nm.

Retention times:

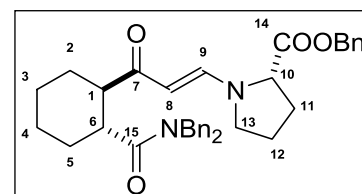
Diastereomer I: $t_r = 4.7$ min

Diastereomer II: $t_r = 5.1$ min

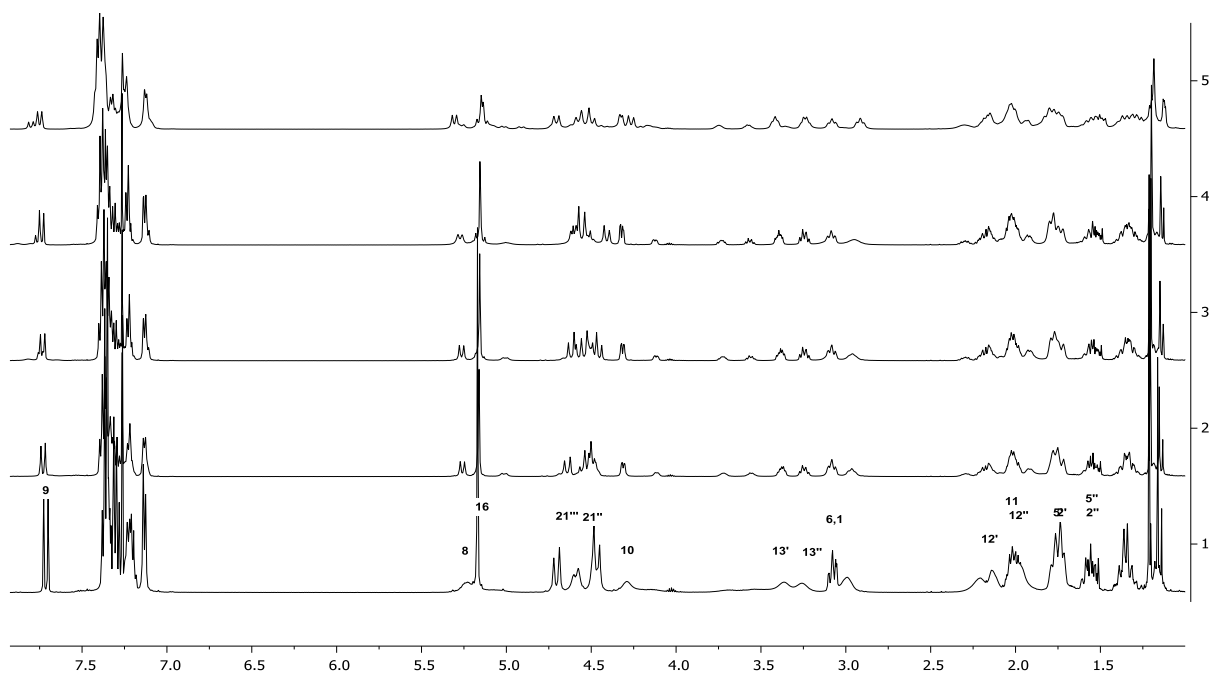
An unambiguous assignment of the diastereomers was not successful due to broadening of all the NMR signals. The given structures represent the proposed diastereomers based on the results at low temperatures for the deprotected enaminones.

Diastereomer I

Variable temperature measurements were performed to find the optimal measurement conditions:



Experimental Section



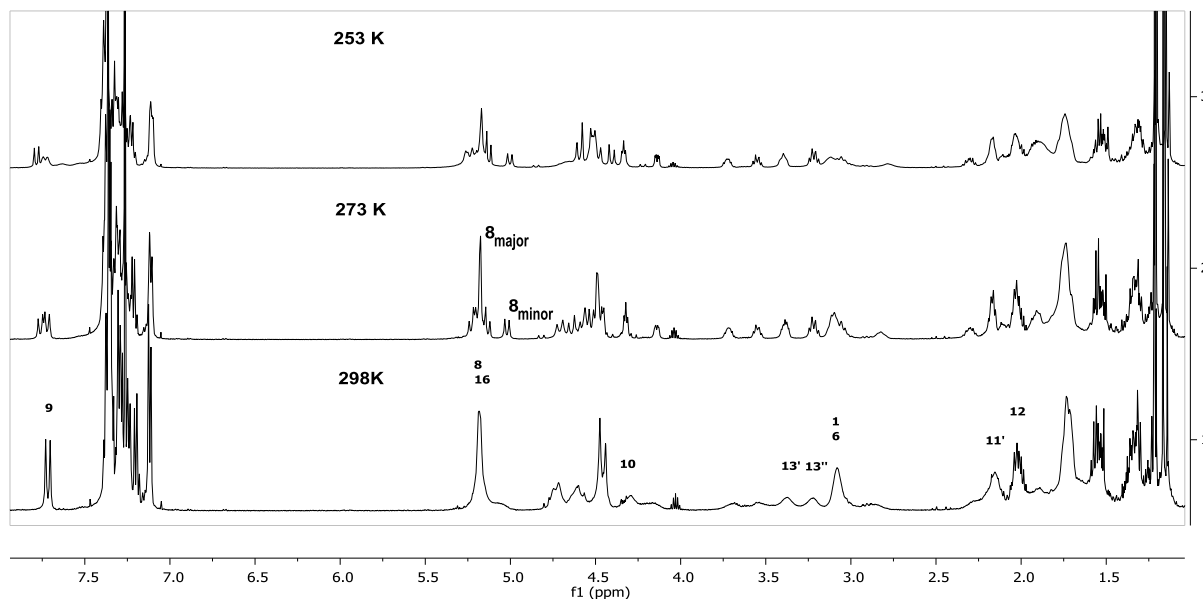
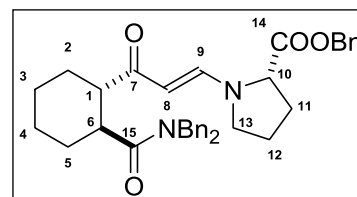
The best signals were obtained at 273 K (0 °C). At this temperature two enamine rotamers (ratio = 3:1) are visible. Both are (*E*)-configured ($^3J = 12.5$ Hz). An NMR assignment could be obtained for the major enamine rotamer at 273 K. Due to missing HMBC peaks, an assignment of the cyclohexyl ring was not successful. The unambiguous results are presented in the following table:

Assignments		
Atom	Chemical Shift	HMBC
1 C		
H	3.08	
6 C		
H	3.08	
7 C	200.42	9, 8
8 C	98.20	
H	5.26	7
9 C	147.74	
H	7.73	7, 10, 13
10 C	64.12	9, 13'
H	4.30	
11 C	23.70	13', 13''
H2	2.04	
12 C	30.07	13'
H'	2.17	
H''	2.00	

Assignments		
Atom	Chemical Shift	HMBC
13 C	47.37	9
H'	3.40	10, 12, 11
H''	3.21	11
14 C	171.91	
15 C	176.51	
16 C	67.37	
H2	5.16	
17 C	135.15	
18 C	128.34	

Diastereomer II

Variable temperature measurements were performed to find optimal measurement conditions. The best signals were obtained at 273 K (0 °C). At this temperature two enamine rotamers (ratio = 2:1) are visible. Both are (*E*)-configured ($^3J = 13.2$ Hz).



An NMR assignment could be obtained for the major enamine rotamer at 273 K. Due to missing HMBC peaks, an assignment of the cyclohexyl ring was not successful. The unambiguous results are presented in the following table:

Assignments		
Atom	Chemical Shift	HMBC
7 C	200.06	
8 C	99.16	8
H	5.20	8
9 C	148.25	
H	7.72	13, 10
10 C	64.05	9, 13', 11', 12
H	4.32	11, 12, 13, 14
11 C	29.38	13', 10
H2	2.17	14, 12, 13, 10
12 C	23.63	13', 10, 11'
H2	2.03	10, 13
13 C	47.37	9, 10, 11', 12
H'	3.37	12, 11, 10
H''	3.22	
14 C	171.76	10, 11'

((E)-3-(trans-2-(Dibenzylcarbamoyl)cyclohexyl)-3-oxoprop-1-en-1-yl)-L-proline (50)

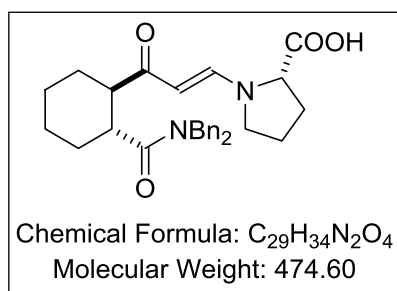
To enaminone **57** (25 mg, 0.044 mmol) in EtOAc (5.0 mL) 10% Pd/C (4.7 mg) was added and stirred atmosphere of hydrogen overnight. After removing the solid components by zentrifugation, the solvent was removed under reduced pressure. The product (17.4 mg, 0.27 mmol, 83%) was used for the NMR analysis without further purification. Purification on silica led to decomposition of the compound.

MS (EI) m/z: 91 (100%, **Bn**⁺) 106 (50%, **BnNH**⁺), 124 (82%), 234 (70%, **M-Bn**), 335 (34%, **M**⁺), 430 (8%, **M-COOH**)

MS (ESI-pos) m/z: 475.2 (M+H)

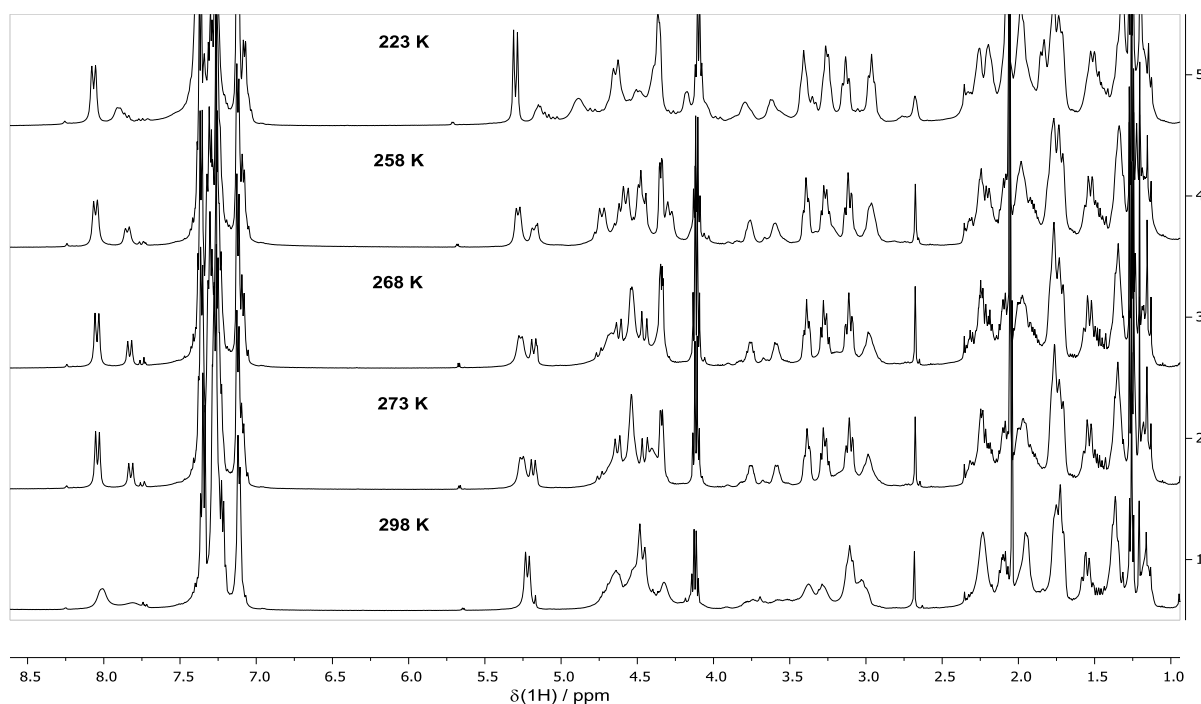
HRMS (ESI-neg) m/z (M-H): calcd: 473.244586 found: 473.244807

Diastereomer I

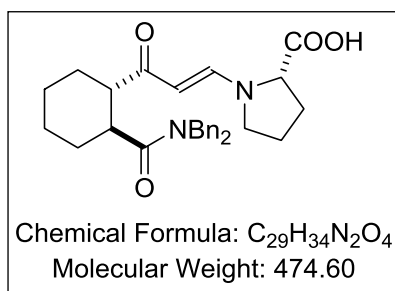


Variable temperature measurements were performed to find optimal measurement conditions. No conditions could be found, that enabled good measurement conditions to determine the 3D structure of the molecule with NOESY measurements. As in **57** two different (*E*)-enamine rotamers were observed (³*J* = 12.7 and 13.2 Hz) at 273 K.

¹H-NMR spectra at various temperatures:

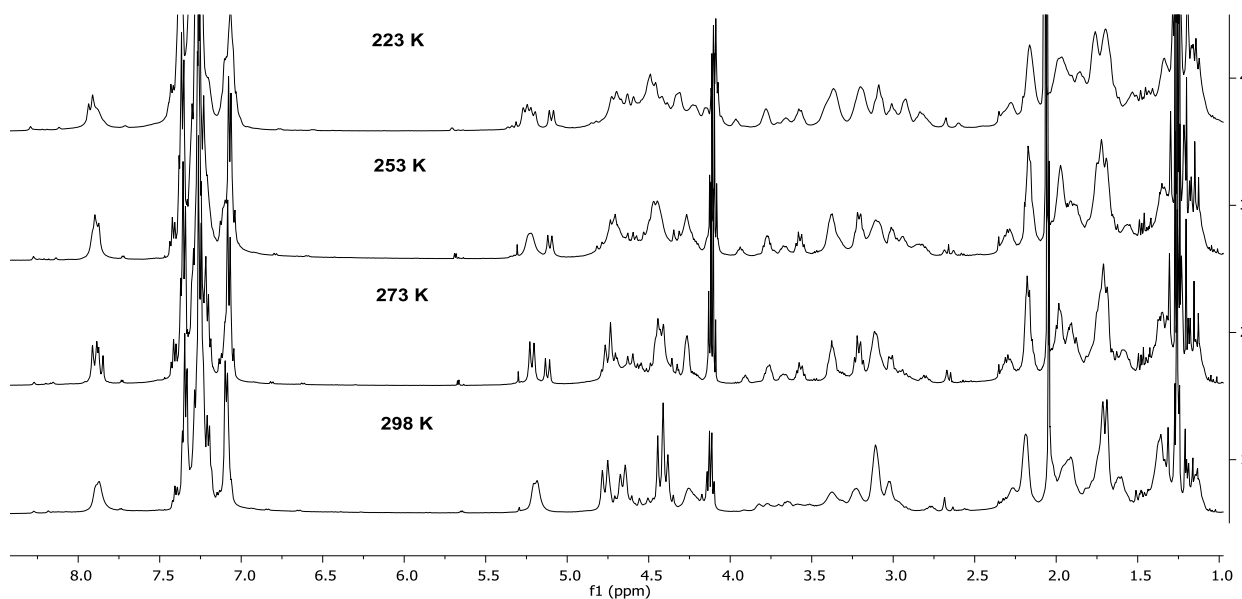


Diastereomer II

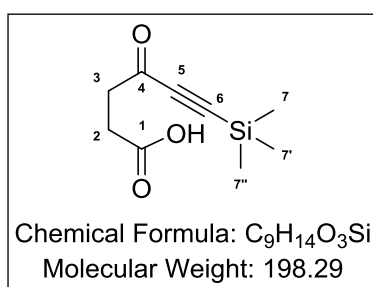


Variable temperature measurements were performed to find optimal measurement conditions. No conditions could be found, that enabled good measurement conditions to determine the 3D structure of the molecule with NOESY measurements. As in **57** two different (*E*)-enamine rotamers were observed ($^3J = 13.2$ and 14.0 Hz) at 273 K.

1H -NMR spectra at various temperatures:

4-Oxo-6-(trimethylsilyl)hex-5-ynoic acid (**59**)

To a suspension of powdered $AlCl_3$ (1.46 g, 11.0 mmol) in dry CH_2Cl_2 (20 mL) a mixture of succinic anhydride (1.00 g, 10.0 mmol) and bis(TMS)acetylene in CH_2Cl_2 (20 mL) was added dropwise at $0^\circ C$. After stirring for 45 min, the solution was poured on ice/ 10% HCl (50 mL). After separation of the phases, the aq. phase was extracted with CH_2Cl_2 (2x 25 mL). The combined phases were dried over $MgSO_4$ and the solvent was removed under reduced pressure. After washing with pentanes, the product was obtained as a white solid (610 mg, 3.08 mmol, 31%).



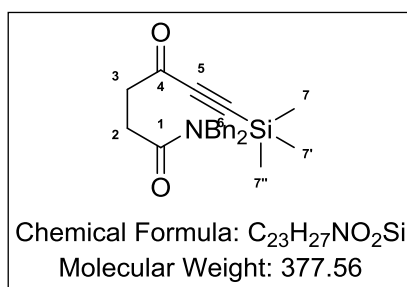
1H NMR (500 MHz, $CDCl_3$) $\delta = 11.28$ (bs, 1H, COOH), 2.90 (t, $J=6.6$, 2H, H-3), 2.69 (t, $J=6.6$, 2H, H-2), 0.24 (s, 9H, H-7, H-7', H-7'').

^{13}C NMR (126 MHz, $CDCl_3$) $\delta = 184.9$ (C-4), 178.3 (C-1), 101.3 (C-5), 99.0 (C-6), 39.5 (C-3), 27.6 (C-2), -0.8 (C-7, C-

7', C-7'').

N,N-Dibenzyl-4-oxo-6-(trimethylsilyl)hex-5-ynamide (60)

To a stirred solution of 2-chloro-4,6-dimethoxy-1,3,5-triazine (CDMT) (292 mg 1.66 mmol) and acid **59** (300.0 mg, 1.51 mmol) in dry CH₂Cl₂ (4.5 mL) N-methylmorpholine (117 μl, 1.66 mmol) was added dropwise so that the temperature remained at 0-5 °C. After further stirring for 2 h at 0 °C all the CDMT was consumed. To this suspension, dibenzylamine was added at -5 °C (351 μl, 1.82 mmol). Then the solution was slowly warmed up to rt and stirred for further 20 h. Afterwards the solvent was removed under reduced pressure and the residue was dissolved in EtOAc (10 mL). The undissolved solids were filtered, and the organic layers washed with 1N HCl, sat. aq. NaHCO₃, water and brine. After drying over MgSO₄ and removal of the solvent, the product was purified by FC (5% EtOAc in hexanes) to obtain the desired amide as yellowish, viscous oil (551 mg, 1.46 mmol, 96%).



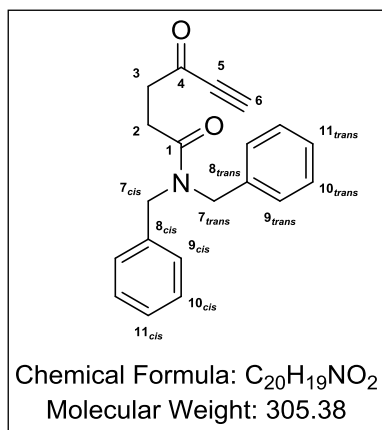
¹H NMR (500 MHz, CDCl₃) δ = 7.42 – 7.35 (m, 2H, H_{meta,arom}), 7.34 – 7.24 (m, 4H, 2x H_{meta,arom}, 2x H_{para,arom}), 7.20 (m, 4H, H_{ortho,arom}), 4.60 (d, J=2.6, 2H, *trans*-Ph-CH₂-NCO), 4.49 (s, 2H, *cis*-Ph-CH₂-N), 3.04 (t, J=6.4, 2H, H-3), 2.75 (t, J=6.4, 2H, H-2), 0.24 (s, 8H, H-7, H-7', H-7'').

¹³C NMR (126 MHz, CDCl₃) δ = 186.2 (C-4), 171.5 (C-1), 137.2 (C_{ipso,arom}), 136.2 (C_{ipso,arom}), 129.0 (2x C_{meta,arom}), 128.6 (2x C_{meta,arom}), 128.2 (2x C_{ortho,arom}), 127.6 (C_{para,arom}), 127.4 (C_{para,arom}), 126.4 (2x C_{ortho,arom}), 101.8 (C-5), 98.1 (C-6), 49.8 (*cis*-Ph-CH₂-N), 48.4 (*trans*-Ph-CH₂-N), 40.3 (C-3), 26.9 (C-2), -0.8 (C-7, C-7', C-7'').

The NMR assignment was supported by ¹H-¹H-NOESY and *edited* ¹H-¹³C-HSQC measurements.

N,N-Dibenzyl-4-oxohex-5-ynamide (61)

To the TMS-protected alkyne (550 mg, 1.46 mmol) in MeOH (2.9 mL) Borax (0.01 M in water, 0.29 mL) was added. After full consumption of the SM as monitored by TLC, MeOH was removed under reduced pressure, the mixture was extracted with EtOAc. After purification by FC (gradient: 9% to 17% EtOAc/Hexanes), the desired alkyne was obtained.

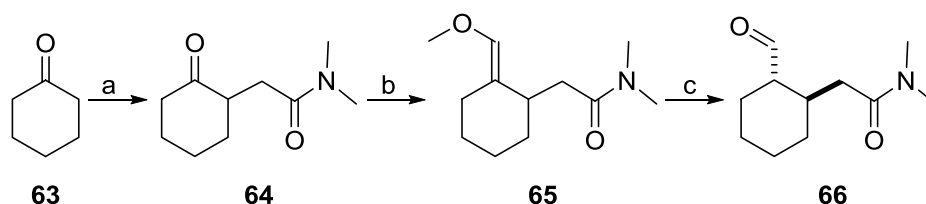


¹H NMR (500 MHz, CDCl₃) δ = 7.38 (t, *J*=7.5, 2H, **H-10_{cis}**), 7.36 – 7.23 (m, 4H, **H-10_{trans}**, **H-11**), 7.23 – 7.18 (m, 4H, **H-9**), 4.60 (s, 2H, **H-7_{trans}**), 4.49 (s, 2H, **H-7_{cis}**), 3.23 (s, 1H, **H-6**), 3.05 (t, *J*=6.3, 2H, **H-3**), 2.77 (t, *J*=6.3, 2H, **H-2**).

¹³C NMR (126 MHz, CDCl₃) δ = 185.9 (**C-4**), 171.3 (**C-1**), 137.1 (**C-8_{trans}**), 136.1 (**C-8_{cis}**), 129.0 (**C-10_{cis}**), 128.6 (**C-10_{trans}**), 128.2 (**C-9_{trans}**), 127.7 (**C-11**), 127.4 (**C-11**), 126.4 (**C-9_{cis}**), 81.3 (**C-5**), 78.7 (**C-6**), 49.8 (**C-7_{cis}**), 48.5 (**C-7_{trans}**), 40.3 (**C-3**), 27.0 (**C-2**).

The NMR assignment was supported by comparison with **60** and ed. ¹H-¹³C-HSQC and ¹H-¹³C-HMBC measurements.

2-(*trans*-2-Formylcyclohexyl)-*N,N*-dimethylacetamide (**66**)



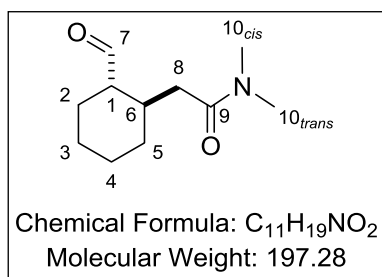
a) To a solution of cyclohexanone **63** (250 μL, 2.4 mmol) in THF (10 ml) LDA (2 M in THF, 1.3 mL) was added slowly at 0 °C. After stirring for 30 min at 0 °C, 2-Chloro-*N,N*-dimethylacetamide (262 μL, 2.54 mmol) was added dropwise and stirred for further one hour at rt. Afterwards the reaction was quenched with H₂O (10 mL) and extracted 3x with EtOAc (3x 10 mL) The combined organic layers were washed with brine, dried over NaSO₄ and the solvent was removed under reduced pressure. After FC (80% EtOAc in hexanes), the impure product (233 mg) was directly used for the next step.

b) To a solution of (methoxymethyl)triphenylphosphonium chloride (310 mg, 0.9 mmol) in THF (10 mL) was added NaOtBu (100 mg, 0.9 mmol) at -10 °C and stirred for 30 min. Afterwards ketone **64** was added. The mixture was warmed up to rt and stirred overnight. Then water was added (5 mL) and the mixture was extracted with EtOAc (3x 10 mL). The combined org. layers were washed with brine, dried over NaSO₄ and afterwards the solvent was removed under reduced pressure. After FC (50% EtOAc in hexanes) the product was obtained as E/Z mixture (230 mg) with impurities of OPh₃.

c) The enol ether **66** (230 mg) was dissolved in CH₂Cl₂ (5 mL) and TFA (340 μL) was added dropwise. After stirring for 2 h sat. aq. NaHCO₃ was added. The phases were separated and the org. phase was washed once more with sat. aq. NaHCO₃ aa(3 mL)

Experimental Section

and brine (3 mL). The organic layer was dried over NaSO₄ and the solvent was removed under reduced pressure. After flash chromatography (40% EtOAc/ hexanes) the product was obtained as colorless oil (115 mg, 0.58 mmol, 24% over 3 steps).



¹H NMR (501 MHz, CDCl₃) δ = 9.50 (d, *J*=3.9, 1H, **H-7**), 2.99 (s, 2H, **H-10_{cis}**), 2.91 (s, 2H, **H-10_{trans}**), 2.38 (dd, *J*=15.2, 5.1, 1H, **H-8'**), 2.29 – 2.19 (m, 1H, **H-6**), 2.12 (dd, *J*=15.2, 7.7, 1H, **H-8''**), 2.05 (dddd, *J*=11.6, 10.4, 3.9, 3.7, 1H, **H-1**), 1.88 (dddd, *J*=13.3, 4.4, 3.7, 3.3, 1H, **H-5_α**), 1.83 – 1.76 (m, 2H, **H-3_α**, **H-2_β**), 1.75 – 1.68 (m, 1H, **H-4_β**), 1.44 – 1.24 (m, 3H, **H-2_α**, **H-4_α**, **H-3_β**), 1.04 (dddd, *J*=13.3, 12.5, 11.3, 3.8, 1H, **H-5_β**).

¹³C NMR (126 MHz, CDCl₃) δ = 204.8 (**C-7**), 171.5 (**C-9**), 55.9 (**C-1**), 38.3 (**C-8**), 37.3 (**C-10_{cis}**), 35.4 (**C-10_{trans}**), 33.3 (**C-6**), 31.6 (**C-5**), 26.1 (**C-2**), 25.2 (**C-4**), 24.6 (**C-3**).

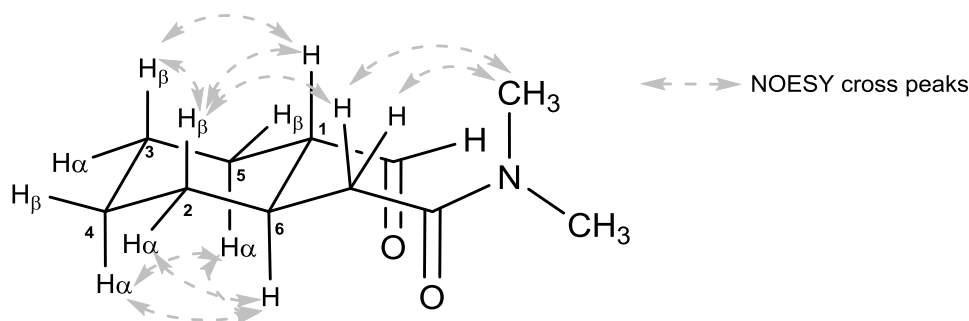
The structure was analyzed by ¹H, ¹³C, ¹H-¹H-COSY, ed. ¹H-¹³C-HSQC and HMBC measurements. The important cross peaks are concluded in the following table:

Assignments					
Atom	Chemical Shift	COSY	HSQC	HMBC	NOESY
1 C	55.85		1	8', 8''	
H	2.05	7, 2 _α , 2 _β , 6	1	2	2 _β , 5 _β , 2 _α , 3 _β , 7
2 C	26.05		2 _α , 2 _β	1	
Ha	1.39	3 _α , 3 _β , 2 _β , 1	2		1, 6, 3 _α , 2 _β , 7
Hβ	1.79	3 _α , 3 _β , 2 _α , 1	2		1, 2 _α , 3 _β , 7
3 C	24.60		3 _α , 3 _β		
Ha	1.79	2 _α , 4 _α , 4 _β , 3 _β , 2 _β	3		2 _α , 3 _β
Hβ	1.28	2 _α , 4 _α , 4 _β , 3 _α , 2 _β	3		1, 3 _α , 2 _β
4 C	25.16		4 _α , 4 _β		
Ha	1.30	3 _α , 5 _α , 5 _β , 4 _β , 3 _β	4		6, 5 _α , 4 _β
Hβ	1.71	3 _α , 5 _α , 5 _β , 4 _α , 3 _β	4		5 _β , 4 _α
5 C	31.62		5 _α , 5 _β	8', 8''	
Ha	1.88	4 _α , 6, 5 _β , 4 _β	5		6, 8'', 5 _β , 4 _α
Hβ	1.04	4 _α , 6, 5 _α , 4 _β	5		1, 6, 8'', 5 _α , 4 _β
6 C	33.34		6	8', 8''	
H	2.23	8', 8'', 5 _α , 5 _β , 1	6	8	5 _α , 5 _β , 2 _α , 4 _α , 7
7 C	204.79		7		
H	9.50	1	7		8', 1, 6, 2 _α , 2 _β
8 C	38.19		8', 8''	6	
H'	2.38	6, 8''	8	9, 1, 5, 6	7, 10 _{cis}
H''	2.12	8', 6	8	9, 1, 5, 6	5 _α , 5 _β , 10 _{cis}
9 C	171.47			10 _{trans} , 10 _{cis} , 8',	

		8"	
10cis C	37.33	10cis	10trans
H3	2.99	10cis	10trans, 9
10trans C	35.43	10trans	10cis
H3	2.91	10trans	10cis, 9

The relative configuration of the product was determined with the coupling constants of **H-1** and by 2D-NOESY.

The most important NOE correlations are visualized in the next figure:



GC-MS: GC System 1, t_r = 10.93 min

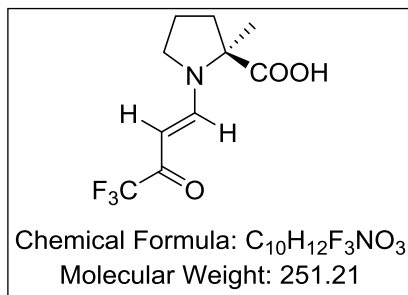
GC (GC, EI) m/z: 111 (100 %, **M-CH₂CONMe₂**), 166.1 (93.9%, **M-CO₂H**), 93 (42%) 81.1 (32%), 137.1 (19%)

(S,E)-2-methyl-1-(4,4,4-trifluoro-3-oxobut-1-en-1-yl)pyrrolidine-2-carboxylic acid (67b)

L- α -Methyl-proline (38.7 mg, 0.30 mmol) was dissolved in 2 N NaOH (0.5 mL) and cooled down to 0 °C. Then 4-ethoxy-1,1,1-trifluoro-3-buten-2-one (36 μ L, 0.25 mmol) in 0.2 mL THF was slowly added and stirred overnight. The solution was acidified with 3 Drops of HCl_{conc} and then extracted with EtOAc. The organic solvent was removed under reduced pressure.

Experimental Section

The product was analyzed by NMR without further purification to show the effect of the methyl group.



1H NMR δ = 8.21 (d, $J=12.1$, 1H), 5.40 (d, $J=12.1$, 1H), 3.65 – 3.45 (m, 2H), 2.59 (ddd, $J=12.8$, 6.6, 4.1, 1H), 2.16 – 1.93 (m, 1H), 1.68 (s, 3H).

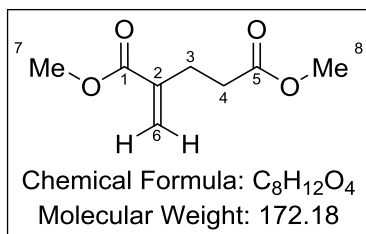
(S,E)-2-methyl-1-(3-oxobut-1-en-1-yl)pyrrolidine-2-carboxylic acid (67c)

L- α -Methyl-proline (38.7 mg, 0.30 mmol) was dissolved in 2N NaOH (0.1 mL) and cooled down to 0 °C. Then 4-methoxy-3-buten-2-one (25 μ L, 0.25 mmol) in 50 μ L THF was slowly added and stirred overnight. The solution was acidified of HCl (pH=3) and then extracted with EtOAc. The organic solvent was removed under reduced pressure.

Dimethyl 2-methylenepentanedioate (72)

The compound was synthesized following a literature procedure.^[141]

Methyl acrylate **71** (5 mL, 55.5 mmol) was degassed by one freeze-thaw cycle and cooled to -10 °C. Then tri-*n*-octylphosphine (2.5 mL, 5.6 mmol) was added slowly. After 20 min the reaction was warmed up to rt and stirred for another 30 min. The volatiles were removed on a rotary evaporator. After distillation the desired product was obtained as colorless liquid (3.2 g, 27.8 mol, 66%).



1H NMR (500 MHz, $CDCl_3$) δ 6.18 (s, 1H, **H-6_{cis}**), 5.61 – 5.57 (m, 1H, **H-6_{trans}**), 3.74 (s, 3H, **H-7**), 3.65 (s, 3H, **H-8**), 2.63 (t, $J = 7.5$ Hz, 2H, **H-3**), 2.51 (t, $J = 7.8$ Hz, 2H, **H-4**).

^{13}C NMR (126 MHz, $CDCl_3$) δ = 173.1 (**C-5**), 167.1 (**C-1**), 138.8 (**C-2**), 125.9 (**C-6**), 51.9 (**C-7**), 51.6(**C-8**), 32.9 (**C-4**),

27.3 (**C-3**).

The assignment was achieved using *edited*- 1H - ^{13}C -HSQC and 1H - ^{13}C -HMBC experiments.

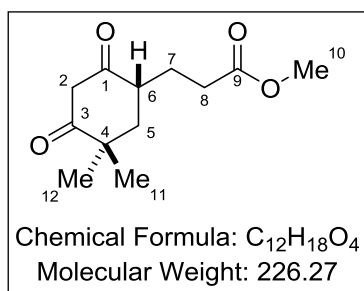
MS (EI) m/z: 141 (41%, **M-OMe**), 140 (66%, **M-OMe-H**), 113 (39%, **M-CO₂Me**), 112 (100%, **M-CO₂Me-H**), 81 (33%), 59 (32%)

HRMS (ESI-pos) m/z (M+Na): calcd: 195.062779 found: 195.062800

The physical data is in good agreement to those previously reported.^[140]

Methyl 3-(5,5-dimethyl-2,4-dioxocyclohexyl)propanoate (**70**)

To 3-Methyl-2-butanone (2.42 mL, 22.65 mmol) in THF (19 mL) KO^tBu (2.35 g, 20.91 mmol) was added at 0 °C and stirred for 10 min at that temperature. Then the methyl methacrylate derivative **70** (3.00 g, 17.42 mmol) was added dropwise. A white precipitate formed. The suspension was stirred for 2 h at rt and afterwards quenched with conc. HCl (2.48 mL, 26.14 mmol). The solvents were removed under reduced pressure. After FC (20% EtOAc/hexanes) the product was obtained as a slightly yellow powder (2.34 g, 17.42 mmol, 59 %).

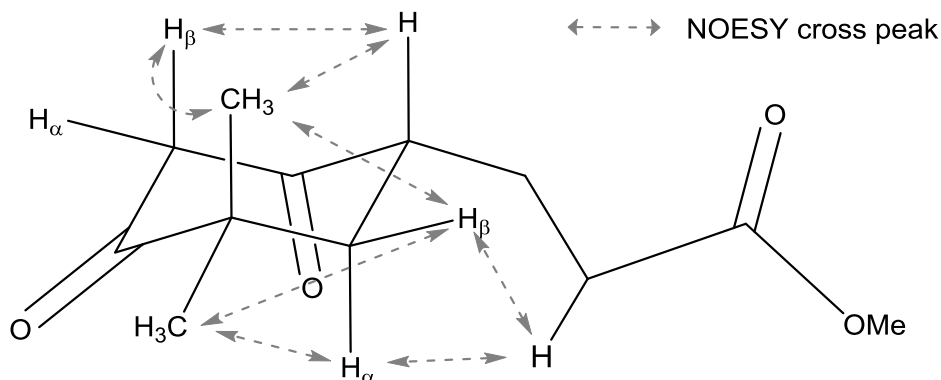


¹H NMR (501 MHz, CDCl₃) δ 3.68 (s, 3H, **H-10**), 3.58 (dd, *J* = 16.6, 0.9 Hz, 1H, **H-2β**), 3.35 (d, *J* = 16.6 Hz, 1H, **H-2α**), 2.74 (ddtd, *J* = 13.7, 7.2, 5.6, 0.9 Hz, 1H, **H-6**), 2.53 – 2.40 (m, 2H, **H-8**), 2.12 (dq, *J* = 14.4, 7.2 Hz, 1H, **H-7'**), 1.89 (dd, *J* = 14.0, 5.5 Hz, 1H, **H-5β**), 1.69 (dtd, *J* = 14.4, 7.8, 7.0, 5.6 Hz, 1H, **H-7''**), 1.48 (t, *J* = 13.7 Hz, 1H, **H-5α**), 1.30 (s, 3H, **H-11**), 1.17 (s, 3H, **H-12**).

¹³C NMR (126 MHz, CDCl₃) δ 207.7 (**C-3**), 204.1 (**C-1**), 173.6 (**C-9**), 55.6 (**C-2**), 51.7 (**C-10**), 45.3 (**C-6**), 44.9 (**C-4**), 39.9 (**C-5**), 31.3 (**C-8**), 24.7 (**C-12**), 24.6 (**C-11**), 24.4 (**C-7**).

The assignment was achieved using ¹H-¹H-COSY, ¹H-¹H-NOESY, *edited*-¹H-¹³C-HSQC and ¹H-¹³C-HMBC experiments.

Stereo information extracted from ^1H - ^1H -NOESY:



There are small amounts of the enol-form present in solution ($\delta_{\text{H-2}} = 5.32$ ppm). Interestingly the exchange of rate of the axial H-2 β is bigger the one of the H-2 α presumably due to its better transition state towards the enol form.

MS (EI) m/z: 226 (8%, **M**⁺), 194 (47%, **M-OMe-H**), 176 (32%), 100 (100%), 70 (54%)

HRMS (ESI-pos) m/z (M+Na): calcd: 249.109729 found: 249.109790

7.4 Synthesis of an Proline Derived Aryl Amine with an Intramolecular Hydrogen Bond Acceptor

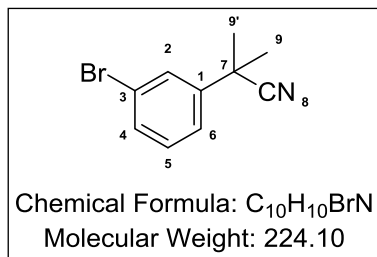
The reactions presented here have not been optimized. The most reactions have been run only once to see, whether the desired target structure can be synthesized and if it shows the elusive hydrogen bond or not.

2-(3-Bromophenyl)-2-methylpropanenitrile (76)

The compound was synthesized following a literature procedure.^[143]

To a stirring solution of 3'-bromophenylacetonitril (3.24 g, 16.52 mmol, 1 equiv) in 45 mL dry THF at -50°C KOtBu (4.08 g, 36.36 mmol, 2.2 equiv) was added and the mixture was stirred for some minutes. After the dropwise addition of MeI (2.6 mL, 41.32 mmol, 2.5 equiv), the cooling bath was removed and the reaction was stirred at rt. GC-MS analysis (after mini-workup with 1M HCl, EtOAc) indicated that the reaction had proceeded to completion after ~ 2 h. To the pink suspension aq. HCl (1M, 15 mL) was added and the yellow mixture was poured into H₂O (20 mL), followed by extraction with EtOAc (3x 30 mL). After washing with 30 mL brine/ sat. aq NaHCO₄-solution (ratio 1:2) and drying over NaSO₄, the solvent was removed under reduced. The residual brownish oil was 2x

filtered over SiO₂ (20% Et₂O / Pentane) and dried overnight at high vacuum. The product was obtained as a colorless oil (3.66 g, 15.48 mmol, 99%).



¹H NMR (501 MHz, CDCl₃) δ = 7.60 (t, *J*=1.9, 1H, **H-2**), 7.46 (ddd, *J*=7.9, 1.9, 1.0, 1H, **H-4**), 7.43 (ddd, *J*=7.9, 1.9, 1.0, 1H, **H-5**), 7.27 (t, *J*=7.9, 1H, **H-6**), 1.72 (s, 6H, **H-9**)

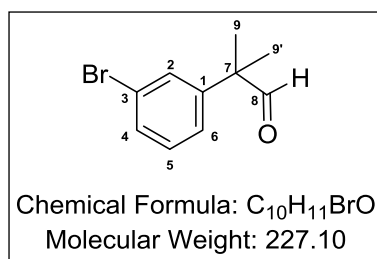
¹³C NMR (126 MHz, CDCl₃) δ 143.6 (**C-1**), 131.0 (**C-4**), 130.5 (**C-5**), 128.3 (**C-2**), 123.9 (**C-6**), 123.9 (**C-8**), 123.0 (**C-3**), 37.0 (**C-10**), 29.0 (**C-9**, **C-9'**).

The physical data is in good agreement to those previously reported.^[143]

2-(3-Bromophenyl)-2-methylpropanal (77)

The compound was synthesized following a literature procedure.^[143]

To a stirring solution of cyanide **76** (3.45 g, 15.39 mmol, 1 equiv) in THF at -78 °C was added DIBAL-H (1.0 M in THF, 15.4 mL) dropwise over 10 min. After the addition was complete, the mixture was stirred for 2 h at the same temperature. 6 M HCl was added, the cooling bath was removed and the reaction mixture was stirred for 1 h. The mixture was poured into 40 mL CH₂Cl₂ and the phases were separated. The water phase was extracted with CH₂Cl₂ (3 × 50mL) and the combined organic fractions were washed with brine, dried over NaSO₄, and concentrated under reduced pressure. After drying at high vacuum the product was obtained as colorless oil (3.30 g, 14.73 mmol, 96%).



¹H NMR (501 MHz, CDCl₃) δ = 9.49 (s, 1H, **H-8**), 7.45 – 7.40 (m, 2H, 4, **H-2**), 7.25 (t, *J*=8.4, 7.9, 1H, **H-5**), 7.19 (ddd, *J*=7.9, 1.8, 1.2, 1H, **H-6**), 1.46 (s, 7H, **H-9**, **H-9'**).

¹³C NMR (126 MHz, CDCl₃) δ = 201.4 (**C-8**), 143.6 (**C-1**), 130.4 (**C-4**), 130.3 (**C-5**), 129.9 (**C-2**), 125.5 (**C-6**), 123.1 (**C-3**), 50.4 (**C-7**), 22.5 (**C-9**, **C-9'**).

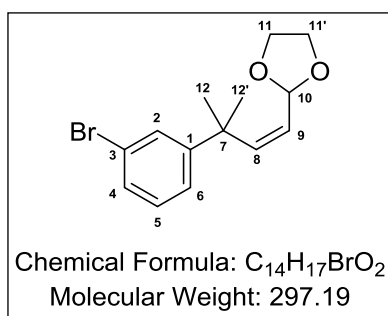
MS (EI) m/z: 228 (12%, **M⁺**), 226 (12%, **M⁺**), 199 (98%, **M-CHO**), 197 (100%, **M-CHO**), 171 (30%, **3-Br-Ph-CH₂⁺**), 169 (31%, **3-Br-Ph-CH₂⁺**), 118 (38%)

HRMS (EI) m/z (M⁺): calcd: 225.999340 found: 225.999577

The physical data is in good agreement to those previously reported.^[143]

(Z)-2-(3-(3-bromophenyl)-3-methylbut-1-en-1-yl)-1,3-dioxolane (135)

To (1,3-Dioxolan-2-ylmethyl)triphenylphosphonium bromide (1.0 g, 2.33 mmol) in dry THF (3.5 mL) in a flame dried Schlenk flask KOtBu (252 mg, 2.24 mmol) was added at -40°C and stirred for 30 min. Afterwards aldehyde **77** (196 mg, 0.86 mmol) in THF (0.7 mL) was added to the yellow suspension, stirred for 30 min at -40°C and then warm up to rt and stirred for further 3d. No full conversion was observed after this time and more Wittig reagent was added. When the reaction was fully converted (10 d), the reaction was quenched with water (10 mL) and extracted with MTBE (2x 20 mL). After drying over NaSO₄ the solvent was removed under reduced pressure. The crude product was purified by FC (30% EtOAc/hexanes). The product was obtained as colorless oil (104 mg, 0.35 mmol, 41%). No *E*-product was observed in the crude mixture of the compound.



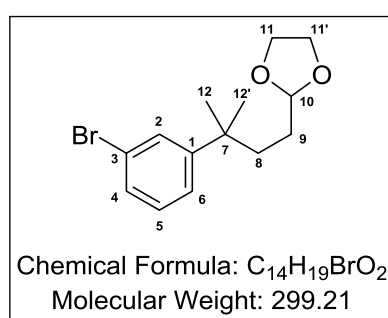
¹H NMR (501 MHz, CDCl₃) δ = 7.53 (t, *J*=1.9, 1H, **H-2**), 7.35 – 7.30 (m, 2H, **H-4**, **H-6**), 7.17 (t, *J*=7.9, 1H, **H-5**), 5.97 (dd, *J*=12.0, 1.0, 1H, **H-8**), 5.39 (dd, *J*=12.0, 7.7, 1H, **H-9**), 4.98 (dd, *J*=7.8, 1.0, 1H, **H-10**), 3.95 – 3.86 (m, 2H, **H'-11**, **H'-11'**), 3.74 – 3.63 (m, 2H, **H''-11**, **H''-11'**), 1.48 (s, 6H, **H-12**, **H-12'**).

GC-MS GC System 1, *t_r* = 13.98 min

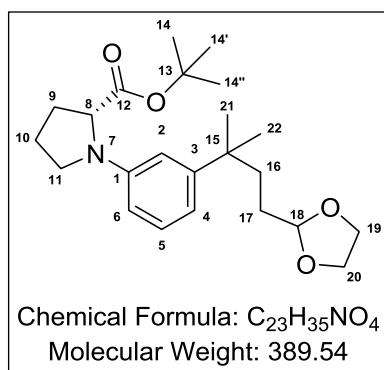
MS (GC, EI) *m/z*: 99.1 (100%, **M-[3-Br-Ph-C(CH₃)₂]**), 140.1 (97%, **M-[3-Br-Ph]**), 73.1 (43%, **(-OCH₂CH₂O)-C⁺H**), 86.1(30%, **(-OCH₂CH₂O)-C=C⁺H**), 295 (4%, **M-H**), 297 (4%, **M-H**)

2-(3-(3-bromophenyl)-3-methylbutyl)-1,3-dioxolane (78)

To olefin **135** (100 mg, 0.34 mmol) in EtOAc (1.0 mL) 10% Pd/C (36 mg) was added and stirred for 18h under hydrogen atmosphere. After filtering over Celite, the solvent was removed under reduced pressure. The product (80 mg, 0.27 mmol, 80%) was used in the next reaction without further purification.



¹H NMR (501 MHz, CDCl₃) δ = 7.45 (t, *J*=1.9, 1H, **H-2**), 7.30 (dt, *J*=7.8, 1.9, 1.1, 1H, **H-4**), 7.26 (dt, *J*=7.8, 1.9, 1.1, 1H, **H-6**), 7.16 (t, *J*=7.8, 1H, **H-5**), 4.76 (t, *J*=4.7, 1H, **H-10**), 3.95 – 3.90 (m, 2H, **H'-11**, **H'-11'**), 3.84 – 3.78 (m, 2H, **H''-11**, **H''-11'**), 1.74 – 1.68 (m, 2H, **H-9**), 1.47 – 1.39 (m, 2H, **H-8**), 1.30 (s, 6H, **H-12'**, **H-12**).

tert-butyl (3-(4-(1,3-dioxolan-2-yl)-2-methylbutan-2-yl)phenyl)-L-prolinate (79)

A mixture of Pd₂(dba)₃ (2.4 mg, 0.0027 mmol), RuPhos (5.0 mg, 0.011 mmol), NaOtBu (41.1 mg, 0.43 mmol) and 4Å MS in a flamed dry Schlenk flask was set under argon atmosphere. After adding dry toluene (0.55 mL), Arylbromide **78** (80.0 mg, 0.27 mmol) and L-Proline *tert*-butylester (64.1 mg, 0.37 mmol) were added and the red suspension was heated overnight at 100°C. Afterwards sat. aq. NaHCO₃ (1 mL) was added and the mixture was

extracted with EtOAc (3x 5 mL). After drying over Na₂SO₄ the solvent was removed under reduced pressure. After prep. TLC (10% EtOAc/ hexanes) the product (18.0 mg) was obtained as a inseparable mixture with 2-(3-phenyl-3-methylbutyl)-1,3-dioxolane and was used directly in the next reaction.

The compound was characterized by NMR from the mixture by ¹H, ¹³C, ¹H-¹H-COSY, ¹H-¹³C-HSQC and ¹H-¹³C-HMBC.

The assignments can be found in the following table:

Assignments					Assignments				
Atom	Chemical Shift	COSY	HSQC	HMBC	Atom	Chemical Shift	COSY	HSQC	HMBC
1 C	146.67			5	14 C	28.00		14	14', 14''
2 C	109.75		2	4, 6	H3	1.42		14	13, 14', 14''
H	6.51		2	15, 6, 4	14' C	28.00		14'	14, 14''
3 C	149.74			5, 22, 21	H3	1.42		14'	14, 14'', 13
4 C	114.34		4	2, 6	14'' C	28.00		14''	14, 14'
H	6.69	5	4	15, 6, 2	H3	1.42		14''	14', 14, 13
5 C	128.74		5		15 C	37.33			4, 2, 16, 22, 21
H	7.14	4, 6	5	1, 6, 3	16 C	38.18		16	18, 17, 22, 21
6 C	109.33		6	4, 2, 5	H2	1.74	17	16	15, 17, 22, 21
H	6.37	5	6	2, 4	17 C	29.40		17	18, 16
8 C	61.67		8	11'	H2	1.45	16	17	16, 18
H	4.12	9', 9''	8	10, 11, 9, 12	18 C	105.02		18	19', 19'', 20', 20'', 17
9 C	30.90		9', 9''	8, 11', 10', 10''	H	4.75		18	16, 20, 19, 17
H'	2.24	8, 10', 10''	9	12, 11, 10	19 C	64.75		19',	18, 20',
H''	2.09	8, 10', 10''	9	12, 11, 10					
10 C	23.87		10'	8, 11', 11'', 9', 9''					
H'	2.17	11', 11'', 9', 9''	10	9					

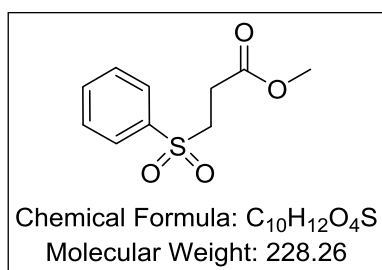
Experimental Section

H''	2.03	11', 11'', 9', 9''	9			19''	20''
11 C	48.25		11', 11''	8, 9', 9''			
H'	3.53	10', 10''	11	8, 9, 10			
H''	3.35	10', 10''	11	10			
12 C	173.97			8, 9', 9''			
13 C	80.86			14, 14', 14''			
H'	3.91					19	20, 18
H''	3.80					19	20, 18
20 C	64.75					20', 20''	18, 19', 19''
H'	3.91					20	19, 18
H''	3.80					20	19, 18
21 C	29.09					21	16, 22
H3	1.29					21	3, 15, 22, 16
22 C	28.76					22	16, 21
H3	1.29					22	3, 15, 21, 16

Methyl 3-(phenylsulfonyl)propanoate (82)

The compound was synthesized following a literature procedure.^[144]

Sodium benzenesulfinate **81** (250 mg, 1.5 mmol) was dissolved in 0.25 M HCl (6 mL). Then methacrylate **71** (275 μ l, 3.0 mmol) was added and stirred overnight at 70 °C. Afterwards the biphasic solution was extracted with EtOAc (3x 15 mL). After drying with NaSO₄ the organic solvent was removed under reduced pressure and the product was obtained as a colorless crystalline solid after drying at high vacuum overnight (342.0 mg, 1.5 mmol, 98%). The product was used without further purification for the next step.



¹H NMR (501 MHz, CDCl₃) δ = 7.94 – 7.87 (m, 2H, **H-2**, **H-2'**), 7.71 – 7.61 (m, 1H, **H-4**), 7.61 – 7.53 (m, 2H, **H-3**, **H-3'**), 3.62 (s, 3H, **H-8**), 3.46 – 3.38 (m, 2H, **H-5**), 2.79 – 2.70 (m, 2H, **H-6**).

¹³C NMR (126 MHz, CDCl₃) δ = 170.4 (**C-7**), 138.4 (**C-1**), 134.0 (**C-4**), 129.4 (**C-3**, **C-3'**), 128.2 (**C-2**, **C-2'**), 52.3 (**C-5**), 51.4 (**C-8**), 27.6 (**C-6**).

GC-MS GC System 1, t_r = 13.90 min

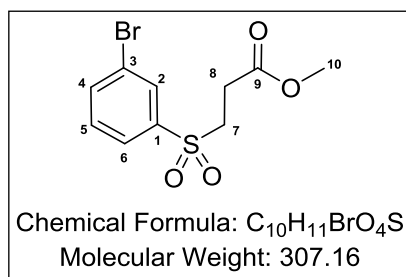
MS (GC, EI) m/z : 77.1 (100%, **Ph**⁺), 104.1 (62%), 125 (51%), 87.1 (38%, **MeOOCCH₂CH₂**⁺), 59.1 (33%, **[CO₂Me]**⁺), 141 (25%, **PhSO₂**⁺)

The physical data is in good agreement to those previously reported.^[144]

A single crystal suitable for X-ray analysis (see 9.1, page 145) could be obtained by recrystallization from EtOAc/Et₂O.

Methyl 3-((3-bromophenyl)sulfonyl)propanoate (83)

A 1:1 mixture of H₂SO₄/ H₂O (15 mL) was heated to 60 °C. Then sulfone **82** (2.5 g, 11.0 mmol) and NBS (2.2 g, 12.6 mmol) were added and stirred for 2.5 h at this temperature. Afterwards methanol (75 mL) was added to the suspension and stirred for 3h at rt. The yellowish solution was neutralized with sat. aq. NaHCO₃ and addition Na₂SO₃ to quench bromine. The mixture was extracted with MTBE(3x). After drying over NaSO₄, the solvent was removed. After recrystallization in 20%EtOAc/ hexanes, the product was obtained colorless needles (2.5g, 8.14 mmol).



¹H NMR (501 MHz, CDCl₃) δ = 8.06 (dd, *J*=1.9, 1.8, 1H, **H-2**), 7.85 (ddd, *J*=7.8, 1.8, 1.0, 1H, **H-6**), 7.81 (ddd, *J*=8.0, 1.9, 1.0, 1H, **H-4**), 7.47 (dd, *J*=8.0, 7.8, 1H, **H-5**), 3.66 (s, 3H, **H-10**), 3.45 (t, *J*=7.6, 2H, **H-7**), 2.78 (t, *J*=7.6, 2H, **H-8**).

¹³C NMR (126 MHz, CDCl₃) δ = 170.2 (**C-9**), 140.4 (**C-1**), 137.1 (**C-4**), 131.1 (**C-2**), 130.9 (**C-5**), 126.7 (**C-6**), 123.4 (**C-3**), 52.4 (**C-10**), 51.5 (**C-7**), 27.5 (**C-8**).

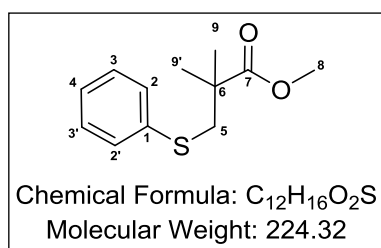
GC-MS GC System 1, *t_r* = 15.36 min

MS (GC, EI) m/z: 59.1 (100 %, [CO₂Me]⁺), 155 (81%, 3-Br-Ph⁺), 156.9 (81%, 3-Br-Ph⁺), 87.1 (75%, MeOOCCH₂CH₂⁺), 202.9 (37%), 204.9 (38%), 306 (16%, M⁺), 308 (19%, M⁺)

Methyl 2,2-dimethyl-3-(phenylthio)propanoate (88)

The compound was synthesized following a literature procedure. ^[145]

To a solution of methyl-2,2-dimethyl-3-hydroxypropionat **87** (2.69 g, 20.4 mmol) and diphenyl disulfide **86** (4.9 g 22.4 mmol) in DMF (100 mL) trioctylphosphine (10.9 mL, 24.5 mmol) was added. The mixture was stirred at 70 °C for 24h. After quenching with 200 mL sat. aq. NaHCO₃/H₂O (1:1), the mixture was extracted with 66% Hexanes/MTBE. The organic phase was washed with brine, dried with NaSO₄ and the solvent was removed under reduced pressure. After FC with MTBE/hexanes (0 -> 10%) the product was obtained as colorless oil (3.18 g, 20.4 mmol, 70%).



¹H NMR (501 MHz, CDCl₃) δ = 7.40 – 7.36 (m, 2H, **H-2**, **H-2'**), 7.29 – 7.24 (m, 3H, **H-3**, **H-3'**), 7.20 – 7.15 (m, 1H, **H-4**), 3.57 (s, 3H, **H-8**), 3.18 (s, 2H, **H-5**), 1.29 (s, 6H, **H-9'**, **H-9**).

Experimental Section

^{13}C NMR (126 MHz, CDCl_3) δ = 176.6 (**C-7**), 137.0 (**C-1**), 130.1 (**C-2**, **C-2'**), 128.8 (**C-3**, **C-3'**), 126.2 (**C-4**), 51.8 (**C-8**), 44.9 (**C-5**), 43.9 (**C-6**), 24.8 (**C-9**, **C-9'**).

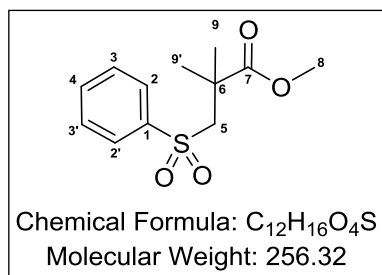
GC-MS: GC System 1, t_r = 12.11 min

GC (GC, EI) m/z: 123 (100 %, PhSCH_2^+), 109 (53%, PhS^+) 59.1 (40%, $[\text{CO}_2\text{Me}]^+$), 224.1 (32%, M^+)

The physical data is in good agreement to those previously reported. ^[146]

Methyl 2,2-dimethyl-3-(phenylsulfonyl)propanoate (**89**)

Thioether **88** (3.15 g, 14.0 mmol) was dissolved in a 1:1:1 mixture of THF, H_2O and MeOH (30 mL). After cooling the solution to 0 °C Oxone (24.2 g, 39.3 mmol) was slowly added. When no full conversion of the SM was observed by TLC additional Oxon was added (5 g, 8.1 mmol). After completion the mixture was poured onto water (250 mL) and extracted with CH_2Cl_2 (3x 150 mL). After drying over NaSO_4 the solvent was removed under reduced pressure. The product was obtained as a slightly yellow solid (1.3 g, 14.0 mmol, 36%) and used without further purification for the next step.



^1H NMR (501 MHz, CDCl_3) δ = 7.94 – 7.88 (m, 2H, **H-2**, **H-2'**), 7.67 – 7.62 (m, 1H, **H-4**), 7.59 – 7.53 (m, 2H, **H-3**, **H-3'**), 3.68 (s, 3H, **H-8**), 3.47 (s, 2H, **H-5**), 1.41 (s, 6H, **H-9**, **H-9'**).

^{13}C NMR (126 MHz, CDCl_3) δ = 175.4 (**C-7**), 141.1 (**C-1**), 133.6 (**C-4**), 129.2 (**C-3**, **C-3'**), 127.8 (**C-2**, **C-2'**), 64.7 (**C-5**), 52.4 (**C-8**), 41.5 (**C-6**), 25.4 (**C-9**, **C-9'**).

The assignment of the ^{13}C spectra was supported by an ed. ^1H - ^{13}C -HSQC.

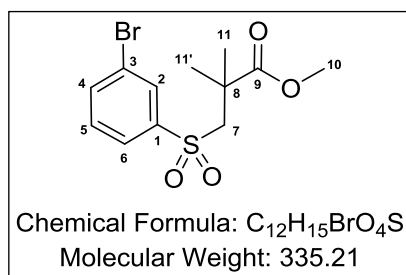
The physical data is in good agreement to those previously reported. ^[147]

A single crystal suitable for X-ray analysis (see 9.1, page 145) could be obtained by recrystallization in MTBE.

Methyl 3-((3-bromophenyl)sulfonyl)-2,2-dimethylpropanoate (**90**)

A 1:1 mixture of $\text{H}_2\text{SO}_4/\text{H}_2\text{O}$ was heated 60 °C. Then sulfone **89** (100.0 mg, 0.39 mmol) and NBS (78.8 mg, 0.45 mmol) were added and stirred for 2.5h at this temperature. Afterwards methanol (0.8 mL) was added to the suspension and stirred for 3h at rt. The yellowish solution was neutralized with sat. aq. NaHCO_3 and Na_2SO_3 . The

mixture was extracted MTBE (3x 10 mL). After drying over NaSO₄, the product was obtained as an inseparable mixture with the SM (70% pure) and was directly used for the next step.



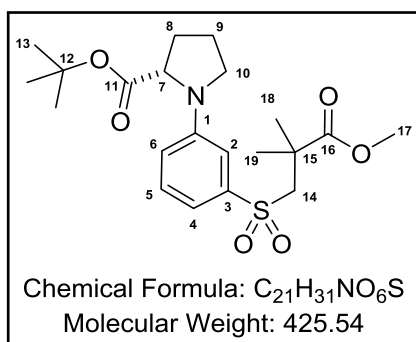
¹H NMR (501 MHz, CDCl₃) δ = 8.04 (t, *J*=1.9, 1H, **H-2**), 7.84 (ddd, *J*=7.9, 1.9, 1.1, 1H, **H-6**), 7.77 (ddd, *J*=7.9, 1.9, 1.1, 1H, **H-4**), 7.45 (t, *J*=7.9, 1H, **H-5**), 3.71 (s, 3H, **H-10**), 3.47 (s, 3H, **H-7**), 1.42 (s, 6H, **H-11**, **H-11'**).

GC-MS: GC System 1, *t_r* = 15.60 min

MS (GC, EI) m/z: 59.1 (100 %, [CO₂Me]⁺), 55.1 (66%), 154.9 (41 %, 3-Br-Ph⁺), 156.9 (40 %, 3-Br-Ph⁺), 202.9 (23%), 204.9 (26%), 339.9 (2%, M⁺), 335.9 (3%, M⁺)

tert-Butyl 3-((3-methoxy-2,2-dimethyl-3-oxopropyl)sulfonyl)phenyl)-L-prolinate (91)

Methyl 3-((3-bromophenyl)sulfonyl)-2,2-dimethylpropanoate (70.0 mg, 0.23 mmol, 55% purity (impurity: **89**)), Pd₂(dba)₃ (5.2 mg, 0.0060 mmol), (*rac*)-BINAP (8.5 mg, 0.014 mmol) and CsCO₃ (96.5 mg, 0.30 mmol) were mixed in a flamed dry Schlenk flask and set under argon atmosphere. After adding dry toluene (0.42 mL), L-Proline *tert*-butylester (50.7 mg, 0.30 mmol) was added and the red suspension was heated for 14 h at 100°C. Afterwards sat. aq. NaHCO₃ (1 mL) was added and the mixture was extracted with EtOAc (3x 5 mL). After drying over Na₂SO₄ the solvent was removed under reduced pressure. After prep. TLC (50% EtOAc / hexanes, blue fluorescing under UV) the product was obtained in 40% purity.



¹H NMR (501 MHz, CDCl₃) δ = 7.34 (t, *J*=8.4, 7.7, 1H, **H-5**), 7.17 (ddd, *J*=7.7, 1.9, 1.0, 1H, **H-4**), 7.00 (dd, *J*=2.6, 1.9, 1H, **H-2**), 6.72 (dt, *J*=8.4, 2.6, 1.0, 1H, **H-6**), 4.18 (dd, *J*=8.5, 2.2, 1H, **H-7**), 3.69 (s, 3H, **H-17**), 3.57 (td, *J*=8.7, 3.6, 1H, **H-10'**), 3.46 (d, *J*=14.9, 1H, **H-14''**), 3.45 – 3.39 (m, 1H, **H-10''**), 3.41 (d, *J*=14.2, 1H, **H-14'**), 2.34 – 2.24 (m, 1H, **H-8'**), 2.23 – 2.12 (m, 2H, **H-9'**, **H-8''**), 2.12 – 2.06 (m, 1H, **H-9''**), 1.44 (s, 9H, **H-13**), 1.41 (s, 3H, **H-19**), 1.40 (s, 3H, **H-18**).

The assignment was performed in by comparison with **85** and using ¹H-¹H-COSY. Observed cross peaks:

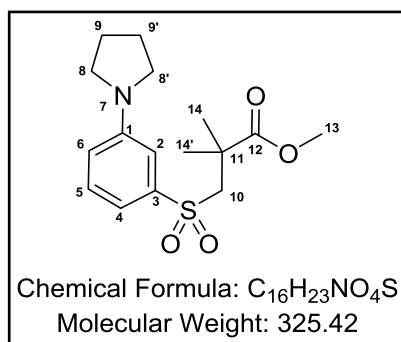
Assignments

Assignments

Atom	COSY	Atom	COSY
2 C		8 C	
H	6	H'	7, 8"
4 C		H''	8'
H	5	9 C	
5 C		H'	10', 10", 9"
H	4, 6	H''	10', 10", 9'
6 C		10 C	
H	5, 2	H'	9', 9"
7 C		H''	9', 9"
H	8'		

Methyl 2,2-dimethyl-3-((3-(pyrrolidin-1-yl)phenyl)sulfonyl)propanoate (**92**)

The mixture of **92** and **89** was dissolved in 50% TFA/CH₂Cl₂ and stirred at stirred for 2 h at rt. Afterwards the mixture was quenched with sat. aq. NaHCO₃ and extracted with CH₂Cl₂. After drying over Na₂SO₄ the solvent was removed under reduced pressure. A crude NMR analysis revealed the formation of the undesired decarboxylated product as major product.



¹H NMR (501 MHz, CDCl₃) δ = 7.33 (t, *J*=7.9, 1H, **H-5**), 7.10 (ddd, *J*=7.7, 1.9, 0.9, 1H, **H-4**), 6.97 (dd, *J*=2.4, 1.8, 1H, **H-2**), 6.72 (dd, *J*=7.8, 2.4, 1H, **H-6**), 3.69 (s, 3H, **H-13**), 3.46 (s, 2H, **H-10**), 3.36 – 3.28 (m, 4H, **H-8,H-8'**), 2.08 – 1.99 (m, 4H, **H-9, H-9'**), 1.40 (s, 6H, **H-14, H-14'**).

¹³C NMR (126 MHz, CDCl₃) δ = 175.6 (**C-12**), 148.0 (**C-1**), 141.6 (**C-3**), 129.9 (**C-5**), 116.1 (**C-6**), 113.6 (**C-4**), 109.7 (**C-2**), 64.5 (**C-10**), 52.4 (**C-13**), 47.7 (**C-8,C-8'**), 41.4 (**C-11**), 25.5 (**C-9,C-9'**), 25.4 (**C-14,C-14'**).

¹⁵N NMR (51 MHz, CDCl₃) δ = -302.1 (**N-7**).

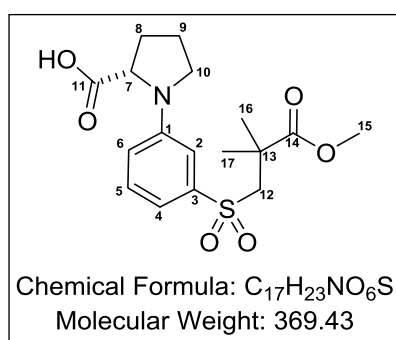
The assignment was achieved from the crude mixture using ¹H-¹H-COSY, ¹H-¹H-NOESY, *edited*-¹H-¹³C-HSQC and ¹H-¹³C-HMBC and ¹H-¹⁵N-HSQC experiments.

Observed cross peaks in the 2D spectra at 298 K:

Assignments					Assignments				
Atom	COSY	HSQC	HMBC	NOESY	Atom	COSY	HSQC	HMBC	NOESY
1 C			5		9 C		9	9', 8, 8'	
2 C		2	5, 4, 6		H2	8, 8'	9	7, 9', 8, 8'	8', 8
H	6	2	6, 4	14, 14', 8', 8	9' C		9'	9, 8, 8'	
3 C			5		H2	8, 8'	9'	7, 9, 8, 8'	8', 8
4 C		4	5, 6, 2		10 C		10	14, 14'	
H	5	4	2, 6	14, 14', 10	H2		10	12, 11, 14, 14'	4, 14, 14'
5 C		5			11 C			10, 14, 14'	
H	6, 4	5	2, 6, 4, 3, 1	6	12 C			14, 14', 10, 13	
6 C		6	5, 4, 2		13 C		13		
H	2, 5	6	2, 4	5, 8', 8	H3		13	12	
7 N			9, 9'		14 C		14	10, 14'	
8 C		8	8', 9, 9'		H3		14	12, 11, 10, 14'	4, 2, 10
H2	9', 9	8	9, 9', 8'	2, 6, 9', 9	14' C		14'	10, 14	
8' C		8'	8, 9, 9'		H3		14'	12, 11, 10, 14	4, 2, 10
H2	9', 9	8'	9, 9', 8	2, 6, 9', 9					

3-((3-Methoxy-2,2-dimethyl-3-oxopropyl)sulfonyl)phenyl)-L-proline (85)

The crude Methyl 3-((3-bromophenyl)sulfonyl)-2,2-dimethylpropanoate (50.0 mg, 70% pure, (impurity: **89**)), L-Proline (18.7 mg, 0.16 mmol), CuI (3.1 mg, 0.016 mmol) and K₂CO₃ (33.7 mg, 0.24 mmol) were transferred into a dried Schlenk flask and then DMF (0.2 mL) was added. The heterogeneous dark mixture was stirred at 90°C for 48h. Afterwards the mixture was diluted with EtOAc (10 mL) and Water (5 mL) and the solution was carefully acidified with HCl (pH = 3) to pH=3-4. The mixture was extracted with EtOAc (4 x 10 mL). After drying over NaSO₄, the solvent was evaporated under reduced pressure. After purification by preparative TLC (80% EtOAc/Hexanes + 1% AcOH) the product was obtained as yellowish oil (5.0 mg, 0.014 mmol)



¹H NMR (500 MHz, CDCl₃) δ = 7.36 (t, *J*=8.0, 1H, **H-5**), 7.24 – 7.18 (m, 1H, **H-4**), 7.04 (t, *J*=2.1, 1H, **H-2**), 6.74 (dd, *J*=8.3, 2.6, 1H, **H-6**), 4.32 (dd, *J*=8.6, 2.6, 1H, **H-7**), 3.68 (s, 3H, **H-15**), 3.61 (td, *J*=8.4, 3.2, 1H, **H-10'**), 3.45 (s, 2H, 12), 3.42 (td, *J*=8.7, 7.1, 1H, **H-10''**), 2.42 – 2.25 (m, 2H, **H-8**), 2.24 – 2.07 (m, 2H, **H-9**), 1.40 (s, 3H, **H-17**), 1.39 (s, 3H, **H-16**).

¹³C NMR (126 MHz, CDCl₃) δ = 177.5 (**C-11**), 175.6 (**C-14**), 146.9 (**C-1**), 141.9 (**C-3**), 130.1 (**C-5**), 116.7 (**C-6**), 115.5 (**C-4**), 110.5 (**C-2**), 64.6 (**C-12**), 60.5 (**C-7**), 52.4 (**C-15**), 48.6 (**C-10**), 41.4 (**C-13**), 30.9 (**C-8**), 25.41 (**C-17**), 25.38 (**C-16**), 23.7 (**C-9**).

Experimental Section

The assignment was achieved using ^1H - ^1H -COSY, ^1H - ^1H -NOESY, *edited*- ^1H - ^{13}C -HSQC and ^1H - ^{13}C -HMBC experiments.

Observed cross peaks in the 2D spectra at 298 K:

Assignments					Assignments				
Atom	COSY	HSQC	HMBC	NOESY	Atom	COSY	HSQC	HMBC	NOESY
1 C			5		10 C		10', 10''		
2 C		2	4, 6		H'	9	10		9, 10'', 6, 2
H	6, 4	2	4, 6, 3	10', 10'', 7	H''	9	10		9, 10', 6, 2
3 C			5, 2		11 C			7, 8	
4 C		4	2, 6		12 C		12	17, 16	
H	2, 6, 5	4	2, 6	12	H2		12	14, 13, 17, 16	17, 4
5 C		5			13 C			12, 17, 16	
H	6, 4	5	1, 3	6	14 C			15, 12, 17, 16	
6 C		6	4, 2		15 C		15		
H	2, 5, 4	6	2, 4	5, 7, 10', 10''	H3		15	14	
7 C		7			16 C		16	12, 17	
H	8	7	11	8, 6, 2	H3		16	14, 12, 13, 17	
8 C		8			17 C		17	12, 16	
H2	9, 7	8	11	7	H3		17	14, 12, 13, 16	12
9 C		9			25 O				
H2	10', 10'', 8	9		10', 10''	H				

MS (EI) m/z: 369 (6.77 %, M^+), 338 (2.28%, M^+ -OMe), 324 (100%, M-COOH), 210 (16.27%), 145 (34.08%)

HRMS (ESI-neg) m/z (M-H): calcd: 368.117336 found: 368.117680

7.5 Kinetic NMR Experiments

7.5.1 Torgov Cyclisation

Sample Preparation and Data Acquisition

The diketone **29a** (5.3 mg, 0.017 mol) and tetrakis(trimethylsilyl)silan (4.3 mg, 0.017 mmol, 1 equiv) as internal reference were dissolved in 0.6 mL of toluene-*d*₈. The solution was transferred into a 5mm NMR tube. After cooling the sample to 0°C in the magnet a first proton NMR spectrum was measured. This proton spectrum was used as reference for $t = 0$ s. Then the sample was cooled in a dry ice bath and the catalyst **96** (~0.5 mg, 1.5 mol%) was added and the sample was transferred again to the spectrometer at 0°C. After approximately 3 min the first proton spectrum was measured. During the first hour, every 3 min one proton was acquired, after this time every 10 minutes. All the acquired ¹H-NMR spectra were recorded with the standard proton pulse sequence (zg, 90° pulse, ns=1, d1=10s, no rotation).

Data Processing

All the NMR spectra were acquired with Bruker TOPSPIN 3.1 on an Bruker Ascend AVIII 500 MHz NMR spectrometer (11.7 Tesla) equipped with an Bruker 5mm BBFOplus 500 MHz SmartProbeTM (PA BBO 500S1 BBF-H-D-05 Z Plus) and referenced to the residual solvent signal of toluene-*d*₇ ($\delta = 2.08$ ppm). The spectra were imported into MestreNova 9.01 (Mestrelab Research, Santiago de Compostela, Spain) and a stack plot of all the spectra was generated. For the generation of the kinetic curve the reaction monitoring plugin of the program was used. For the observation of the product formation the olefinic protons and the aliphatic methyl groups were chosen. The different compounds had no overlap in these regions and seemed to be suitable for this investigation. When the signal of one compound was gone, the integral region was reduced to minimize errors from appearing and overlapping broad polar signals. In addition all the integrals were referenced to the internal standard.

7.5.2 Mannich Reaction

Sample Preparation and Data Acquisition

N-Boc-Sulfone **31a** (17.5 mg) was dissolved in dry CDCl₃ and dry toluene (0.011 mL) was added as an internal standard. The solution was cooled to 0°C and a ¹H NMR spectrum was measured. After the addition of silyl ketene acetal **32** (0.042 mL) at 0°C,

Experimental Section

another ^1H NMR spectrum was measured. This proton spectrum was used as reference for $t = 0$ s. Then the catalyst **13b** (2 mg, 5 mol%) was added and a ^1H NMR spectrum was measured every 30 minutes until the starting material was fully converted (24h).

Data Processing

All the NMR spectra were acquired with Bruker TOPSPIN 3.1 on an Bruker Ascend AVIII 500 MHz NMR spectrometer (11.7 Tesla) equipped with an Bruker 5mm BBFOplus 500 MHz SmartProbeTM (PA BBO 500S1 BBF-H-D-05 Z Plus). The single spectra were processed with Bruker TOPSPIN 3.1 and after phasing and baseline correction, the CHN-protons were integrated using $\text{CH}_3\text{-Ph}$ as the internal standard. The plot was then generated with Microsoft Excel.

7.6 PHIP Experiments

7.6.1 Sample Preparation

The CD_2Cl_2 used in these experiments was dried by distillation over CaCO_3 and stored in a Schlenk-flask in a glovebox. The catalyst **24** and **133** (*Strem Chemicals*) were stored under argon.

All the samples were carefully prepared in a glovebox. After transferring the material into the pressure NMR-tube (5 mm medium wall precision pressure/vacuum valve NMR sample tube, Wilmad) the tube was connected to the pH_2 -storage container or directly to the generator. The tubing was flushed with pH_2 to ensure that no other gases are present. Then the Swagelok connection to the NMR tube was tightened and the pressure valve opened to fill the tube with hydrogen. After closing the valve, the tube was shaken and directly transferred into the NMR magnet.

7.6.2 NMR Measurements

All the spectra were acquired on an Bruker Ascend AVIII 500 MHz NMR spectrometer (11.7 Tesla) equipped with an Bruker 5mm BBFO^{plus} 500 MHz SmartProbeTM (PA BBO 500S1 BBF-H-D-05 Z Plus) or Bruker 5mm TBI Probe (PH TBI 500S1 H/C-BB-D-05 Z) at 298 K unless otherwise mentioned.

The acquired ^1H -NMR spectra were referenced to the residual solvent signal ($\delta(\text{CHDCl}_2)=5.32$ ppm)^[137]. The ^{13}C -spectra were referenced indirectly to the referenced proton frequency with the Ξ -scale^[138,139].

NMR data was processed with Bruker's Topspin 3.2 and MestreNova 9.1.

7.6.3 Parahydrogen Enrichment

The hydrogen used in this work was produced in two different ways. An enrichment of 92 % was reached with *Para*-Hydrogen Generator by *Bruker BioSpin GmbH*

The *p*- H_2 was enriched to 50% by the usage of a U-shaped tube.^[148] The tube was produced in the workshops of the Max Planck Institute. The tube was filled with a mixture (3:1) an activated charcoal (Norit PK1-3, Sigma Aldrich) and iron(III) oxide (99%, meshed powder, Alfa Aesar). The filled tube was evacuated and heated with a heat gun (150 °C) to remove all the water and oxygen from the catalyst. Then the tube was used multiple times before the catalyst needs to be reactivated. To enrich the hydrogen the

Experimental Section

tube was loaded with 20 bar of hydrogen gas (99.995%, dry) and placed in a Dewar flask filled with liquid nitrogen ($-196\text{ }^{\circ}\text{C}$). After an equilibration time of 1h the enriched hydrogen was transferred to an evacuated storage bottle or directly transferred to the NMR tube.

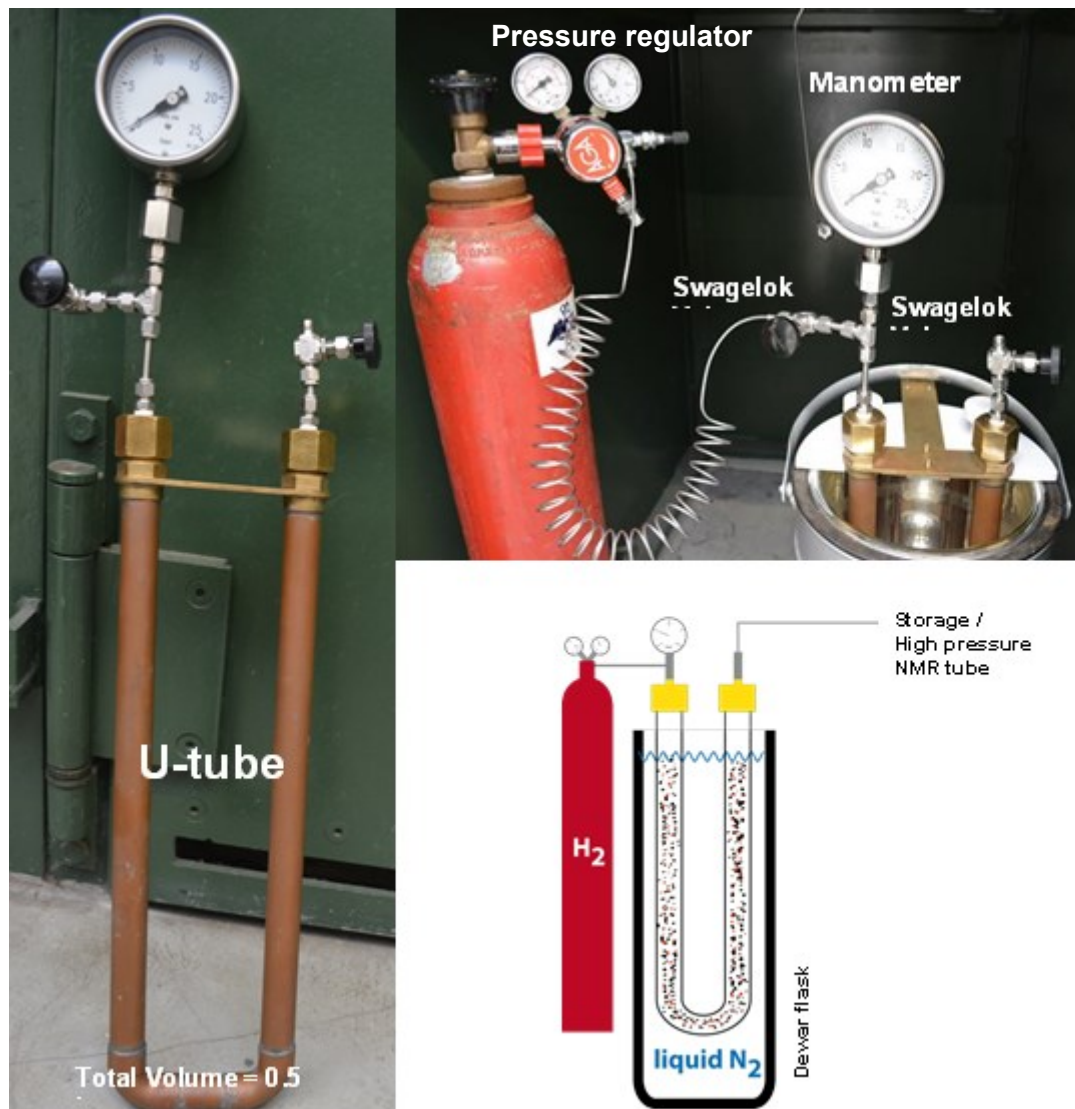


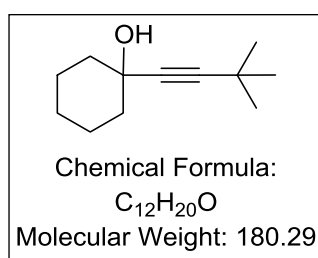
Figure 7.1: Apparatus for the *parahydrogen* enrichment to 50%

7.6.4 Substrates

The alkynes unless otherwise mentioned were purchased from commercial sources. Mono- and di-methylated diols **116b** and **116c** as well as 1-OMe-propynyl-cyclohexanol **112b** were kindly provided by Dr. M. Fuchs. 1-(1-butynyl)cyclohexanol **112c** was kindly provided by Dr. D.-A. Roşca.

1-(3,3-Dimethylbut-1-yn-1-yl)cyclohexan-1-ol (**112d**)

To 3.2 mL THF in a flame dried Schlenk-flask 200 μ L *tert*-butylacetylene (132 mg, 1.61 mmol, 1.0 equiv) were added and cooled to -78 °C. After dropwise addition of 68 μ L *n*-BuLi (2.5 M in hexanes, 1.70 mmol, 1.05 equiv) the solution was stirred for 30 min. Then 170 μ L dry cyclohexanone (1.61 mmol, 1.0 equiv) were added, the dry ice bath was removed and the mixture was stirred at rt overnight. The reaction was quenched with 4 mL sat. NaHCO₃ and the aqueous phase was extracted 3 times with 5 mL CH₂Cl₂. After washing with brine, the solvent was reduced pressure evaporated. Drying at high vacuum overnight yielded of a white, crystalline solid (100 mg, 0.55 mmol, 34%) were obtained.



¹H NMR (500 MHz, CD₂Cl₂) δ = 1.86 (s, 1H, OH), 1.83 – 1.76 (m, 2H, C-CH'H''-C), 1.65 (m, 2H C-CH'H''-C), 1.59 – 1.43 (m, 6H, C_{alip}H), 1.21 (s, 9H, C(CH₃)₃)

¹³C NMR (126 MHz, CD₂Cl₂) δ = 93.1, 82.3, 68.4, 40.4, 30.8, 27.1, 25.3, 23.5.

MS (EI) m/z: 180 (8%, M⁺), 165 (68%, M - CH₃), 137 (100%), 109 (47%), 67 (64%)

HRMS (ESI-pos) m/z (M+Na): calcd: 203.140634 found: 203.140710

7.6.5 Theoretical Methods

Density functional theory (DFT) was used to elucidate the mechanism of the Ru(II) catalyzed hydrogenation of alkynes. All geometry optimizations were performed using the M06^[149] functional. The triple- ζ quality def2-TZVP^[150–152] basis set was used for all atoms. The 28 inner-shell core electrons of the ruthenium atom were described by the corresponding def2 effective core potential^[153] accounting for scalar relativistic effects (def2-ecp).

Stationary points were characterized by evaluating the harmonic vibrational frequencies at the optimized geometries. Zero-point vibrational energies (ZPVE) were computed from the corresponding harmonic vibrational frequencies without scaling. Relative free energies (ΔG) were determined at standard pressure (1 bar) and at room temperature (298 K). The thermal and entropic contributions were evaluated within the rigid-rotor harmonic-oscillator approximation. Solvation contributions were included for dichloromethane on the optimized gas-phase geometries employing the SMD solvation model^[154] using the same functional and basis set. All calculations were performed using Gaussian09 with the ultrafine grid.^[155]

Dr. L. M. Wolf and Dr. P. Gupta from the group of Prof. W. Thiel at the Max-Planck-Institut für Kohlenforschung performed the computations. Further information about the computations including all the calculated structures are included in the supporting information of our common publication.^[156]

8. Bibliography

- [1] I. I. Rabi, J. R. Zacharias, S. Millman, P. Kusch, *Phys. Rev.* **1938**, *53*, 318–318.
- [2] E. D. Becker, *Anal. Chem.* **1993**, *65*, 295A–302A.
- [3] H. Pfeifer, *Magn. Reson. Chem.* **1999**, *37*, S154–S159.
- [4] J. T. Arnold, S. S. Dharmatti, M. E. Packard, *J. Chem. Phys.* **1951**, *19*, 507.
- [5] B. List, R. A. Lerner, C. F. Barbas, *J. Am. Chem. Soc.* **2000**, *122*, 2395–2396.
- [6] H. (2005). A. O. W. W.-V. Berkessel, A., Groeger, *Asymmetric Organocatalysis*, Wiley-VCH, **2005**.
- [7] J. Seayad, B. List, *Org. Biomol. Chem.* **2005**, *3*, 719.
- [8] B. List, Ed. , *Asymmetric Organocatalysis*, Springer Berlin Heidelberg, Berlin, Heidelberg, **2009**.
- [9] J. von Liebig, *Ann. der Chemie und Pharm.* **1860**, *113*, 246–247.
- [10] B. List, *Angew. Chem. Int. Ed.* **2010**, *49*, 1730–1734.
- [11] E. Knoevenagel, *Berichte der Dtsch. Chem. Gesellschaft* **1898**, *31*, 2596–2619.
- [12] W. Ostwald, *Zeitschrift für Phys. Chemie* **1900**, *34*, 510.
- [13] W. Langenbeck, *Die Organischen Katalysatoren Und Ihre Beziehungen Zu Den Fermenten*, Springer Berlin Heidelberg, Berlin, Heidelberg, **1935**.
- [14] G. Bredig, P. S. Fiske, *Biochem Z* **1912**, *7*.
- [15] D. R. P. Z. G. Hajos, *Asymetrische Synthese Polyzyclischer Organischer Verbindungen*, **1971**, DE 2102623.
- [16] Z. G. Hajos, D. R. Parrish, *J. Org. Chem.* **1974**, *39*, 1615–1621.
- [17] U. Eder, G. Sauer, R. Wiechert, *Angew. Chem. Int. Ed.* **1971**, *10*, 496–497.
- [18] K. A. Ahrendt, C. J. Borths, D. W. C. MacMillan, *J. Am. Chem. Soc.* **2000**, *122*, 4243–4244.
- [19] W. J. Rutter, *Fed. Proc.* **1964**, *23*, 1248–1257.
- [20] M. E. Jung, *Tetrahedron* **1976**, *32*, 3–31.
- [21] K. L. Brown, L. Damm, J. D. Dunitz, A. Eschenmoser, R. Hobi, C. Kratky, *Helv. Chim. Acta* **1978**, *61*, 3108–3135.
- [22] C. Agami, F. Meynier, C. Puchot, J. Guilhem, C. Pascard, *Tetrahedron* **1984**, *40*, 1031–1038.
- [23] C. Agami, C. Puchot, H. Sevestre, *Tetrahedron Lett.* **1986**, *27*, 1501–1504.
- [24] D. Rajagopal, M. . Moni, S. Subramanian, S. Swaminathan, *Tetrahedron: Asymmetry* **1999**, *10*, 1631–1634.
- [25] B. List, L. Hoang, H. J. Martin, *Proc. Natl. Acad. Sci.* **2004**, *101*, 5839–5842.
- [26] L. Hoang, S. Bahmanyar, K. N. Houk, B. List, *J. Am. Chem. Soc.* **2003**, *125*, 16–17.

Bibliography

- [27] H. Zhu, F. R. Clemente, K. N. Houk, M. P. Meyer, *J. Am. Chem. Soc.* **2009**, *131*, 1632–1633.
- [28] B. List, R. A. Lerner, C. F. Barbas, S. Bahmanyar, W. Notz, K. N. Houk, *Chemtracts* **2000**, *13*, 904–911.
- [29] W. Notz, B. List, *J. Am. Chem. Soc.* **2000**, *122*, 7386–7387.
- [30] S. Bahmanyar, K. N. Houk, H. J. Martin, B. List, *J. Am. Chem. Soc.* **2003**, *125*, 2475–2479.
- [31] S. Bahmanyar, K. N. Houk, *J. Am. Chem. Soc.* **2001**, *123*, 11273–11283.
- [32] D. Seebach, A. K. Beck, D. M. Badine, M. Limbach, A. Eschenmoser, A. M. Treasurywala, R. Hobi, W. Prikoszovich, B. Linder, *Helv. Chim. Acta* **2007**, *90*, 425–471.
- [33] A. K. Sharma, R. B. Sunoj, *Angew. Chem. Int. Ed.* **2010**, *49*, 6373–6377.
- [34] D. A. Bock, C. W. Lehmann, B. List, *Proc. Natl. Acad. Sci.* **2010**, *107*, 20636–20641.
- [35] M. B. Schmid, K. Zeitler, R. M. Gschwind, *Angew. Chem. Int. Ed.* **2010**, *49*, 4997–5003.
- [36] R. J. Andrew, J. M. Mellor, *Tetrahedron* **2000**, *56*, 7267–7272.
- [37] D. A. Bock, Chirale Co-Kristallisation Und Kristallstrukturen von Prolin-Enaminen, Bergische Universität Wuppertal, **2014**.
- [38] N. Zotova, A. Franzke, A. Armstrong, D. G. Blackmond, *J. Am. Chem. Soc.* **2007**, *129*, 15100–15101.
- [39] N. Zotova, L. J. Broadbelt, A. Armstrong, D. G. Blackmond, *Bioorg. Med. Chem. Lett.* **2009**, *19*, 3934–3937.
- [40] J. Burés, A. Armstrong, D. G. Blackmond, *Chem. Sci.* **2012**, *3*, 1273.
- [41] H. Iwamura, S. P. Mathew, D. G. Blackmond, *J. Am. Chem. Soc.* **2004**, *126*, 11770–11771.
- [42] S. P. Mathew, M. Klussmann, H. Iwamura, D. H. Wells, Jr., A. Armstrong, D. G. Blackmond, *Chem. Commun.* **2006**, 4291.
- [43] J. E. Hein, A. Armstrong, D. G. Blackmond, *Org. Lett.* **2011**, *13*, 4300–4303.
- [44] B. List, *Tetrahedron* **2002**, *58*, 5573–5590.
- [45] S. Mukherjee, J. W. Yang, S. Hoffmann, B. List, *Chem. Rev.* **2007**, *107*, 5471–5569.
- [46] P. M. Pihko, I. Majander, A. Erkkilä, in *Asymmetric Organocatalysis* (Ed.: B. List), Springer Berlin Heidelberg, **2010**, pp. 145–200.
- [47] B. M. Trost, C. S. Brindle, *Chem. Soc. Rev.* **2010**, *39*, 1600.
- [48] D. Kampen, C. M. Reisinger, B. List, *Asymmetric Organocatalysis*, Springer Berlin Heidelberg, Berlin, Heidelberg, **2009**.
- [49] D. Parmar, E. Sugiono, S. Raja, M. Rueping, *Chem. Rev.* **2014**, *114*, 9047–9153.
- [50] T. Akiyama, J. Itoh, K. Fuchibe, *Adv. Synth. Catal.* **2006**, *348*, 999–1010.

- [51] M. S. Sigman, E. N. Jacobsen, *J. Am. Chem. Soc.* **1998**, *120*, 4901–4902.
- [52] Y. Huang, A. K. Unni, A. N. Thadani, V. H. Rawal, *Nature* **2003**, *424*, 146–146.
- [53] J. Seayad, A. M. Seayad, B. List, *J. Am. Chem. Soc.* **2006**, *128*, 1086–1087.
- [54] D. Uraguchi, K. Sorimachi, M. Terada, *J. Am. Chem. Soc.* **2004**, *126*, 11804–11805.
- [55] S. Hoffmann, A. M. Seayad, B. List, *Angew. Chem. Int. Ed.* **2005**, *44*, 7424–7427.
- [56] D. Nakashima, H. Yamamoto, *J. Am. Chem. Soc.* **2006**, *128*, 9626–9627.
- [57] P. García-García, F. Lay, P. García-García, C. Rabalakos, B. List, *Angew. Chem. Int. Ed.* **2009**, *48*, 4363–4366.
- [58] T. James, M. van Gemmeren, B. List, *Chem. Rev.* **2015**, *115*, 9388–9409.
- [59] L.-Y. Chen, H. He, W.-H. Chan, A. W. M. Lee, *J. Org. Chem.* **2011**, *76*, 7141–7147.
- [60] S. Prévost, N. Dupré, M. Leutzsch, Q. Wang, V. Wakchaure, B. List, *Angew. Chem. Int. Ed.* **2014**, *53*, 8770–8773.
- [61] T. Hashimoto, K. Maruoka, *J. Am. Chem. Soc.* **2007**, *129*, 10054–10055.
- [62] T. Akiyama, Y. Saitoh, H. Morita, K. Fuchibe, *Adv. Synth. Catal.* **2005**, *347*, 1523–1526.
- [63] G. B. Rowland, H. Zhang, E. B. Rowland, S. Chennamadhavuni, Y. Wang, J. C. Antilla, *J. Am. Chem. Soc.* **2005**, *127*, 15696–15697.
- [64] I. Čorić, S. Müller, B. List, *J. Am. Chem. Soc.* **2010**, *132*, 17370–17373.
- [65] I. Čorić, B. List, *Nature* **2012**, *483*, 315–319.
- [66] J. H. Kim, I. Čorić, S. Vellalath, B. List, *Angew. Chem. Int. Ed.* **2013**, *52*, 4474–4477.
- [67] J. H. Kim, I. Čorić, C. Palumbo, B. List, *J. Am. Chem. Soc.* **2015**, *137*, 1778–1781.
- [68] S. Liao, I. Čorić, Q. Wang, B. List, *J. Am. Chem. Soc.* **2012**, *134*, 10765–10768.
- [69] G. C. Tsui, L. Liu, B. List, *Angew. Chem. Int. Ed.* **2015**, *54*, 7703–7706.
- [70] G. N. Lewis, *From Valence and the Structure of Atoms and Molecules*, **1923**.
- [71] Z.-X. Wang, Y. Tu, M. Frohn, J.-R. Zhang, Y. Shi, *J. Am. Chem. Soc.* **1997**, *119*, 11224–11235.
- [72] U. H. Dolling, P. Davis, E. J. J. Grabowski, *J. Am. Chem. Soc.* **1984**, *106*, 446–447.
- [73] L. Ratjen, M. van Gemmeren, F. Pesciaioli, B. List, *Angew. Chem. Int. Ed.* **2014**, *53*, 8765–8769.
- [74] A. Berkessel, V. R. Yatham, S. Elfert, J.-M. Neudörfl, *Angew. Chem.* **2013**, *125*, 11364–11369.
- [75] L. T. Kuhn, Ed. , *Hyperpolarization Methods in NMR Spectroscopy*, Springer Berlin Heidelberg, Berlin, Heidelberg, **2013**.
- [76] K.-G. Seifert, *Chemie unserer Zeit* **1976**, *10*, 84–93.
- [77] H. R. Ward, *Acc. Chem. Res.* **1972**, *5*, 18–24.
- [78] J. Natterer, J. Bargon, *Prog. Nucl. Magn. Reson. Spectrosc.* **1997**, *31*, 293–315.

Bibliography

- [79] Simon B. Duckett, in *Encycl. Magn. Reson.* (Ed.: R.K. Harris), John Wiley & Sons, Ltd, Chichester, UK, **2009**, pp. 3283–3293.
- [80] C. R. Bowers, D. P. Weitekamp, *J. Am. Chem. Soc.* **1987**, *109*, 5541–5542.
- [81] T. C. Eisenschmid, R. U. Kirss, P. P. Deutsch, S. I. Hommeltoft, R. Eisenberg, J. Bargon, R. G. Lawler, A. L. Balch, *J. Am. Chem. Soc.* **1987**, *109*, 8089–8091.
- [82] M. G. Pravica, D. P. Weitekamp, *Chem. Phys. Lett.* **1988**, *145*, 255–258.
- [83] L. Buljubasich, M. B. Franzoni, K. Münnemann, *Top. Curr. Chem.* **2013**, *338*, 33–74.
- [84] J. F. Young, J. A. Osborn, F. H. Jardine, G. Wilkinson, *Chem. Commun.* **1965**, 131.
- [85] S. B. Duckett, C. L. Newell, R. Eisenberg, *J. Am. Chem. Soc.* **1994**, *116*, 10548–10556.
- [86] J. M. Brown, P. L. Evans, A. R. Lucy, *J. Chem. Soc. Perkin Trans. 2* **1987**, 1589.
- [87] J. M. Brown, *Chem. Soc. Rev.* **1993**, *22*, 25.
- [88] S. B. Duckett, C. L. Newell, R. Eisenberg, *J. Am. Chem. Soc.* **1997**, *119*, 2068–2068.
- [89] J. a Osborn, R. R. Schrock, *J. Am. Chem. Soc.* **1971**, *2143*, 2143–2147.
- [90] H. Lindlar, *Helv. Chim. Acta* **1952**, *35*, 446–450.
- [91] R. R. Burch, E. L. Muetterties, R. G. Teller, J. M. Williams, *J. Am. Chem. Soc.* **1982**, *104*, 4257–4258.
- [92] R. R. Burch, A. J. Shusterman, E. L. Muetterties, R. G. Teller, J. M. Williams, *J. Am. Chem. Soc.* **1983**, *105*, 3546–3556.
- [93] K. Tani, A. Iseki, T. Yamagata, *Chem. Commun.* **1999**, 1821–1822.
- [94] D. Schleyer, H. G. Niessen, J. Bargon, *New J. Chem.* **2001**, *25*, 423–426.
- [95] H. G. Niessen, D. Schleyer, S. Wiemann, J. Bargon, S. Steines, B. Driessen-Hoelscher, *Magn. Reson. Chem.* **2000**, *38*, 747–750.
- [96] J. P. Dunne, S. Aiken, S. B. Duckett, D. Konya, K. Q. Almeida Leñero, E. Drent, *J. Am. Chem. Soc.* **2004**, *126*, 16708–16709.
- [97] J. López-Serrano, S. B. Duckett, A. Lledós, *J. Am. Chem. Soc.* **2006**, *128*, 9596–9597.
- [98] J. López-Serrano, S. B. Duckett, S. Aiken, K. Q. Almeida Leñero, E. Drent, J. P. Dunne, D. Konya, A. C. Whitwood, *J. Am. Chem. Soc.* **2007**, *129*, 6513–6527.
- [99] J. López-Serrano, S. B. Duckett, J. P. Dunne, C. Godard, A. C. Whitwood, *Dalt. Trans.* **2008**, 4270.
- [100] K. Radkowski, B. Sundararaju, A. Fürstner, *Angew. Chem.* **2013**, *125*, 373–378.
- [101] B. Sundararaju, A. Fürstner, *Angew. Chem. Int. Ed.* **2013**, *52*, 14050–14054.
- [102] S. M. Rummelt, A. Fürstner, *Angew. Chem. Int. Ed.* **2014**, *53*, 3626–3630.
- [103] S. M. Rummelt, K. Radkowski, D.-A. Roşca, A. Fürstner, *J. Am. Chem. Soc.* **2015**, *137*, 5506–5519.
- [104] L. W. Chung, Y.-D. Wu, B. M. Trost, Z. T. Ball, *J. Am. Chem. Soc.* **2003**, *125*, 11578–11582.

- [105] Q. Wang, M. Leutzsch, M. van Gemmeren, B. List, *J. Am. Chem. Soc.* **2013**, *135*, 15334–15337.
- [106] T. Steiner, *New J. Chem.* **1998**, *22*, 1099–1103.
- [107] T. Steiner, *Angew. Chem. Int. Ed.* **2002**, *41*, 48–76.
- [108] C. R. Kemnitz, M. J. Loewen, *J. Am. Chem. Soc.* **2007**, *129*, 2521–2528.
- [109] R. Thomas, C. B. Shoemaker, K. Eriks, *Acta Crystallogr.* **1966**, *21*, 12–20.
- [110] A. Martínez, K. Zumbansen, A. Döhring, M. van Gemmeren, B. List, *Synlett* **2014**, *25*, 932–934.
- [111] L. E. Luna, G. Seoane, R. M. Cravero, *European J. Org. Chem.* **2008**, *2008*, 1271–1277.
- [112] B. List, I. Čorić, O. O. Grygorenko, P. S. J. Kaib, I. Komarov, A. Lee, M. Leutzsch, S. Chandra Pan, A. V. Tymtsunik, M. van Gemmeren, *Angew. Chem. Int. Ed.* **2014**, *53*, 282–285.
- [113] M. B. Schmid, K. Zeitler, R. M. Gschwind, *Chem. Eur. J.* **2012**, *18*, 3362–3370.
- [114] T. Kita, A. Georgieva, Y. Hashimoto, T. Nakata, K. Nagasawa, *Angew. Chem. Int. Ed.* **2002**, *41*, 2832–2834.
- [115] A. Blaschette, E. Wieland, T. Hamann, R. K. Harris, *Zeitschrift für Naturforsch. B* **1992**, *47*, 1693–1700.
- [116] G. Simchen, S. Jonas, *J. für Prakt. Chemie* **1998**, *340*, 506–512.
- [117] A. Vij, Y. Y. Zheng, R. L. Kirchmeier, J. M. Shreeve, *Inorg. Chem.* **1994**, *33*, 3281–3288.
- [118] A. G. Wenzel, E. N. Jacobsen, *J. Am. Chem. Soc.* **2002**, *124*, 12964–12965.
- [119] B. P. Stoicheff, *Can. J. Phys.* **1957**, *35*, 730–741.
- [120] B. A. Tom, S. Bhasker, Y. Miyamoto, T. Momose, B. J. McCall, *Rev. Sci. Instrum.* **2009**, *80*, 016108.
- [121] B. Feng, A. M. Coffey, R. D. Colon, E. Y. Chekmenev, K. W. Waddell, *J. Magn. Reson.* **2012**, *214*, 258–262.
- [122] M. Mahlau, B. List, *Angew. Chem. Int. Ed.* **2013**, *52*, 518–533.
- [123] H. Suzuki, T. Kakigano, K. Tada, M. Igarashi, K. Matsubara, A. Inagaki, M. Oshima, T. Takao, *Bull. Chem. Soc. Jpn.* **2005**, *78*, 67–87.
- [124] H. Suzuki, *Eur. J. Inorg. Chem.* **2002**, *2002*, 1009–1023.
- [125] H. Suzuki, H. Omori, D. H. Lee, Y. Yoshida, Y. Morooka, *Organometallics* **1988**, *7*, 2243–2245.
- [126] G. Jia, W. S. Ng, C. P. Lau, *Organometallics* **1998**, *17*, 4538–4540.
- [127] H. Günther, *NMR Spectroscopy - Basic Principles, Concepts, and Applications in Chemistry*, **2013**.

- [128] R. H. Grubbs, T. M. Trnka, in *Ruthenium Org. Synth.*, Wiley-VCH Verlag GmbH & Co. KGaA, Weinheim, FRG, **2005**, pp. 153–177.
- [129] J. a Aguilar, R. W. Adams, S. B. Duckett, G. G. R. Green, R. Kandiah, *J. Magn. Reson.* **2011**, *208*, 49–57.
- [130] J. a Aguilar, P. I. P. Elliott, J. López-Serrano, R. W. Adams, S. B. Duckett, *Chem. Commun.* **2007**, 1183.
- [131] A. Fürstner, L. Ackermann, B. Gabor, R. Goddard, C. W. Lehmann, R. Mynott, F. Stelzer, O. R. Thiel, *Chem. Eur. J.* **2001**, *7*, 3236–3253.
- [132] M. R. Monaco, B. Poladura, M. Diaz de Los Bernardos, M. Leutzsch, R. Goddard, B. List, *Angew. Chem. Int. Ed.* **2014**, *53*, 7063–7067.
- [133] M. R. Monaco, S. Prévost, B. List, *Angew. Chem. Int. Ed.* **2014**, *53*, 8142–5.
- [134] M. R. Monaco, S. Prévost, B. List, *J. Am. Chem. Soc.* **2014**, *136*, 16982–16985.
- [135] Mattia Monaco, Activation of Carboxylic Acid via Self-Assembly Organocatalysis, Universität Köln, **2015**.
- [136] L. Liu, M. Leutzsch, Y. Zheng, M. W. Alachraf, W. Thiel, B. List, *J. Am. Chem. Soc.* **2015**, *137*, 13268–13271.
- [137] G. R. Fulmer, A. J. M. Miller, N. H. Sherden, H. E. Gottlieb, A. Nudelman, B. M. Stoltz, J. E. Bercaw, K. I. Goldberg, *Organometallics* **2010**, *29*, 2176–2179.
- [138] R. K. Harris, E. D. Becker, S. M. Cabral de Menezes, P. Granger, R. E. Hoffman, K. W. Zilm, *Pure Appl. Chem.* **2008**, *80*, 59–84.
- [139] M. Findeisen, S. Berger, *50 and More Essential NMR Experiments: A Detailed Guide*, Wiley-VCH, **2013**.
- [140] C. Hardouin, M. J. Kelso, F. A. Romero, T. J. Rayl, D. Leung, I. Hwang, B. F. Cravatt, D. L. Boger, *J. Med. Chem.* **2007**, *50*, 3359–3368.
- [141] Y. Feng, J. K. Coward, *J. Med. Chem.* **2006**, *49*, 770–788.
- [142] J. A. Murphy, A. G. J. Commeureuc, T. N. Snaddon, T. M. McGuire, T. A. Khan, K. Hisler, M. L. Dewis, R. Carling, *Org. Lett.* **2005**, *7*, 1427–1429.
- [143] E. De Gussem, J. Cornelus, S. Pieters, D. Van den Bossche, J. Van der Eycken, W. Herrebout, P. Bultinck, *ChemPhysChem* **2013**, *14*, 3255–3262.
- [144] Y. Yang, L. Tang, S. Zhang, X. Guo, Z. Zha, Z. Wang, *Green Chem.* **2014**, *16*, 4106.
- [145] E. A. Voight, P. A. Roethle, S. D. Burke, *J. Org. Chem.* **2004**, *69*, 4534–4537.
- [146] J. Gracia, E. J. Thomas, *J. Chem. Soc. Perkin Trans. 1* **1998**, 2865–2872.
- [147] K. J. Hale, M. Frigerio, S. Manaviazar, *Org. Lett.* **2001**, *3*, 3791–3794.
- [148] J. Bargon, J. Kandels, K. Woelk, *Zeitschrift für Phys. Chemie* **1993**, *180*, 65–93.
- [149] Y. Zhao, D. G. Truhlar, *Theor. Chem. Acc.* **2008**, *120*, 215–241.
- [150] A. Schäfer, H. Horn, R. Ahlrichs, *J. Chem. Phys.* **1992**, *97*, 2571.
- [151] F. Weigend, R. Ahlrichs, *Phys. Chem. Chem. Phys.* **2005**, *7*, 3297.

- [152] F. Weigend, *Phys. Chem. Chem. Phys.* **2006**, *8*, 1057.
- [153] D. Andrae, U. Häußermann, M. Dolg, H. Stoll, H. Preuß, *Theor. Chim. Acta* **1990**, *77*, 123–141.
- [154] M. J. Frisch, G. W. Trucks, H. B. Schlegel, G. E. Scuseria, M. A. Robb, J. R. Cheeseman, G. Scalmani, V. Barone, B. Mennucci, G. A. Petersson, et al., *Gaussian 09, Revision D.01*, Gaussian, Inc., Wallingford CT, **2009**.
- [155] C. Y. Legault, *CYLview, 1.0b*, Université De Sherbrooke, **2009**.
- [156] M. Leutzsch, L. M. Wolf, P. Gupta, M. Fuchs, W. Thiel, C. Farès, A. Fürstner, *Angew. Chem.* **2015**, *127*, 12608–12613.

9. Appendix

9.1 Pulse Sequences

OPSY-EXSY

For the generation of the new pulse sequence the pulse sequence noesygpqh by Bruker was modified

```
;noesygpqhOPSY.leu
;avance-version (12/01/11)
;2D homonuclear correlation via dipolar coupling
;dipolar coupling may be due to noe or chemical exchange.
;phase sensitive
;with gradient pulses in mixing time
;with OPSY filter
```

```
;$CLASS=HighRes
;$DIM=2D
;$TYPE=
;$SUBTYPE=
;$COMMENT=
```

```
#include <Avance.incl>
#include <Grad.incl>
#include <Delay.incl>
```

```
"p2=p1*2"
```

```
"in0=inf1"
```

```
"d0=in0/2-p1*4/3.1416"
```

```
"p17=cnst1*p16"
```

```
"TAU=d8*0.5-p16-d16-50u"
```

```
"acqt0=-p1*2/3.1416"
```

Appendix

```
1 ze
2 d1
3 p1 ph1
  50u UNBLKGRAD
  p16:gp1
  d16
  p1 ph1
  p17:gp1
  d0
  p1 ph2
  TAU
  50u
  p16:gp2
  d16
  3u
  (p2 ph4):f1
  3u
  p16:gp2*-1
  d16
  50u BLKGRAD
  TAU
  p1 ph3
  go=2 ph31
  d1 mc #0 to 2 F1PH(calph(ph1, +90), caldel(d0, +in0))
exit
```

```
ph1=0 2
ph2=0 0 0 0 0 0 0 2 2 2 2 2 2 2
ph3=0 0 2 2 1 1 3 3
ph4=0
ph31=0 2 2 0 1 3 3 1 2 0 0 2 3 1 1 3
```

```
;p1 : f1 channel - power level for pulse (default)
;p1 : f1 channel - 90 degree high power pulse
;p2 : f1 channel - 180 degree high power pulse
;p16: homospoil/gradient pulse          [1 msec]
;d0 : incremented delay (2D)
```

```
;d1 : relaxation delay; 1-5 * T1
;d8 : mixing time
;d16: delay for homospoil/gradient recovery
;inf1: 1/SW = 2 * DW
;in0: 1/(1 * SW) = 2 * DW
;nd0: 1
;ns: 2 * n
;ds: 0
;td1: number of experiments
;FnMODE: States-TPPI, TPPI, States or QSEQ

;use gradient ratio:  gp 1
;                      40

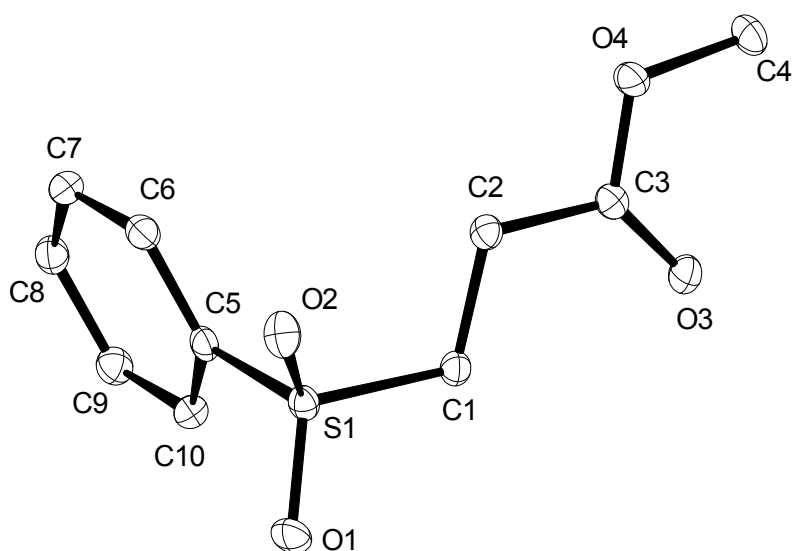
;for z-only gradients:
;gpz1: 100%
;gpz2: 40%

;use gradient files:
;gpnam1: SINE.100
;gpnam2: SINE.100
```

9.2 X-Ray Structures

The structures were analyzed by the X-Ray department of the institute (J. Rust & C. W. Lehmann)

Solid State Structure of Methyl 3-(phenylsulfonyl)propanoate (82)



Crystal data and structure refinement.

Identification code	9336	
Empirical formula	C ₁₀ H ₁₂ O ₄ S	
Color	colorless	
Formula weight	228.26 g · mol ⁻¹	
Temperature	100 K	
Wavelength	1.54178 Å	
Crystal system	MONOCLINIC	
Space group	P2₁/c, (no. 14)	
Unit cell dimensions	a = 7.7284(4) Å	α = 90°.
	b = 9.9308(5) Å	β = 95.8497(11)°.
	c = 13.6281(7) Å	γ = 90°.
Volume	1040.50(9) Å ³	
Z	4	
Density (calculated)	1.457 Mg · m ⁻³	
Absorption coefficient	2.727 mm ⁻¹	
F(000)	480 e	

Crystal size	0.47 x 0.35 x 0.27 mm ³	
θ range for data collection	5.522 to 67.371°.	
Index ranges	-9 \leq h \leq 9, -11 \leq k \leq 11, -16 \leq l \leq 16	
Reflections collected	23479	
Independent reflections	1857 [$R_{\text{int}} = 0.0313$]	
Reflections with $I > 2\sigma(I)$	1842	
Completeness to $\theta = 67.371^\circ$	99.5 %	
Absorption correction	Gaussian	
Max. and min. transmission	0.60 and 0.39	
Refinement method	Full-matrix least-squares on F^2	
Data / restraints / parameters	1857 / 0 / 137	
Goodness-of-fit on F^2	1.088	
Final R indices [$I > 2\sigma(I)$]	$R_1 = 0.0301$	$wR^2 = 0.0752$
R indices (all data)	$R_1 = 0.0303$	$wR^2 = 0.0753$
Largest diff. peak and hole	0.3 and -0.6 e \cdot \AA^{-3}	

Atomic coordinates and equivalent isotropic displacement parameters (\AA^2).

U_{eq} is defined as one third of the trace of the orthogonalized U_{ij} tensor.

	x	y	z	U_{eq}
S(1)	0.4113(1)	0.5453(1)	0.2931(1)	0.013(1)
O(1)	0.4649(2)	0.4524(1)	0.2207(1)	0.020(1)
O(2)	0.3297(1)	0.4928(1)	0.3759(1)	0.019(1)
O(3)	0.8574(1)	0.8064(1)	0.4328(1)	0.020(1)
O(4)	0.6779(1)	0.8869(1)	0.5386(1)	0.018(1)
C(1)	0.5980(2)	0.6394(2)	0.3391(1)	0.014(1)
C(2)	0.5636(2)	0.7225(2)	0.4288(1)	0.014(1)
C(3)	0.7179(2)	0.8083(2)	0.4644(1)	0.013(1)
C(4)	0.8140(2)	0.9758(2)	0.5810(1)	0.019(1)
C(5)	0.2695(2)	0.6649(2)	0.2312(1)	0.014(1)
C(6)	0.1284(2)	0.7145(2)	0.2755(1)	0.016(1)
C(7)	0.0206(2)	0.8092(2)	0.2253(1)	0.017(1)

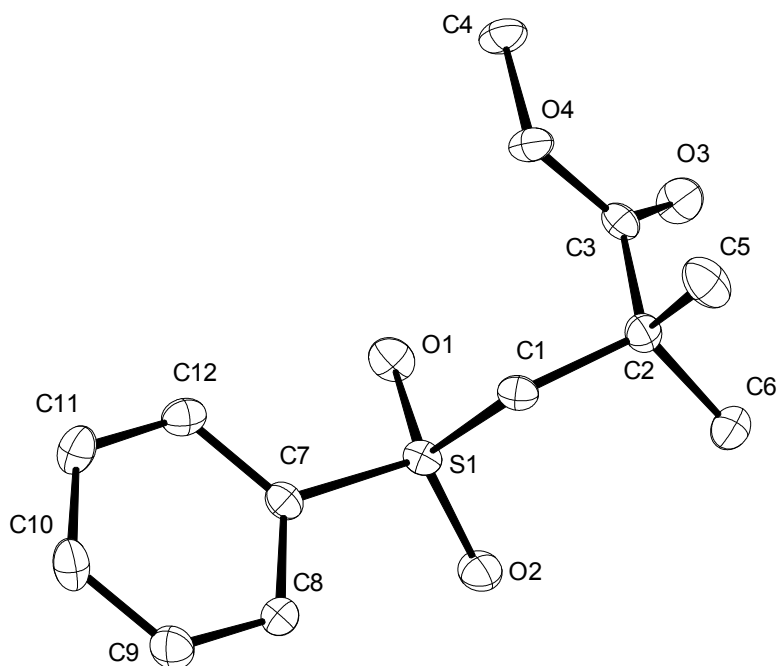
Appendix

C(8)	0.0548(2)	0.8529(2)	0.1324(1)	0.017(1)
C(9)	0.1968(2)	0.8028(2)	0.0892(1)	0.017(1)
C(10)	0.3053(2)	0.7079(2)	0.1381(1)	0.016(1)

Bond lengths [Å] and angles [°].

S(1)-O(1)	1.4423(11)	S(1)-O(2)	
1.4446(11)	S(1)-C(1)	1.7788(15)	S(1)-
C(5)	1.7698(15)	O(3)-C(3)	
1.2011(18)	O(4)-C(3)	1.3387(18)	O(4)-
C(4)	1.4473(19)	C(1)-C(2)	1.520(2)
C(2)-C(3)	1.505(2)	C(5)-C(6)	1.389(2)
C(5)-C(10)	1.393(2)	C(6)-C(7)	1.390(2)
C(7)-C(8)	1.388(2)	C(8)-C(9)	1.389(2)
C(9)-C(10)	1.386(2)		
O(1)-S(1)-O(2)	118.80(7)	O(1)-S(1)-C(1)	
107.36(7)	O(1)-S(1)-C(5)	108.08(7)	O(2)-
S(1)-C(1)	108.48(7)	O(2)-S(1)-C(5)	
108.42(7)	C(5)-S(1)-C(1)	104.84(7)	C(3)-
O(4)-C(4)	116.22(12)	C(2)-C(1)-S(1)	
111.52(10)	C(3)-C(2)-C(1)	111.65(12)	O(3)-
C(3)-O(4)	124.41(14)	O(3)-C(3)-C(2)	
125.88(14)	O(4)-C(3)-C(2)	109.70(12)	C(6)-
C(5)-S(1)	120.43(12)	C(6)-C(5)-C(10)	
121.62(14)	C(10)-C(5)-S(1)	117.95(11)	C(5)-
C(6)-C(7)	118.94(14)	C(8)-C(7)-C(6)	
120.02(14)	C(7)-C(8)-C(9)	120.40(15)	C(10)-
C(9)-C(8)	120.35(14)	C(9)-C(10)-C(5)	
118.66(14)			

Solid State Structure of Methyl 2,2-dimethyl-3-(phenylthio)propanoate (89)



Crystal data and structure refinement.

Identification code	9575	
Empirical formula	$C_{12}H_{16}O_4S$	
Color	colorless	
Formula weight	$256.31 \text{ g} \cdot \text{mol}^{-1}$	
Temperature	100 K	
Wavelength	1.54178 \AA	
Crystal system	Orthorhombic	
Space group	Pca2₁ , (no. 29)	
Unit cell dimensions	$a = 12.3908(4) \text{ \AA}$	$\alpha = 90^\circ$.
	$b = 8.0508(3) \text{ \AA}$	$\beta = 90^\circ$.
	$c = 12.8841(4) \text{ \AA}$	$\gamma = 90^\circ$.
Volume	$1285.26(7) \text{ \AA}^3$	
Z	4	
Density (calculated)	$1.325 \text{ Mg} \cdot \text{m}^{-3}$	
Absorption coefficient	2.264 mm^{-1}	
F(000)	544 e	
Crystal size	$0.22 \times 0.06 \times 0.03 \text{ mm}^3$	
θ range for data collection	5.495 to 67.516° .	
Index ranges	$-14 \leq h \leq 14$, $-9 \leq k \leq 9$, $-15 \leq l \leq 15$	
Reflections collected	28311	

Appendix

Independent reflections	2280 [R _{int} = 0.0384]	
Reflections with I > 2σ(I)	2215	
Completeness to θ = 67.516°	99.7 %	
Absorption correction	Gaussian	
Max. and min. transmission	0.94 and 0.69	
Refinement method	Full-matrix least-squares on F ²	
Data / restraints / parameters	2280 / 1 / 157	
Goodness-of-fit on F ²	1.064	
Final R indices [I > 2σ(I)]	R ₁ = 0.0243	wR ² = 0.0591
R indices (all data)	R ₁ = 0.0255	wR ² = 0.0597
Absolute structure parameter	-0.001(7)	
Largest diff. peak and hole	0.173 and -0.313 e · Å ⁻³	

Atomic coordinates and equivalent isotropic displacement parameters (Å²).
U_{eq} is defined as one third of the trace of the orthogonalized U_{ij} tensor.

	x	y	z	U _{eq}
S(1)	0.7066(1)	0.2695(1)	0.5026(1)	0.015(1)
O(1)	0.6722(2)	0.2125(2)	0.4019(1)	0.021(1)
O(2)	0.8185(1)	0.2499(2)	0.5301(1)	0.023(1)
O(3)	0.7342(1)	0.5607(2)	0.2513(2)	0.024(1)
O(4)	0.5711(1)	0.5303(2)	0.3242(1)	0.019(1)
C(1)	0.6680(2)	0.4813(3)	0.5171(2)	0.016(1)
C(2)	0.7147(2)	0.6033(3)	0.4364(2)	0.017(1)
C(3)	0.6768(2)	0.5608(3)	0.3276(2)	0.016(1)
C(4)	0.5282(2)	0.4878(3)	0.2234(2)	0.022(1)
C(5)	0.6686(2)	0.7752(3)	0.4644(2)	0.027(1)
C(6)	0.8380(2)	0.6098(4)	0.4396(2)	0.025(1)
C(7)	0.6275(2)	0.1694(3)	0.5982(2)	0.016(1)
C(8)	0.6643(2)	0.1647(3)	0.7005(2)	0.019(1)
C(9)	0.6000(2)	0.0901(3)	0.7754(2)	0.024(1)
C(10)	0.5013(2)	0.0220(3)	0.7483(2)	0.025(1)
C(11)	0.4657(2)	0.0273(3)	0.6462(2)	0.023(1)
C(12)	0.5285(2)	0.1021(3)	0.5706(2)	0.019(1)

Bond lengths [Å] and angles [°].

S(1)-O(1)	1.4407(18)	S(1)-O(2)	1.4397(18)
S(1)-C(1)	1.781(2)	S(1)-C(7)	1.768(2)
O(3)-C(3)	1.213(3)	O(4)-C(3)	1.334(3)
O(4)-C(4)	1.444(3)	C(1)-C(2)	1.543(3)
C(2)-C(3)	1.518(3)	C(2)-C(5)	1.540(3)
C(2)-C(6)	1.529(3)	C(7)-C(8)	1.394(3)
C(7)-C(12)	1.387(3)	C(8)-C(9)	1.388(4)
C(9)-C(10)	1.385(4)	C(10)-C(11)	1.387(4)
C(11)-C(12)	1.385(4)	O(1)-S(1)-C(1)	108.63(11)
O(1)-S(1)-C(7)	108.59(12)	O(2)-S(1)-O(1)	118.15(11)
O(2)-S(1)-C(1)	109.72(10)	O(2)-S(1)-C(7)	108.21(11)
C(7)-S(1)-C(1)	102.38(11)	C(3)-O(4)-C(4)	115.74(19)
C(2)-C(1)-S(1)	116.00(17)	C(3)-C(2)-C(1)	111.30(19)
C(3)-C(2)-C(5)	107.7(2)	C(3)-C(2)-C(6)	110.0(2)
C(5)-C(2)-C(1)	105.9(2)	C(6)-C(2)-C(1)	112.2(2)
C(6)-C(2)-C(5)	109.5(2)	O(3)-C(3)-O(4)	123.3(2)
O(3)-C(3)-C(2)	124.6(2)	O(4)-C(3)-C(2)	112.1(2)
C(8)-C(7)-S(1)	119.31(19)	C(12)-C(7)-S(1)	119.28(18)
C(12)-C(7)-C(8)	121.4(2)	C(9)-C(8)-C(7)	118.8(2)
C(10)-C(9)-C(8)	120.2(2)	C(9)-C(10)-C(11)	120.5(2)
C(12)-C(11)-C(10)	120.1(2)	C(11)-C(12)-C(7)	119.1(2)

9.3 Eigenständigkeitserklärung

"Ich versichere, dass ich die von mir vorgelegte Dissertation selbständig angefertigt, die benutzten Quellen und Hilfsmittel vollständig angegeben und die Stellen der Arbeit – einschließlich Tabellen, Karten und Abbildungen –, die anderen Werken im Wortlaut oder dem Sinn nach entnommen sind, in jedem Einzelfall als Entlehnung kenntlich gemacht habe; dass diese Dissertation noch keiner anderen Fakultät oder Universität zur Prüfung vorgelegen hat; dass sie – abgesehen von unten angegebenen Teilpublikationen – noch nicht veröffentlicht worden ist, sowie, dass ich eine solche Veröffentlichung vor Abschluss des Promotionsverfahrens nicht vornehmen werde. Die Bestimmungen der Promotionsordnung sind mir bekannt. Die von mir vorgelegte Dissertation ist von Prof. Dr. Benjamin List betreut worden."

Mülheim an der Ruhr, Oktober 2015

(M. Leutzsch)

Bisher sind folgende Teilpublikationen veröffentlicht worden:

- (1) Q. Wang, **M. Leutzsch**, M. van Gemmeren, B. List, *J. Am. Chem. Soc.* **2013**, *135*, 15334–15337.
- (2) B. List, I. Čorić, O. O. Grygorenko, P. S. J. Kaib, I. Komarov, A. Lee, **M. Leutzsch**, S. Chandra Pan, A. V. Tyntsunik, M. van Gemmeren, *Angew. Chem. Int. Ed.* **2014**, *53*, 282–285.
- (3) M. R. Monaco, B. Poladura, M. Diaz de Los Bernardos, **M. Leutzsch**, R. Goddard, B. List, *Angew. Chem. Int. Ed.* **2014**, *53*, 7063–7067.
- (4) S. Prévost, N. Dupré, **M. Leutzsch**, Q. Wang, V. Wakchaure, B. List, *Angew. Chem. Int. Ed.* **2014**, *53*, 8770–8773..
- (5) V. N. Wakchaure, P. S. J. Kaib, **M. Leutzsch**, B. List, *Angew. Chem. Int. Ed.* **2015**, *54*, 11852–11856.
- (6) **M. Leutzsch**, L. M. Wolf, P. Gupta, M. Fuchs, W. Thiel, C. Farès, A. Fürstner, *Angew. Chem. Int. Ed.* **2015**, *54*, 12431–12436.
- (7) L. Liu, **M. Leutzsch**, Y. Zheng, M. W. Alachraf, W. Thiel, B. List, *J. Am. Chem. Soc.* **2015**, *137*, 13268–13271.

9.4 Curriculum Vitae / Lebenslauf

Markus H. Leutzsch

Geburtsdatum: 06.12.1987
 Geburtsort: Meerane (Sachsen)
 Staatsangehörigkeit: deutsch

Akademischer Werdegang

Promotion

11.2011 – 11.2015 Dissertation im Arbeitskreis von Prof. Dr. Benjamin List
 Max-Planck-Institut für Kohlenforschung, Mülheim an der
 Ruhr.

Titel: *“NMR Spectroscopic Investigations of Catalyzed Reactions - Mechanisms, Kinetics & Unexpected Intermediates”*

Hochschulstudium

10.2009 – 10.2011 Masterstudium Chemie an der Universität Leipzig
 Masterarbeit im Arbeitskreis von Prof. Dr. Stefan Berger;
 Thema *“Anwendung moderner
 Kernresonanzspektroskopischer Methoden zur
 Konformationsanalyse von (Bio-)Molekülen”*

10.2006 – 10.2009 Bachelorstudium Chemie an der Universität Leipzig
 Bachelorarbeit im Arbeitskreis von Prof. Dr. Stefan Berger;
 Thema: *“Isolierung und Strukturaufklärung von
 Boswelliasäuren aus Weihrauch“*

Schulbildung

09.1998 – 07.2006 Europäisches Gymnasium Waldenburg, Waldenburg,
 Deutschland

10.1994 – 07.1998 Altstädter Grundschule Waldenburg, Waldenburg,
 Deutschland